[redacted]

Downgraded at 3 year intervals
Declassified after 12 years
DOD DIR 5200.10 per E Hodgman
by E Bartlett 3/31/64

COMPARISON OF AUTOMATIC TRACKING SYSTEMS FOR INTERCEPTOR AIRCRAFT

by

ROBERT C. SEAMANS, JR.

S.B., Harvard University
1939

S.M., Massachusetts Institute of Technology
1942

SUBMITTED IN PARTIAL FULFILLMENT OF THE
REQUIREMENTS FOR THE DEGREE OF
DOCTOR OF SCIENCE

at

MASSACHUSETTS INSTITUTE OF TECHNOLOGY
1951

Signature of Author: _____
Department of Aeronautical Engineering
May 11, 1951

Certified by: _____
Thesis Supervisor

_____
Chairman, Departmental Committee on Graduate Students

[redacted]

COMPARISON OF AUTOMATIC TRACKING SYSTEMS FOR INTERCEPTOR AIRCRAFT

by

Robert C. Seamans, Jr.

Submitted for the degree of Doctor of Science in the Department of Aeronautical Engineering at Massachusetts Institute of Technology on May 11, 1951.

ABSTRACT

The object of this thesis is to compare the performance of automatic tracking systems for interceptor aircraft. Interceptor aircraft must track the target in order to fire the weapon best suited to the tactical situation. Possible weapon systems involve the use of guns, rockets, bombs or guided missiles.

Interceptor aircraft will be vectored into close proximity with the target on the basis of information received from a computer on the ground. Upon nearing the target, radar in the interceptor aircraft must search for, then acquire, signals from the target in order that tracking may commence. Although the course followed during tracking may initially be the same for any weapon, at the instant of fire consideration must be given to a particular projectile. At present, interceptor aircraft are controlled manually; but it is felt that, with the short times available at transonic speeds, the tracking should be automatic as soon as engineering developments permit.

Five different tracking systems were investigated from the standpoint of the dispersion from gust and radar interference and on the basis of the forced dynamic errors caused by particular tactical situations. These results are presented in graphic form in Chapters I through V. It was found that of the two general types of tracking systems, namely, the open-chain and the closed-loop, the closed-loop tracking system showed a decided superiority from the standpoint of dynamic errors. On the basis

of idealized components, the dispersion when using either type of system appears comparable. The results indicate that, with any type of system, there is difficulty in tracking with sufficient accuracy for nose and beam attacks to be effective. Inasmuch as interceptor aircraft should not be required to fly in the tail cone of the target, it is felt that considerable emphasis should be placed on means for minimizing the error during nose and beam attacks.

Basic data important to the design of an automatic tracking system are presented in the appendices of this thesis. This information covers the effects of atmospheric turbulence and radar interference, both of which affect the dispersion of the projectile impact with respect to a target.

May 11, 1951

Prof. Joseph S. Newell
Secretary of the Faculty
Massachusetts Institute of Technology
Cambridge 39, Massachusetts

Dear Professor Newell:

In accordance with the regulations of the faculty, I hereby submit a thesis entitled COMPARISON OF AUTOMATIC TRACKING SYSTEMS FOR INTERCEPTOR AIRCRAFT, in partial fulfillment of the requirements for the degree of Doctor of Science.

ACKNOWLEDGMENT

The author is indebted to the following persons and organizations for their assistance in the analysis described in this thesis:

Dr. C. S. Draper, who contributed many useful ideas and, more important, set an example of great technical skill and professional integrity.

The civilian and military students, who have contributed directly in the form of their theses and, indirectly, through classroom discussions.

Dr. E. Frey, Mr. William Greene, Mr. D. E. Kendall, Jr. and Dr. J. H. Laning, Jr. of the Instrumentation Laboratory, MIT, for paving the way to many solutions on the REAC.

Miss Madeline Sullivan, who kept the REAC wheels turning.

The Staff of the Statistical Services, MIT; especially, to Mr. F. M. Verzuh for this supervision, Mr. I. Pfeffer for the operation of the Rockefeller Differential Analyzer, and Mr. R. Lesser for the operation of the IBM equipment.

Mrs. R. C. Seamans for maintaining order at home.

Mr. J. Ward of the Servomechanisms Research Laboratory, MIT, for correlating a sample of radar data.

Mr. J. Angell of the Research Laboratory of Electronics, MIT, for advice on radar interference problems.

Jackson & Moreland for reproducing the manuscript.

Comdr. J. Wootton of the Bureau of Aeronautics, U.S. Navy, for supplying valuable radar information.

Col. G. Blake, Chief, Armament Laboratory, Air Materiel Command, for providing material pertaining to the interception problem.

This thesis was prepared under the auspices of DIC Project 6822, sponsored by the Office of Air Research and Armament Laboratory, Engineering Division, Air Materiel Command, through contract W33-038-ac-13969.

TABLE OF CONTENTS

LIST OF ILLUSTRATIONS

INTRODUCTION

Interceptor Aircraft Armament

The interceptor aircraft of today is manually operated and carries either 50-cal or 20 mm machine guns, and may have racks for 2.75-inch and 5-inch rockets. The guns are used in air-to-air attacks, whereas the rockets are held in reserve for ground and sea targets. Rockets have been employed successfully against air targets, using experimental fire control equipment, but as yet computers for air-to-air rocketfire are not operational. If such computers can be made available, rockets may well become the primary armament of the interceptor aircraft. This possibility is pictured in Fig. 1, which shows a rocket salvo being launched against an enemy bomber. The present rate of development promises that the military advantages stemming from the use of rockets against airborne targets can be realized in the near future.

Other weapons carried by interceptor aircraft include bombs and guided missiles. Bombs have excessively long times of flight and present a difficult storage problem. Air-to-air guided missiles offer the hope of high kill probability per pound of armament, with increased safety to the interceptor aircraft because of the relatively long ranges at which they can be fired while still maintaining a high hit probability. However, guided missiles are not yet production items; hence, it is felt that the development of tracking systems for interceptor aircraft should be concentrated at this time on gunfire and rocketfire. But it should be fairly easy to keep sufficient flexibility in the equipment so that guided missiles could be effectively utilized when they become available.

The Lead Angle in Interception

Much has been published in post war literature concerning fire against a moving target, so that today it is common knowledge that non-homing missiles must be fired at a calculated, future position of the target rather than at the instantaneous position apparent to the interceptor pilot.

Line of Sight For the purpose of calculating, or predicting, some future position of the target, certain facts concerning the target must be ascertained. The most available fact is the instantaneous position of the target with respect to the attacking interceptor. The straight line determined by the interceptor and a selected target at any instant of time is called the line of sight.

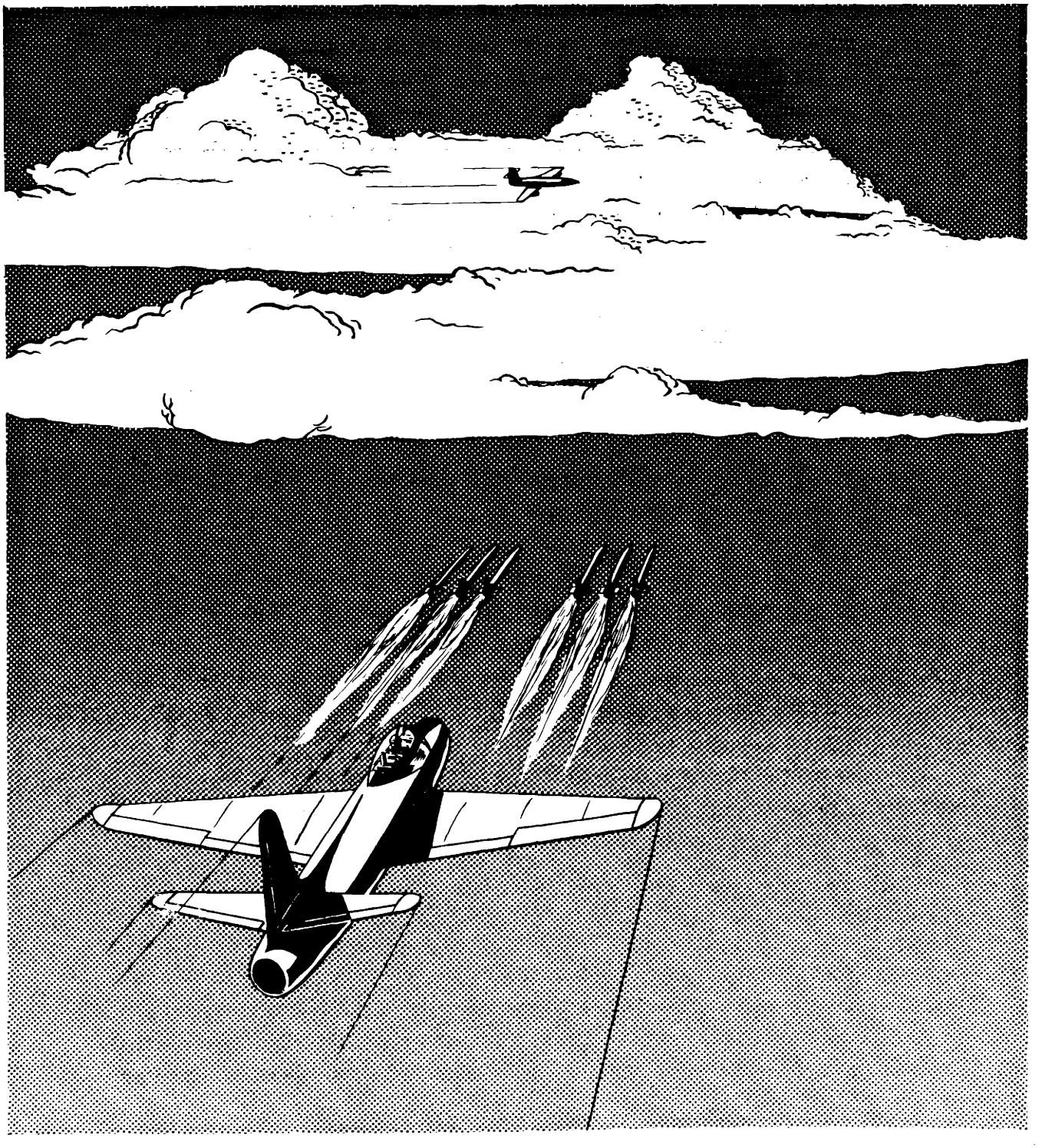

Fig. 1.—Diagram showing interceptor aircraft firing a rocket salvo against an enemy target.

Radar Tracking It is shown later that accurate, instantaneous knowledge of both the position and the angular velocity of the line of sight established by the target's position is necessary in fire control. Automatic systems use radar equipment to measure the target's position with respect to the interceptor aircraft. The radar has an antenna mounted in the nose of the interceptor in such a manner that the antenna can rotate in elevation and deflection. The center axis of the radar antenna establishes a direction called the tracking line. The radar receiver provides a voltage proportional to the displacement of this tracking line away from the line of sight. In all automatic systems this signal is used to drive the tracking line into alignment with the line of sight. This procedure is called tracking. The tracking line is fixed to the radar antenna, and is along the line of sight when the voltage signals from the radar receiver are a minimum. An angular displacement of the tracking line from the line of sight is called a tracking line inaccuracy, (I)TL, as shown in Fig. 2. Ideally, the tracking line inaccuracy is zero at all times.

Future Line of Sight

For the instant at which we choose to fire a projectile with the expectation that it will hit the target at some future position, we would like to know the direction along which to start the projectile so that the collision will occur. The straight line from the target to the hoped-for collision point we call the future line of sight.

The Lead Angle

The angle from the line of sight to the future line of sight is called the lead angle, because it is the angle by which we must lead the target in its present position to bring about a collision after the time of flight of the missile.

Mathematics of the Lead Angle The factors which affect the lead angle are shown in Fig. 3. The diagram depicts the interceptor-target-collision point triangle, which includes the lead angle. In terms of the target velocity, V_T, the target angle, A_T, and the average velocity of the missile over its course to the collision point, $V_{p(av)}$; and with the reasonable assumption that the lead angle is equal to its sine; the lead angle, L, is shown to be given by

$$L = \frac{V_T}{V_{p(av)}} \sin A_T \qquad (1)$$

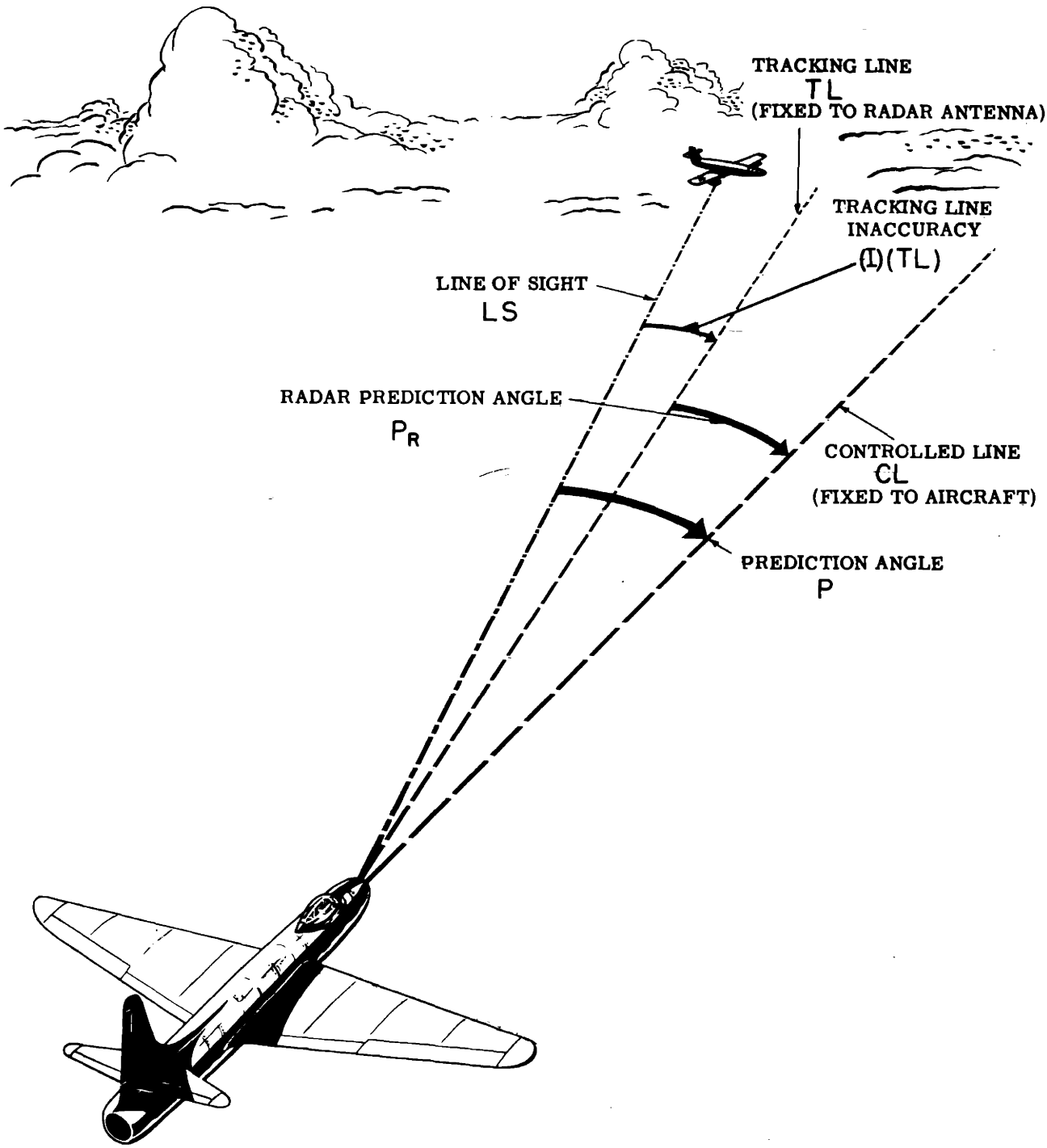

Fig. 2.—Diagram showing an interceptor aircraft tracking the target.

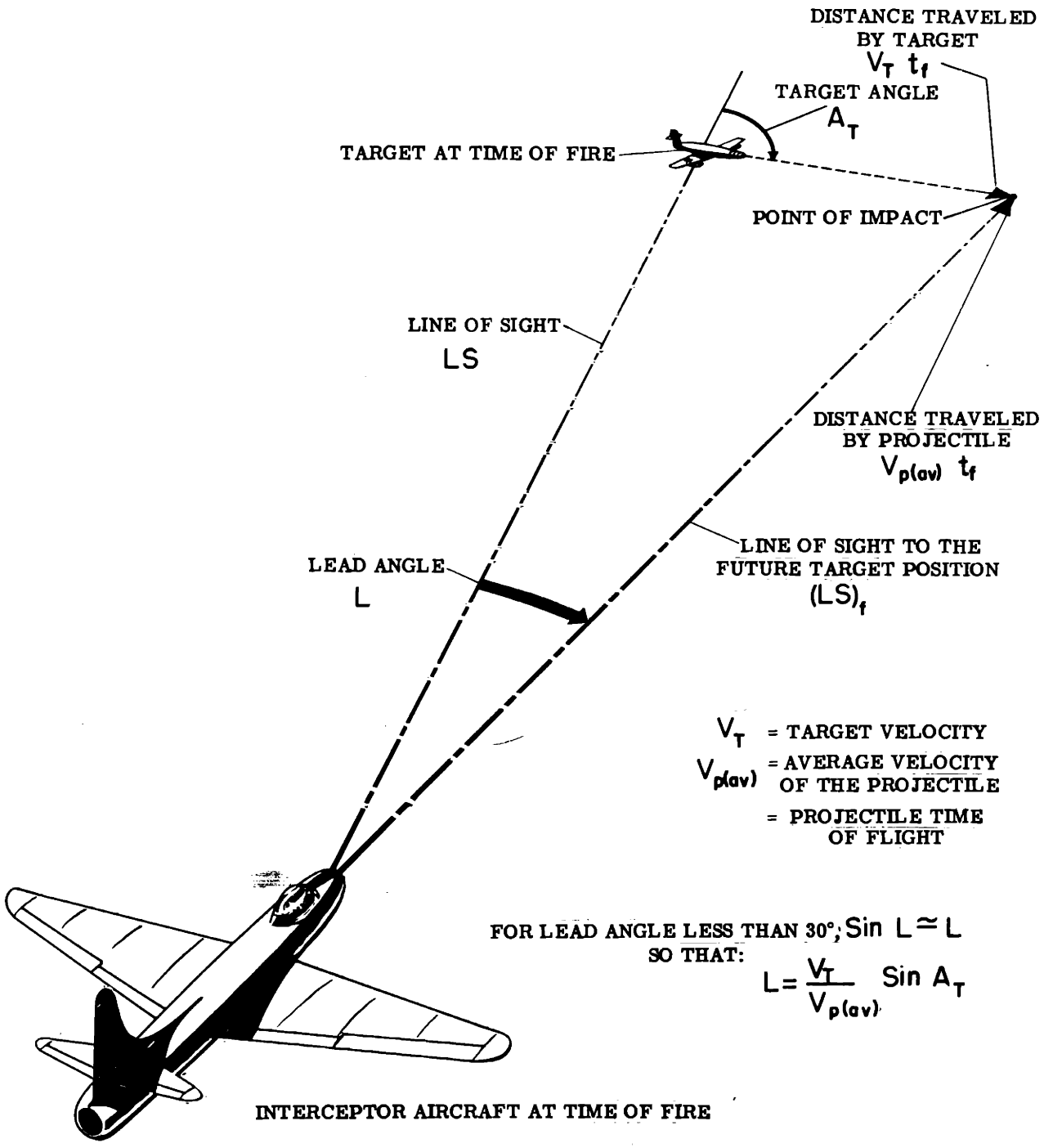

Fig. 3.—Diagram showing the factors which affect the lead angle.

That is, the lead angle is equal to the quotient of the component of target velocity perpendicular to the line of sight ($V_T \sin A_T$) and the average projectile (missile) velocity.

The Prediction Angle

Although the lead angle determines the future line of sight, it does not fix the line of fire. This would be so if lead - which corrects for target travel during the time of flight of the missile — were the only correction to be considered. But the missile gets part of its initial velocity from that of the interceptor, which may alter the line of departure (this is called velocity jump), and the missile will fall during its passage to the target because of the pull of gravity (this is called gravity drop). The angle compounded of lead, the correction for velocity jump and the correction for gravity drop is called the prediction angle. In interceptor problems where velocity jump and gravity drop are both relatively minor, the prediction angle is often loosely referred to as the lead angle since, in such cases, the latter constitutes almost the entire prediction angle.

Controlled Line

If we can predetermine with reasonable accuracy the amount of lead, velocity jump and gravity drop that will enter into a particular missile's passage to the collision point, we can fix the line of the missile-launching equipment so that a hit will be scored. In gunfire, this line is the axis of the gun bore; in rocketfire it is the line established by the launcher rails or tube; for generalized fire control use it is referred to as the controlled line. With the "fixed" guns or rockets of interceptor aircraft, by so harmonizing the equipment that the controlled line is parallel to the velocity vector (flight path) of the aircraft, velocity jump can be effectively minimized.

The correct orientation of the controlled line for a hit must be predicted on the basis of the target motion preceding the time of fire. As already noted, the predicted orientation of the controlled line is called the prediction angle, P, when measured with respect to the line of sight. It is called the radar prediction angle, P_R, when measured with respect to the tracking line.

In order to establish the proper controlled-line position, a computer carried in the interceptor aircraft generates an output voltage proportional to the desired prediction angle. In some tracking systems this voltage is used to position the radar antenna. In other systems the computer output

voltage is compared with a voltage indication of the radar prediction angle in order to obtain a measure of the aiming error of the interceptor aircraft. A comparison of the two methods is brought out in more detail later in the thesis.

Causes of Impact Errors

When a projectile is fired from an interceptor aircraft, it may miss the target for a variety of reasons. One is the tracking inaccuracy, caused by dynamic lags in the tracking system and by interference effects associated with the radar receiver. Another reason is the inaccuracy introduced by the prediction computer, which may result from either faulty calibration or dynamic effects. In addition, it must be remembered that the interceptor aircraft is flying through a turbulent air mass, which causes the controlled line to wander in a random manner. Finally, the projectiles have a dispersion with respect to the interceptor aircraft due to imperfections in their manufacture and to the method of firing.

Center-of-Impact Error

The probability of hitting the vulnerable area of the target depends upon the sum of the inaccuracies. It is useful to distinguish between the error components and the uncertainty components of inaccuracies. Errors are considered to be those components that can be predicted on the basis of static calibrations and dynamic analyses. Uncertainties, on the other hand, can only be treated statistically. A typical projectile pattern is shown in Fig. 4. The impact points are the intersections of the projectiles with a plane passing through the center of the target and normal to the line of fire. The center of impact is the average, or mean, position of all the impact points; the error in the center of impact is the distance from the target to this average position. It is assumed in this thesis that the error in the center of impact is equal to the aiming error of the interceptor aircraft.

Standard Deviation as a Measure of Scatter

The scatter of the impact points with respect to the center of impact is commonly measured in terms of the standard deviation. The standard deviation is the root mean square of the angular displacement of all the impact points with respect to their average position. When the pattern is represented by a Gaussian distribution, 40 percent of the impact points fall within a circle with a radius equal to the standard deviation. The standard deviation results from a random wander of the interceptor due to the effects

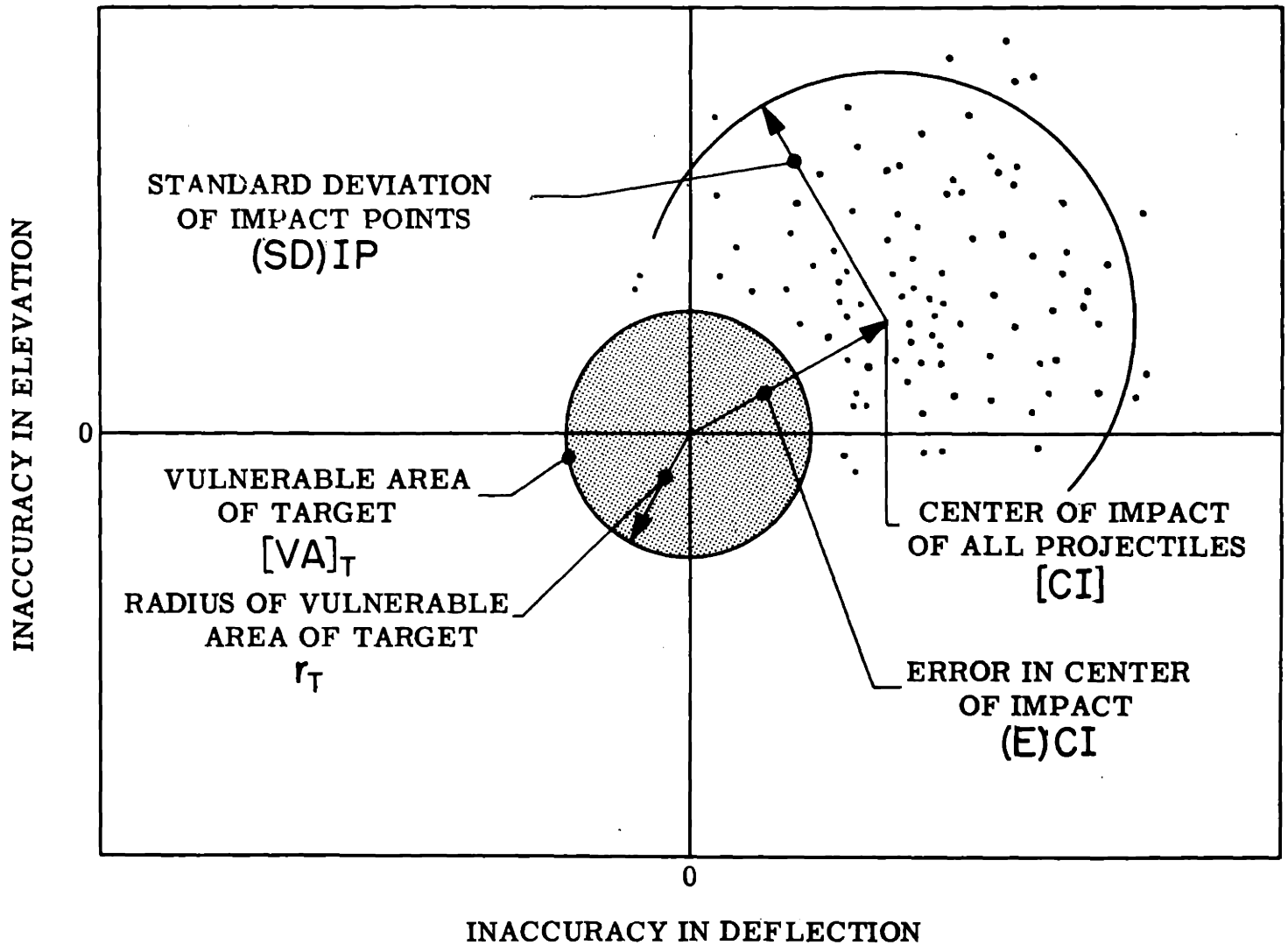

Fig. 4.—Impact of projectiles with the plane containing the target and normal to the line of fire.

of gusts and radar interference, and also depends on the dispersion of the projectiles measured with respect to the interceptor. In order to facilitate the analysis, the vulnerable area of the target is assumed to be circular, with a radius r_T. However, it must be realized that few targets are truly circular and that their projected areas may be quite irregular in shape.

Hit Probability

The probability of hitting the vulnerable area of the target, $P(VA)_T$, clearly depends on the error of the center of impact and the standard deviation of the impact points. When the center of impact is well off the target and the standard deviation is small in comparison with the target radius, there will be a low hit probability, for in this case most of the projectiles will pass by one side of the target. Under the same conditions of center-of-impact error, when the standard deviation – the scatter – is increased, there is increased probability of hits. However, when the standard deviation is much larger than the target radius, the impact points are scattered over a relatively wide area, hence are thinly distributed over the target and the hit probability is decreased. Obviously, when the error in the center of impact is greater than the target radius, the standard deviation has an optimum value that gives a maximum probability of a hit. This is shown in Fig. 5, in which the hit probability is plotted as a function of the standard deviation of the impact points for various errors in the center of impact. In these plots, the values of standard deviation and error are divided by the target radius in order to non-dimensionalize them and render them applicable to any size of circular target, provided the projectile pattern is Gaussian. For example, from Fig. 5 it can be seen that, with a (non-dimensional) error of 1.5, the maximum hit probability is 17 percent. This maximum is achieved with a non-dimensional standard deviation of 0.9. For greater accuracy in determining the hit probability for a given error and standard deviation, use can be made of Fig. G-2 in Appendix G.

Lead Pursuit Course

Attention must be given to the hit probability when selecting the course[1] to be followed prior to firing. Of the many possible courses that an aircraft can follow in the attack, the lead pursuit course and the straight line approach course are discussed here, as representing the two extremes of maximum acceleration and zero acceleration. When the interceptor flies an ideal lead-pursuit course, a projectile can be fired at any instant and a hit will be scored.

1 Numbered references are to bibliography, page 262.

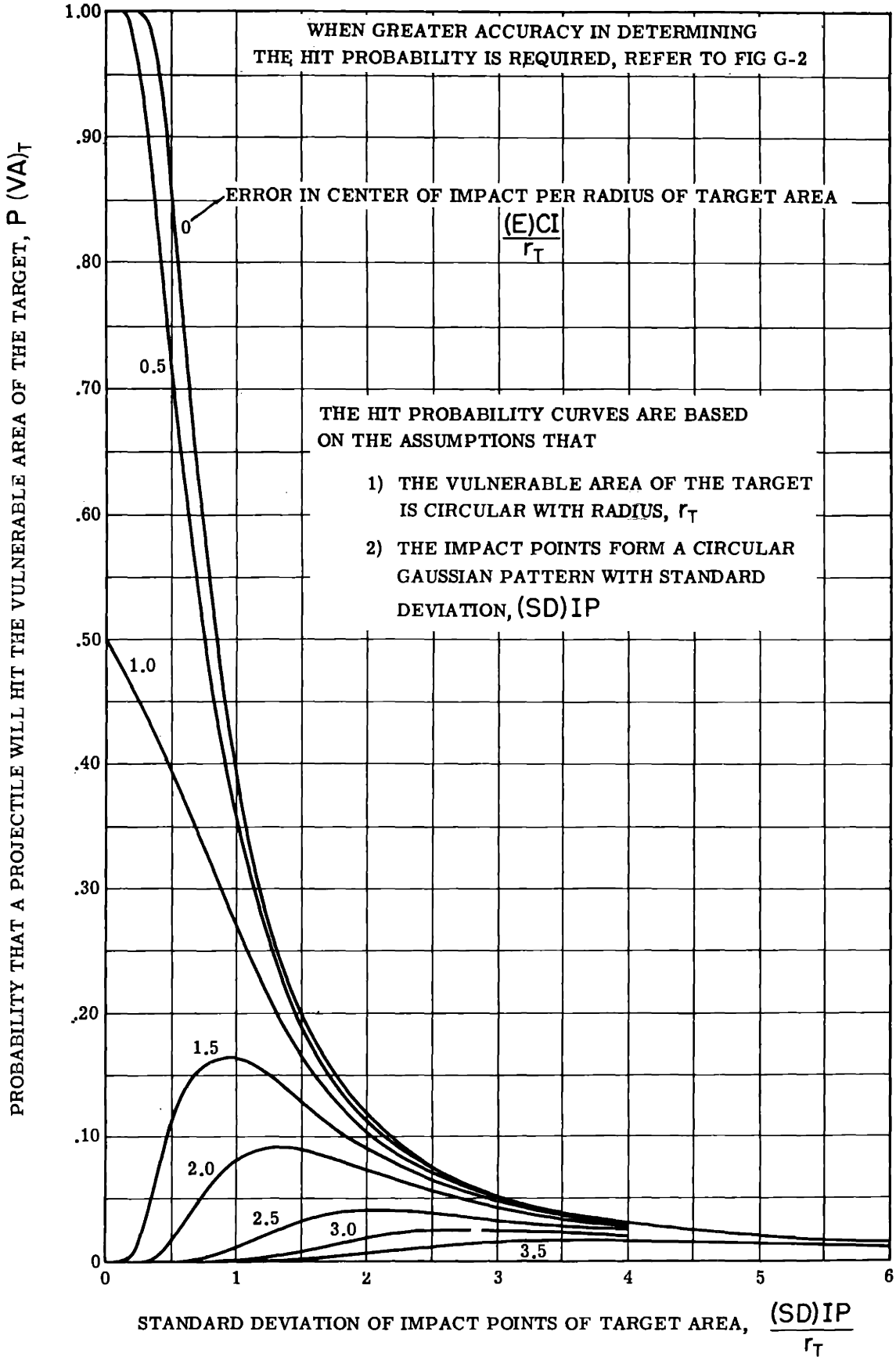

Fig. 5.–Effect of dispersion and aiming error on the probability of a hit.

This course has the advantage that the duration of the time within which effective fire is possible is sufficiently long that the pilot can watch instruments in the cockpit and select the time of fire when the aiming error is a minimum. Secondly, although the hit probability of a single round is low, a long burst can be fired in order to increase the number of hits on the target. Although the lead-pursuit course is usually preferable to other types of courses, there may be cases at high altitude where it is impossible for the interceptor aircraft to hold a sufficient acceleration to maintain such a course. In this case a path requiring less acceleration is required. In such circumstances it is advisable to fly the aircraft at its maximum turning rate, in order for the interval of effective fire to be as large as possible.

Straight Line Approach Course

On a straight-line approach course there is only a brief interval in which the firing can take place. This is a most important consideration when guns are used, for the rate of fire is limited with 0.50 cal weapons to 20 rounds per second for each gun. Since the interval for achieving a hit is a fraction of a second, there is little likelihood of scoring more than a few hits. Rockets cannot be fired together from free launchers without incurring some interference in their flight paths. However, they can be launched nearly simultaneously, and hence the probability of a hit is not as seriously reduced with this type weapon when flying straight-line approaches.

Open-Chain Tracking Systems

No matter what type of course is selected, it is essential to track the target so that the interceptor aircraft follows a prescribed path with respect to the target. The number of possible tracking systems is staggering when consideration is given to all the possible methods of stabilization and compensation. However, all tracking systems can be catalogued into two distinct types; namely, open-chain and closed-loop. In an open-chain tracking system, the radar tracking line is maintained along the line of sight by the action of the radar receiver and the radar antenna drive. An attempt is made to keep the tracking line orientation independent of the output from the prediction computer and the motion of the interceptor aircraft.

Lead Computation in Open-Chain Tracking Systems

The computation of the lead angle is based on the angular velocity of the radar tracking line which, ideally, is along the line of sight. Figure 6 shows

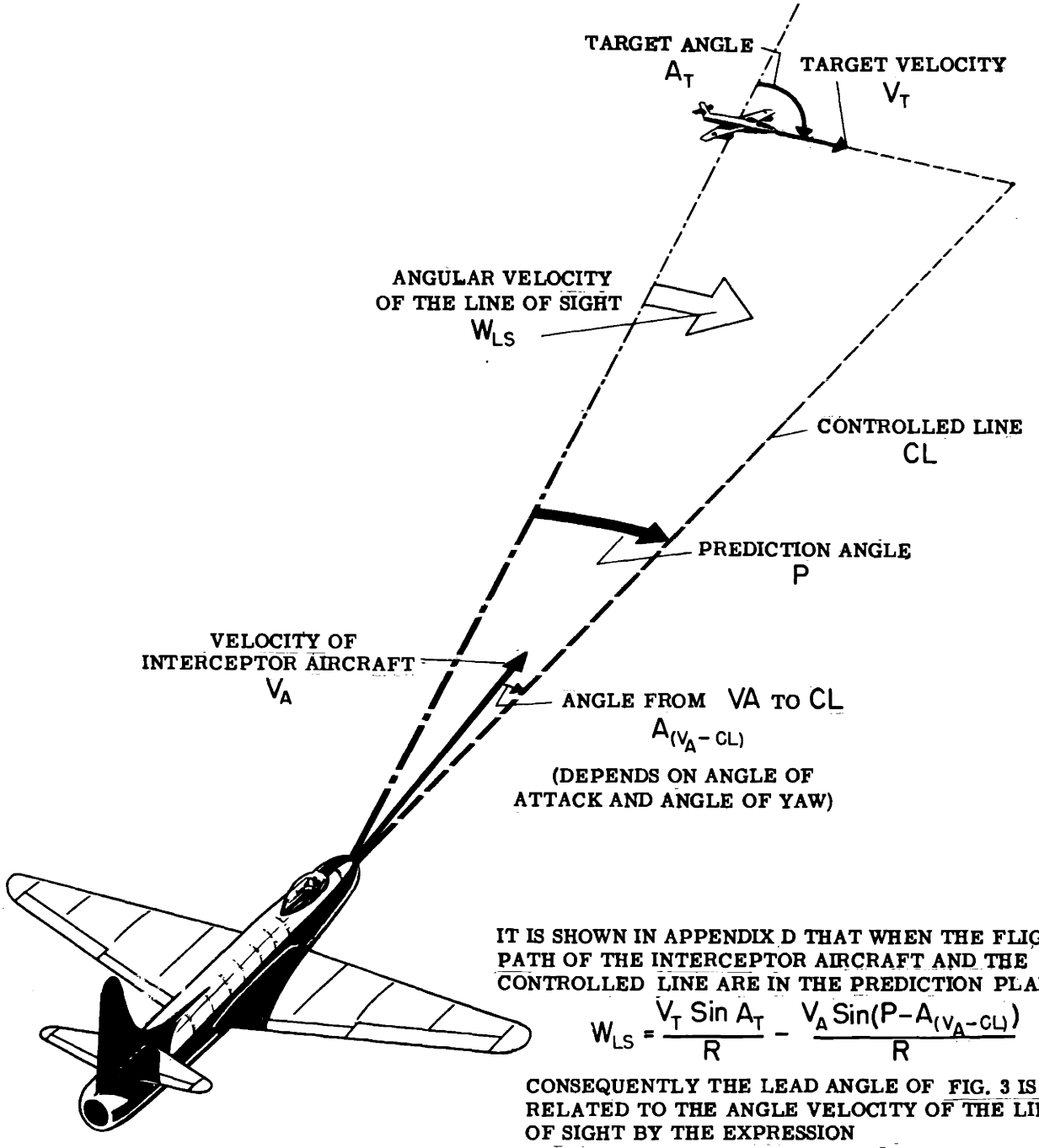

IT IS SHOWN IN APPENDIX D THAT WHEN THE FLIGHT PATH OF THE INTERCEPTOR AIRCRAFT AND THE CONTROLLED LINE ARE IN THE PREDICTION PLANE

$$W_{LS} = \frac{V_T \sin A_T}{R} - \frac{V_A \sin(P - A_{(V_A - CL)})}{R}$$

CONSEQUENTLY THE LEAD ANGLE OF FIG. 3 IS RELATED TO THE ANGLE VELOCITY OF THE LINE OF SIGHT BY THE EXPRESSION

$$L = \left[\frac{R}{V_{P(av)} - V_A}\right] W_{LS} + \left[\frac{V_a}{V_{P(av)} - V_A}\right] (P - L - A_{(V_A - CL)})$$

Fig. 6.–Relationship between the lead angle and the angular velocity of the line of sight.

the relationship between the lead angle and the angular velocity of the line of sight, W_{LS}. The line-of-sight angular velocity is proportional to the quotient of the target velocity normal to the line of sight and the range R, or stated mathematically

$$W_{LS} = \frac{V_T \sin A_T}{R} - \frac{V_A \sin \left[P - A_{(V_A - CL)}\right]}{R} \qquad (2)$$

The second term in Eq. (2) accounts for the velocity of the interceptor aircraft normal to the line of sight. The angle $A_{(V_A - CL)}$ depends upon the angle of attack and the angle of yaw. The first term of Eq. (2) is related to the lead angle of Eq. (1). The two expressions can be combined to give

$$L = \frac{R}{V_{p(av)} - V_A} W_{LS} + \left[\frac{V_A}{V_{p(av)} - V_A}\right] \left[P - L - A_{(V_A - CL)}\right] \qquad (3)$$

The average projectile velocity with respect to the interceptor, $[V_{p(av)} - V_A]$ is a function of range, since the projectile slows down in its passage through the air. Consequently, the first term in Eq. (3) can be computed given an indication of the range and the angular velocity of the line of sight. Range information is provided by the radar equipment, and in an open-chain tracking system the angular velocity of the line of sight is measured by single-degree-of-freedom gyros mounted in the radar antennas. The second term of this equation is small. Its significance in the total amount of the lead angle is considered in Appendix D.

Closed-Loop Tracking Systems

In a closed-loop tracking system, rather than to attempt to remove the effect of the computer on the tracking, the computer action is included in the tracking loop, that is, any effect generated by the computer is immediately manifested in the position of the tracking line. In steady-state conditions, under which the lead angle changes slowly or not at all, the angular velocity of the controlled line equals the angular velocity of the line of sight; consequently, in a closed-loop tracking system the lead computation is carried

out on the basis of the motion required of the aircraft when tracking the target. This is possible since the aircraft is integral with the controlled line and partakes of the same angular motion. The output of the prediction computer is used (in effect) to offset the radar tracking line by an amount proportional to the desired prediction angle. The resulting inaccuracy in tracking is detected by the radar receiver, which supplies a voltage proportional to this quantity to the interceptor controls to rehead the aircraft so as to keep the radar line in coincidence with the line of sight. Hence, in the process of tracking, the aircraft is advanced ahead of the line of sight by an amount proportional to the computer output.

Tracking Systems Investigated in This Thesis

The five tracking systems investigated in this thesis are:

I Open-Chain Tracking System with Tracking-Line Prediction

II* Open-Chain Tracking System with Tracking-Inaccuracy Prediction and Tight-Loop Stabilization of the Radar Antenna

III Closed-Loop Tracking System with Controlled-Line Prediction

IV Closed-Loop Tracking System with Controlled-Line Prediction and Tight-Loop Stabilization of the Aircraft

V Closed-Loop Tracking System with Tracking Inaccuracy Prediction and Tight-Loop Stabilization of the Aircraft

It can be seen that, of the five tracking systems investigated, two are open-chain and three are closed-loop. Functional diagrams of these five systems are contained in the respective Fig. I-1, II-1, III-1, IV-1, and V-1.

The open-chain systems differ according to the input supplied to the prediction computer. In system I a gyro mounted on the radar antenna measures the tracking-line angular velocity and provides this input to the prediction computer. In system II an integrating rate gyro is used to provide tight-loop stabilization of the radar antenna. The output from the gyro is applied to the radar antenna drive in such a way that the tracking line is held fixed with respect to inertial space, provided no electrical currents are applied to a torque generator in the integrating rate gyro. However, when a current is applied to the torque generator the tracking line rotates with a proportional angular velocity and, consequently, the input current can be used as a measure of the anticipated rotation of the

* Two variations of system II, referred to as IIa and IIb, are investigated: system IIb differs from system IIa in the inclusion of integration in the signal modifier - See Fig. II-24,-26,-28,-30.

tracking line. In order to maintain the tracking line along the line of sight, this current is provided by an amplifier associated with the radar receiver and, as a result of the tight-loop stabilization, this current can be used for prediction purposes.

In closed-loop tracking systems III and IV, gyros are used to measure the angular velocity of the controlled line about the respective elevation and deflection axes.* In both tracking systems III and IV, the radar antenna is rotated about the elevation and deflection axes by amounts proportional to the input angular velocity about these axes. However, in system IV a second integrating rate gyro, mounted so as to be fixed with respect to the controlled line, is used to stabilize the aircraft in a manner similar to the radar antenna stabilization of system II. In system V, integrating rate gyros are mounted fixed with respect to the controlled line as in System IV, rather than with respect to the tracking line as in System II. The current from the radar receiver, which serves as the tracking-inaccuracy detector, is used as the input to the integrating rate gyro and also as the primary input to the computer. The output from the gyro, properly modified by integral and lead networks, is transmitted to the servo system that positions the control surface.

The results of the analyses of the five tracking systems are presented in graphical form in Chapters I - V. A discussion of the results is contained in the following section.

* In this orthogonal axis system the elevation and deflection axes are normal to the controlled line, with the deflection axis taken downward in the plane of symmetry, and the elevation axis perpendicular to the plane of symmetry, positive along the right wing.

DISCUSSION OF RESULTS

Analytical Procedure

The analysis of the five tracking systems described herein was carried out in two parts: (1) The standard deviation of the controlled line, caused by gust and radar interferences, was obtained analytically — using IBM equipment made available by Statistical Services, M.I.T. (2) In order to determine the controlled-line error, solutions of the system equations and the target-interceptor kinematic equations were obtained on a REAC. The REAC solutions were obtained by restricting the approach courses to a vertical plane. This restriction imposed by the limitations of the equipment made it necessary to determine the response of the interceptor aircraft only about its pitch axis. The initial conditions shown in Fig. E-8 provided tail, beam, and head-on attacks with initial target angles of 30, 90 and 150 degrees. (The target angle is measured from the line of sight to the direction of the target flight path.) The ratio of initial range to interceptor velocity was either 20 or 40 seconds, giving absolute ranges of 14,500 feet and 29,000 feet for the interceptor flying at a Mach number of 0.7 at 20,000 feet.

System Comparison on the Basis of the Controlled-Line Errors

The controlled-line errors for the various tracking systems are plotted for comparison as functions of time, as shown in Chapters I through V. Included with the controlled-line error is the associated range, the sine of the target angle, and the angle of attack of the interceptor aircraft. The best results for both the open-chain tracking system and the closed-loop tracking system are shown in Fig. 7 for a beam attack. It can be seen that both systems I and IV are definitely unsatisfactory, with controlled-line errors of 50 and 20 mils respectively at a distance of 0.85 (corresponding to a range of approximately 1.5 miles). System II is equally unsatisfactory without integration in the signal modifier.

The angular velocity of the line of sight is inversely proportional to the range, as indicated in Eq. (2). Hence at short range the interceptor aircraft must have a large turning rate in order to keep the controlled line aimed ahead of the target. Without integration in the signal modifier, the turning rate is proportional to the correction signal introduced into the signal modifier, and hence to the controlled-line error. The curve for system IIb shows

that the controlled-line error can be reduced by increasing the forward gain, determined by the ratio of the controlled line angular velocity to the correction signal supplied to the signal modifier.

The distinct advantage of the closed-loop tracking systems III and V over the open-chain systems I and IIa is due to the difference in forward gain. The forward gain is 0.26 mil per second per mil for system I, 0.59 mil per second per mil for system IIa, 4.3 mils per second per mil for system III, and 3 mils per second per mil for system V. In none of the systems can these respective gains be increased without causing an appreciable increase in the deviation of the controlled line caused by gust and radar interference. But the closed-loop tracking systems can have the larger forward gain because of the attenuation in tracking-line motion introduced by the prediction computer.

In an effort to improve tracking system II, integration was introduced in the signal modifier in order to increase the forward gain, thereby decreasing the tracking correction required for a given aircraft turning rate. The curves of Fig. 7 show that at a non-dimensional range of 0.85, the controlled-line error is reduced by this means to only a quarter of the amount preceding the change.

The controlled-line errors of systems IIb, III and V are replotted in Fig. 8 as functions of the target range — the instantaneous distance from interceptor to target. At ranges useful for gunfire and rocketfire, the closed-loop tracking systems have controlled-line errors less than half the controlled-line errors of the open-chain tracking systems. The performance of closed-loop tracking systems will show to even greater advantage when integration is incorporated in their controls.

Comparison of Standard Deviations of Controlled-Line Displacement

The power spectral densities of the controlled-line displacements resulting from gusts and radar interference have been determined, and the results are plotted in Chapters I through V as functions of frequency. The power spectral densities provide a measure of the controlled-line wander at angular frequencies, ω, from 0.1 to 10 radians per second. The standard deviation of the controlled-line displacement [(SD)CL] can be readily determined by integrating the power spectral density (PSD) CL, since

I WITH TRACKING LINE PREDICTION (ref. Fig. I-17).

IIa WITH TRACKING INACCURACY PREDICTION AND TIGHT-LOOP STABILIZATION OF THE RADAR ANTENNA (ref. Fig. II-14).

IIb WITH TRACKING INACCURACY PREDICTION, TIGHT-LOOP STABILIZATION OF THE RADAR ANTENNA, AND INTEGRATION IN THE SIGNAL MODIFIER (ref. Figs. II-24 & II-28).

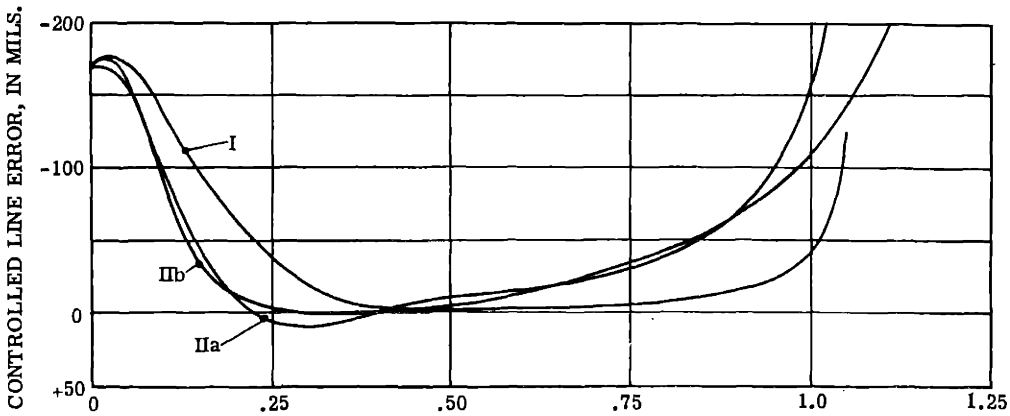

RATIO OF THE DISTANCE TRAVELLED BY THE INTERCEPTOR AIRCRAFT TO THE INITIAL RANGE

OPEN-CHAIN TRACKING SYSTEM.

III WITH CONTROLLED LINE PREDICTION (ref. Fig. III-44).

IV WITH CONTROLLED LINE PREDICTION AND TIGHT-LOOP STABILIZATION OF THE AIRCRAFT (ref. Fig. IV-11).

V WITH TRACKING INACCURACY PREDICTION AND TIGHT-LOOP STABILIZATION OF THE AIRCRAFT (ref. Fig. V-3).

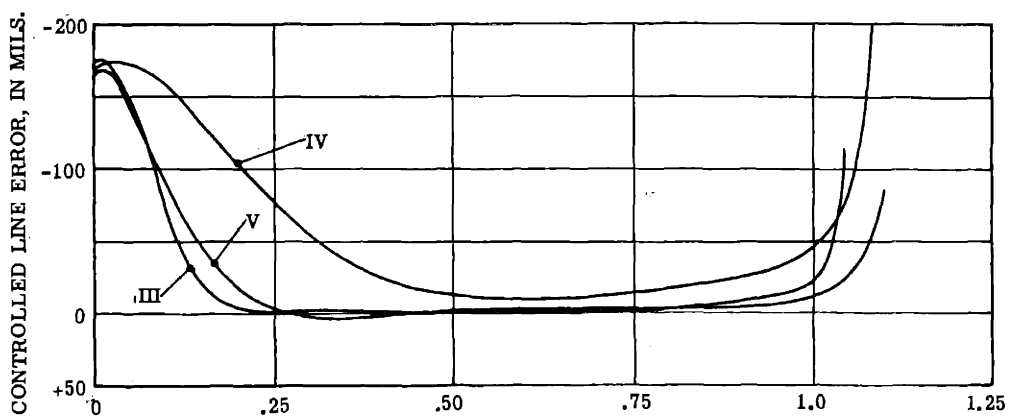

RATIO OF THE DISTANCE TRACKED BY THE INTERCEPTOR AIRCRAFT TO THE INITIAL RANGE

CLOSED-LOOP TRACKING SYSTEM.

INITIAL RANGE = 29,000 FEET
INITIAL TARGET ANGLE = 90°
AIRCRAFT MACH NUMBER = 0.70
TARGET MACH NUMBER = 0.35
PRESSURE ALTITUDE = 20,000 FEET

Fig. 7.–Controlled-line errors of open-chain and closed-loop tracking systems.

$$[(SD)CL]^2 = \frac{1}{\pi}\int_0^{\infty} [(PSD)CL]\, d\omega \qquad (4)$$

In this thesis the power spectral density is expressed in mils^2 per cps, the angular frequency, ω, in radians per second, and the standard deviation of the controlled-line displacement in mils.

The power spectral density of the controlled-line displacement for tracking system IIb is shown in Fig. II-34. The system parameters for this system have essentially the same values as used in the determination of the controlled-line curve of Fig. 8 at a target range of 18,000 feet. At this range the prediction computer has a sensitivity of 13.85 seconds.

The standard deviation of the controlled-line displacement caused by gust disturbances is $\sqrt{9.6}$, or 3.1 mils, and the standard deviation resulting from radar interference is 4.9 mils. In order to evaluate the standard deviation resulting from radar interference, use must also be made of Fig. I-1 in Appendix I, which gives the power spectral density of the radar interference at zero frequency, $[(PSD)q_{RI}]_{[\omega = 0]} S^2_{TS[q_{RI},TL]}$. Fig. I-1 shows that, at a range of 18,000 feet, $[(PSD)q_{RI}]_{[\omega = 0]} S^2_{TS[q_{RI},TL]}$ equals 2 mils^2/cps.

Values of the power spectral densities for tracking systems III and V are included in Fig. III-56 and V-26 for a prediction sensitivity of 13.85 seconds. Integration of the power spectral densities of these figures permits the standard deviation of the controlled-line displacement resulting from gust and radar interference to be evaluated. Values of the standard deviation of the controlled line for systems III and V, as well as for tracking system IIb, are summarized in Table 1.

TABLE 1

Standard Deviation of the Controlled-line Displacement Resulting from Gust and Radar Interference for Tracking Systems IIb, III, and V at a range of 18,000 feet

	Gust Interference (mils)	Radar Interference (mils)
Tracking System IIb	3.1	4.9
Tracking System III	2.3	4.3
Tracking System V	3.2	4.6

— — — OPEN-CHAIN TRACKING SYSTEM WITH TRACKING INACCURACY PREDICTION, TIGHT LOOP STABILIZATION OF THE RADAR ANTENNA, AND INTEGRATION IN THE SIGNAL MODIFIER (REF. FIGS. II-24 AND II-28)

—·— CLOSED-LOOP TRACKING SYSTEM WITH CONTROLLED LINE PREDICTION (REF. FIG. III-44)

——— CLOSED-LOOP TRACKING SYSTEM WITH TRACKING INACCURACY PREDICTION AND TIGHT LOOP STABILIZATION OF THE AIRCRAFT (REF. FIG. V-3)

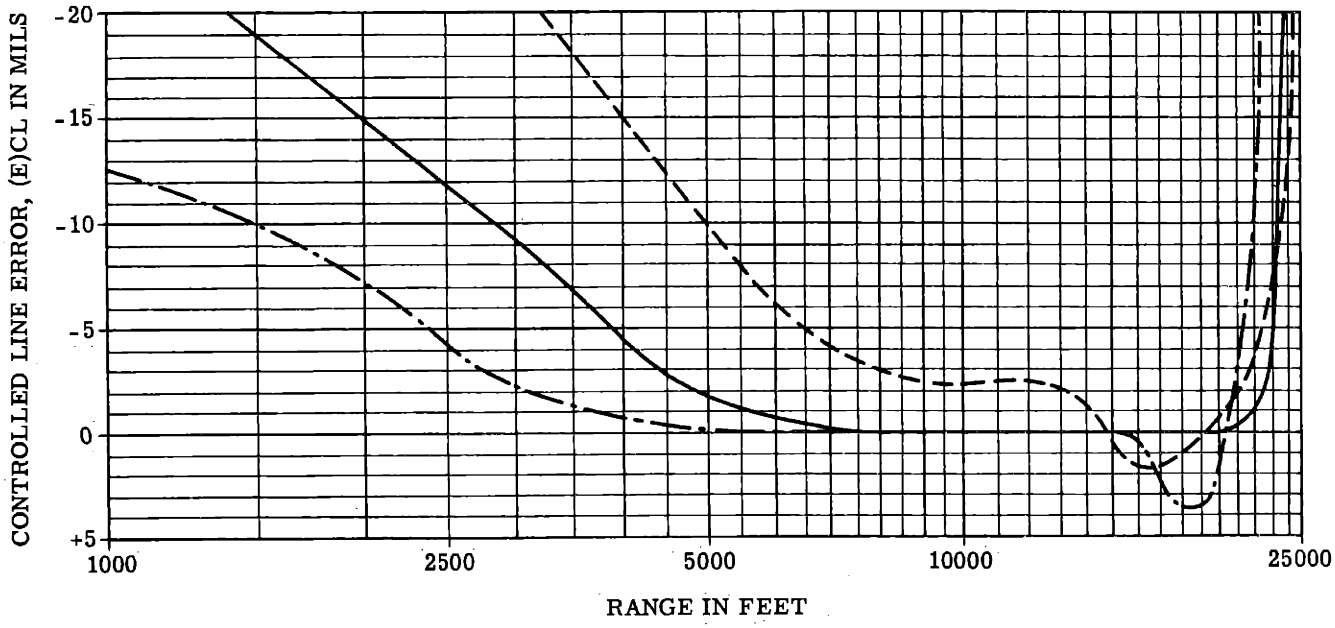

INITIAL RANGE = 29,000 FEET; AIRCRAFT MACH NUMBER = 0.70

INITIAL TARGET ANGLE = 90°; TARGET MACH NUMBER = 0.35

PRESSURE ALTITUDE = 20,000 FEET

Fig. 8.—Aiming errors of several tracking systems for interceptor aircraft as a function of range.

The results of Table 1 indicate that tracking systems IIb, III, and V have approximately the same standard deviation of the controlled-line displacement when the characteristic parameters of these systems are adjusted in such a manner that the controlled-line error is minimized. It is conceivable that a tracking system can be designed which considerably reduces the effect of gusts. The effect of radar interference can be minimized by fundamental improvements in radar design; for example, by using monopulse and by reducing the ratio of controlled-line displacement to line-of-sight displacement. In order to obtain an appreciable reduction in this ratio, the stability number must be increased by a large factor. Such an increase makes it impossible to fly lead-pursuit courses without incurring an excessive controlled-line error.

Hit Probability Comparison

The results of the analysis can be used to determine the hit probability for either gunfire or rocketfire. For example, when guns are fired at 3000 feet against a 15-foot circular target, the angle subtended by the target is 5 mils. At this range tracking system III has a controlled-line error of 2.2 mils, as seen from Fig. 8; a standard deviation of 2.3 mils resulting from gust interference; and a standard deviation of 3.9 mils resulting from radar interference. Then, with a standard deviation of the bullet pattern of 1.5 mils with respect to the interceptor aircraft[33], the standard deviation of the impact pattern becomes

$$[(SD)IP] = \sqrt{[(SD)CL]^2_{[q_{in} = W_G]} + [(SD)CL]^2_{[q_{in} = q_{RI}]} + [(SD)BP]^2}$$

$$= \sqrt{(2.3)^2 + (3.9)^2 + (1.5)^2}$$

$$= 4.8 \text{ mils}$$

In this example the ratio of the controlled-line error to the target radius is 0.44, and the ratio of the standard deviation of the impact pattern to the target radius is 0.96, giving a hit probability (Fig. 5) of 37 percent. Consequently, 54 rounds of ammunition must be fired to ensure 20 hits in the vulnerable area of the target. The hit probability for system V is 12 percent, and for system IIb it is 0.6 percent, against the same target at 3000 feet.

When 5-inch rockets with proximity fuzes are fired, the target may be destroyed even though the rocket impact point falls outside the vulnerable area of the target. For this discussion the reasonable assumption is made that the fuze and warhead have effective lethality at 15 feet. In this case the target of the previous example has an effective radius of 30 feet. Then, at a range of 6000 feet, the angle subtended by the target radius is 5 mils. Allowing for a rocket dispersion of 5 mils with respect to the interceptor aircraft,the ratio of the standard deviation of the impact pattern to the target radius proved to be 1.23 for tracking system III. The controlled-line error for system III is negligibly small and, as seen from Fig. 5, the hit probability is 28 percent. Hence, 11 rockets must be fired to ensure 3 hits on the target. Allowing for one failure due to faulty fuzing, it is felt that this result is comparable to 20 direct hits with 0.50 cal ammunition.

On the same basis as for system III, the hit probability of tracking system V is 24 percent and the hit probability of tracking system IIb is 15 percent. Consequently, 13 and 20 rockets must be fired in order to ensure three hits with system V and IIb respectively. However, with these same systems, 170 and 3300 rounds of 0.50 cal ammunition must be fired at 3000 feet in order to obtain 20 hits.

It can be seen from these examples that there is an advantage in firing at 6000 feet rather than at 3000 feet, since the controlled-line errors are considerably less at the longer range. However, to be effective at ranges greater than one mile, it is felt that proximity fuzes are required, in order to ease the aiming tolerance.

Possibility for Further Reducing the Controlled-Line Error

The controlled-line error can undoubtedly be further reduced by refinements to the tracking systems analyzed in this thesis. Integration in the signal modifier of system III, and in the tracking inaccuracy detector of system V, will probably reduce the error by a factor of two. Other methods for reducing the error center around the tactics. In a tail attack the angular velocities are low, but the danger to the interceptor is increased. In a straight-line approach, the controlled line angular velocity is nearly zero and the resulting controlled-line error is negligible. Further study is required to determine whether the hit probability can be increased by a more thorough and understanding application of tactics.

CONCLUSIONS

1. The controlled-line errors of closed-loop tracking systems are 1/2 to 1/3 the errors that occur with open-chain tracking systems. Furthermore, the controlled-line error of a closed-loop tracking system probably can be reduced by a factor of 50 percent by including integration in the tracking inaccuracy detector.
2. The standard deviation of the controlled-line displacement resulting from gust and radar interference is comparable for tracking systems with characteristics adjusted to minimize the controlled-line error.
3. The standard deviation of the controlled-line displacement resulting from gust interference is of the same order of magnitude as the standard deviation resulting from radar interference.
4. Cross-roll corrections must be applied to the prediction computers of both open-chain and closed-loop tracking systems.
5. With an open-chain system which computes with respect to the antenna axes of Fig. D-5: a coordinate transformation is required between the prediction computer and the controls of the interceptor aircraft, which operate about aircraft body axes.
6. The closed-loop tracking system with tracking inaccuracy prediction has the shortest solution time, and is least sensitive to the direction of attack (head-on, beam, or tail). In addition, this system offers the possibility of aircraft stabilization during all phases of the interceptor operation.
7. The closed-loop tracking system with controlled-line prediction has the lowest values of controlled-line errors on tail and beam attacks.
8. It appears that rockets can be fired effectively at twice the range for effective gunfire, provided the rockets have reliable warheads and proximity fuzes.
9. When long-range, air-to-air guided missiles become available, problems associated with tracking by interceptor aircraft will be considerably reduced.
10. For interceptor aircraft that are to be used for head-on and beam attacks, the stability number must be in the vicinity of 0.3.
11. Tracking must commence when the interceptor is at least 15 seconds away from the target. This time is nearly equal to the ratio of range to rate of change of range.

12. The controlled-line error appears to be the most important consideration in a comparison of tracking systems with idealized components. With actual systems, in which discrepancies are introduced by such effects as gearing, hysteresis and flexibility, the error may not be the dominant factor.

RECOMMENDATIONS FOR FUTURE INVESTIGATIONS

1. An analysis of the lateral control of interceptor aircraft should be carried out in a manner similar to the longitudinal investigation in this thesis.
2. The hit probability should be evaluated for gunfire and rocketfire when used in conjunction with straight-line approach courses.
3. In the analysis of this thesis, no angle-of-attack information was introduced into the prediction computer for compensation of the jump angle since this correction is not required in "fixed" gunfire when the projectile velocity is nearly constant. However, in rocketfire the jump angle is significant and must be accounted for by a correction proportional to the angle of attack. Solutions should be obtained using the REAC with the angle-of-attack indication introduced (1) as a torque on the computer shaft, and (2) as an addition to the voltage output from the signal generator on the prediction computer. The second method is simpler to mechanize, but may introduce instability.
4. "Second-order Computers" evaluate changes in the target direction during the time of flight of the projectile, and require an angular acceleration input. A tracking system with a "Second-order Computer" should be investigated from the standpoint of hit probability.
5. In the prediction computer analysis of Appendix D, the prediction angle is assumed to be small. The effect of large angles on the accuracy of closed-loop and open-chain tracking systems should be considered.
6. The measurements of atmospheric turbulence by Clementson should be extended, using higher-speed aircraft. It is recommended that pitch angle, rather than pitch rate, be recorded. Measurements should be made for diving courses as well as for level flight, for application to ground and sea attack.
7. It is felt that more radar interference data are required and that the effort should be made by all agencies working on this problem to present their results in a general form applicable to all types of tracking systems.

CHAPTER I

OPEN-CHAIN TRACKING SYSTEM WITH TRACKING LINE PREDICTION

Figure I-1 is a functional diagram of the open-chain tracking system with tracking line prediction. The responses of this tracking system, in the absence of gust and radar interference, are contained in Fig. 1-2 through I-21. These responses are obtained primarily for tail attacks. However, Fig. I-17 and I-20 give the responses for a 90-degree beam attack, and Fig. I-18 and I-21 give the responses for a 150-degree nose attack. The effects of gust and radar interference are indicated in Fig. I-22 through I-28. These results are based on the gust data of Appendix H and the radar interference data of Appendix I.

The results contained in this chapter were obtained by using Eq. B-8 and B-9 to represent the performance of the aircraft, and supplemented with the following differential equations, which are derived in Appendices C, D, and E:

For the tracking radar —

$$(CT)_R \dot{P}_R + P_R = LS - CL \qquad \text{I-1}$$

For the prediction computer —

$$S_{p(W,P)}[SN][-S_{(sg)(V,P)}]\dot{V}_{PC} + [-S_{(sg)(V,P)}]V_{PC} = S_{p(W,P)} W_{TL} \qquad \text{I-2}$$

where

$$S_{p(W,P)} = (PSR)\frac{R}{V_{p\,(av)} - V_A} \qquad \text{I-3}$$

and

$$W_{TL} = W_{CL} - \dot{P}_R \qquad \text{I-4}$$

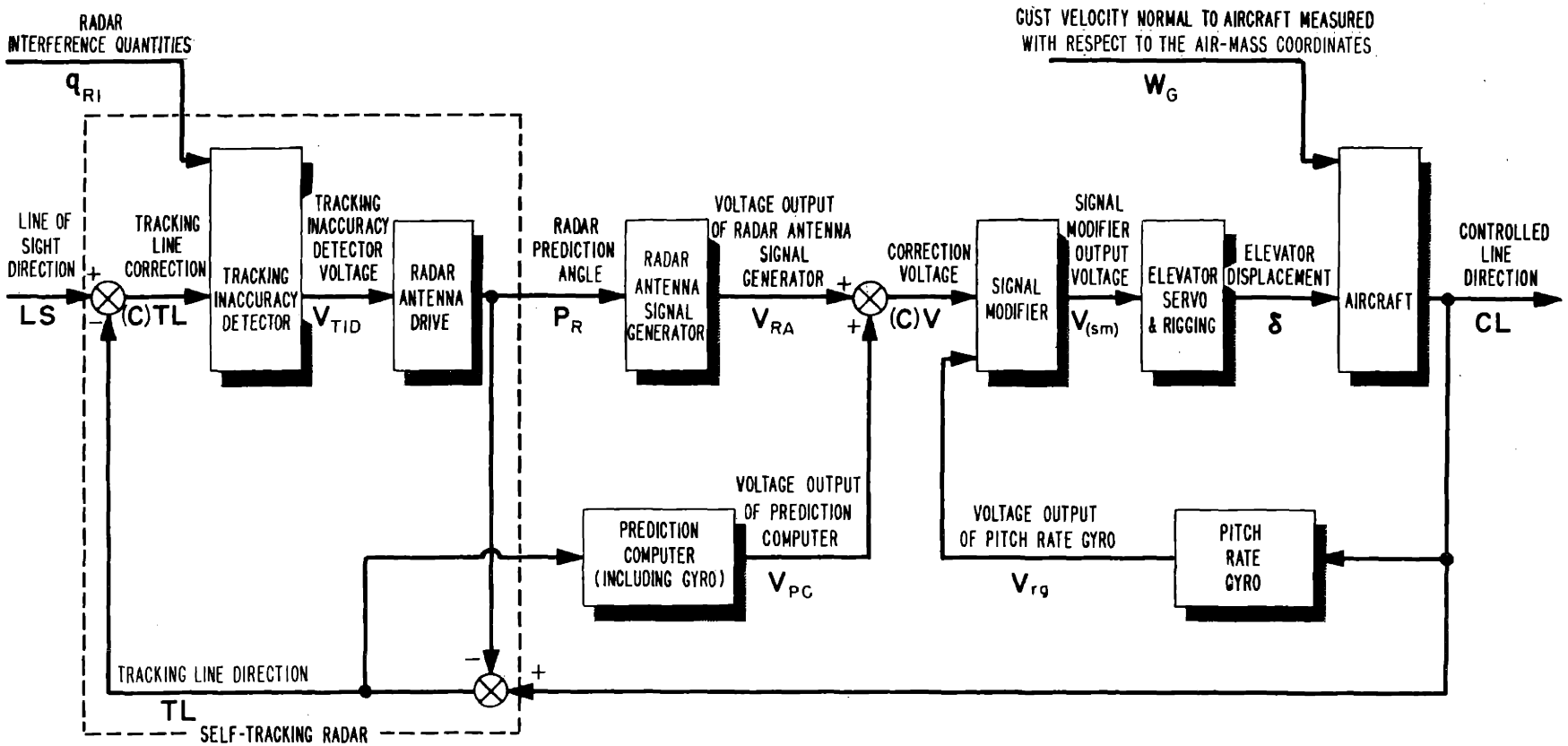

FIG I-1 FUNCTIONAL DIAGRAM OF OPEN-CHAIN TRACKING SYSTEM WITH TRACKING LINE PREDICTION

For the signal modifier elevator servo and rigging –

$$\delta = [S_{(sg)(P,V)}S_{(sm)p}S_{(s,r)}][P_R + S_{(sg)(V,P)}V_{PC}] + [S_{rg}S_{(sm)\theta}S_{(s,r)}]W_{CL} \qquad \text{I-5}$$

The radar prediction angle, P_R, is measured from the radar tracking line to the controlled line. The radar tracking line, $(TL)_R$, is fixed to the radar antenna and is along the target line of sight, LS, when the radar is correctly tracking the target. When the tracking line is not along the line of sight, a correction must be applied to the radar prediction angle. This action is accomplished by means of the tracking inaccuracy detector and the radar antenna drive. The tracking inaccuracy detector senses the magnitude and the direction of the desired correction and provides a proportional voltage signal. This signal is the input to the radar antenna drive. It is assumed in Eq. I-1 that the radar antenna is driven at a rate proportional to the input voltage.

The prediction computer includes a gyro that detects the angular velocity of the tracking line, W_{TL}. The voltage output from the prediction computer, V_{PC}, is proportional to the angular velocity of the tracking line. Although zero solution time is the goal of all tracking systems, damping of the computer output is always required. This smoothing action is accomplished by the action of a viscous damper in a mechanical computer. The voltage output from the prediction computer is compared with the voltage from a signal generator on the radar antenna. When these two voltages are equal, the aircraft is considered to be on the correct course. However, when they differ, the actual prediction angle as measured by the radar is not equal to the desired prediction angle as established by the prediction computer, and a reorientation of the aircraft is required to reduce the aiming error. Equation I-2 has been written in terms of the desired prediction angle by multiplying the voltage from the prediction computer by the reciprocal of the sensitivity of the radar antenna signal generator, $S_{(sg)(V,P)}$. In this thesis the sensitivities are used to determine sense; that is, they carry an algebraic sign. A positive radar prediction angle must give a negative voltage; consequently, the sensitivity of the signal generator carries a minus sign. For this reason the sensitivity of the signal generator is preceded by a minus sign in Eq. I-2 in order that the quantity $[-S_{(sg)(V,P)}]$ will be positive.

The angular velocity – prediction angle sensitivity, $S_{p(W,P)}$, establishes the magnitude of the prediction angle for a given angular velocity of the tracking line. It is shown in Appendix D that for tracking systems with no smoothing this sensitivity must be proportional to the range, R, divided by the average velocity of the projectile with respect to the interceptor aircraft, $[V_{p\ (av)} - V_A]$. In order to account for dynamic lags introduced by the smoothing, the prediction sensitivity is modified by the prediction sensitivity ratio, PSR, shown in Eq. I-3.

The signal modifier receives the correction voltage, (C)V, as an input as well as a signal from a pitch rate gyro used to increase the stability of the tracking system. The output from the signal modifier may include not only terms proportional to the inputs, but also terms proportional to either the derivatives or the integrals of the input quantities. This output voltage is applied to the elevator servo that actuates the controlled servos through a rigging system, which includes pulleys and cables. In this thesis it is assumed that the lags in the servo and rigging are negligible and hence the ratio of the elevator displacement to the output voltage of the signal modifier is equal to the sensitivity, $S_{(s,r)}$. This sensitivity accounts for the performance of the servo and rigging in combination, and includes the effect of restraining hinge moments on the elevator. Equation I-5 shows that in the analysis of this tracking system only proportional signals are generated by the signal modifier.

The performance equations of the interceptor aircraft are considered in Appendix B. As noted earlier, these aircraft performance equations, along with Eq. I-1, I-2, I-3, I-4 and I-5, are used to obtain the results presented in this chapter. In order to evaluate the tracking line correction for different tactical situations, the target interceptor kinematic equations of Appendix C are also included. These kinematic equations include expressions for the angular velocity of the line of sight, the target range, and the correct direction of the controlled line. The results presented in Fig. I-2 through I-21 are obtained by assuming an average projectile velocity three times the velocity of the interceptor aircraft, or 2180 feet per second. This projectile velocity is low for gunfire and greater than that experienced with five-inch rockets. A low value for the projectile velocity was purposely selected inasmuch as larger prediction angles are required, leading to a more difficult situation for the tracking system from a

stability standpoint. A projectile jump factor of one-third is used for all solutions. This jump factor is correct for gunfire and is approximately one half that required in rocketfire. Time did not permit an investigation of the effect of a larger projectile jump factor.

The results of Fig. I-2 through I-21 assume a radar characteristic time of .15 second and a signal modifier characteristic time of zero. The values of the forward gain, $[S_{(sg)(P,V)}S_{(sm)p}S_{(s,r)}]$, are equal to .06, .09, and .12. The pitch rate stabilization gain, $[S_{rg}S_{(sm)\dot{\theta}}S_{(s,r)}]$, is either 0 or .05 second. For the prediction computer, stability numbers of .15, .25, and .50 are used, and the prediction sensitivity ratio, PSR, is either 1.0 or 1.3. Examination of Fig. I-2, I-3, and I-4 indicates that an increase in stability number increases the solution time in direct proportion. The solution time is the time required by the system to reduce the controlled-line error to five percent of its initial value. The forced error in the controlled line that follows after the solution period is nearly independent of the stability number. It can be seen from Fig. I-5 that the forced error can be reduced by increasing the forward gain, or ratio of elevator displacement to correction voltage. When this gain is increased to .12, as indicated in Fig. I-8, an underdamped oscillation appears which indicates close proximity to instability. The effect of this oscillatory mode can be reduced by increasing the stability number, as shown by Fig. I-9 and I-10. The effect of the oscillatory mode can also be reduced by incorporating pitch rate feedback in the control system, as can be seen by a comparison of Fig. I-8 and I-14. However, no combination of system parameters yields a satisfactory system inasmuch as, even for tail attacks, the controlled-line error is excessively large at most ranges. Integration in the signal modifier would improve this tracking system, but probably not a sufficient amount.

The standard deviation of the controlled line can be determined for certain system parameters from Fig. I-22 through I-28. In each figure, the power spectral density of the controlled line is plotted as a function of frequency, for both gust and radar interference. The integral of the power spectral density of the controlled line is proportional to the square of the standard deviation, as discussed in Appendix F. Values for the standard deviation are tabulated in each figure. For example, in Fig. I-22 it can be seen that the standard deviation of the controlled line resulting from gust input velocities equals $\sqrt{42.4}$, or 6.5 mils. In order to evaluate the stan-

dard deviation of the controlled line resulting from radar interference, the power spectral density of the radar interference at zero frequency must be known. With this tracking system, a prediction sensitivity of 13.85 seconds is required at a range of 15,500 feet. Reference to Fig. I-1 in Appendix I shows that at this range the power spectral density of the radar interference is 1.5 $mils^2/cps$; consequently, the standard deviation of the controlled line resulting from the radar interference is 4.4 mils.

It can be seen that an increase in stability number decreases the standard deviation of the controlled line. An increase in the forward gain decreases the effect of the gust interference but causes an increase in the effect of radar interference. At short ranges, as for example when the prediction sensitivity is equal to 2.77 seconds, the standard deviation of the controlled line is 5.0 mils and the standard deviation resulting from radar interference is 1.0 mil, as shown in Fig. I-28. Although it is desirable to have the standard deviation as low as possible, the decrease must not be obtained at the expense of a large controlled-line error, as is the case with this tracking system.

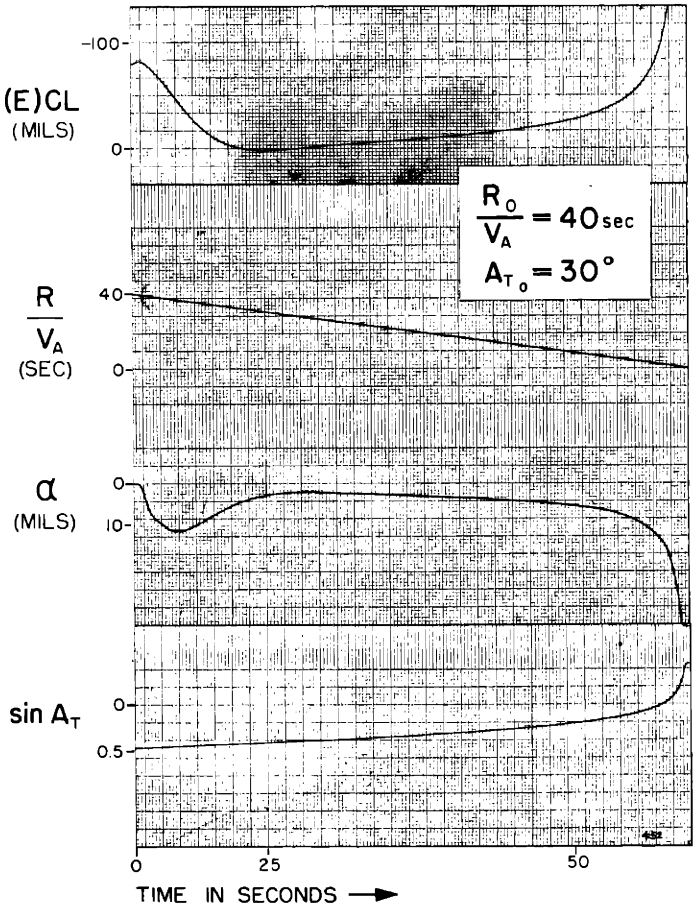

$S_{sg(P,V)} S_{(sm)p} S_{(s,r)} = 0.06$ SN = 0.15

$S_{sg(P,V)} S_{(sm)i} S_{(s,r)} = 0$ $(CT)_R = 0.15$ sec

$S_{rg} S_{(sm)\dot{\theta}} S_{(s,r)} = 0$ PSR = 1.3

$(CT)_{(sm)} = 0$ sec

AIRCRAFT CHARACTERISTICS OF APP B

FIG I - 2

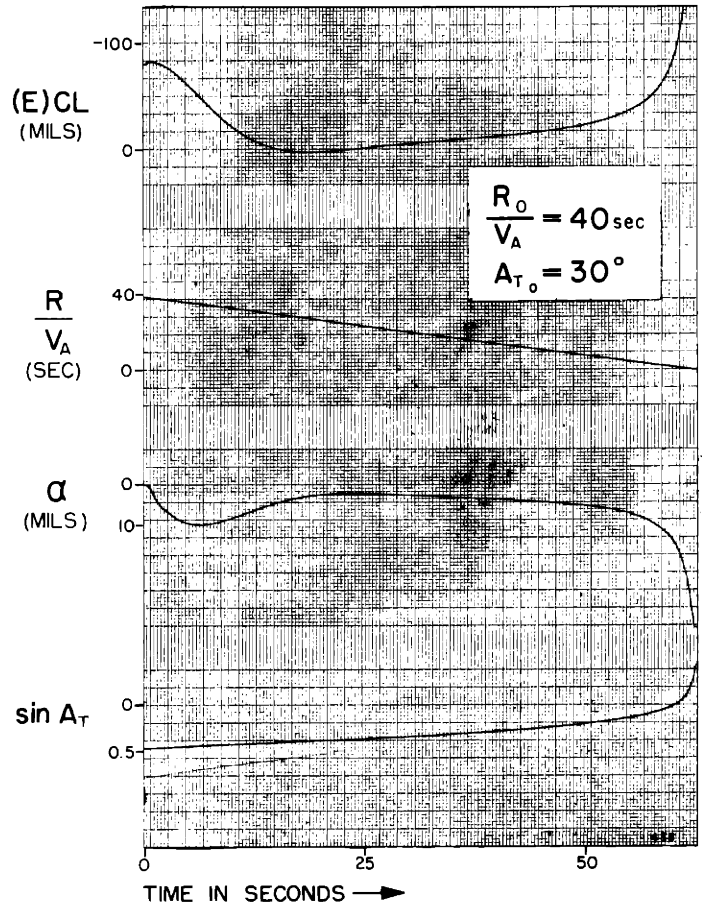

$S_{sg(P,V)} S_{(sm)p} S_{(s,r)} = 0.06$ SN = 0.25

$S_{sg(P,V)} S_{(sm)i} S_{(s,r)} = 0$ $(CT)_R = 0.15$ sec

$S_{rg} S_{(sm)\dot{\theta}} S_{(s,r)} = 0$ PSR = 1.3

$(CT)_{(sm)} = 0$ sec

AIRCRAFT CHARACTERISTICS OF APP B

FIG I-3

RESPONSE OF OPEN-CHAIN TRACKING SYSTEM WITH TRACKING LINE PREDICTION IN THE ABSENCE OF GUST AND RADAR INTERFERENCE

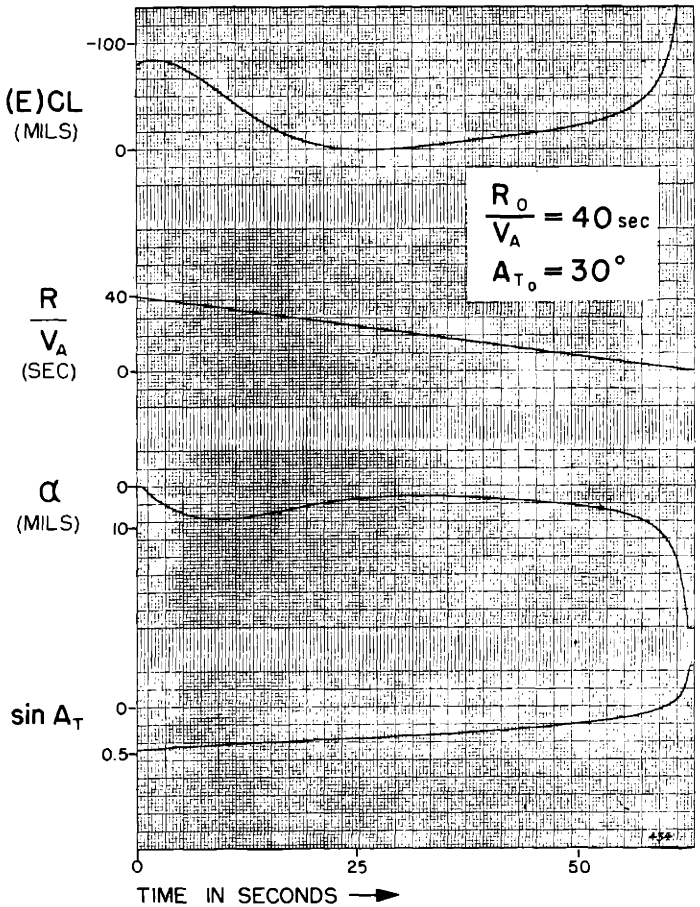

$S_{sg(P,V)} S_{(sm)p} S_{(s,r)} = 0.06$ SN = 0.50

$S_{sg(P,V)} S_{(sm)i} S_{(s,r)} = 0$ $(CT)_R = 0.15$ sec

$S_{rg} S_{(sm)\dot{\theta}} S_{(s,r)} = 0$ PSR = 1.3

$(CT)_{(sm)} = 0$ sec

AIRCRAFT CHARACTERISTICS OF APP B

FIG I - 4

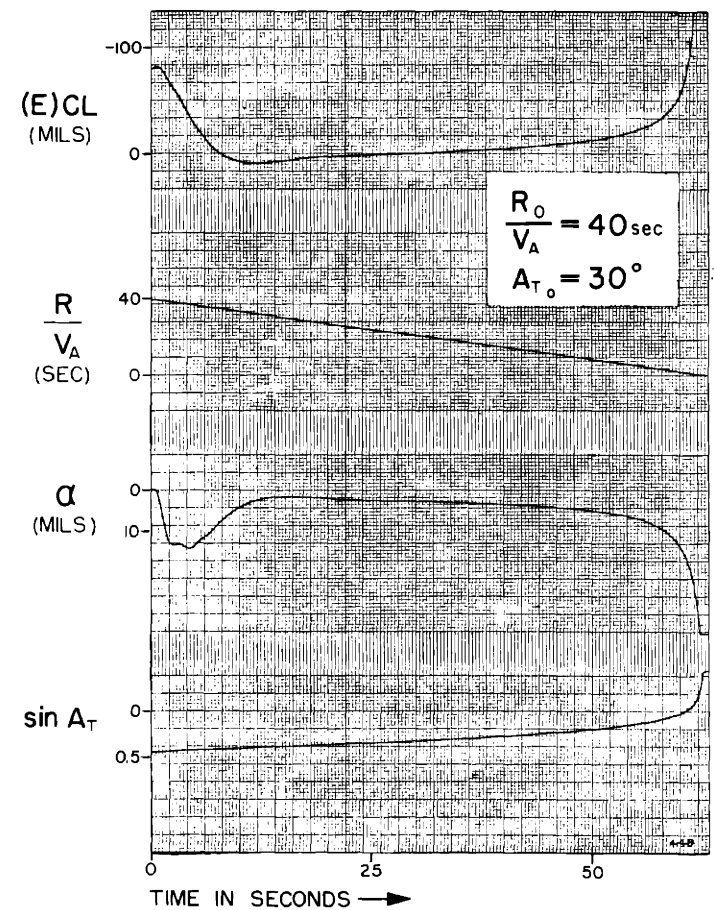

$S_{sg(P,V)} S_{(sm)p} S_{(s,r)} = 0.09$ SN = 0.15

$S_{sg(P,V)} S_{(sm)i} S_{(s,r)} = 0$ $(CT)_R = 0.15$ sec

$S_{rg} S_{(sm)\dot{\theta}} S_{(s,r)} = 0$ PSR = 1.3

$(CT)_{(sm)} = 0$ sec

AIRCRAFT CHARACTERISTICS OF APP B

FIG I - 5

RESPONSE OF OPEN-CHAIN TRACKING SYSTEM WITH TRACKING LINE PREDICTION IN THE ABSENCE OF GUST AND RADAR INTERFERENCE

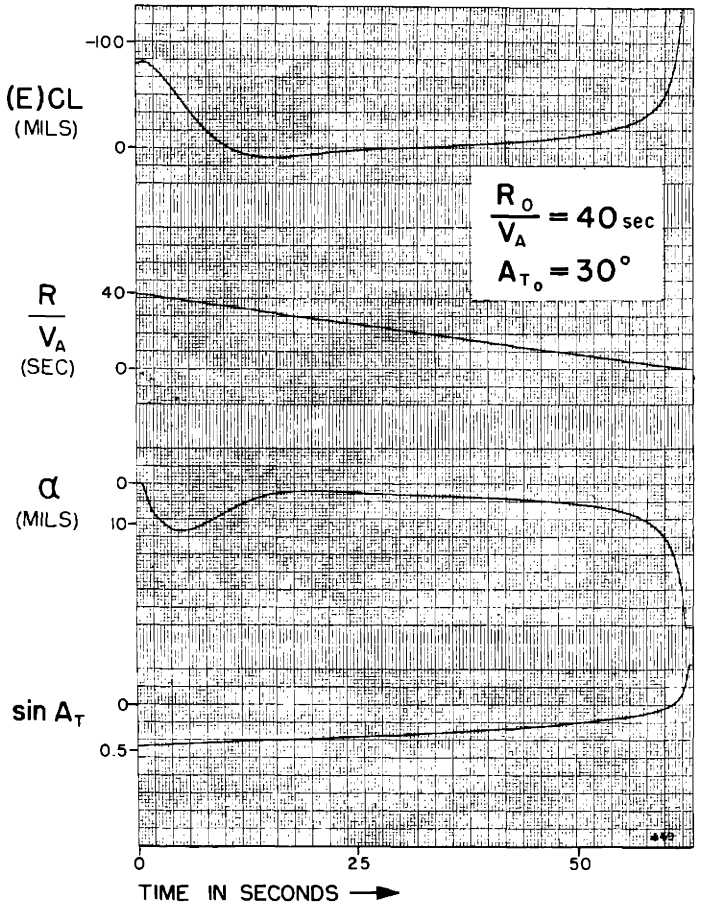

$S_{sg(P,V)} S_{(sm)p} S_{(s,r)} = 0.09$ SN = 0.25

$S_{sg(P,V)} S_{(sm)i} S_{(s,r)} = 0$ $(CT)_R = 0.15$ sec

$S_{rg} S_{(sm)\dot{\theta}} S_{(s,r)} = 0$ PSR = 1.3

$(CT)_{(sm)} = 0$ sec

AIRCRAFT CHARACTERISTICS OF APP B

FIG I-6

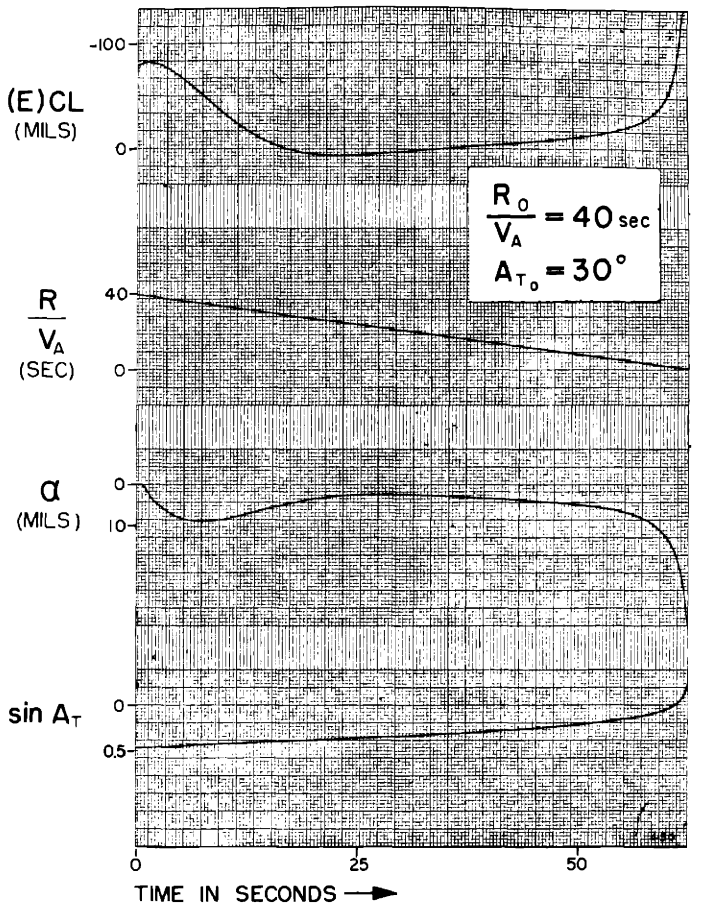

$S_{sg(P,V)} S_{(sm)p} S_{(s,r)} = 0.09$ SN = 0.50

$S_{sg(P,V)} S_{(sm)i} S_{(s,r)} = 0$ $(CT)_R = 0.15$ sec

$S_{rg} S_{(sm)\dot{\theta}} S_{(s,r)} = 0$ PSR = 1.3

$(CT)_{(sm)} = 0$ sec

AIRCRAFT CHARACTERISTICS OF APP B

FIG I-7

RESPONSE OF OPEN-CHAIN TRACKING SYSTEM WITH TRACKING LINE PREDICTION IN THE ABSENCE OF GUST AND RADAR INTERFERENCE

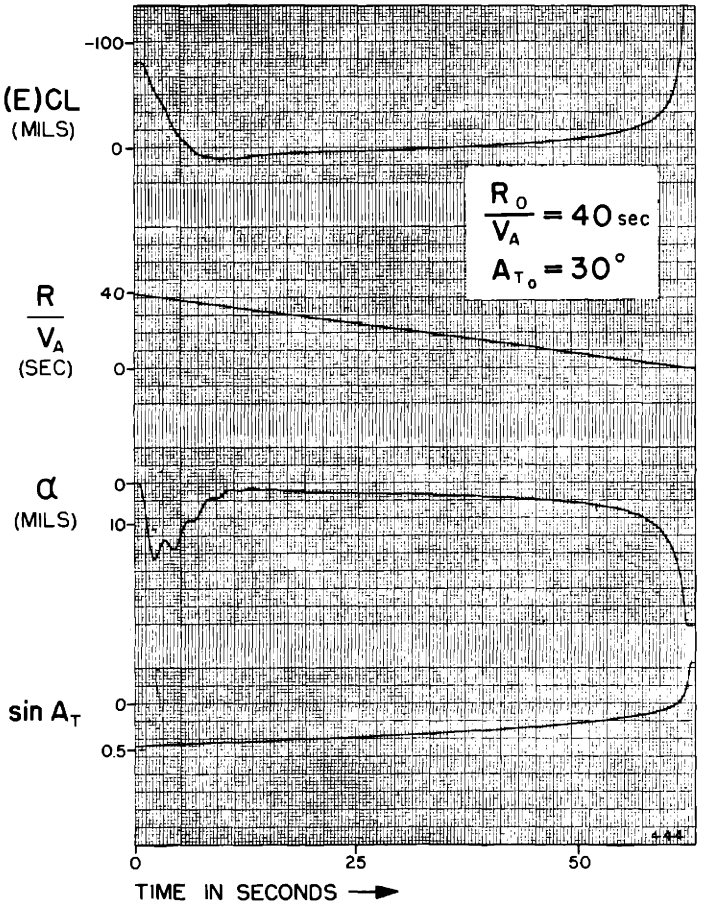

$S_{sg(P,V)} S_{(sm)p} S_{(s,r)} = 0.12$ SN = 0.15

$S_{sg(P,V)} S_{(sm)i} S_{(s,r)} = 0$ $(CT)_R = 0.15$ sec

$S_{rg} S_{(sm)\dot{\theta}} S_{(s,r)} = 0$ PSR = 1.3

$(CT)_{(sm)} = 0$ sec

AIRCRAFT CHARACTERISTICS OF APP B

FIG I - 8

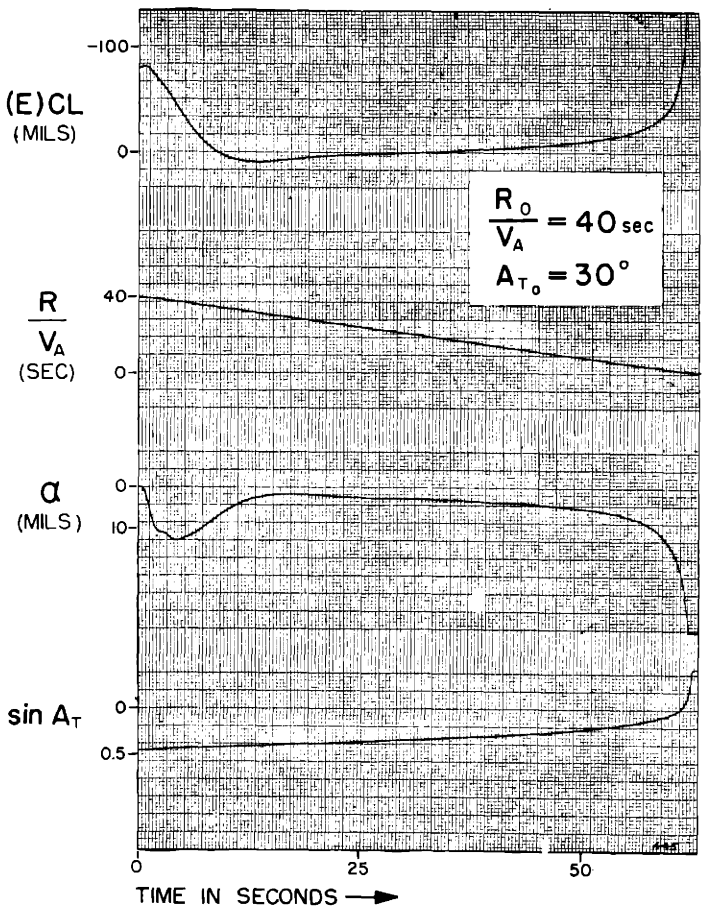

$S_{sg(P,V)} S_{(sm)p} S_{(s,r)} = 0.12$ SN = 0.25

$S_{sg(P,V)} S_{(sm)i} S_{(s,r)} = 0$ $(CT)_R = 0.15$ sec

$S_{rg} S_{(sm)\dot{\theta}} S_{(s,r)} = 0$ PSR = 1.3

$(CT)_{(sm)} = 0$ sec

AIRCRAFT CHARACTERISTICS OF APP B

FIG I - 9

RESPONSE OF OPEN-CHAIN TRACKING SYSTEM WITH TRACKING LINE PREDICTION IN THE ABSENCE OF GUST AND RADAR INTERFERENCE

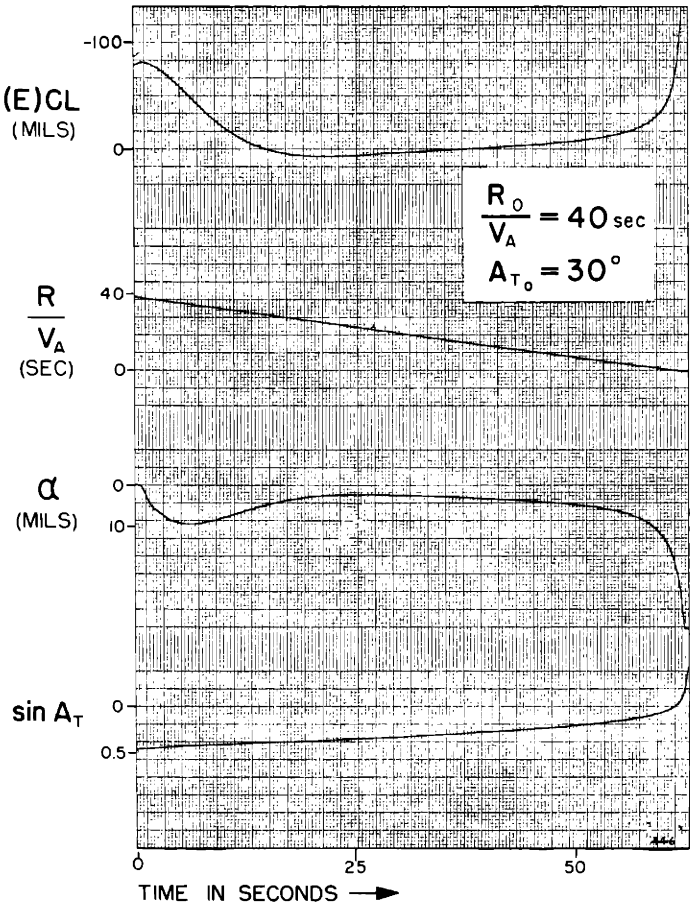

$S_{sg(P,V)} S_{(sm)p} S_{(s,r)} = 0.12$ SN = 0.50

$S_{sg(P,V)} S_{(sm)i} S_{(s,r)} = 0$ $(CT)_R = 0.15$ sec

$S_{rg} S_{(sm)\dot{\theta}} S_{(s,r)} = 0$ PSR = 1.3

$(CT)_{(sm)} = 0$ sec

AIRCRAFT CHARACTERISTICS OF APP B

FIG I-10

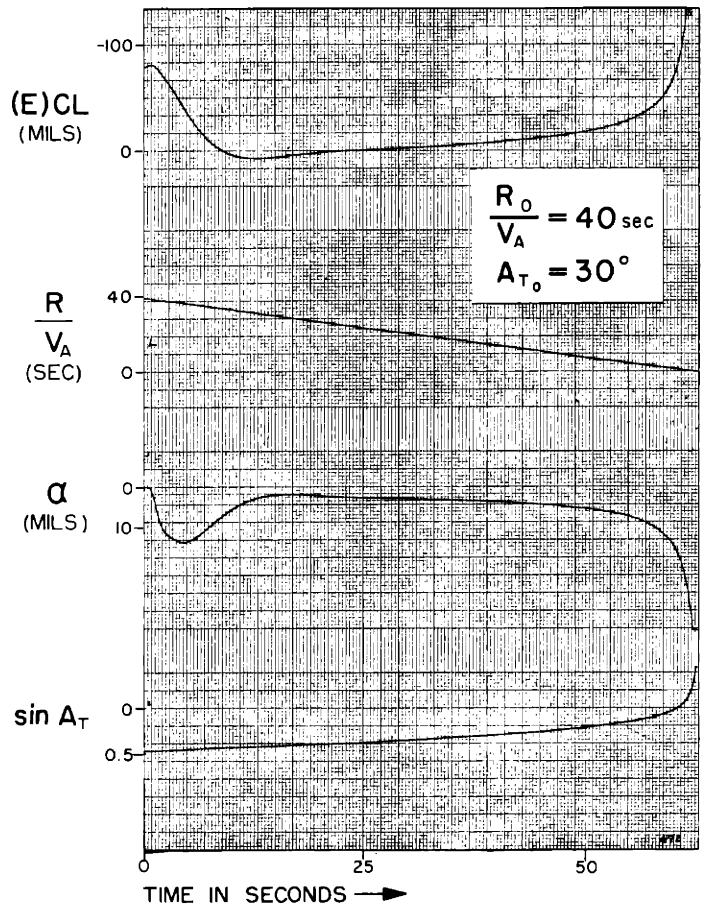

$S_{sg(P,V)} S_{(sm)p} S_{(s,r)} = 0.09$ SN = 0.15

$S_{sg(P,V)} S_{(sm)i} S_{(s,r)} = 0$ $(CT)_R = 0.15$ sec

$S_{rg} S_{(sm)\dot{\theta}} S_{(s,r)} = 0.05$ PSR = 1.3

$(CT)_{(sm)} = 0$ sec

AIRCRAFT CHARACTERISTICS OF APP B

FIG I-11

RESPONSE OF OPEN-CHAIN TRACKING SYSTEM WITH TRACKING LINE PREDICTION IN THE ABSENCE OF GUST AND RADAR INTERFERENCE

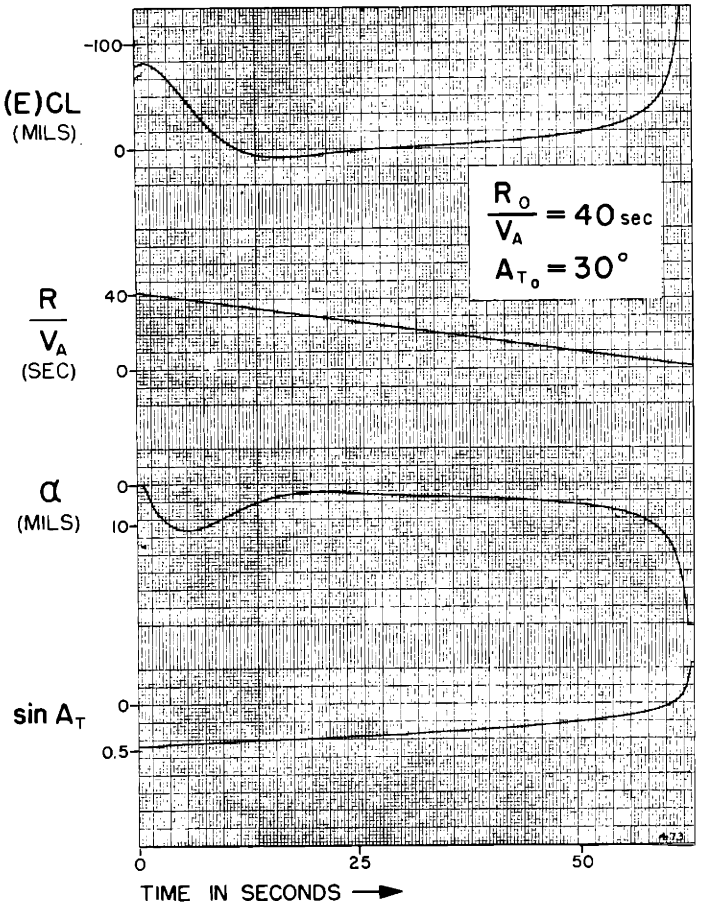

$S_{sg(P,V)} S_{(sm)p} S_{(s,r)} = 0.09$ SN = 0.25

$S_{sg(P,V)} S_{(sm)i} S_{(s,r)} = 0$ $(CT)_R = 0.15$ sec

$S_{rg} S_{(sm)\dot{\theta}} S_{(s,r)} = 0.05$ PSR = 1.3

$(CT)_{(sm)} = 0$ sec

AIRCRAFT CHARACTERISTICS OF APP B

FIG I-12

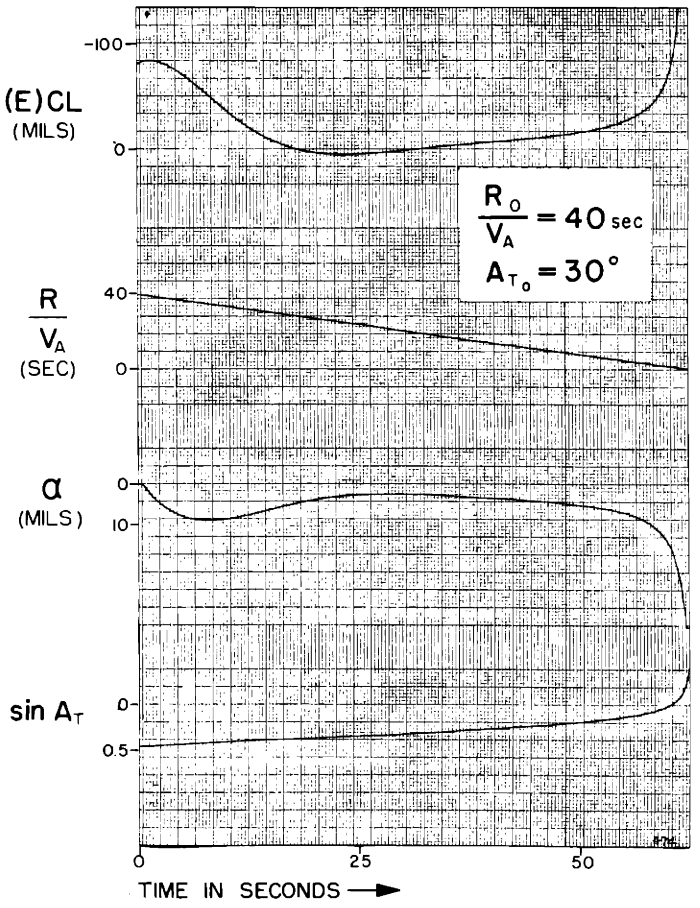

$S_{sg(P,V)} S_{(sm)p} S_{(s,r)} = 0.09$ SN = 0.50

$S_{sg(P,V)} S_{(sm)i} S_{(s,r)} = 0$ $(CT)_R = 0.15$ sec

$S_{rg} S_{(sm)\dot{\theta}} S_{(s,r)} = 0.05$ PSR = 1.3

$(CT)_{(sm)} = 0$ sec

AIRCRAFT CHARACTERISTICS OF APP B

FIG I-13

RESPONSE OF OPEN-CHAIN TRACKING SYSTEM WITH TRACKING LINE PREDICTION IN THE ABSENCE OF GUST AND RADAR INTERFERENCE

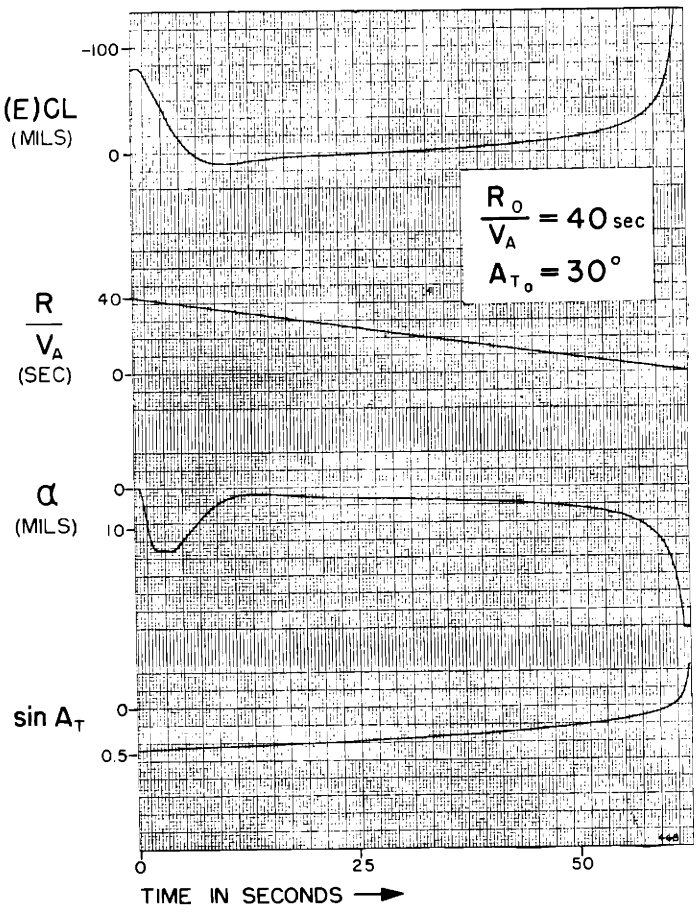

$S_{sg(P,V)} S_{(sm)p} S_{(s,r)} = 0.12$ SN = 0.15

$S_{sg(P,V)} S_{(sm)i} S_{(s,r)} = 0$ $(CT)_R = 0.15$ sec

$S_{rg} S_{(sm)\dot{\theta}} S_{(s,r)} = 0.05$ PSR = 1.3

$(CT)_{(sm)} = 0$ sec

AIRCRAFT CHARACTERISTICS OF APP B

FIG I-14

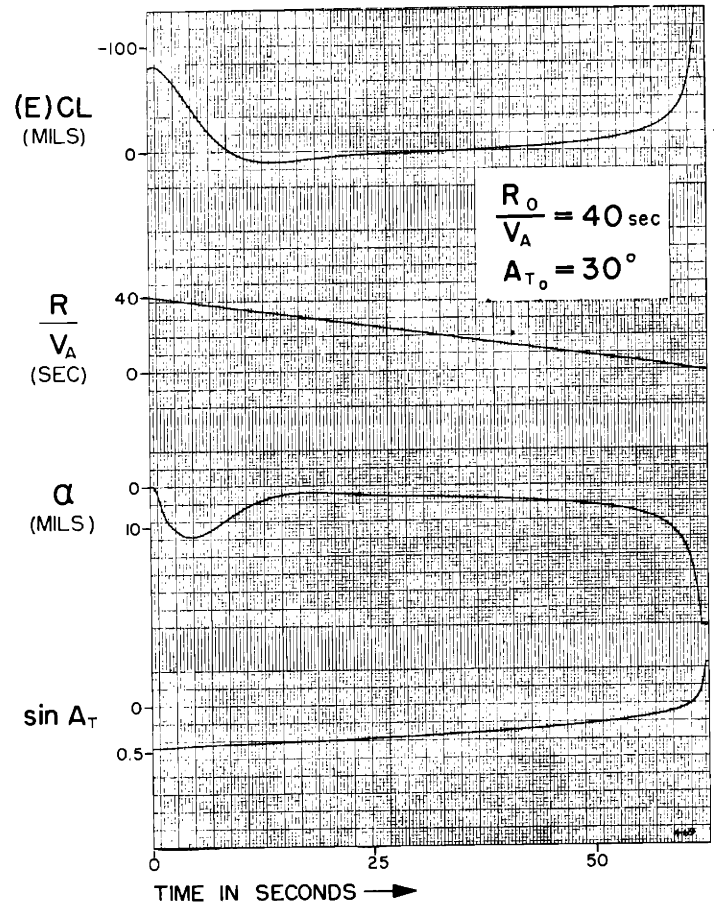

$S_{sg(P,V)} S_{(sm)p} S_{(s,r)} = 0.12$ SN = 0.25

$S_{sg(P,V)} S_{(sm)i} S_{(s,r)} = 0$ $(CT)_R = 0.15$ sec

$S_{rg} S_{(sm)\dot{\theta}} S_{(s,r)} = 0.05$ PSR = 1.3

$(CT)_{(sm)} = 0$ sec

AIRCRAFT CHARACTERISTICS OF APP B

FIG I-15

RESPONSE OF OPEN-CHAIN TRACKING SYSTEM WITH TRACKING LINE PREDICTION IN THE ABSENCE OF GUST AND RADAR INTERFERENCE

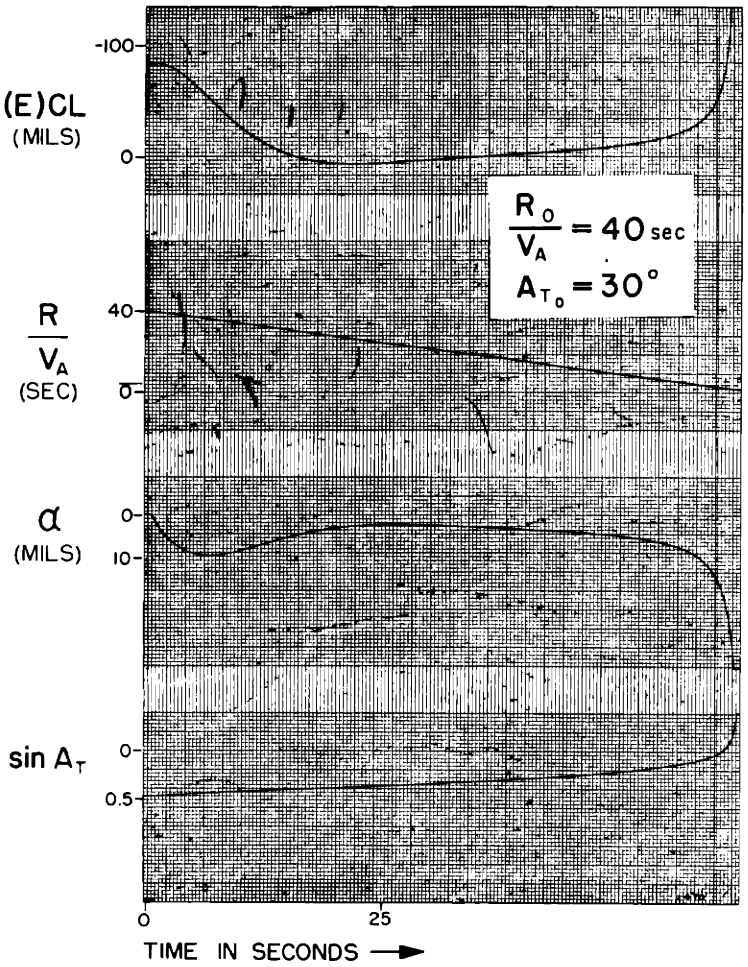

$S_{sg(P,V)} S_{(sm)p} S_{(s,r)} = 0.12$ SN = 0.50

$S_{sg(P,V)} S_{(sm)i} S_{(s,r)} = 0$ $(CT)_R = 0.15$ sec

$S_{rg} S_{(sm)\dot{\theta}} S_{(s,r)} = 0.05$ PSR = 1.3

$(CT)_{(sm)} = 0$ sec

AIRCRAFT CHARACTERISTICS OF APP B

FIG I-16

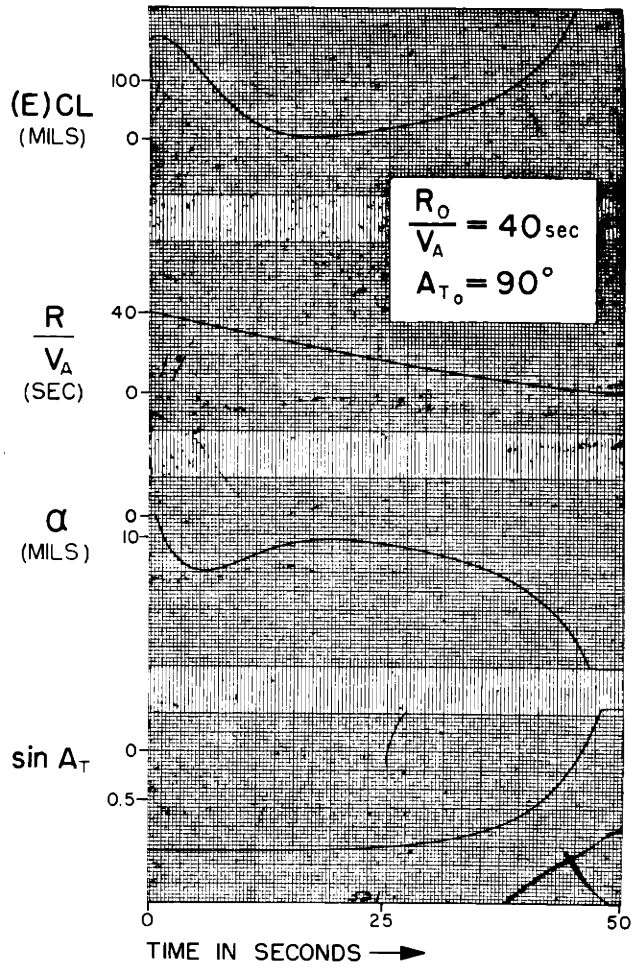

$S_{sg(P,V)} S_{(sm)p} S_{(s,r)} = 0.09$ SN = 0.25

$S_{sg(P,V)} S_{(sm)i} S_{(s,r)} = 0$ $(CT)_R = 0.15$ sec

$S_{rg} S_{(sm)\dot{\theta}} S_{(s,r)} = 0.05$ PSR = 1.3

$(CT)_{(sm)} = 0$ sec

AIRCRAFT CHARACTERISTICS OF APP B

FIG I-17

RESPONSE OF OPEN-CHAIN TRACKING SYSTEM WITH TRACKING LINE PREDICTION IN THE ABSENCE OF GUST AND RADAR INTERFERENCE

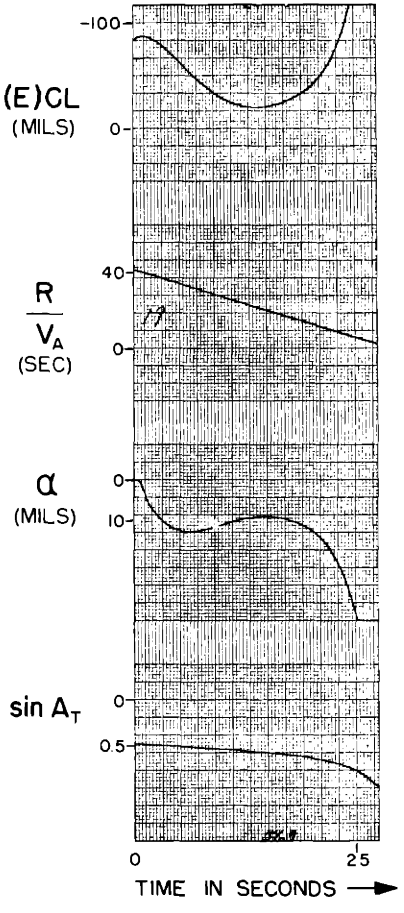

$\frac{R_0}{V_A} = 40$ sec

$A_{T_0} = 150°$

$S_{sg(P,V)} S_{(sm)p} S_{(s,r)} = 0.09$ SN = 0.25

$S_{sg(P,V)} S_{(sm)i} S_{(s,r)} = 0$ $(CT)_R = 0.15$ sec

$S_{rg} S_{(sm)\dot{\theta}} S_{(s,r)} = 0.05$ PSR = 1.3

$(CT)_{(sm)} = 0$ sec

AIRCRAFT CHARACTERISTICS OF APP B

FIG I-18

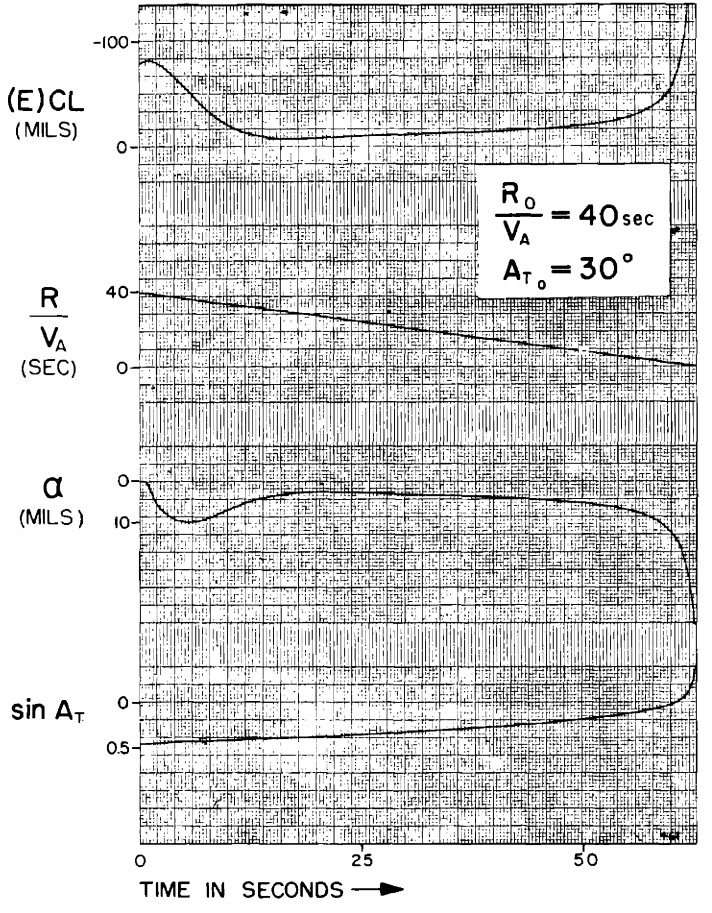

$\frac{R_0}{V_A} = 40$ sec

$A_{T_0} = 30°$

$S_{sg(P,V)} S_{(sm)p} S_{(s,r)} = 0.09$ SN = 0.25

$S_{sg(P,V)} S_{(sm)i} S_{(s,r)} = 0$ $(CT)_R = 0.15$ sec

$S_{rg} S_{(sm)\dot{\theta}} S_{(s,r)} = 0.05$ PSR = 1.0

$(CT)_{(sm)} = 0$ sec

AIRCRAFT CHARACTERISTICS OF APP B

FIG I-19

RESPONSE OF OPEN-CHAIN TRACKING SYSTEM WITH TRACKING LINE PREDICTION IN THE ABSENCE OF GUST AND RADAR INTERFERENCE

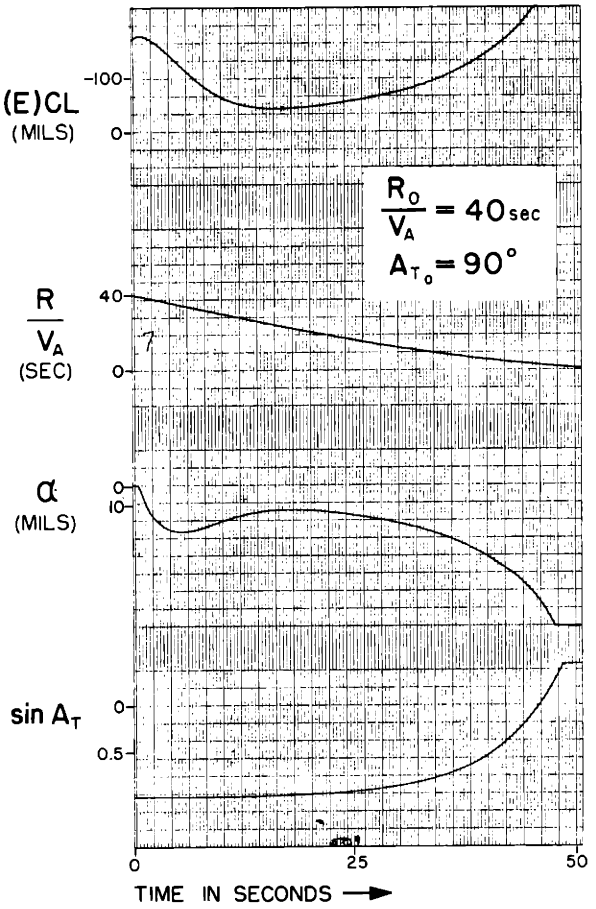

$S_{sg(P,V)} S_{(sm)p} S_{(s,r)} = 0.09$ SN = 0.25

$S_{sg(P,V)} S_{(sm)i} S_{(s,r)} = 0$ $(CT)_R$ = 0.15 sec

$S_{rg} S_{(sm)\dot{\theta}} S_{(s,r)} = .05$ PSR = 1.0

$(CT)_{(sm)}$ = 0 sec

AIRCRAFT CHARACTERISTICS OF APP B

FIG I - 20

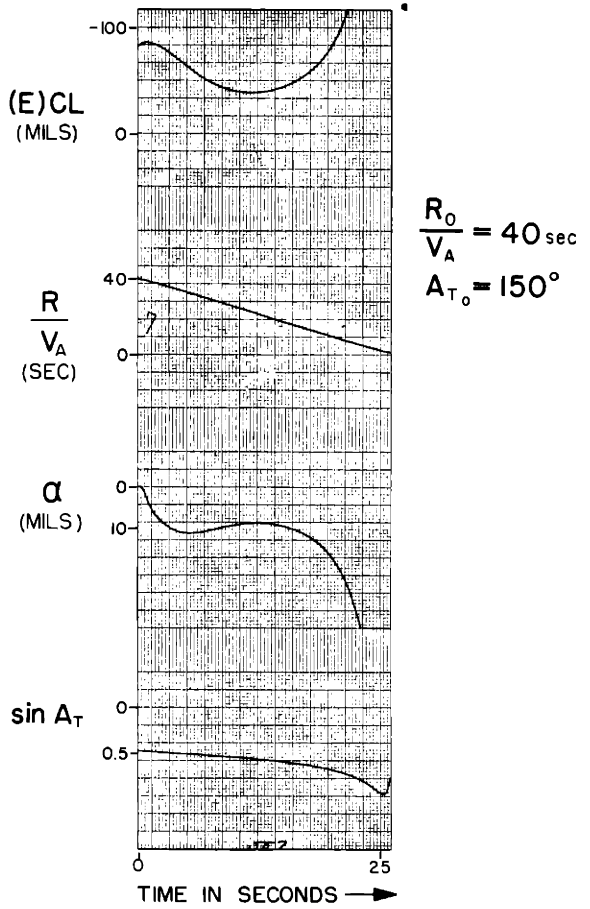

$S_{sg(P,V)} S_{(sm)p} S_{(s,r)} = 0.09$ SN = 0.25

$S_{sg(P,V)} S_{(sm)i} S_{(s,r)} = 0$ $(CT)_R$ = 0.15 sec

$S_{rg} S_{(sm)\dot{\theta}} S_{(s,r)} = 0$ PSR = 1.0

$(CT)_{(sm)}$ = 0 sec

AIRCRAFT CHARACTERISTICS OF APP B

FIG I - 21

RESPONSE OF OPEN-CHAIN TRACKING SYSTEM WITH TRACKING LINE PREDICTION IN THE ABSENCE OF GUST AND RADAR INTERFERENCE

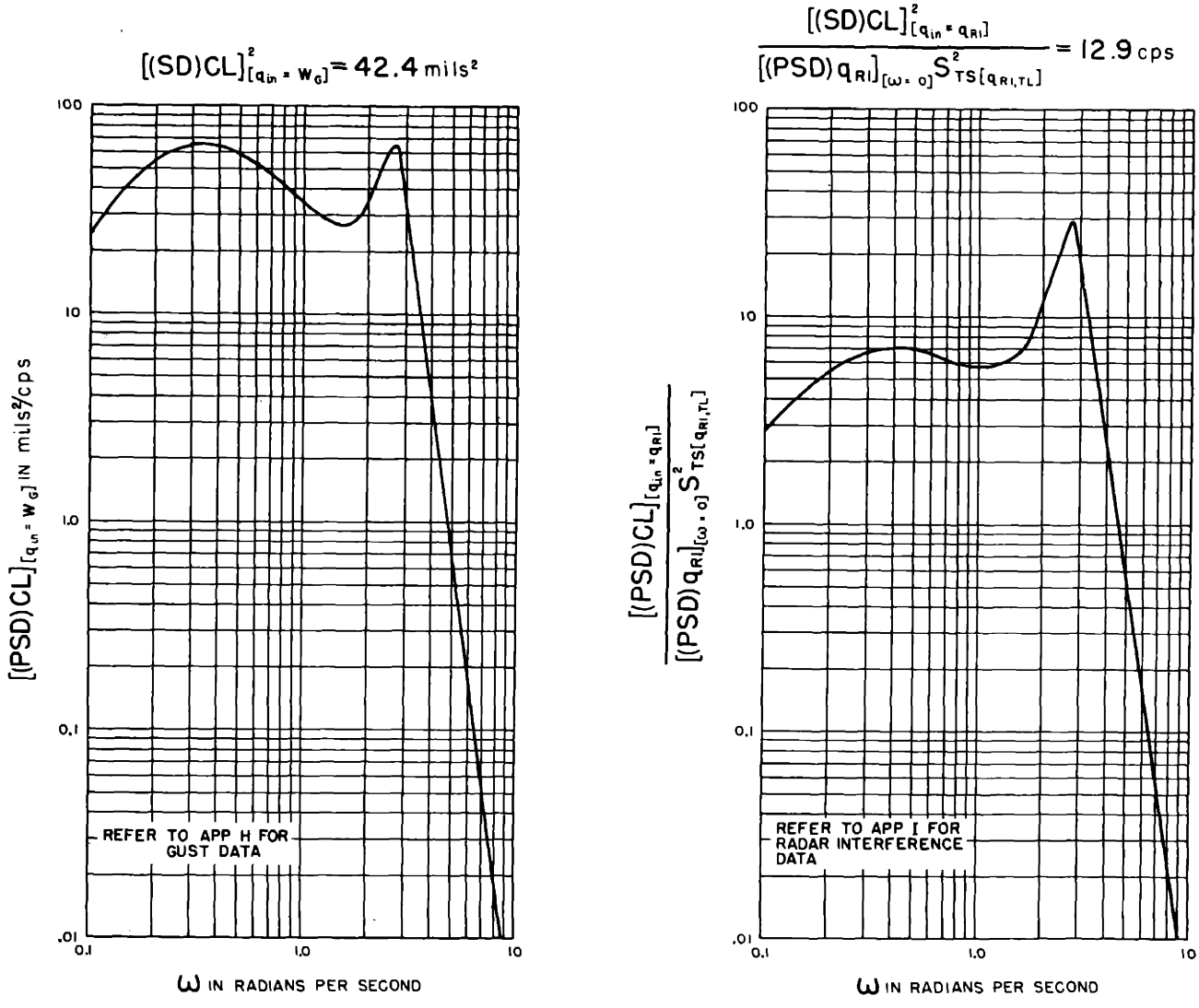

$S_{sg(P,V)}\, S_{(sm)p}\, S_{(s,r)} = 0.09$ $\quad S_{P(\omega,P)} = 13.85$ sec

$S_{sg(P,V)}\, S_{(sm)i}\, S_{(s,r)} = 0$ $\quad SN = 0.15$

$S_{rg}\, S_{(sm)\dot{\theta}}\, S_{(s,r)} = 0$ $\quad (CT)_R = 0.15$ sec

$(CT)_{(sm)} = 0$

AIRCRAFT CHARACTERISTICS OF APP B

FIG I-22 POWER SPECTRAL DENSITIES RESULTING FROM GUST AND RADAR INTERFERENCE OF OPEN-CHAIN TRACKING SYSTEM WITH TRACKING LINE PREDICTION

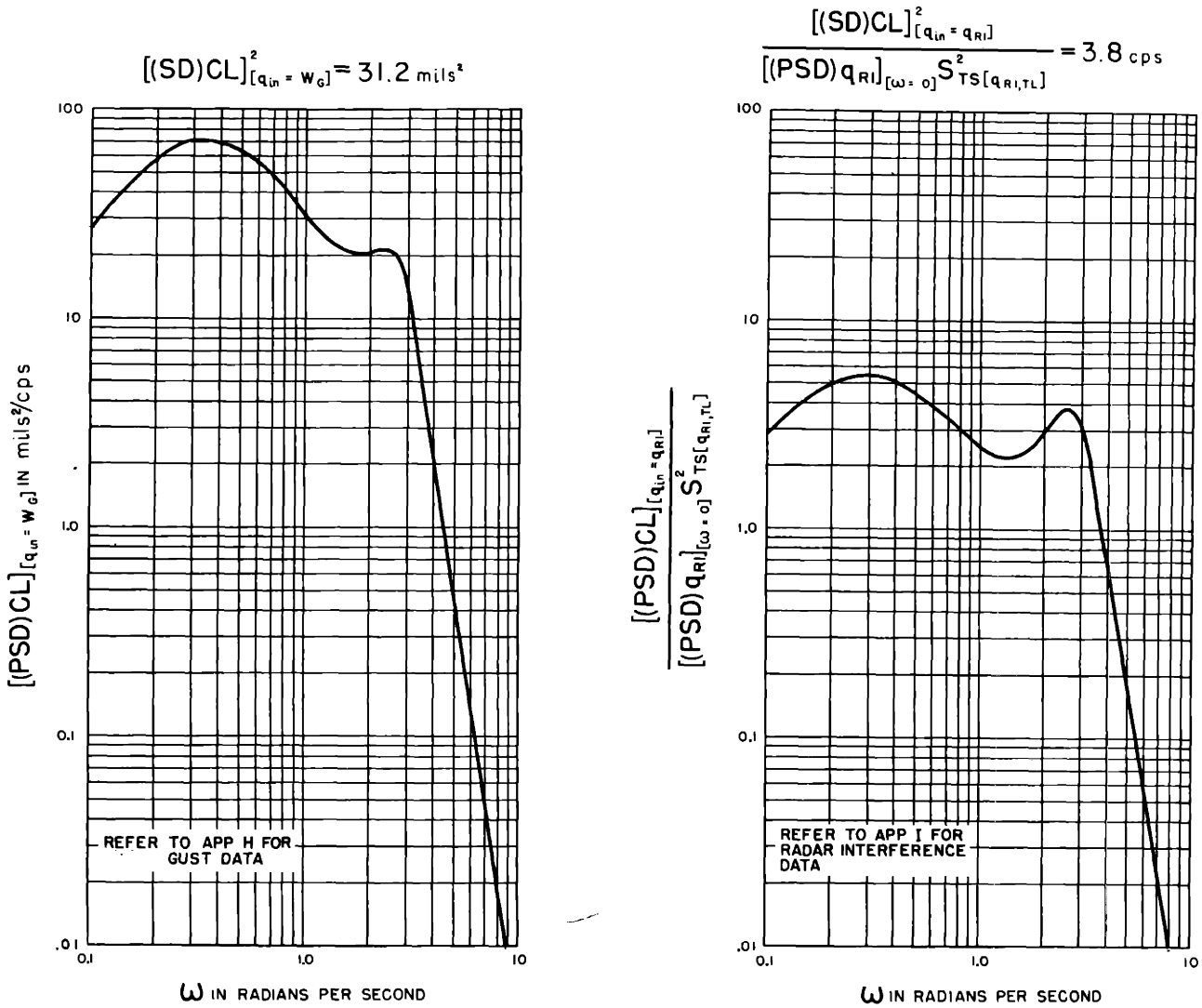

$S_{sg(P,V)}\ S_{(sm)p}\ S_{(s,r)} = 0.09$ $\quad S_{P(\omega,P)} = 13.85$ sec

$S_{sg(P,V)}\ S_{(sm)i}\ S_{(s,r)} = 0$ $\quad SN = 0.25$

$S_{rg}\ S_{(sm)\dot{\theta}}\ S_{(s,r)} = 0$ $\quad (CT)_R = 0.15$ sec

$(CT)_{(sm)} = 0$

AIRCRAFT CHARACTERISTICS OF APP B

FIG I-23 POWER SPECTRAL DENSITIES RESULTING FROM GUST AND RADAR INTERFERENCE OF OPEN-CHAIN TRACKING SYSTEM WITH TRACKING LINE PREDICTION

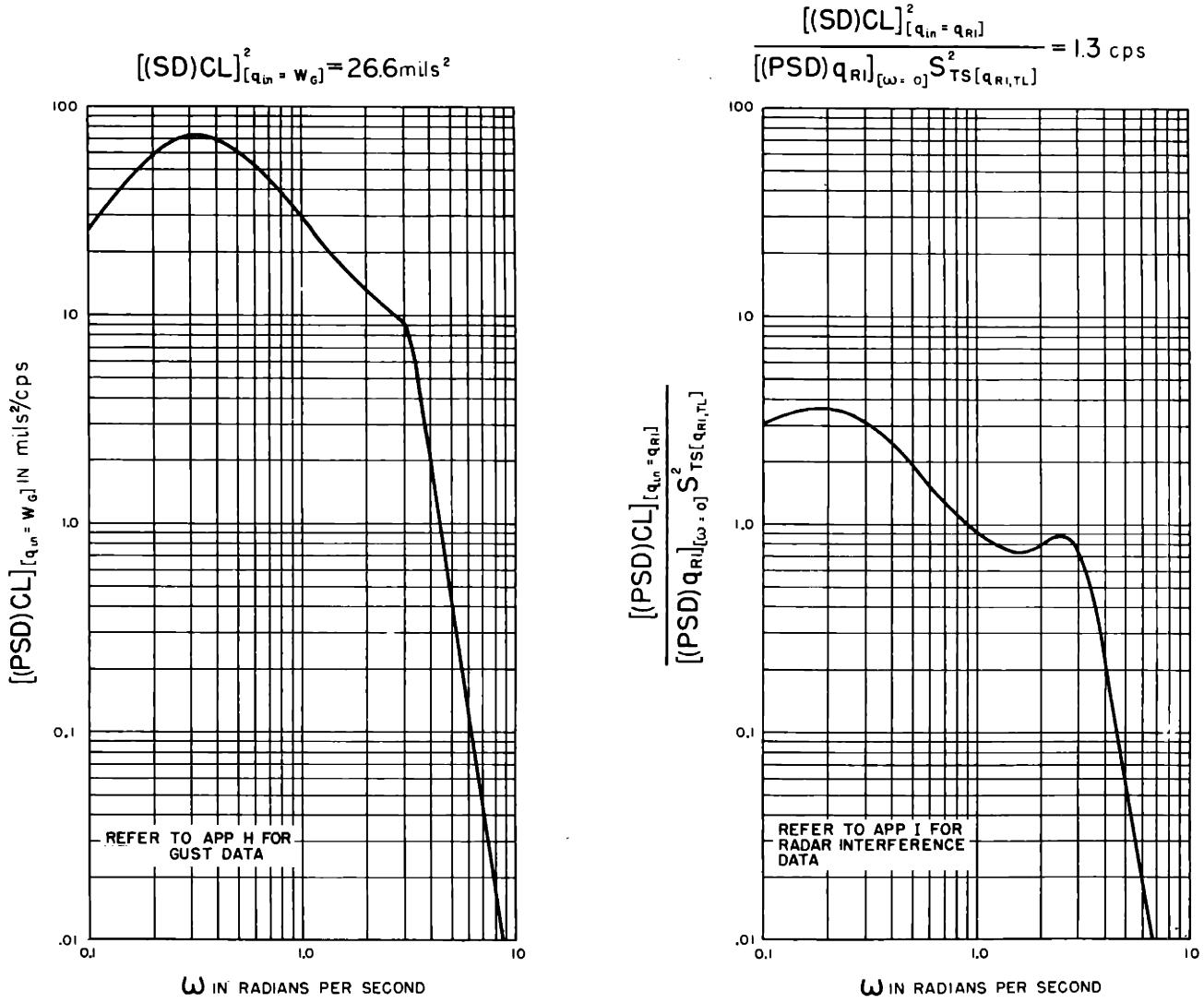

$S_{sg(P,V)}\ S_{(sm)p}\ S_{(S,r)} = 0.09$ $\quad S_{P(\omega,P)} = 13.85$ sec

$S_{sg(P,V)}\ S_{(sm)i}\ S_{(S,r)} = 0$ $\quad SN = 0.50$

$S_{rg}\ S_{(sm)\dot{\theta}}\ S_{(S,r)} = 0$ $\quad (CT)_R = 0.15$ sec

$(CT)_{(sm)} = 0$

AIRCRAFT CHARACTERISTICS OF APP B

FIG I-24 POWER SPECTRAL DENSITIES RESULTING FROM GUST AND RADAR INTERFERENCE OF OPEN-CHAIN TRACKING SYSTEM WITH TRACKING LINE PREDICTION

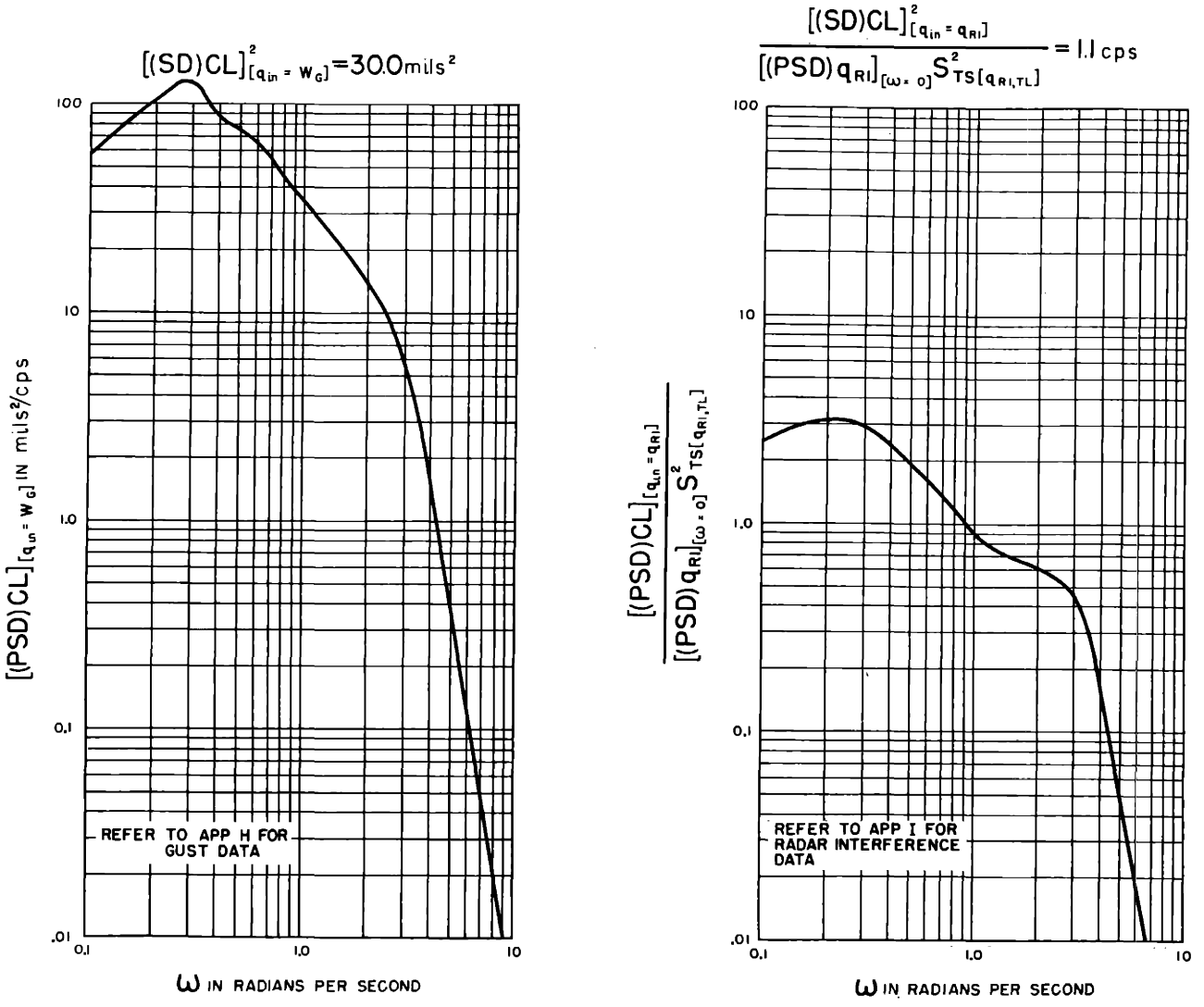

$S_{sg(P,V)}\ S_{(sm)p}\ S_{(S,r)} = 0.06$ $\quad S_{P(\omega,P)} = 13.85$ sec

$S_{sg(P,V)}\ S_{(sm)i}\ S_{(S,r)} = 0$ $\quad SN = 0.25$

$S_{rg}\ S_{(sm)\dot{\theta}}\ S_{(S,r)} = 0.05$ sec $\quad (CT)_R = 0.15$ sec

$(CT)_{(sm)} = 0$

AIRCRAFT CHARACTERISTICS OF APP B

FIG I - 25 POWER SPECTRAL DENSITIES RESULTING FROM GUST AND RADAR INTERFERENCE OF OPEN-CHAIN TRACKING SYSTEM WITH TRACKING LINE PREDICTION

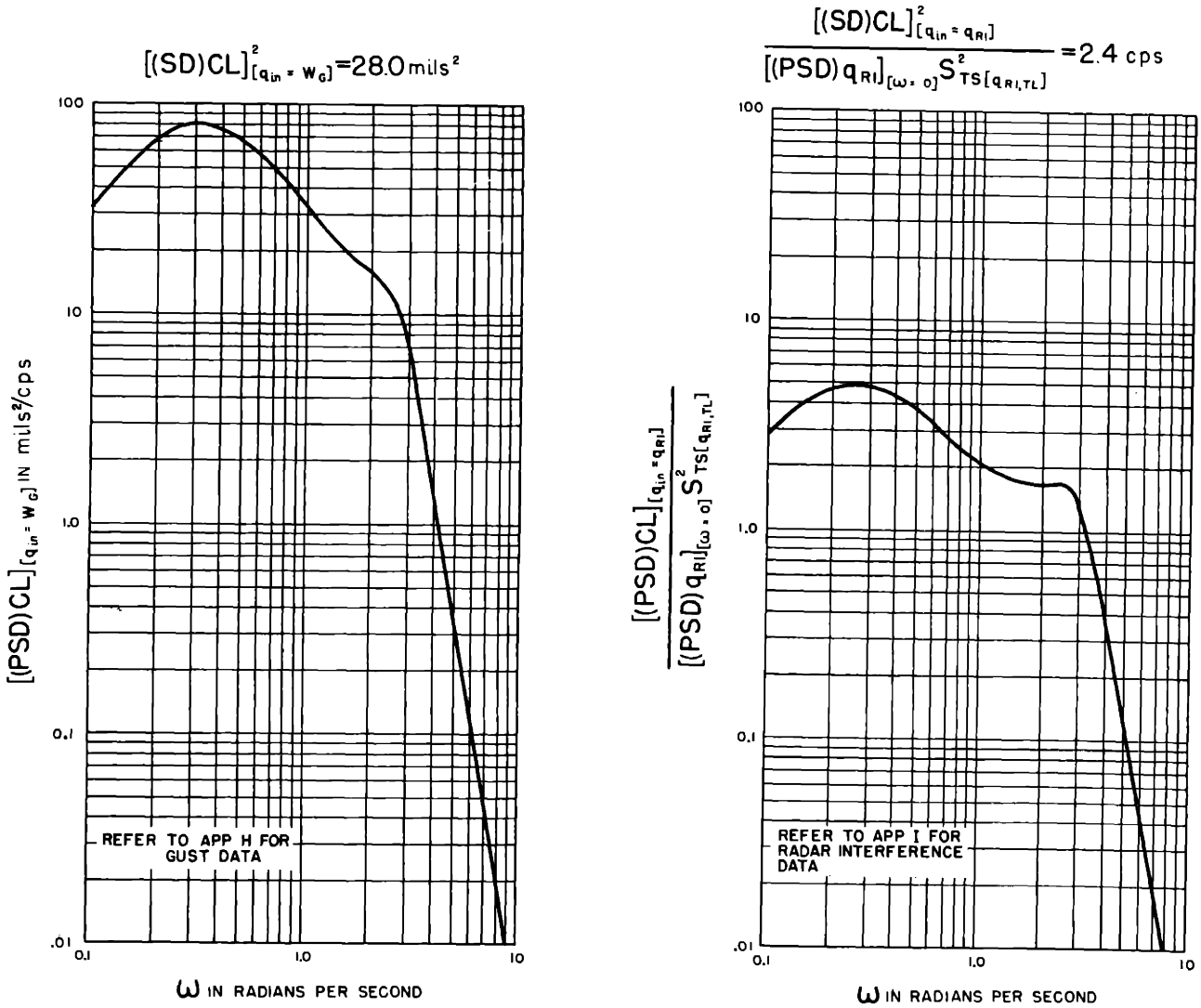

$S_{sg(P,V)}\, S_{(sm)p}\, S_{(s,r)} = 0.09$ $\quad S_{P(\omega,P)} = 13.85$ sec

$S_{sg(P,V)}\, S_{(sm)i}\, S_{(s,r)} = 0$ $\quad SN = 0.25$

$S_{rg}\, S_{(sm)\dot{\theta}}\, S_{(s,r)} = 0.05$ sec $\quad (CT)_R = 0.15$ sec

$(CT)_{(sm)} = 0$

AIRCRAFT CHARACTERISTICS OF APP B

FIG I-26 POWER SPECTRAL DENSITIES RESULTING FROM GUST AND RADAR INTERFERENCE OF OPEN-CHAIN TRACKING SYSTEM WITH TRACKING LINE PREDICTION

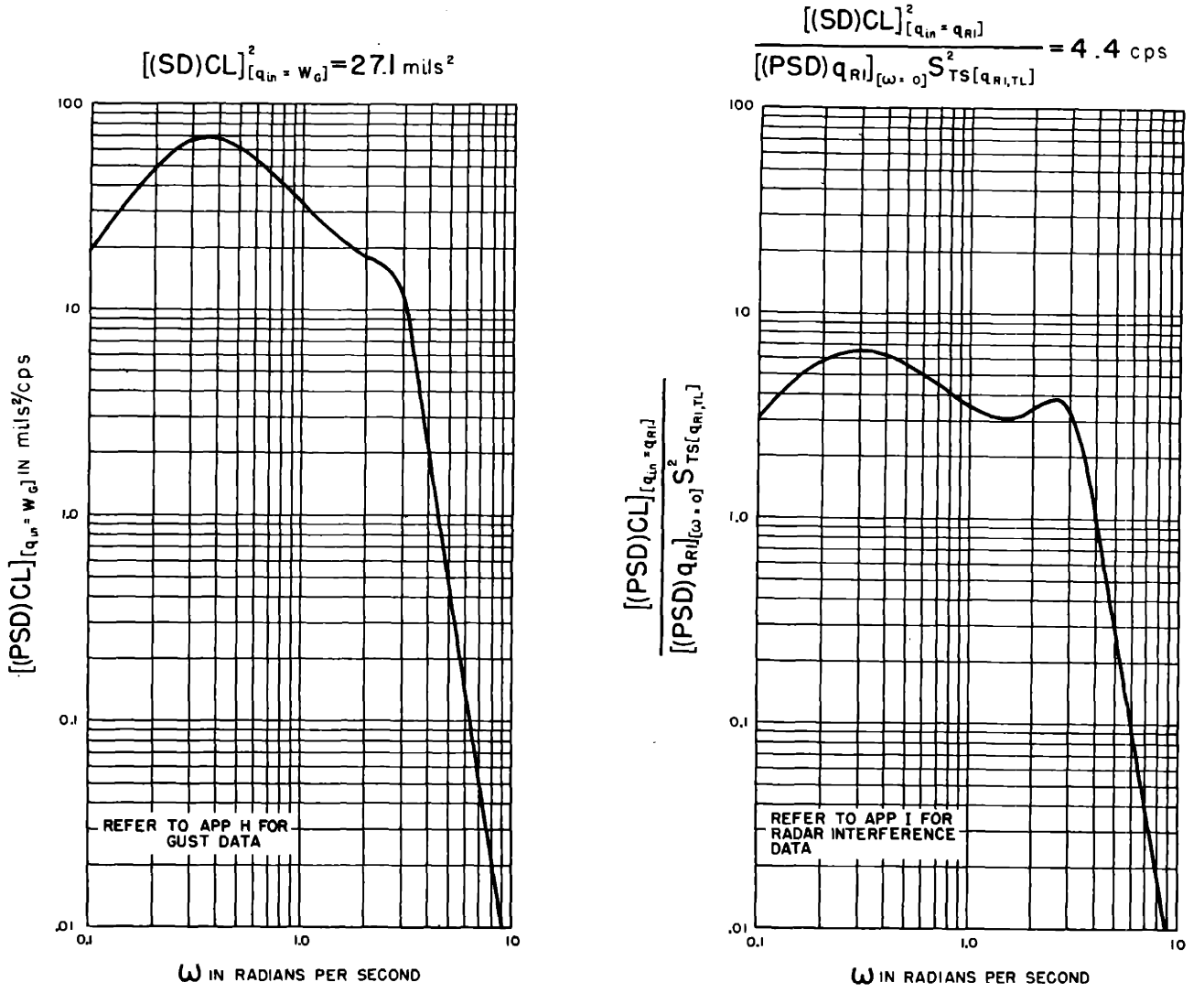

$S_{sg(P,V)}\ S_{(sm)p}\ S_{(s,r)} = 0.12$ $\quad S_{P(\omega,P)} = 13.85$ sec

$S_{sg(P,V)}\ S_{(sm)i}\ S_{(s,r)} = 0$ $\quad SN = 0.25$

$S_{rg}\ S_{(sm)\dot{\theta}}\ S_{(s,r)} = 0.05$ sec $\quad (CT)_R = 0.15$ sec

$(CT)_{(sm)} = 0$

AIRCRAFT CHARACTERISTICS OF APP B

FIG I - 27 POWER SPECTRAL DENSITIES RESULTING FROM GUST AND RADAR INTERFERENCE OF OPEN-CHAIN TRACKING SYSTEM WITH TRACKING LINE PREDICTION

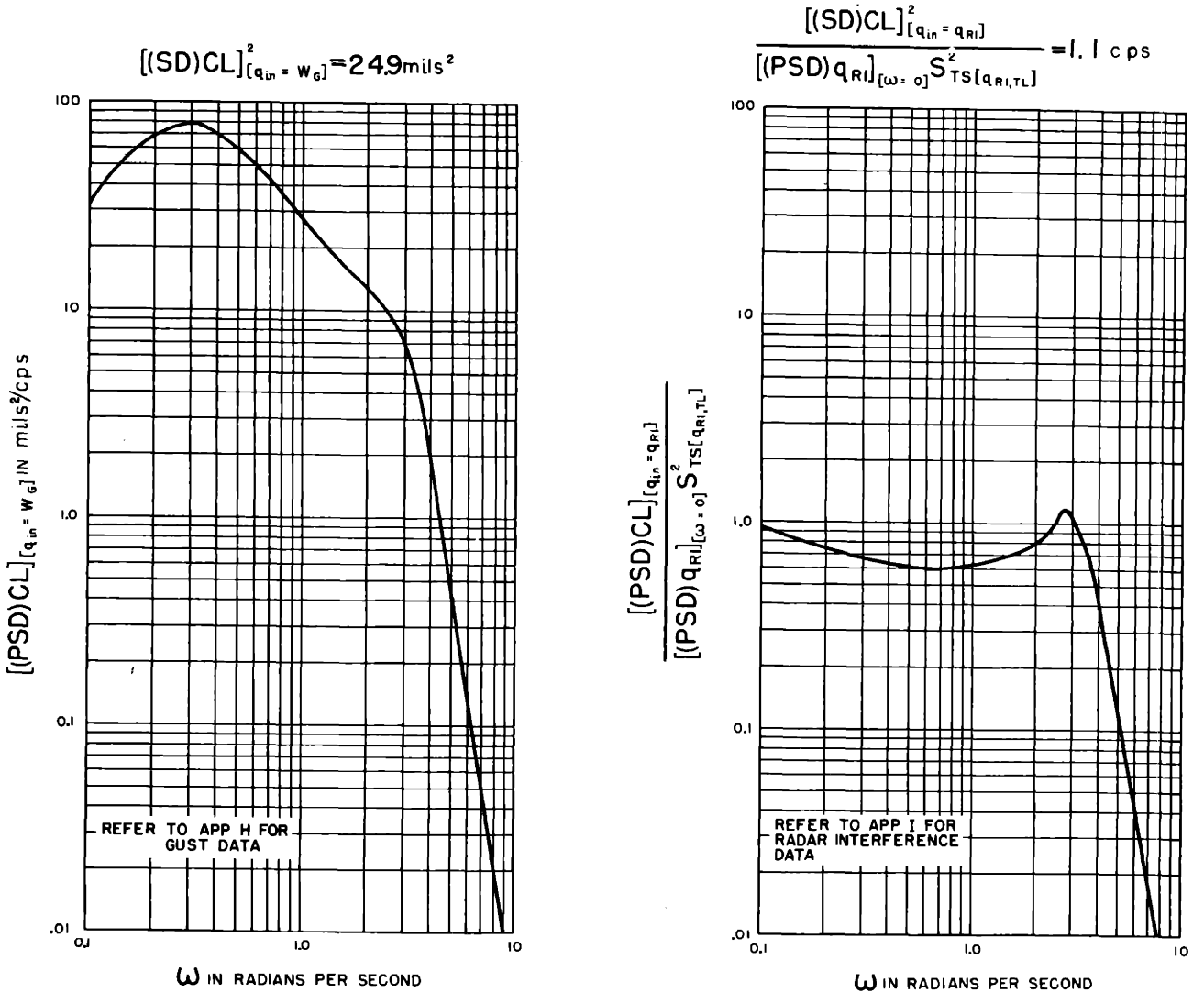

$S_{sg(P,V)}\, S_{(sm)p}\, S_{(s,r)} = 0.09$ $\quad S_{P(\omega,P)} = 2.77$ sec

$S_{sg(P,V)}\, S_{(sm)i}\, S_{(s,r)} = 0$ $\quad SN = 0.25$

$S_{rg}\, S_{(sm)\dot{\theta}}\, S_{(s,r)} = 0.05$ sec $\quad (CT)_R = 0.15$ sec

$(CT)_{(sm)} = 0$

AIRCRAFT CHARACTERISTICS OF APP B

FIG I-28 POWER SPECTRAL DENSITIES RESULTING FROM GUST AND RADAR INTERFERENCE OF OPEN-CHAIN TRACKING SYSTEM WITH TRACKING LINE PREDICTION

CHAPTER II

OPEN-CHAIN TRACKING SYSTEM WITH TRACKING INACCURACY PREDICTION AND TIGHT-LOOP STABILIZATION OF THE RADAR ANTENNA

A functional diagram of this tracking system is contained in Fig. II-1. The response of this tracking system in the absence of gust and radar interference is presented in Fig. II-2 through II-30, and the effects of gusts and radar interference are shown by the power spectral density curves of Fig. II-31 through II-35.

The results contained in this chapter were obtained by using Eq. B-8 and B-9 to represent the performance of the aircraft, and the following different equations which are derived in Appendices C, D, and E:

For the tracking radar –

$$\dot{P}_R = [S_{g(TL,V)} S_{R(V,\dot{P})}] [TL]$$

$$- [S_{TID} S_{RSS(i,W)}][S_{g(TL,V)} S_{R(V,\dot{P})}] \int [(C)TL]dt \qquad \text{II-1}$$

where

$$(C)TL = LS + P_R - CL \qquad \text{II-2}$$

and

$$TL = CL - P_R \qquad \text{II-3}$$

For the prediction computer –

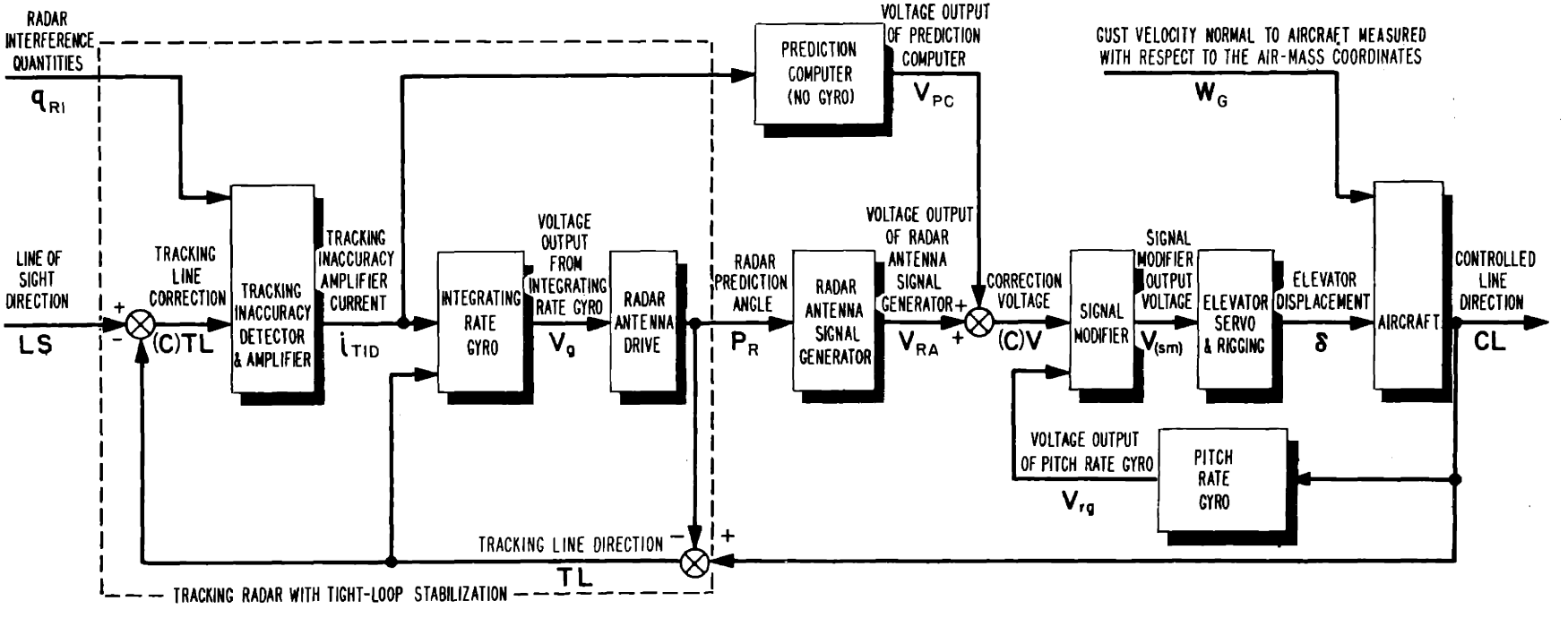

FIG II-1 FUNCTIONAL DIAGRAM OF OPEN-CHAIN TRACKING SYSTEM WITH TRACKING INACCURACY PREDICTION AND TIGHT-LOOP STABILIZATION OF THE RADAR ANTENNA

$$S_{p(W,P)}(SN)[-S_{(sg)(V,P)}]\dot{V}_{PC} + [-S_{(sg)(V,P)}]V_{PC} =$$

$$S_{p(W,P)}[S_{TID}\, S_{RSS(i,W)}][(C)TL] \qquad \text{II-4}$$

where

$$S_{p(W,P)} = (PSR)\frac{R}{V_{p(av)} - V_A} \qquad \text{II-5}$$

For the signal modifier, elevator servo and rigging –

$$\delta = [S_{(sg)(P,V)}S_{(sm)p}\, S_{(s,r)}]\,[P_R + S_{(sg)(V,P)}V_{PC}]$$
$$+ [S_{(sg)(P,V)}S_{(sm)i}\, S_{(s,r)}]\int [P_R + S_{(sg)(V,P)}V_{PC}]\,dt$$
$$+ [S_{rg}\, S_{(sm)}\dot{\theta}\, S_{(s,r)}]\,W_{CL} \qquad \text{II-6}$$

This tracking system differs from the tracking system discussed in Chapter I in two respects. Tight-loop stabilization is provided the tracking radar by the use of integrating rate gyros and, in addition, integration is included in the signal modifier. Equation II-1 indicates that the rate of change of prediction angle is proportional to the displacement of the tracking line and the integral of the tracking line correction. A displacement of the tracking line is detected by the integrating rate gyro, which supplies a proportional voltage to the radar antenna drive. This action is account for by the first term in Eq. II-1. In order to maintain the tracking line along the line of sight, the tracking correction must be detected by the radar receiver, and a proportional current must be supplied to a torque generator in the integrating rate gyro. This current introduces a moment that displaces the gyro gimbal, thereby providing the radar antenna drive with an input voltage that produces a rotation of the tracking line.

It can be seen by differentiating Eq. II-1 that in steady-state conditions where $\ddot{P}_R = 0$, the tracking line angular velocity is proportional to the required tracking correction. Consequently, the current output from the tracking inaccuracy detector can be used not only to drive the integrating rate gyro but also

as the input to the prediction computer. Equation II-4 is the performance equation for the prediction computer, and is obtained from the performance equation of Chapter I by replacing the angular velocity of the tracking line by the corresponding tracking line correction. The outputs from the prediction computer and the radar antenna signal generator are compared as in the system of Chapter I. When the summation of these signals is not zero, a tracking correction voltage results, which is applied to the signal modifier. The elevator is displaced an amount proportional to this signal and to the integral of this signal. Pitch rate stabilization is utilized; hence, Eq. I-6 also contains a term proportional to the angular velocity of the controlled line.

The controlled-line errors are similar to those obtained with the tracking system of Chapter I when no integration is used in the signal modifier. From the angle of attack record of Fig. II-5, it can be seen that with a forward gain of .35, an underdamped oscillation is present with a frequency of approximately one cycle per second. With a gain of .5 the response becomes unstable with a stability number of .15. With a stability number of .25, the stability depends upon the range, as can be seen from Fig. II-8. The effect of this underdamped oscillation can be minimized by increasing the stability number to .5, as shown in Fig. II-9. Consideration is given to pitch rate stabilization in Fig. II-13, II-14, and II-15. These responses were obtained for the same conditions as shown in Fig. II-10, II-11, and II-12, with the pitch rate signal added. It can be seen that the short-period oscillation is practically eliminated but that the forced error of the controlled line is still large. In Fig. II-16, II-17, and II-18 the ratio of tracking line angular velocity to tracking line correction is increased from 2 sec^{-1} to 4 sec^{-1}. As seen from Fig. II-16, this increase accentuates the short-period oscillation and does not improve the performance of the system, measured in terms of controlled-line error.

The performance of the system was markedly improved by incorporating integration in the signal modifier. The responses in Fig. II-24, II-26, II-28, and II-30 are with integration and can be compared with the responses in Fig. II-23, II-25, II-27, and II-29, respectively. The responses with the forward gain, $[S_{(sg)(P,V)}S_{(sm)p}S_{(s,r)}]$, equal to .2 appear slightly better than those with a gain of .5. A comparison of Fig. II-24 and II-28 indicates that a prediction sensitivity ratio of 1.05 would best minimize the controlled-line error. For this reason the results of Fig. 7 and 8 in the Discussion of Results

were obtained by averaging the controlled-line errors contained in Fig. II-24 and II-28.

The power spectral density curves of Fig. II-31 through II-35 show that the standard deviation of the controlled line resulting from gust interference is inversely proportional to the forward gain and nearly independent of all other parameters. With a gain of .2 the standard deviation of the controlled line is 3.3 mils, and with a gain of .5 the standard deviation is 2.4 mils. The standard deviation resulting from radar interference depends upon the forward gain, integration in the signal modifier, the stability number, and the prediction sensitivity. The standard deviation of the controlled line is reduced by increasing the stability number, but this of course is detrimental to the tracking of the interceptor aircraft. Incorporating integration in the signal modifier increases the power spectral density of the controlled line at .7 radian per second from a value of 7 to a value of 27, as can be seen from Fig. II-33 and II-34. This rise causes an increase in the standard deviation of the controlled line. It is felt that the power spectral densities shown in Fig. II-34 represent close to optimum performance for an open-chain tracking system. An increase in pitch rate damping would reduce the resonant peak at 3-1/2 radians per second, but this would decrease the standard deviation by no more than five percent.

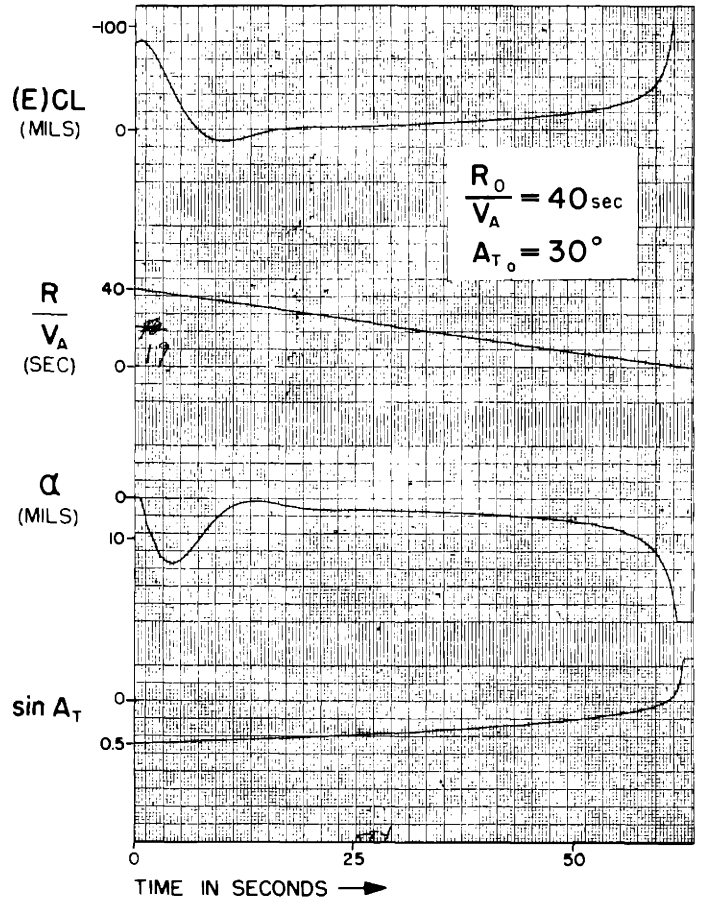

$S_{sg(P,V)}\, S_{(sm)p}\, S_{(s,r)} = 0.20$ PSR = 1.2

$S_{sg(P,V)}\, S_{(sm)\dot{\iota}}\, S_{(s,r)} = 0$ SN = 0.15

$S_{rg}\, S_{(sm)\dot{\theta}}\, S_{(s,r)} = 0\,sec$ $S_{g(TL,V)}\, S_{R(V,\dot{P})} = 6.67\,sec^{-1}$

$(CT)_{(sm)} = 0$ $S_{TID}\, S_{RSS(\dot{\iota},\omega)} = 2.0\,sec^{-1}$

AIRCRAFT CHARACTERISTICS OF APP B

FIG. II - 2

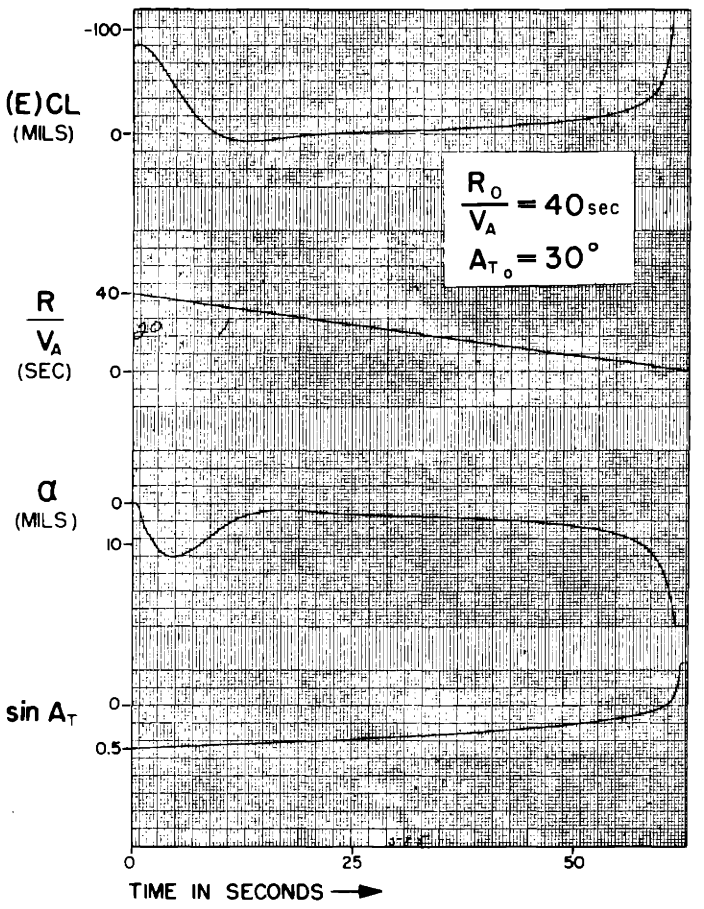

$S_{sg(P,V)}\, S_{(sm)p}\, S_{(s,r)} = 0.20$ PSR = 1.2

$S_{sg(P,V)}\, S_{(sm)\dot{\iota}}\, S_{(s,r)} = 0$ SN = 0.25

$S_{rg}\, S_{(sm)\dot{\theta}}\, S_{(s,r)} = 0\,sec$ $S_{g(TL,V)}\, S_{R(V,\dot{P})} = 6.67\,sec^{-1}$

$(CT)_{(sm)} = 0$ $S_{TID}\, S_{RSS(\dot{\iota},\omega)} = 2.0\,sec^{-1}$

AIRCRAFT CHARACTERISTICS OF APP B

FIG. II - 3

RESPONSE OF OPEN-CHAIN TRACKING SYSTEM WITH TRACKING INACCURACY PREDICTION AND TIGHT-LOOP STABILIZATION OF THE RADAR ANTENNA IN THE ABSENCE OF GUST AND RADAR INTERFERENCE

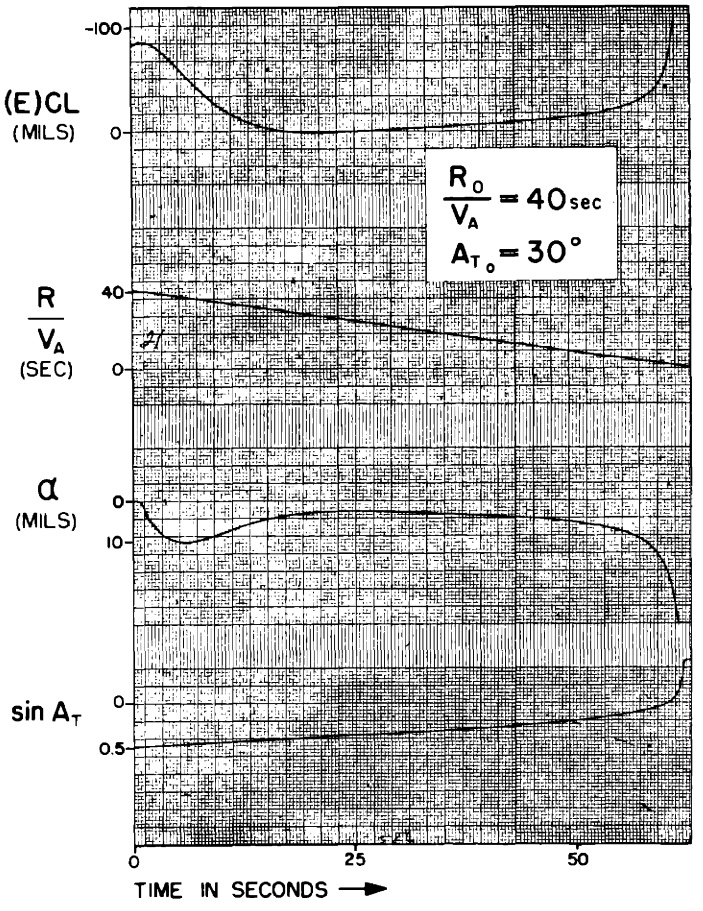

$S_{sg(P,V)}\, S_{(sm)p}\, S_{(s,r)} = 0.20$ PSR = 1.2

$S_{sg(P,V)}\, S_{(sm)i}\, S_{(s,r)} = 0$ SN = 0.50

$S_{rg}\, S_{(sm)\dot{\theta}}\, S_{(s,r)} = 0\,sec$ $S_{g(TL,V)}\, S_{R(V,\dot{P})} = 6.67\,sec^{-1}$

$(CT)_{(sm)} = 0$ $S_{TID}\, S_{RSS(i,\omega)} = 2.0\,sec^{-1}$

AIRCRAFT CHARACTERISTICS OF APP B

FIG. II - 4

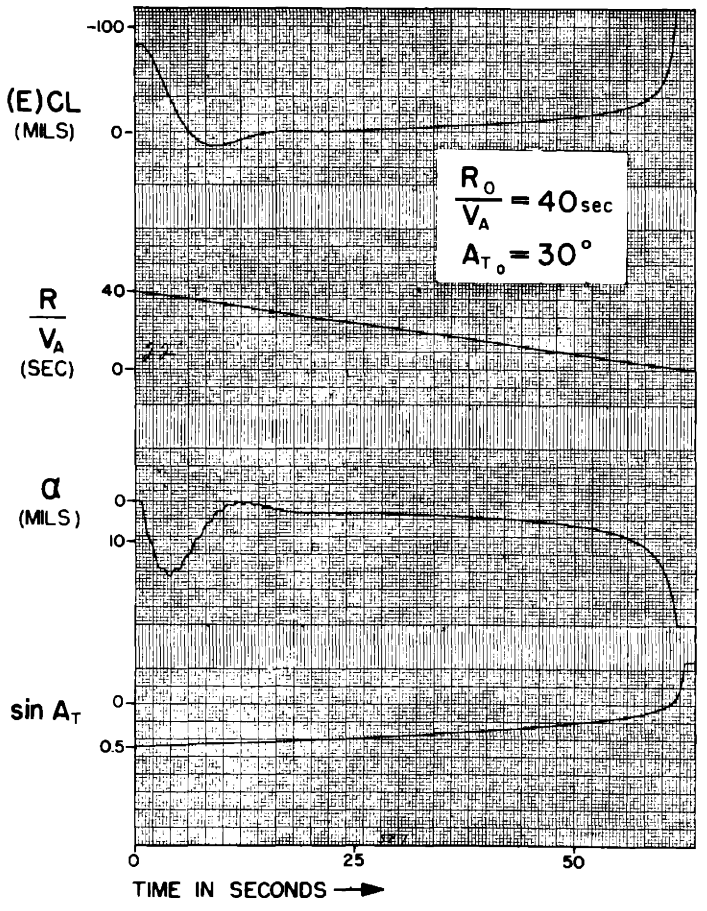

$S_{sg(P,V)}\, S_{(sm)p}\, S_{(s,r)} = 0.35$ PSR = 1.2

$S_{sg(P,V)}\, S_{(sm)i}\, S_{(s,r)} = 0$ SN = 0.15

$S_{rg}\, S_{(sm)\dot{\theta}}\, S_{(s,r)} = 0\,sec$ $S_{g(TL,V)}\, S_{R(V,\dot{P})} = 6.67\,sec^{-1}$

$(CT)_{(sm)} = 0$ $S_{TID}\, S_{RSS(i,\omega)} = 2.0\,sec^{-1}$

AIRCRAFT CHARACTERISTICS OF APP B

FIG. II - 5

RESPONSE OF OPEN-CHAIN TRACKING SYSTEM WITH TRACKING INACCURACY PREDICTION AND TIGHT-LOOP STABILIZATION OF THE RADAR ANTENNA IN THE ABSENCE OF GUST AND RADAR INTERFERENCE

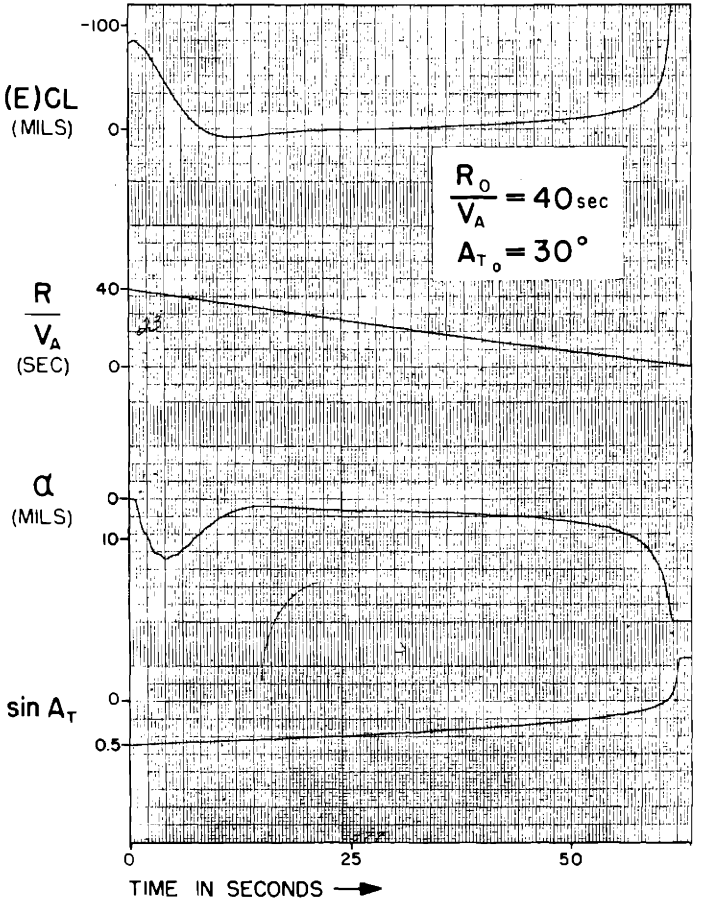

$S_{sg(P,V)}\, S_{(sm)p}\, S_{(s,r)} = 0.35$ PSR = 1.2

$S_{sg(P,V)}\, S_{(sm)i}\, S_{(s,r)} = 0$ SN = 0.25

$S_{rg}\, S_{(sm)\dot{\theta}}\, S_{(s,r)} = 0\,sec$ $S_{g(TL,V)}\, S_{R(V,\dot{P})} = 6.67\,sec^{-1}$

$(CT)_{(sm)} = 0$ $S_{TID}\, S_{RSS(i,\omega)} = 2.0\,sec^{-1}$

AIRCRAFT CHARACTERISTICS OF APP B

FIG. II - 6

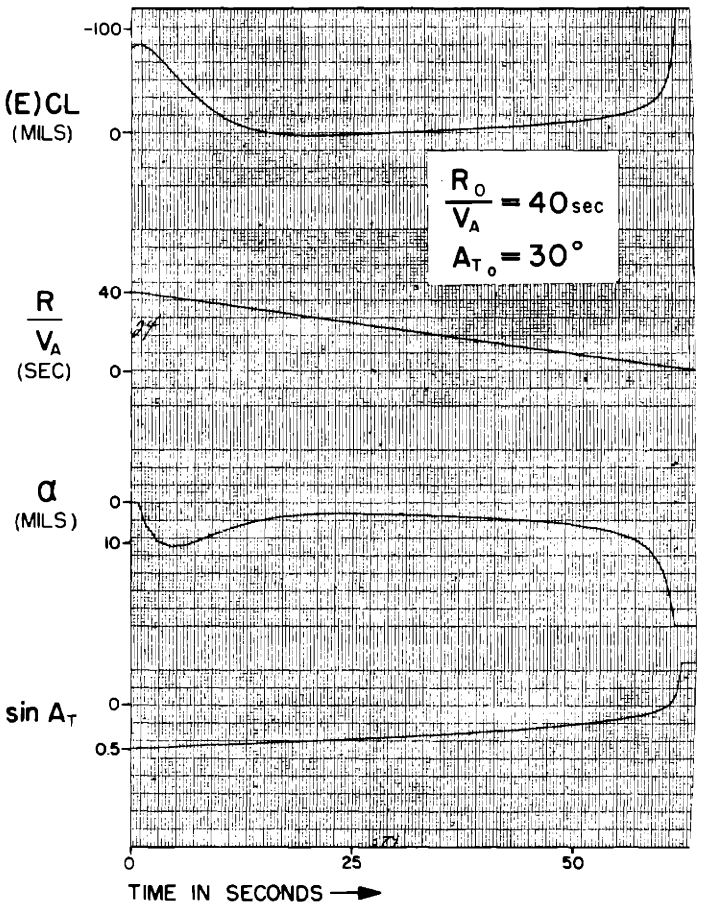

$S_{sg(P,V)}\, S_{(sm)p}\, S_{(s,r)} = 0.35$ PSR = 1.2

$S_{sg(P,V)}\, S_{(sm)i}\, S_{(s,r)} = 0$ SN = 0.50

$S_{rg}\, S_{(sm)\dot{\theta}}\, S_{(s,r)} = 0\,sec$ $S_{g(TL,V)}\, S_{R(V,\dot{P})} = 6.67\,sec^{-1}$

$(CT)_{(sm)} = 0$ $S_{TID}\, S_{RSS(i,\omega)} = 2.0\,sec^{-1}$

AIRCRAFT CHARACTERISTICS OF APP B

FIG. II - 7

RESPONSE OF OPEN-CHAIN TRACKING SYSTEM WITH TRACKING INACCURACY PREDICTION AND TIGHT-LOOP STABILIZATION OF THE RADAR ANTENNA IN THE ABSENCE OF GUST AND RADAR INTERFERENCE

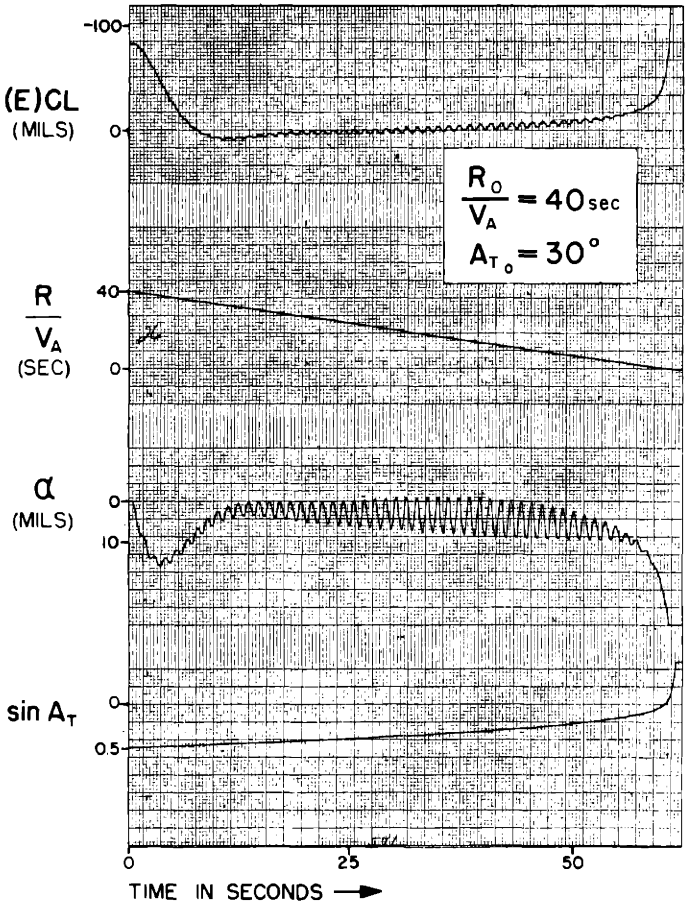

$S_{sg(P,V)}\, S_{(sm)p}\, S_{(s,r)} = 0.50$ PSR = 1.2

$S_{sg(P,V)}\, S_{(sm)\dot{\iota}}\, S_{(s,r)} = 0$ SN = 0.25

$S_{rg}\, S_{(sm)\dot{\theta}}\, S_{(s,r)} = 0$ sec $S_{g(TL,V)}\, S_{R(V,\dot{P})} = 6.67\ \text{sec}^{-1}$

$(CT)_{(sm)} = 0$ $S_{TID}\, S_{RSS(\dot{\iota},\omega)} = 2.0\ \text{sec}^{-1}$

AIRCRAFT CHARACTERISTICS OF APP C

FIG. II - 8

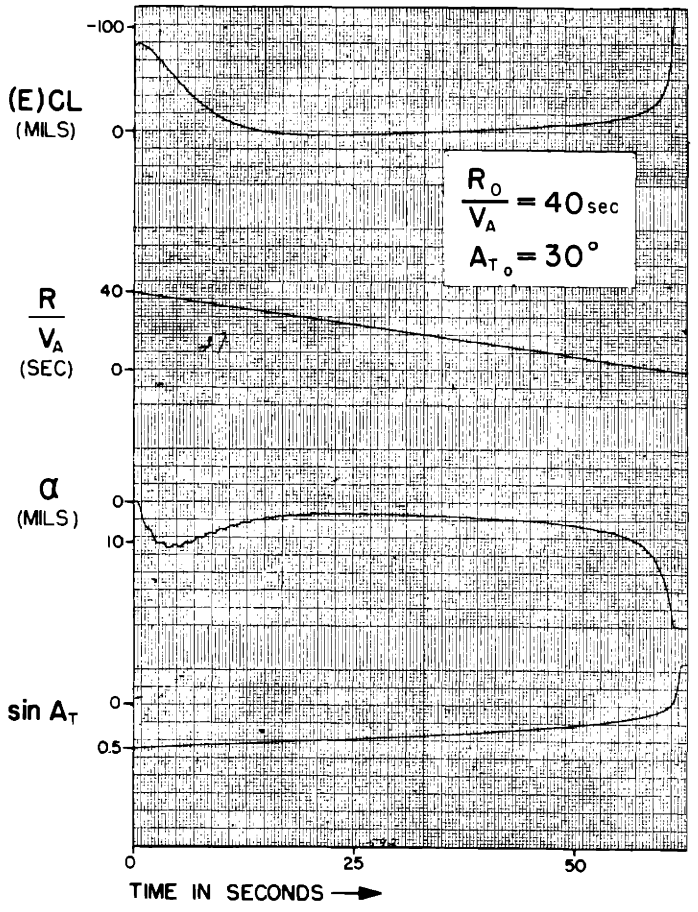

$S_{sg(P,V)}\, S_{(sm)p}\, S_{(s,r)} = 0.50$ PSR = 1.2

$S_{sg(P,V)}\, S_{(sm)\dot{\iota}}\, S_{(s,r)} = 0$ SN = 0.50

$S_{rg}\, S_{(sm)\dot{\theta}}\, S_{(s,r)} = 0$ sec $S_{g(TL,V)}\, S_{R(V,\dot{P})} = 6.67\ \text{sec}^{-1}$

$(CT)_{(sm)} = 0$ $S_{TID}\, S_{RSS(\dot{\iota},\omega)} = 2.0\ \text{sec}^{-1}$

AIRCRAFT CHARACTERISTICS OF APP B

FIG. II - 9

RESPONSE OF OPEN-CHAIN TRACKING SYSTEM WITH TRACKING INACCURACY PREDICTION AND TIGHT-LOOP STABILIZATION OF THE RADAR ANTENNA IN THE ABSENCE OF GUST AND RADAR INTERFERENCE

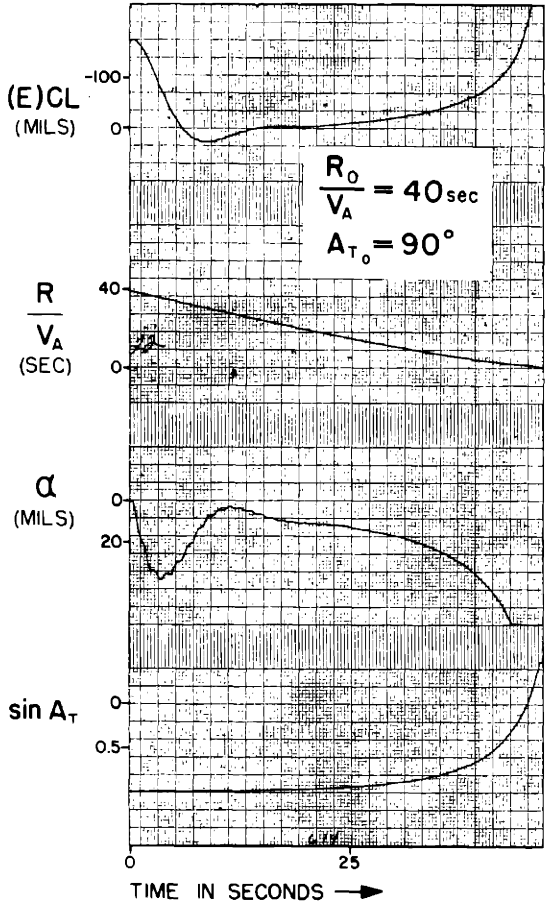

$S_{sg(P,V)}\ S_{(sm)p}\ S_{(s,r)} = 0.35$ PSR = 1.2

$S_{sg(P,V)}\ S_{(sm)i}\ S_{(s,r)} = 0$ SN = 0.15

$S_{rg}\ S_{(sm)\dot{\theta}}\ S_{(s,r)} = 0\ \text{sec}$ $S_{g(TL,V)}\ S_{R(V,\dot{P})} = 6.67\ \text{sec}^{-1}$

$(CT)_{(sm)} = 0$ $S_{TID}\ S_{RSS(i,\omega)} = 2.0\ \text{sec}^{-1}$

AIRCRAFT CHARACTERISTICS OF APP B

FIG. II - 10

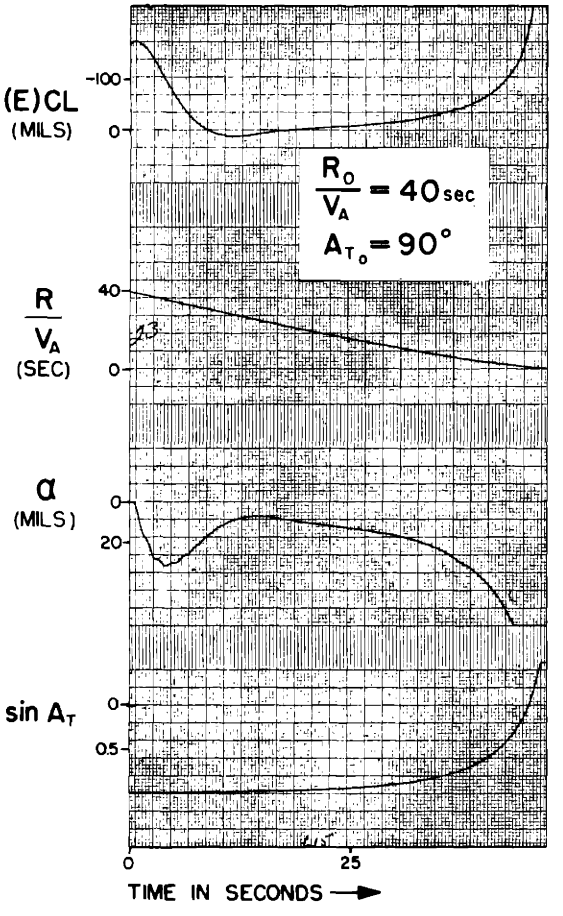

$S_{sg(P,V)}\ S_{(sm)p}\ S_{(s,r)} = 0.35$ PSR = 1.2

$S_{sg(P,V)}\ S_{(sm)i}\ S_{(s,r)} = 0$ SN = 0.25

$S_{rg}\ S_{(sm)\dot{\theta}}\ S_{(s,r)} = 0\ \text{sec}$ $S_{g(TL,V)}\ S_{R(V,\dot{P})} = 6.67\ \text{sec}^{-1}$

$(CT)_{(sm)} = 0$ $S_{TID}\ S_{RSS(i,\omega)} = 2.0\ \text{sec}^{-1}$

AIRCRAFT CHARACTERISTICS OF APP B

FIG. II - 11

RESPONSE OF OPEN-CHAIN TRACKING SYSTEM WITH TRACKING INACCURACY PREDICTION AND TIGHT-LOOP STABILIZATION OF THE RADAR ANTENNA IN THE ABSENCE OF GUST AND RADAR INTERFERENCE

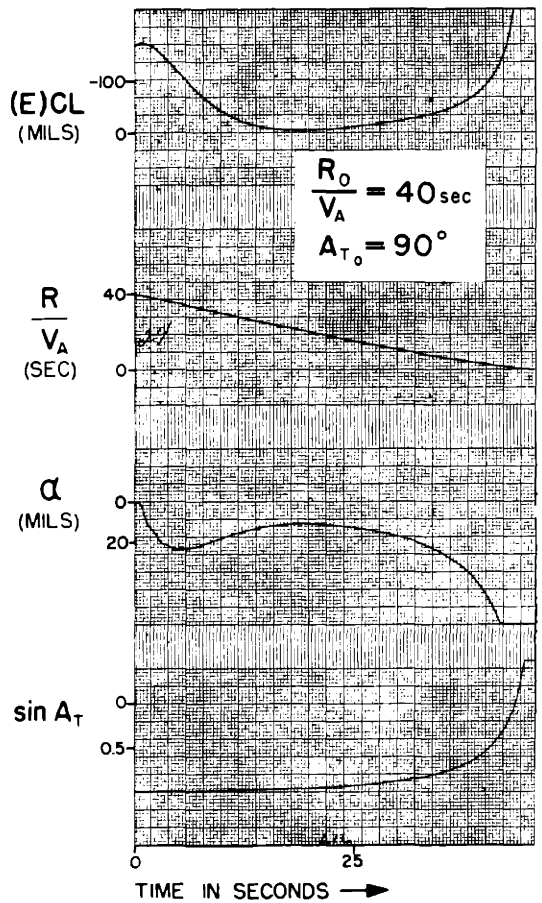

$S_{sg(P,V)}\ S_{(sm)p}\ S_{(S,r)}$ = 0.35 PSR = 1.2

$S_{sg(P,V)}\ S_{(sm)i}\ S_{(S,r)}$ = 0 SN = 0.50

$S_{rg}\ S_{(sm)\dot{\theta}}\ S_{(S,r)}$ = 0 sec $S_{g(TL,V)}\ S_{R(V,\dot{P})}$ = 6.67 sec^{-1}

$(CT)_{(sm)}$ = 0 $S_{TID}\ S_{RSS(i,\omega)}$ = 2.0 sec^{-1}

AIRCRAFT CHARACTERISTICS OF APP B

FIG. II - 12

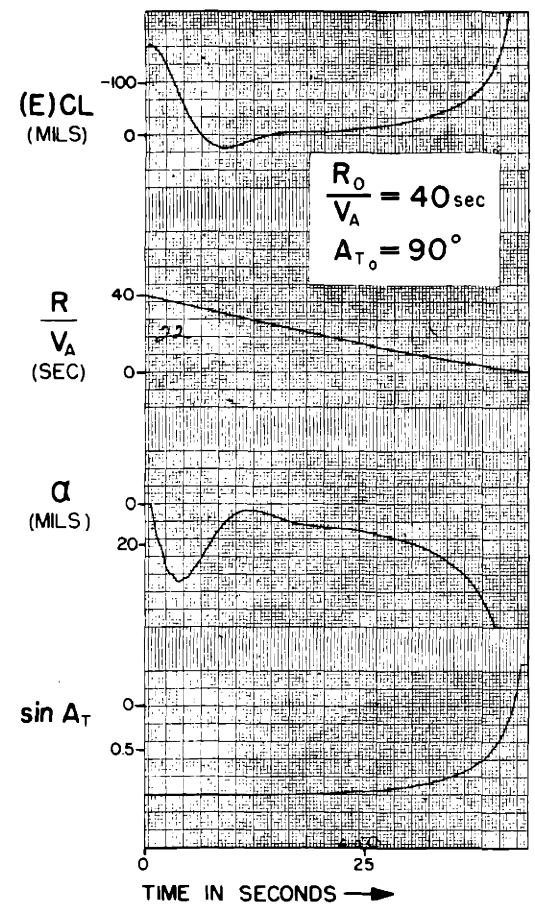

$S_{sg(P,V)}\ S_{(sm)p}\ S_{(S,r)}$ = 0.35 PSR = 1.2

$S_{sg(P,V)}\ S_{(sm)i}\ S_{(S,r)}$ = 0 SN = 0.15

$S_{rg}\ S_{(sm)\dot{\theta}}\ S_{(S,r)}$ = .026 sec $S_{g(TL,V)}\ S_{R(V,\dot{P})}$ = 6.67 sec^{-1}

$(CT)_{(sm)}$ = 0 $S_{TID}\ S_{RSS(i,\omega)}$ = 2.0 sec^{-1}

AIRCRAFT CHARACTERISTICS OF APP B

FIG. II - 13

RESPONSE OF OPEN-CHAIN TRACKING SYSTEM WITH TRACKING INACCURACY PREDICTION AND TIGHT-LOOP STABILIZATION OF THE RADAR ANTENNA IN THE ABSENCE OF GUST AND RADAR INTERFERENCE

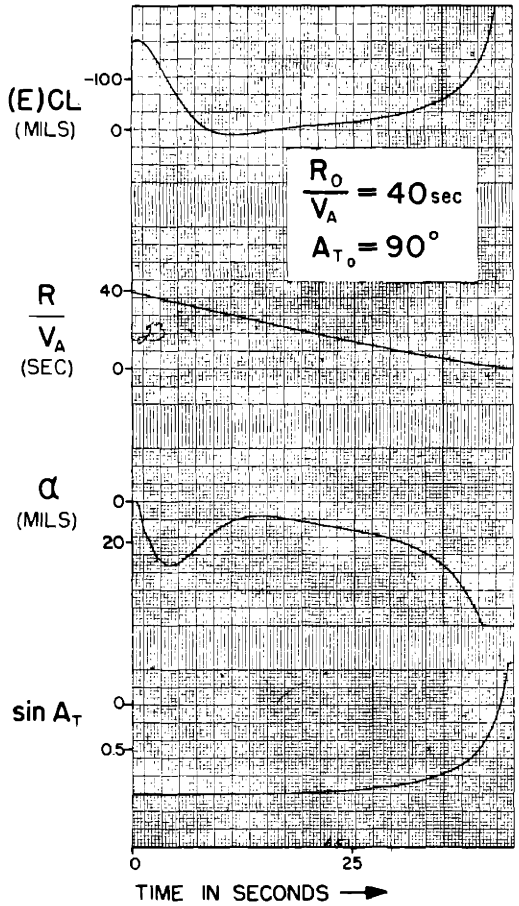

$S_{sg(P,V)}\, S_{(sm)p}\, S_{(s,r)} = 0.35$ PSR = 1.2

$S_{sg(P,V)}\, S_{(sm)i}\, S_{(s,r)} = 0$ SN = 0.25

$S_{rg}\, S_{(sm)\dot{\theta}}\, S_{(s,r)} = .026\,sec.$ $S_{g(TL,V)}\, S_{R(V,\dot{P})} = 6.67\,sec^{-1}$

$(CT)_{(sm)} = 0$ $S_{TID}\, S_{RSS(i,\omega)} = 2.0\,sec^{-1}$

AIRCRAFT CHARACTERISTICS OF APP B

FIG. II - 14

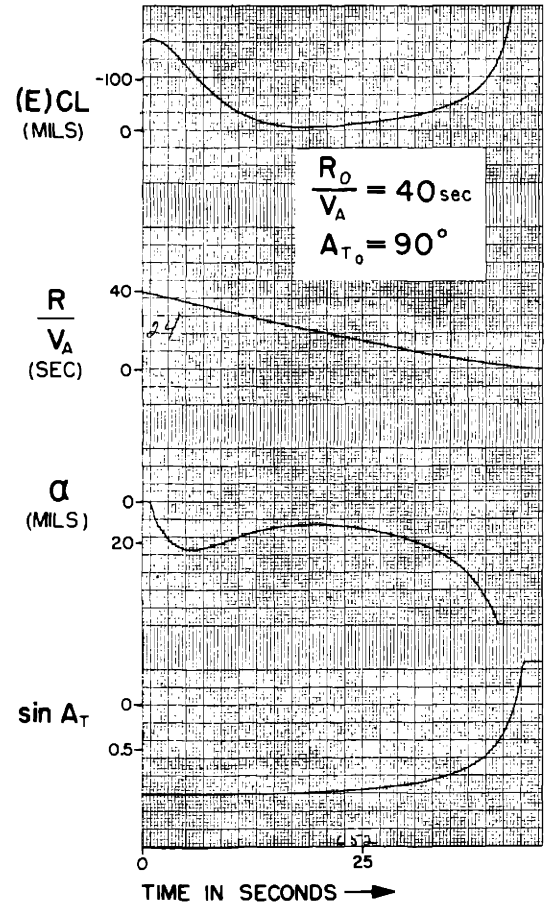

$S_{sg(P,V)}\, S_{(sm)p}\, S_{(s,r)} = 0.35$ PSR = 1.2

$S_{sg(P,V)}\, S_{(sm)i}\, S_{(s,r)} = 0$ SN = 0.50

$S_{rg}\, S_{(sm)\dot{\theta}}\, S_{(s,r)} = .026\,sec$ $S_{g(TL,V)}\, S_{R(V,\dot{P})} = 6.67\,sec^{-1}$

$(CT)_{(sm)} = 0$ $S_{TID}\, S_{RSS(i,\omega)} = 2.0\,sec^{-1}$

AIRCRAFT CHARACTERISTICS OF APP B

FIG. II - 15

RESPONSE OF OPEN-CHAIN TRACKING SYSTEM WITH TRACKING INACCURACY PREDICTION AND TIGHT-LOOP STABILIZATION OF THE RADAR ANTENNA IN THE ABSENCE OF GUST AND RADAR INTERFERENCE

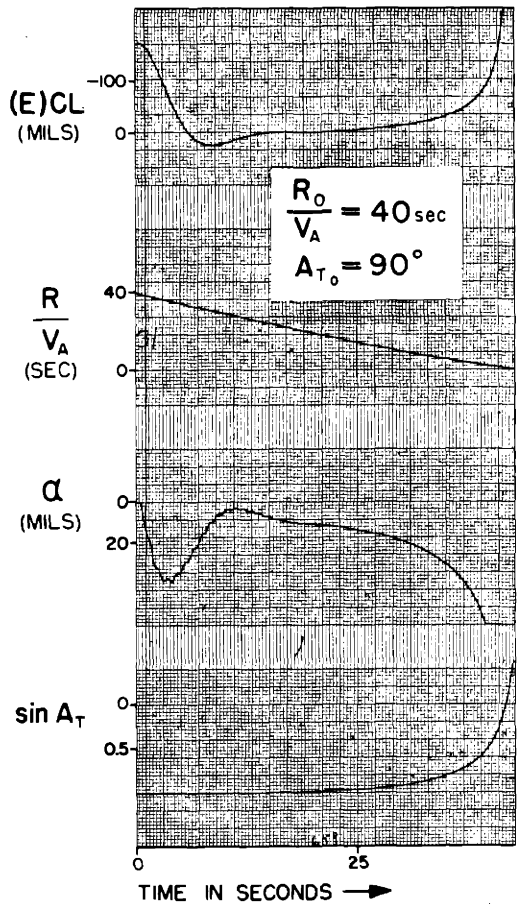

$S_{sg(P,V)}\, S_{(sm)p}\, S_{(s,r)} = 0.35$ PSR = 1.2

$S_{sg(P,V)}\, S_{(sm)i}\, S_{(s,r)} = 0$ SN = 0.15

$S_{rg}\, S_{(sm)\dot{\theta}}\, S_{(s,r)} = .026\,\text{sec}$ $S_{g(TL,V)}\, S_{R(V,\dot{\beta})} = 6.67\,\text{sec}^{-1}$

$(CT)_{(sm)} = 0$ $S_{TID}\, S_{RSS(i,\omega)} = 4.0\,\text{sec}^{-1}$

AIRCRAFT CHARACTERISTICS OF APP B

FIG. II - 16

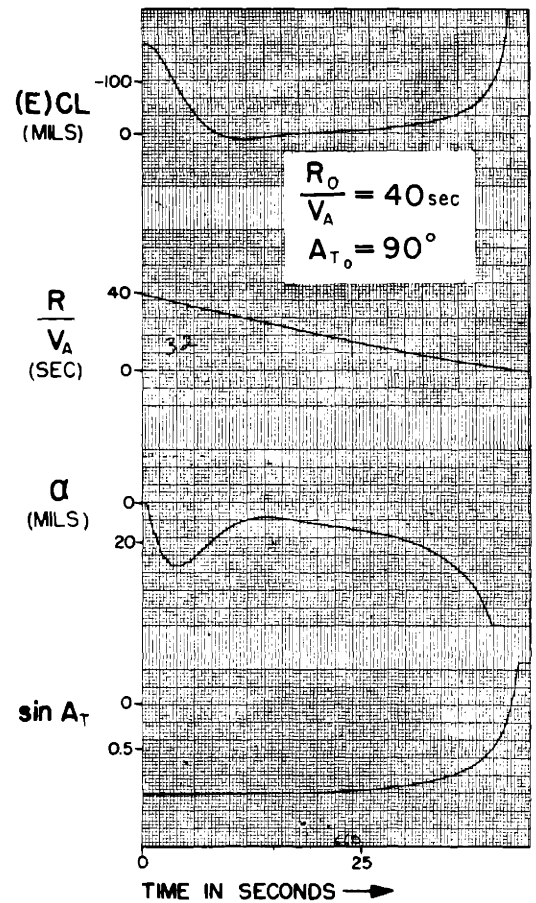

$S_{sg(P,V)}\, S_{(sm)p}\, S_{(s,r)} = 0.35$ PSR = 1.2

$S_{sg(P,V)}\, S_{(sm)i}\, S_{(s,r)} = 0$ SN = 0.25

$S_{rg}\, S_{(sm)\dot{\theta}}\, S_{(s,r)} = .026\,\text{sec}$ $S_{g(TL,V)}\, S_{R(V,\dot{\beta})} = 6.67\,\text{sec}^{-1}$

$(CT)_{(sm)} = 0$ $S_{TID}\, S_{RSS(i,\omega)} = 4.0\,\text{sec}^{-1}$

AIRCRAFT CHARACTERISTICS OF APP B

FIG. II - 17

RESPONSE OF OPEN-CHAIN TRACKING SYSTEM WITH TRACKING INACCURACY PREDICTION AND TIGHT-LOOP STABILIZATION OF THE RADAR ANTENNA IN THE ABSENCE OF GUST AND RADAR INTERFERENCE

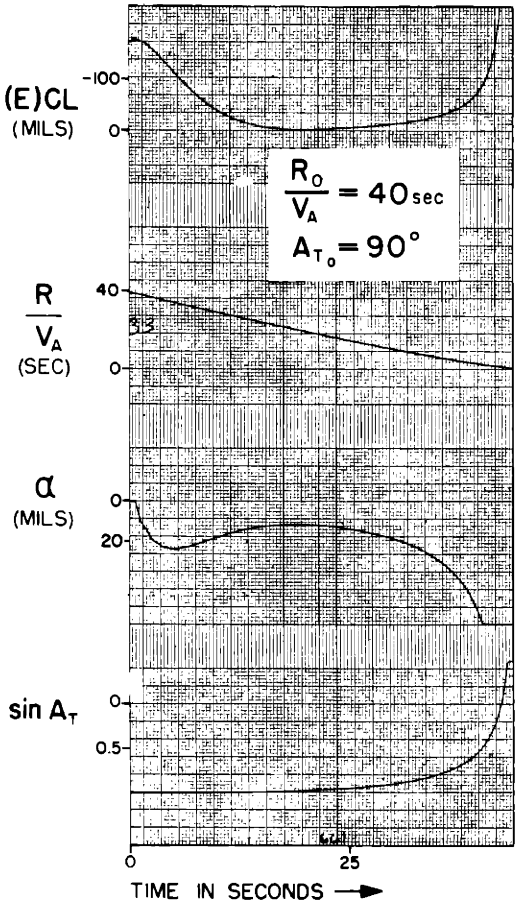

$S_{sg(P,V)}\, S_{(sm)p}\, S_{(s,r)} = 0.35$ PSR = 1.2

$S_{sg(P,V)}\, S_{(sm)i}\, S_{(s,r)} = 0$ SN = 0.50

$S_{rg}\, S_{(sm)\dot{\theta}}\, S_{(s,r)} = .026$ sec $S_{g(TL,V)}\, S_{R(V,\dot{P})} = 6.67\ \text{sec}^{-1}$

$(CT)_{(sm)} = 0$ $S_{TID}\, S_{RSS(i,\omega)} = 4.0\ \text{sec}^{-1}$

AIRCRAFT CHARACTERISTICS OF APP B

FIG. II - 18

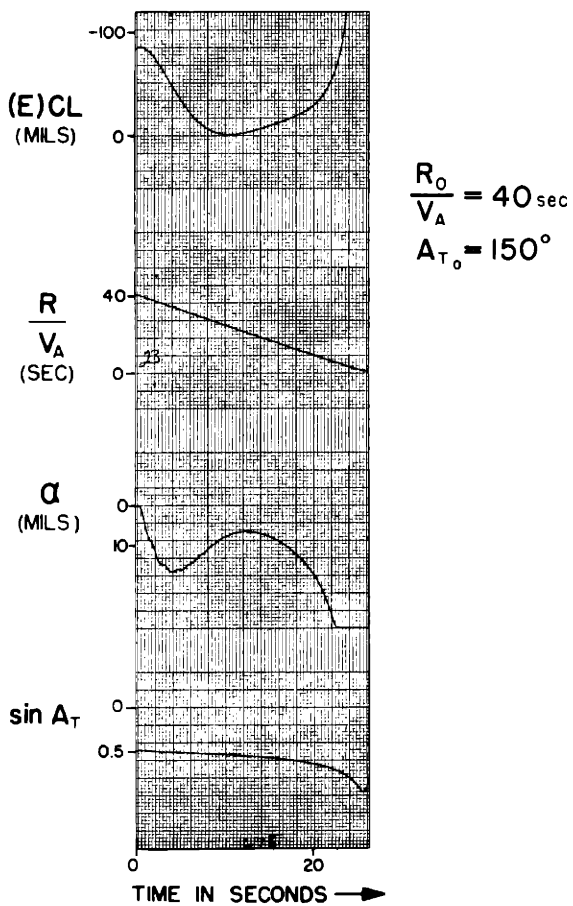

$S_{sg(P,V)}\, S_{(sm)p}\, S_{(s,r)} = 0.35$ PSR = 1.2

$S_{sg(P,V)}\, S_{(sm)i}\, S_{(s,r)} = 0$ SN = 0.25

$S_{rg}\, S_{(sm)\dot{\theta}}\, S_{(s,r)} = 0$ sec $S_{g(TL,V)}\, S_{R(V,\dot{P})} = 6.67\ \text{sec}^{-1}$

$(CT)_{(sm)} = 0$ $S_{TID}\, S_{RSS(i,\omega)} = 2.0\ \text{sec}^{-1}$

AIRCRAFT CHARACTERISTICS OF APP B

FIG. II - 19

RESPONSE OF OPEN-CHAIN TRACKING SYSTEM WITH TRACKING INACCURACY PREDICTION AND TIGHT-LOOP STABILIZATION OF THE RADAR ANTENNA IN THE ABSENCE OF GUST AND RADAR INTERFERENCE

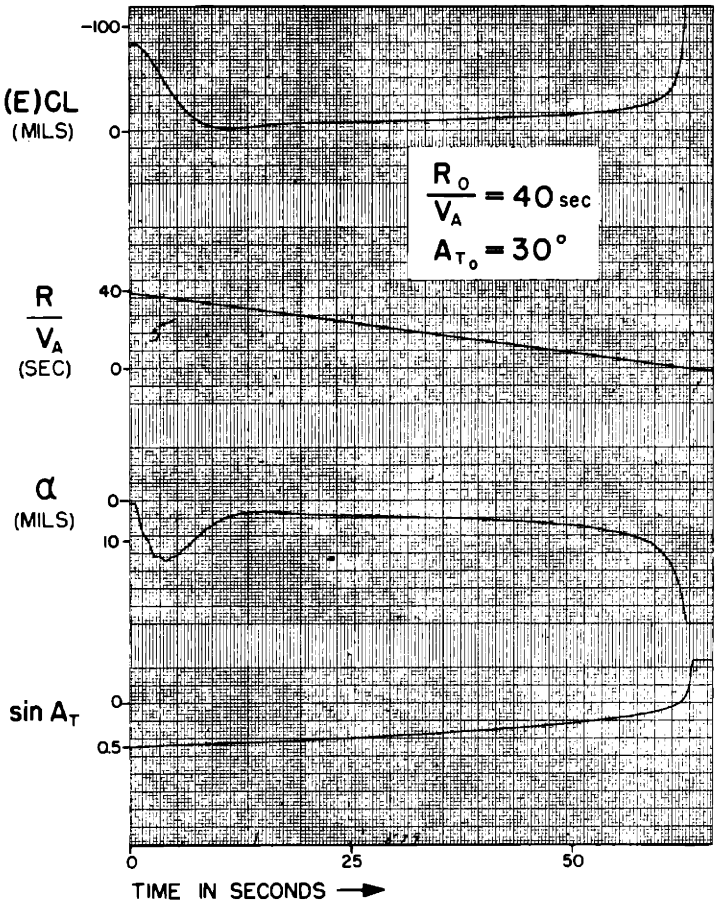

$S_{sg(P,V)}\, S_{(sm)p}\, S_{(s,r)} = 0.35$ PSR = 1.0

$S_{sg(P,V)}\, S_{(sm)i}\, S_{(s,r)} = 0$ SN = 0.25

$S_{rg}\, S_{(sm)\dot{\theta}}\, S_{(s,r)} = 0$ sec $S_{g(TL,V)}\, S_{R(V,\dot{P})} = 6.67\ \text{sec}^{-1}$

$(CT)_{(sm)} = 0$ $S_{TID}\, S_{RSS(i,\omega)} = 2.0\ \text{sec}^{-1}$

AIRCRAFT CHARACTERISTICS OF APP B

FIG. II - 20

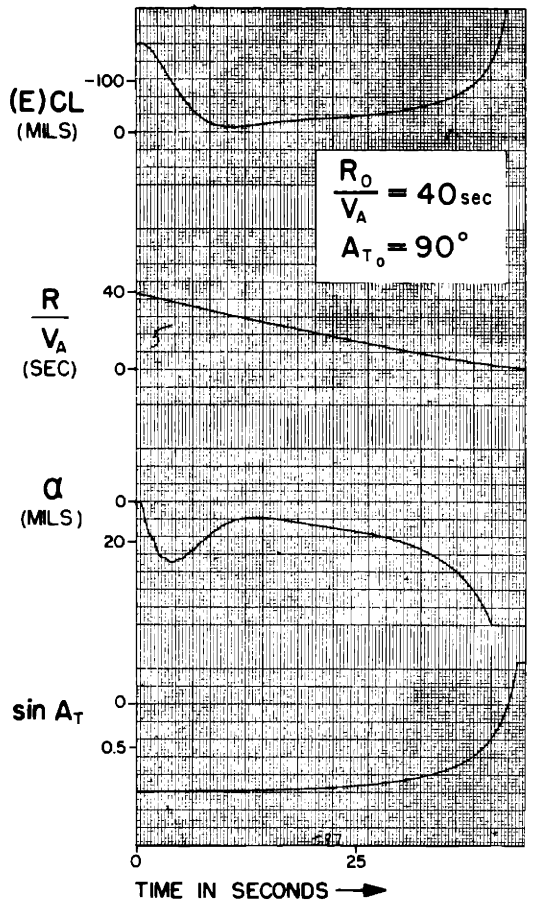

$S_{sg(P,V)}\, S_{(sm)p}\, S_{(s,r)} = 0.35$ PSR = 1.0

$S_{sg(P,V)}\, S_{(sm)i}\, S_{(s,r)} = 0$ SN = 0.25

$S_{rg}\, S_{(sm)\dot{\theta}}\, S_{(s,r)} = 0$ sec $S_{g(TL,V)}\, S_{R(V,\dot{P})} = 6.67\ \text{sec}^{-1}$

$(CT)_{(sm)} = 0$ $S_{TID}\, S_{RSS(i,\omega)} = 2.0\ \text{sec}^{-1}$

AIRCRAFT CHARACTERISTICS OF APP B

FIG. II - 21

RESPONSE OF OPEN-CHAIN TRACKING SYSTEM WITH TRACKING INACCURACY PREDICTION AND TIGHT-LOOP STABILIZATION OF THE RADAR ANTENNA IN THE ABSENCE OF GUST AND RADAR INTERFERENCE

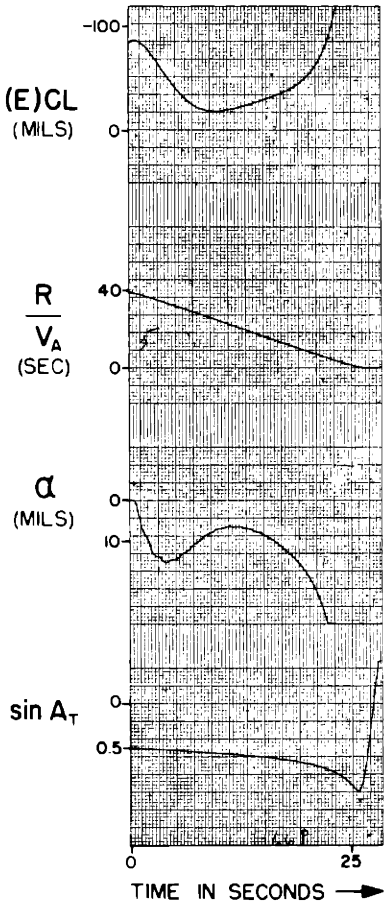

$\frac{R_0}{V_A} = 40\,\text{sec}$

$A_{T_0} = 150°$

$S_{sg(P,V)}\, S_{(sm)p}\, S_{(s,r)} = 0.35$ PSR = 1.0

$S_{sg(P,V)}\, S_{(sm)\dot{\iota}}\, S_{(s,r)} = 0$ SN = 0.25

$S_{rg}\, S_{(sm)\dot{\theta}}\, S_{(s,r)} = 0\,\text{sec}$ $S_{g(TL,V)}\, S_{R(V,\dot{P})} = 6.67\,\text{sec}^{-1}$

$(CT)_{(sm)} = 0$ $S_{TID}\, S_{RSS(\dot{\iota},\omega)} = 2.0\,\text{sec}^{-1}$

AIRCRAFT CHARACTERISTICS OF APP B

FIG. II - 22

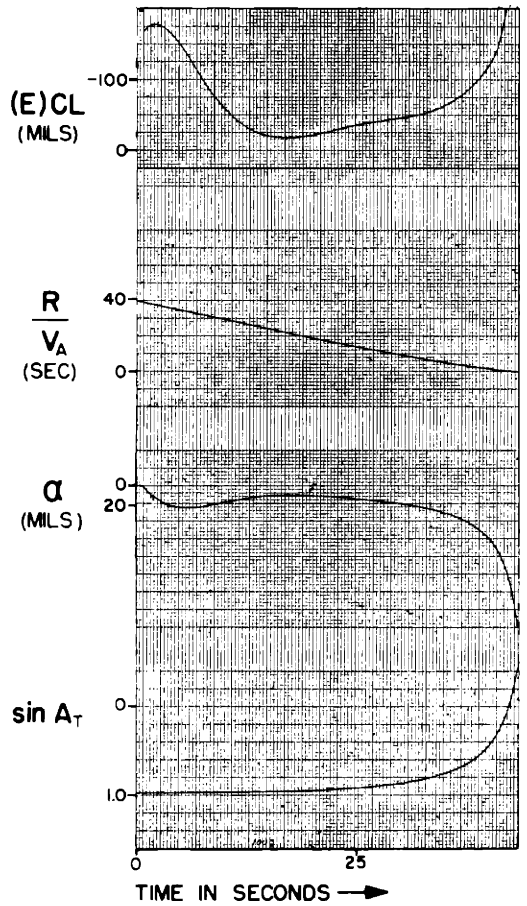

$\frac{R_0}{V_A} = 40\,\text{sec}$

$A_{T_0} = 90°$

$S_{sg(P,V)}\, S_{(sm)p}\, S_{(s,r)} = 0.20$ PSR = 1.0

$S_{sg(P,V)}\, S_{(sm)\dot{\iota}}\, S_{(s,r)} = 0$ SN = 0.35

$S_{rg}\, S_{(sm)\dot{\theta}}\, S_{(s,r)} = 0.05\,\text{sec}$ $S_{g(TL,V)}\, S_{R(V,\dot{P})} = 6.67\,\text{sec}^{-1}$

$(CT)_{(sm)} = 0$ $S_{TID}\, S_{RSS(\dot{\iota},\omega)} = 2.0\,\text{sec}^{-1}$

AIRCRAFT CHARACTERISTICS OF APP B

FIG. II - 23

RESPONSE OF OPEN-CHAIN TRACKING SYSTEM WITH TRACKING INACCURACY PREDICTION AND TIGHT-LOOP STABILIZATION OF THE RADAR ANTENNA IN THE ABSENCE OF GUST AND RADAR INTERFERENCE

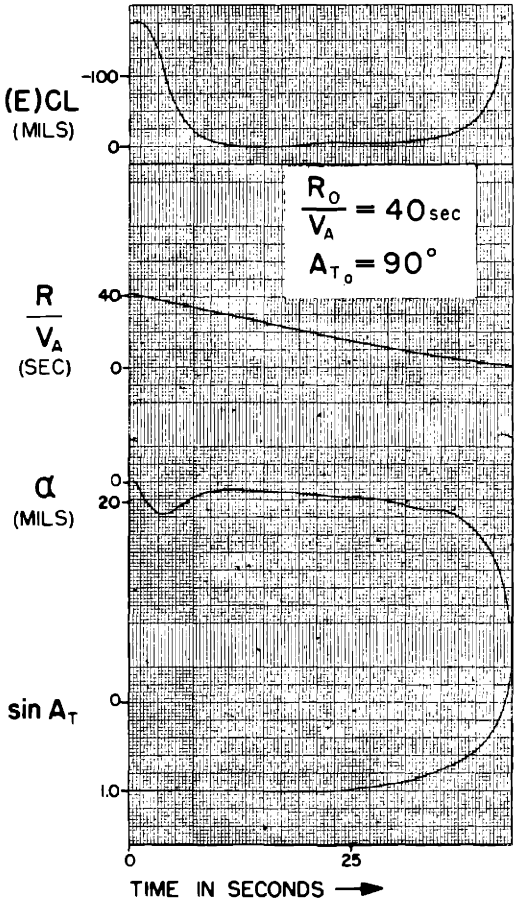

$S_{sg(P,V)}\ S_{(sm)p}\ S_{(s,r)} = 0.20$ PSR = 1.0

$S_{sg(P,V)}\ S_{(sm)i}\ S_{(s,r)} = 0.40$ SN = 0.35

$S_{rg}\ S_{(sm)\dot{\theta}}\ S_{(s,r)} = 0.05\,sec$ $S_{g(TL,V)}\ S_{R(V,\dot{\beta})} = 6.67\,sec^{-1}$

$(CT)_{(sm)} = 0$ $S_{TID}\ S_{RSS(i,\omega)} = 2.0\,sec^{-1}$

AIRCRAFT CHARACTERISTICS OF APP B

FIG. II - 24

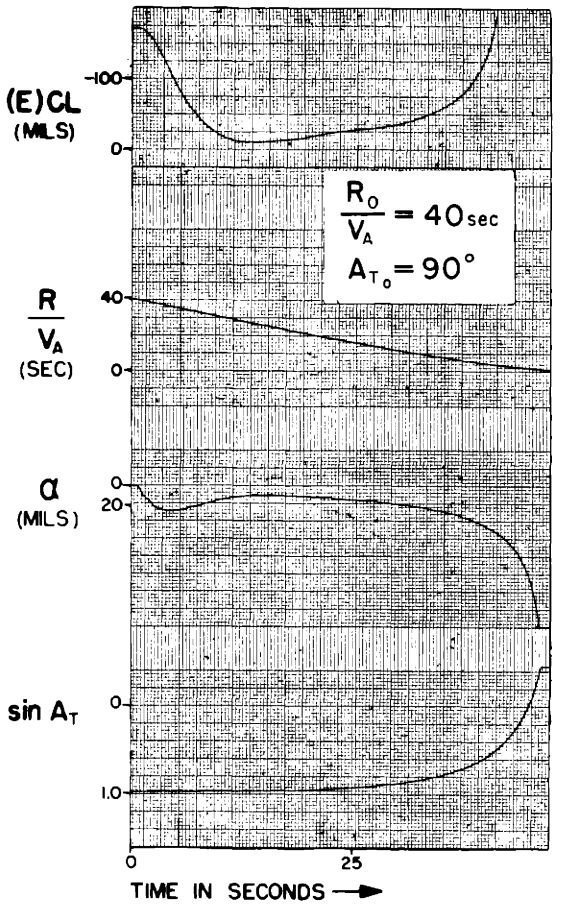

$S_{sg(P,V)}\ S_{(sm)p}\ S_{(s,r)} = 0.50$ PSR = 1.0

$S_{sg(P,V)}\ S_{(sm)i}\ S_{(s,r)} = 0$ SN = 0.35

$S_{rg}\ S_{(sm)\dot{\theta}}\ S_{(s,r)} = 0.05\,sec$ $S_{g(TL,V)}\ S_{R(V,\dot{\beta})} = 6.67\,sec^{-1}$

$(CT)_{(sm)} = 0$ $S_{TID}\ S_{RSS(i,\omega)} = 2.0\,sec^{-1}$

AIRCRAFT CHARACTERISTICS OF APP B

FIG. II - 25

RESPONSE OF OPEN-CHAIN TRACKING SYSTEM WITH TRACKING INACCURACY PREDICTION AND TIGHT-LOOP STABILIZATION OF THE RADAR ANTENNA IN THE ABSENCE OF GUST AND RADAR INTERFERENCE

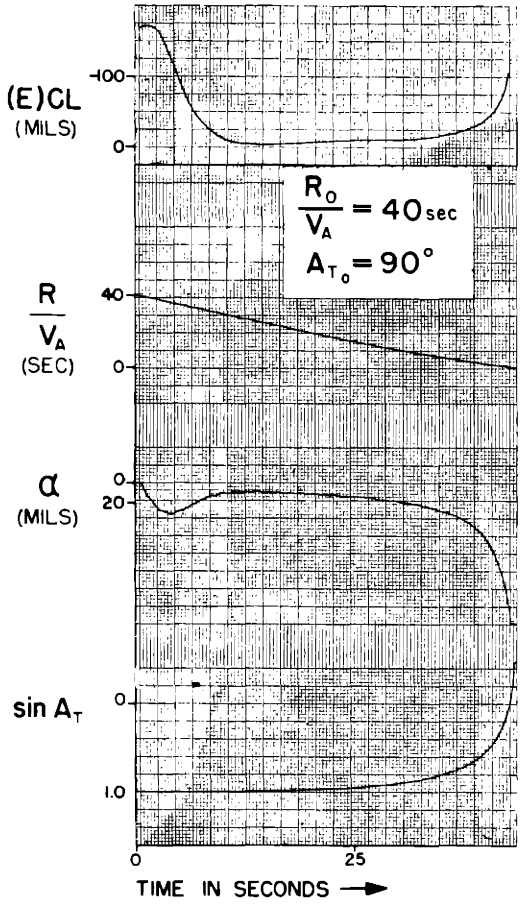

$S_{sg(P,V)}\, S_{(sm)p}\, S_{(s,r)} = 0.50$ PSR = 1.0

$S_{sg(P,V)}\, S_{(sm)\dot{\iota}}\, S_{(s,r)} = 0.40$ SN = 0.35

$S_{rg}\, S_{(sm)\dot{\theta}}\, S_{(s,r)} = 0.05\,\text{sec}$ $S_{g(TL,V)}\, S_{R(V,\dot{P})} = 6.67\,\text{sec}^{-1}$

$(CT)_{(sm)} = 0$ $S_{TID}\, S_{RSS(\dot{\iota},\omega)} = 2.0\,\text{sec}^{-1}$

AIRCRAFT CHARACTERISTICS OF APP B

FIG. II - 26

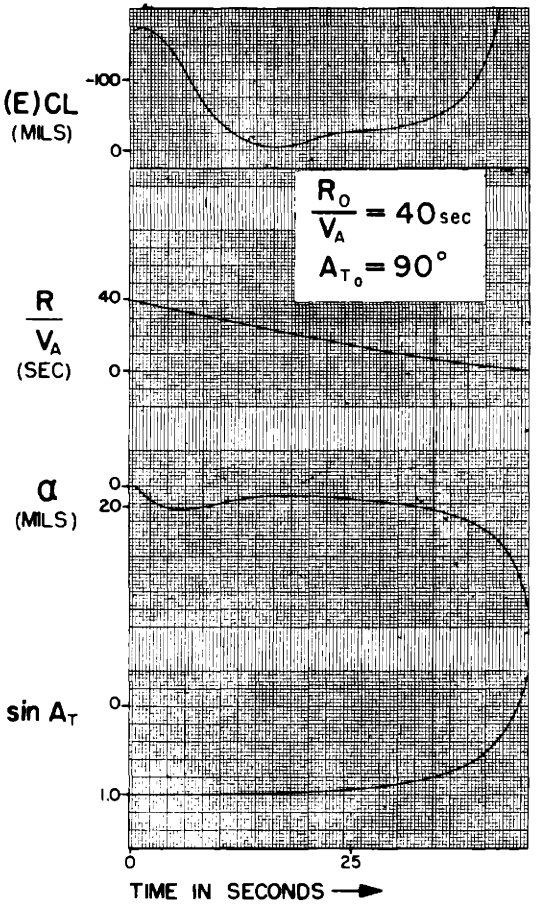

$S_{sg(P,V)}\, S_{(sm)p}\, S_{(s,r)} = 0.20$ PSR = 1.11

$S_{sg(P,V)}\, S_{(sm)\dot{\iota}}\, S_{(s,r)} = 0$ SN = 0.35

$S_{rg}\, S_{(sm)\dot{\theta}}\, S_{(s,r)} = 0.05\,\text{sec}$ $S_{g(TL,V)}\, S_{R(V,\dot{P})} = 6.67\,\text{sec}^{-1}$

$(CT)_{(sm)} = 0$ $S_{TID}\, S_{RSS(\dot{\iota},\omega)} = 2.0\,\text{sec}^{-1}$

AIRCRAFT CHARACTERISTICS OF APP B

FIG. II - 27

RESPONSE OF OPEN-CHAIN TRACKING SYSTEM WITH TRACKING INACCURACY PREDICTION AND TIGHT-LOOP STABILIZATION OF THE RADAR ANTENNA IN THE ABSENCE OF GUST AND RADAR INTERFERENCE

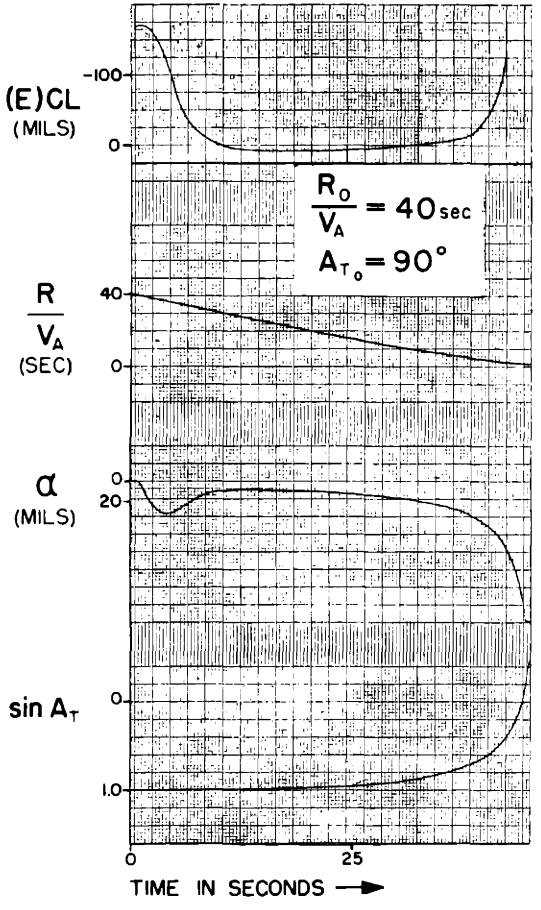

$S_{sg(P,V)}\, S_{(sm)p}\, S_{(s,r)} = 0.20$ PSR = 1.11

$S_{sg(P,V)}\, S_{(sm)i}\, S_{(s,r)} = 0.40$ SN = 0.35

$S_{rg}\, S_{(sm)\dot{\theta}}\, S_{(s,r)} = 0.05\,\text{sec}$ $S_{g(TL,V)}\, S_{R(V,\dot{P})} = 6.67\,\text{sec}^{-1}$

$(CT)_{(sm)} = 0$ $S_{TID}\, S_{RSS(i,\omega)} = 2.0\,\text{sec}^{-1}$

AIRCRAFT CHARACTERISTICS OF APP B

FIG. II - 28

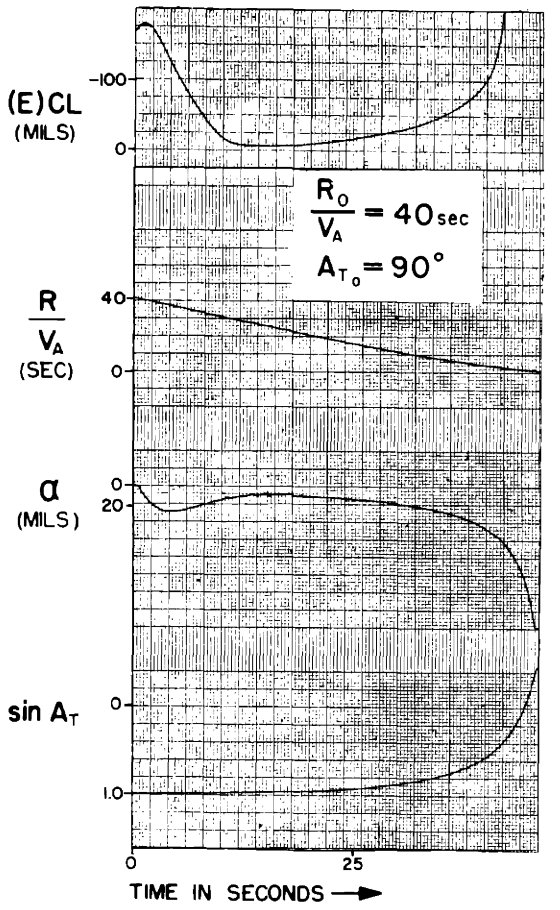

$S_{sg(P,V)}\, S_{(sm)p}\, S_{(s,r)} = 0.50$ PSR = 1.11

$S_{sg(P,V)}\, S_{(sm)i}\, S_{(s,r)} = 0$ SN = 0.35

$S_{rg}\, S_{(sm)\dot{\theta}}\, S_{(s,r)} = 0.05\,\text{sec}$ $S_{g(TL,V)}\, S_{R(V,\dot{P})} = 6.67\,\text{sec}^{-1}$

$(CT)_{(sm)} = 0$ $S_{TID}\, S_{RSS(i,\omega)} = 2.0\,\text{sec}^{-1}$

AIRCRAFT CHARACTERISTICS OF APP B

FIG. II - 29

RESPONSE OF OPEN-CHAIN TRACKING SYSTEM WITH TRACKING INACCURACY PREDICTION AND TIGHT-LOOP STABILIZATION OF THE RADAR ANTENNA IN THE ABSENCE OF GUST AND RADAR INTERFERENCE

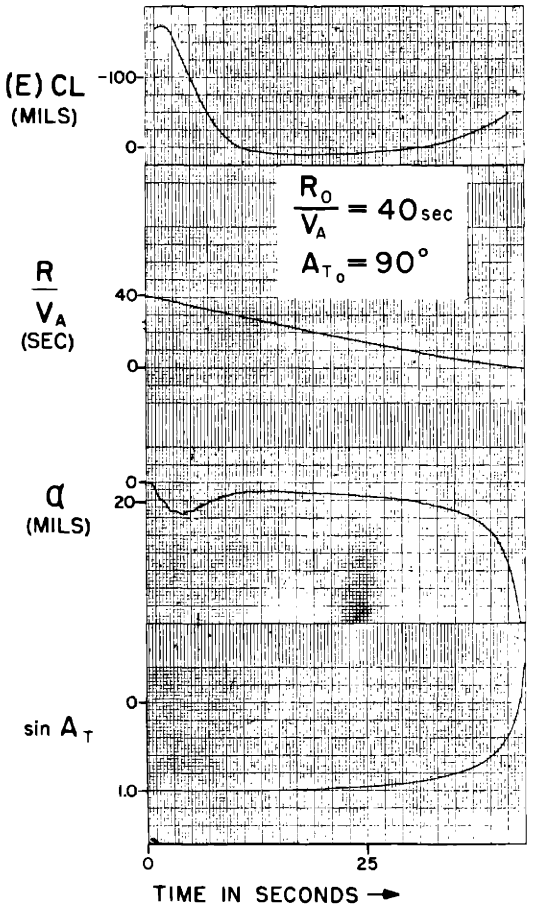

$S_{sg(P,V)}\, S_{(sm)p} S_{(s,r)} = 0.50$ PSR = 1.11

$S_{sg(P,V)}\, S_{(sm)\dot{L}}\, S_{(s,r)} = 0.40$ SN = 0.35

$S_{rg}\, S_{(sm)\dot{\theta}}\, S_{(s,r)} = 0.05\,\text{sec}$ $S_{g(TL,V)}\, S_{R(V,\dot{P})} = 6.67\,\text{sec}^{-1}$

$(CT)_{(sm)} = 0$ $S_{TID}\, S_{RSS(\dot{L},\omega)} = 2.0\,\text{sec}^{-1}$

AIRCRAFT CHARACTERISTICS OF APP B

FIG. II - 30

RESPONSE OF OPEN-CHAIN TRACKING SYSTEM WITH TRACKING INACCURACY PREDICTION AND TIGHT-LOOP STABILIZATION OF THE RADAR ANTENNA IN THE ABSENCE OF GUST AND RADAR INTERFERENCE

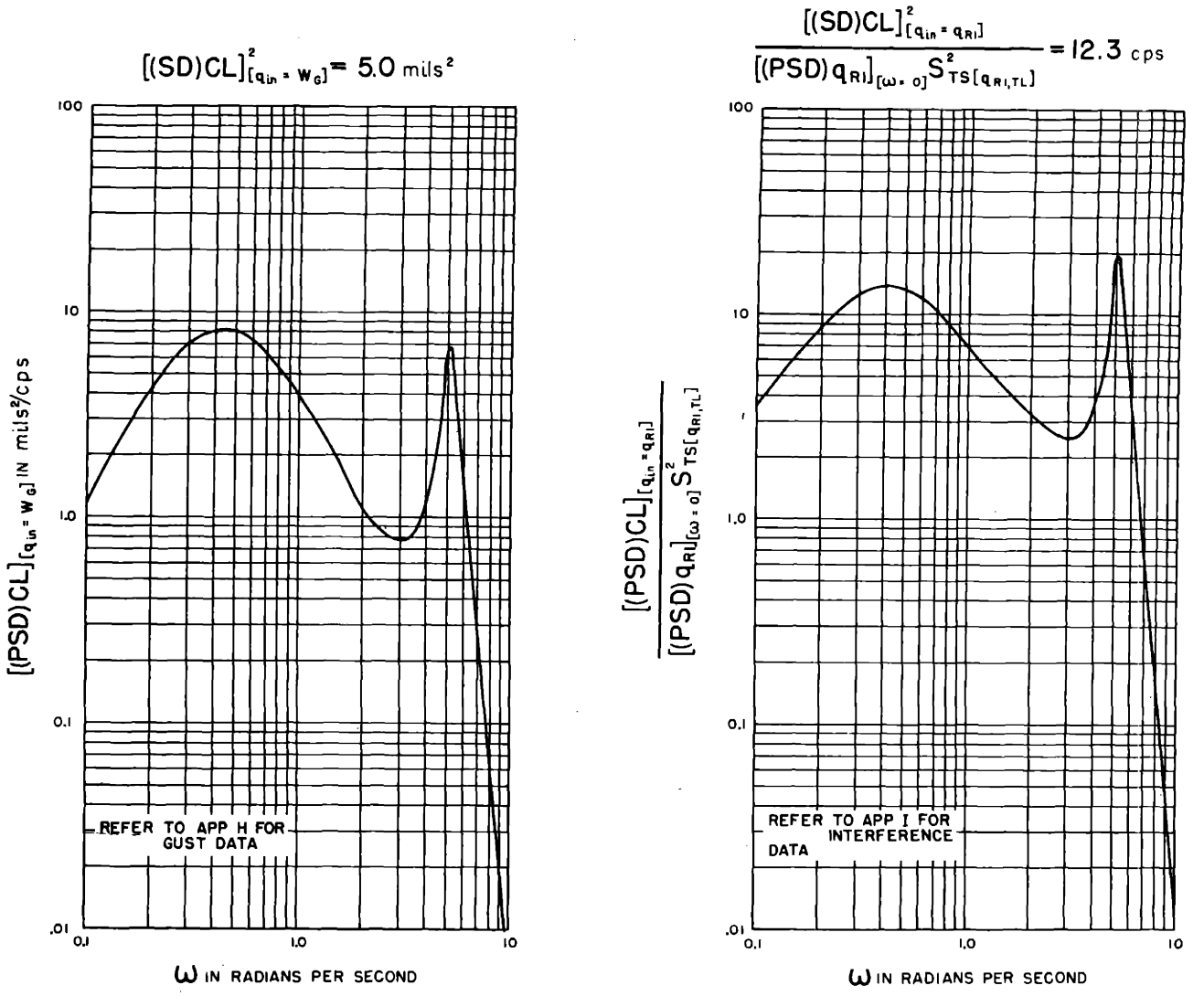

$S_{sg(P,V)}\, S_{(sm)p}\, S_{(S,r)} = 0.50$ $\quad$ $S_{P(\omega,P)} = 13.85$ sec

$S_{sg(P,V)}\, S_{(sm)i}\, S_{(S,r)} = 0$ $\quad$ $SN = 0.25$

$S_{rg}\, S_{(sm)\dot{\theta}}\, S_{(S,r)} = 0.05$ sec $\quad$ $S_{g(TL,V)}\, S_{R(V,\dot{P})} = 6.67$ sec^{-1}

$(CT)_{(sm)} = 0$ $\quad$ $S_{TID}\, S_{RSS(i,\omega)} = 2.0$ sec^{-1}

AIRCRAFT CHARACTERISTICS OF APP B

FIG II - 31 POWER SPECTRAL DENSITIES RESULTING FROM GUST AND RADAR INTERFERENCE OF OPEN-CHAIN TRACKING SYSTEM WITH TRACKING INACCURACY PREDICTION AND TIGHT-LOOP STABILIZATION OF THE RADAR ANTENNA

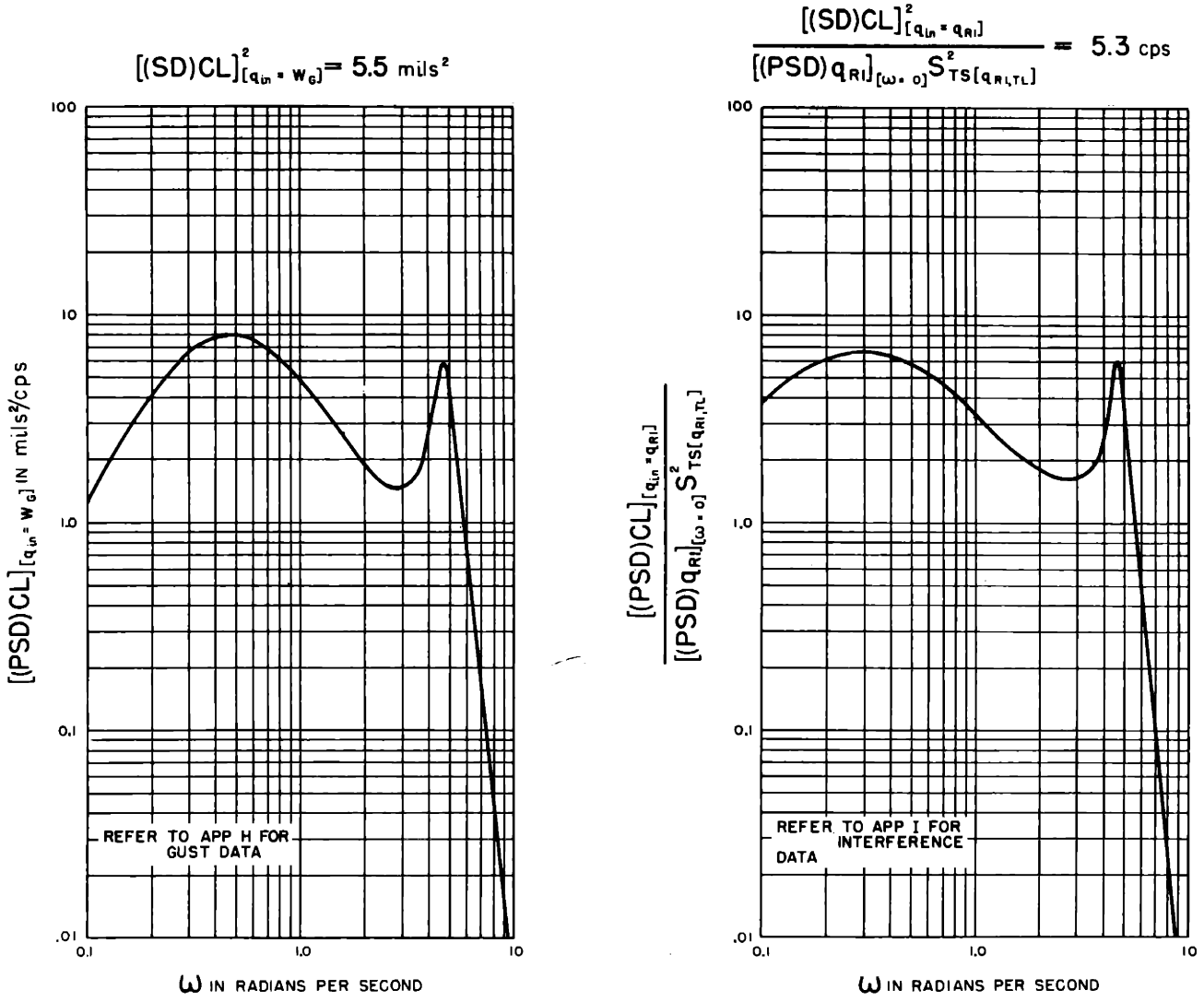

$S_{sg(P,V)}\, S_{(sm)p}\, S_{(s,r)} = 0.50$ $\quad$ $S_{P(\omega,P)} = 13.85$ sec

$S_{sg(P,V)}\, S_{(sm)i}\, S_{(s,r)} = 0$ $\quad$ $SN = 0.50$

$S_{rg}\, S_{(sm)\dot{\theta}}\, S_{(s,r)} = 0.05$ sec $\quad$ $S_{g(TL,V)}\, S_{g(V,\dot{P})} = 6.67$ sec^{-1}

$(CT)_{(sm)} = 0$ $\quad$ $S_{TID}\, S_{RSS(i,\omega)} = 2.0$ sec^{-1}

AIRCRAFT CHARACTERISTICS OF APP B

FIG II-32 POWER SPECTRAL DENSITIES RESULTING FROM GUST AND RADAR INTERFERENCE OF OPEN-CHAIN TRACKING SYSTEM WITH TRACKING INACCURACY PREDICTION AND TIGHT-LOOP STABILIZATION OF THE RADAR ANTENNA

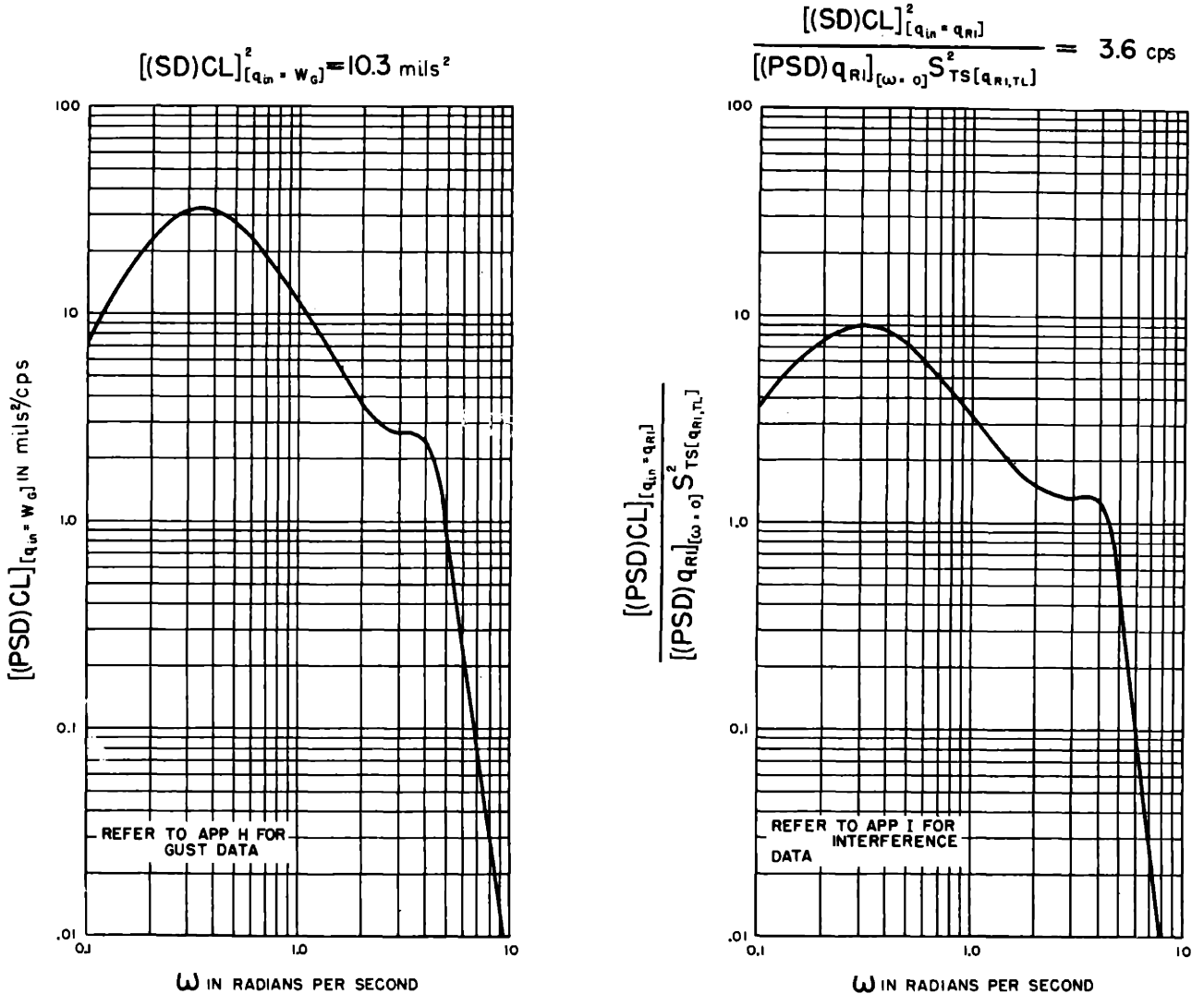

$S_{sg(P,V)}\, S_{(sm)p}\, S_{(S,r)} = 0.20$ $\quad$ $S_{P(\omega,P)} = 13.85$ sec

$S_{sg(P,V)}\, S_{(sm)i}\, S_{(S,r)} = 0$ $\quad$ $SN = 0.25$

$S_{rg}\, S_{(sm)\dot{\theta}}\, S_{(S,r)} = 0.05$ sec $\quad$ $S_{g(TL,V)}\, S_{R(V,\dot{P})} = 6.67$ sec^{-1}

$(CT)_{(sm)} = 0$ $\quad$ $S_{TID}\, S_{RSS(i,\omega)} = 2.0$ sec^{-1}

AIRCRAFT CHARACTERISTICS OF APP B

FIG II-33. POWER SPECTRAL DENSITIES RESULTING FROM GUST AND RADAR INTERFERENCE OF OPEN-CHAIN TRACKING SYSTEM WITH TRACKING INACCURACY PREDICTION AND TIGHT-LOOP STABILIZATION OF THE RADAR ANTENNA

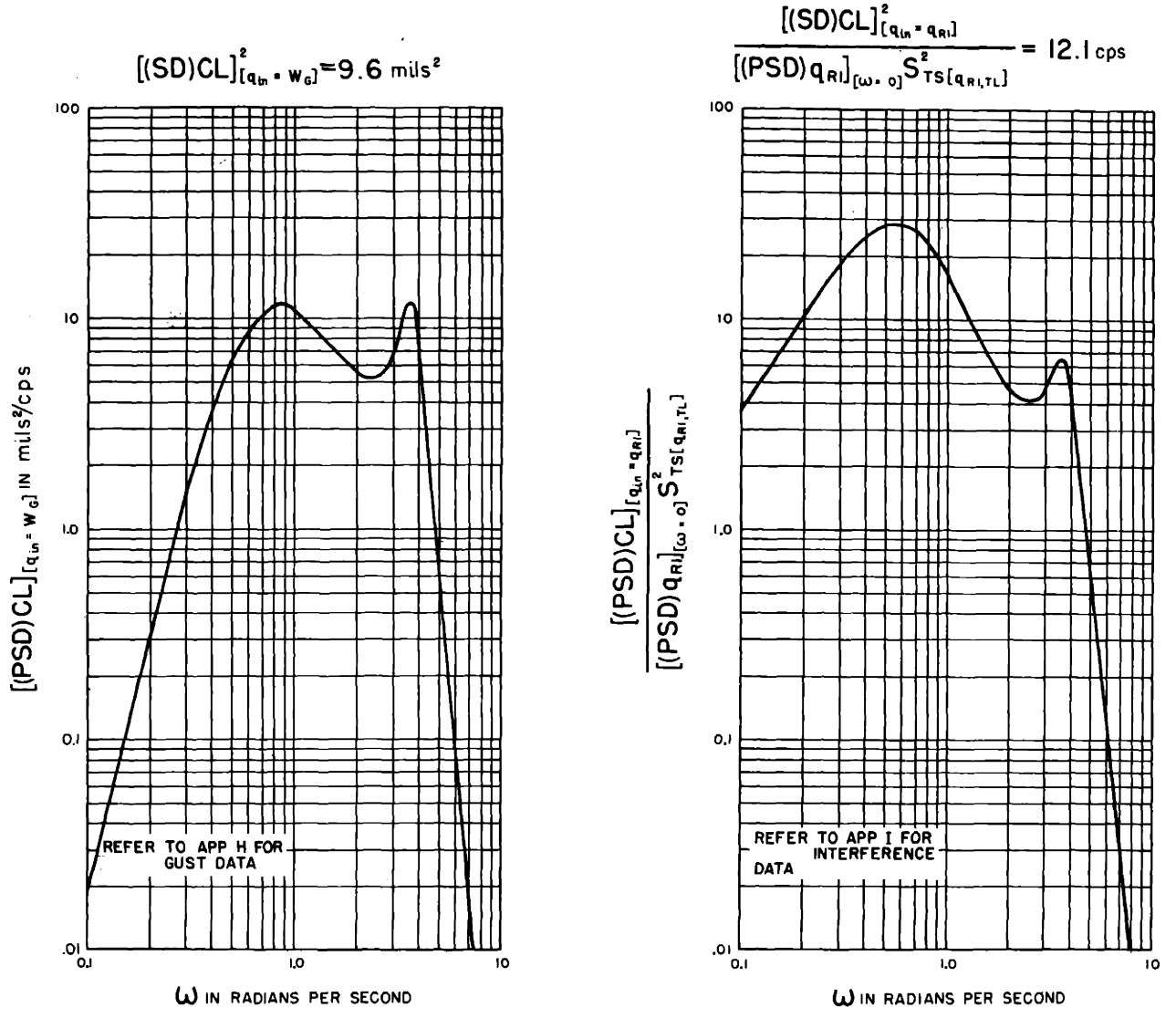

$S_{sg(P,V)}\, S_{(sm)p}\, S_{(S,r)} = 0.20$ $\quad$ $S_{P(\omega,P)} = 13.85$ sec

$S_{sg(P,V)}\, S_{(sm)i}\, S_{(S,r)} = 0.40$ sec^{-1} $\quad$ $SN = 0.25$

$S_{rg}\, S_{(sm)\dot{\theta}}\, S_{(S,r)} = 0.05$ sec $\quad$ $S_{g(TL,V)}\, S_{R(V,\dot{P})} = 6.67$ sec^{-1}

$(CT)_{(sm)} = 0$ $\quad$ $S_{TID}\, S_{RSS(i,\omega)} = 2.0$ sec^{-1}

AIRCRAFT CHARACTERISTICS OF APP B

FIG II-34 POWER SPECTRAL DENSITIES RESULTING FROM GUST AND RADAR INTERFERENCE OF OPEN-CHAIN TRACKING SYSTEM WITH TRACKING INACCURACY PREDICTION AND TIGHT-LOOP STABILIZATION OF THE RADAR ANTENNA

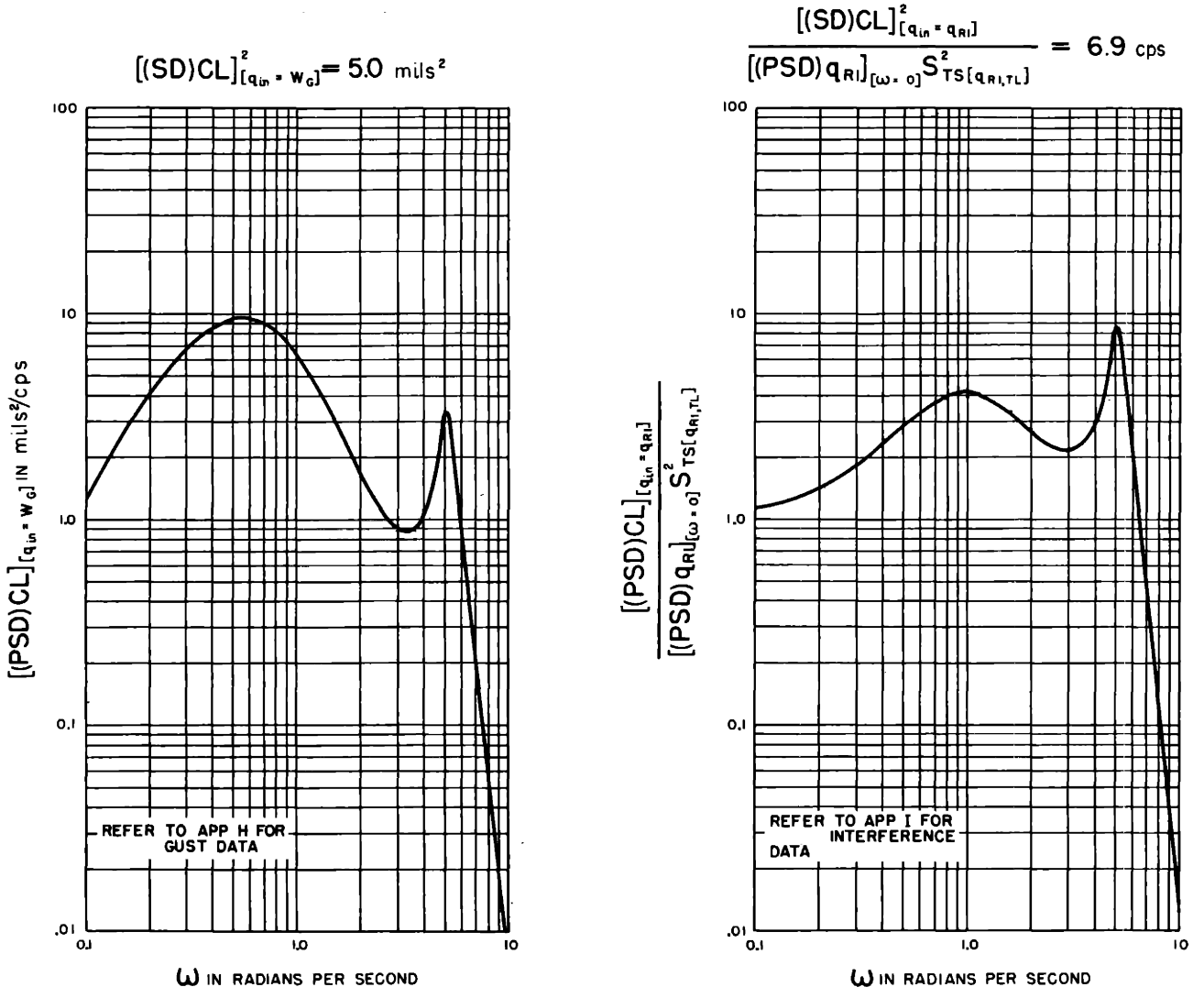

$S_{sg(P,V)}\, S_{(sm)p}\, S_{(s,r)} = 0.50$ $\quad$ $S_{P(\omega,P)} = 2.77$ sec

$S_{sg(P,V)}\, S_{(sm)i}\, S_{(s,r)} = 0$ $\quad$ $SN = 0.25$

$S_{rg}\, S_{(sm)\theta}\, S_{(s,r)} = 0.05$ sec $\quad$ $S_{g(TL,V)}\, S_{R(V,\dot{P})} = 6.67$ sec^{-1}

$(CT)_{(sm)} = 0$ $\quad$ $S_{TID}\, S_{RSS(i,\omega)} = 2.0$ sec^{-1}

AIRCRAFT CHARACTERISTICS OF APP B

FIG II-35 POWER SPECTRAL DENSITIES RESULTING FROM GUST AND RADAR INTERFERENCE OF OPEN CHAIN TRACKING SYSTEM WITH TRACKING INACCURACY PREDICTION AND TIGHT LOOP STABILIZATION OF THE RADAR ANTENNA

CHAPTER III

CLOSED-LOOP TRACKING SYSTEM WITH CONTROLLED-LINE PREDICTION

A functional diagram of the closed-loop tracking system with controlled-line prediction is contained in Fig. III-1. The response of this tracking system in the absence of gust and radar interference is shown in Fig. III-2 through III-46, and the effect of gust and radar interference is presented in the form of power spectral densities in Fig. III-47 through III-57.

The results presented in this chapter were obtained by using Eq. B-8 and B-9 to represent the performance of the aircraft, supplemented with the following differential equations, which are derivedin Appendices C, D, and E:
For the prediction computer –

$$S_{p(W,P)}[\,1 + SN]\,S_{RAS}\,\dot{V}_{PC} + S_{RAS}\,V_{PC} = S_{p(W,P)}{}^{W}CL \qquad \text{III-1}$$

where

$$S_{p(W,P)} = (PSR)\,\frac{R}{V_{p(av)} - V_A} \qquad \text{III-2}$$

For the radar antenna servo –

$$(CT)_R\,\dot{P}_R + P_R = S_{RAS}\,V_{PC} \qquad \text{III-3}$$

and for the tracking inaccuracy detector signal modifier, elevator servo, and rigging –

$$(CT)_{sm}\,\dot{\delta} + \delta = S_{TID}\,S_{(sm)p}S_{(s,r)}[(C)TL] \qquad \text{III-4}$$

in which

$$(C)TL = LS + P_R - CL \qquad \text{III-5}$$

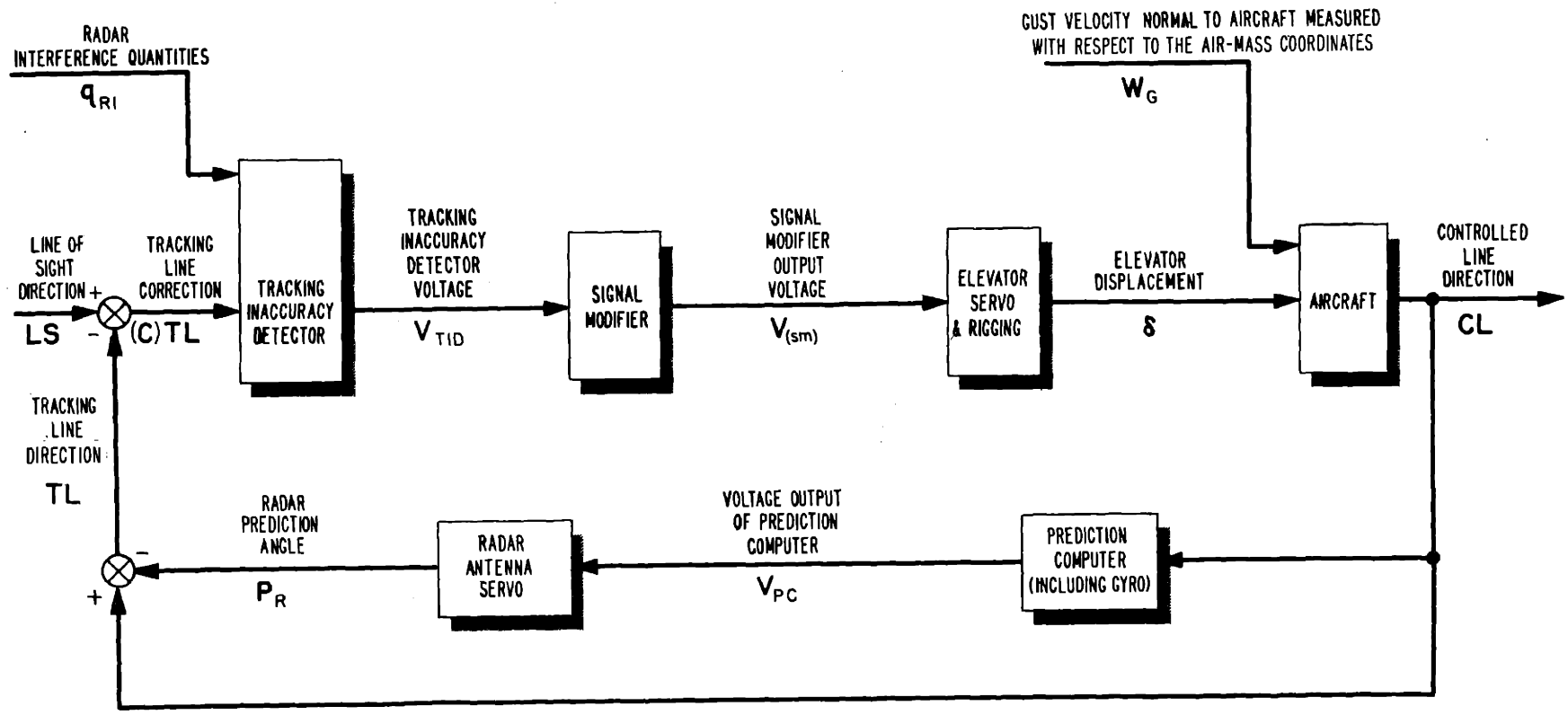

FIG III-1 FUNCTIONAL DIAGRAM OF CLOSED-LOOP TRACKING SYSTEM WITH CONTROLLED LINE PREDICTION

In closed-loop tracking systems, computation and tracking are carried out in cyclic fashion. The computation is based on the angular velocity of the controlled line required in the process of tracking the target. The prediction computer in the tracking system discussed in this chapter includes a gyro that provides an output torque proportional to the angular velocity of the controlled line about the elevation axis. The output from the prediction computer is a voltage that is used as the input to the radar antenna servo. Under steady-state conditions, the radar prediction angle is equal to the product of the voltage from the prediction computer and the sensitivity of the radar antenna servo, S_{RAS}. In order to express the output from the prediction computer in angular units, the prediction computer voltage, V_{PC}, is multiplied by the radar antenna servo sensitivity in Eq. III-1. A comparison of Eq. III-1 with Eq. I-2 shows that the damping in the computer is greater in a closed-loop tracking system than in an open-chain system in the ratio of (1 + SN) to SN. The stability number is defined in Appendix D in such a manner that all systems are unstable when the stability number has a negative value. With a closed-loop tracking system, the tracking line must move upward with respect to the line of sight when the controlled line is moved upward, even though the tracking line must move downward with respect to the interceptor aircraft for the purpose of introducing lead. This fact accounts for the (1 + SN) term in Eq. III-1. When the stability number is positive, the tracking line moves with the proper sense, but when it is negative the tracking line moves in a direction opposite to that of the controlled line. A complete discussion of this effect along with a consideration of cross roll is contained in Appendix D for both closed-loop and open-chain systems.

Equation III-3 is the performance equation for the radar antenna servo drive indicating a first-order lag proportional to the radar characteristic time, $(CT)_R$. The effect of this lag on the performance of the tracking system is small, as the lag serves only to smooth the tracking line motion, thereby increasing the stability of the system. This effect is different in an open-chain system, which becomes unstable when the radar antenna servo lags are large.

In the tracking system discussed in this chapter, errors in tracking are detected by the radar receiver, and proportional voltages are transmitted to the signal modifier. In order to investigate the possibility of filtering radar interference effects, the signal modifier has a first-order lag with character-

istic time, $(CT)_{sm}$. The output from the signal modifier is the input to the elevator servo, which actuates the elevator. The signal modifier characteristic time can also be used in the analysis to represent the effect of lags in the elevator servo and rigging. Pitch rate feedback is not necessary in this system; hence, a pitch rate gyro is not included.

The response of this system to a variety of tactical situations was determined with different combinations of the stability number and the forward gain. Values of the stability number of .25, .50, and .75 were used, as were gains of 1.0, 1.5, and 1.94, leading to nine possible combinations. Figures III-2 through III-10 show the response during a tail attack with the ratio of initial range to aircraft velocity of 40 seconds. With a stability number of .25, the controlled-line error has an overshoot of between 5 and 10 mils in each case. With a stability number of .50, the response appears equivalent to a critically damped second-order system, and with a value of .75 the response appears overdamped. Hence it can be seen that the optimum value for the stability number lies between .25 and .50. An increase in the forward gain reduces the amount of overshoot when the stability number is .25. An increase in the forward gain also introduces an underdamped oscillation at a frequency a little less than one cycle per second. This oscillation is most pronounced with a stability number of .75, as can be seen from Fig. III-10. With a stability number of .75, the tracking line motion is 43 percent of the controlled-line motion; whereas, with a stability number of .25, the tracking line motion is only 20 percent of the controlled-line motion. Hence, with a larger stability number, the loop gain is effectively increased by a factor of 2, giving rise to the oscillatory mode.

The same values of stability number and gain are used in the beam attacks of Fig. III-11 through III-19 with a ratio of initial range to aircraft velocity of 40 seconds. Again, the optimum value for the stability number appears to lie between .25 and .50. The controlled-line error at short range is reduced by an increase in the gain. For example, when the ratio of range to aircraft velocity is two seconds, corresponding to a range of 1400 feet, the error is 26 mils with a gain of 1.0, 13 mils with a gain of 1.5, and 10 mils with a gain of 1.94.

Figures III-20 through III-28 show the errors in a head-on attack. With a stability number of .25, the overshoot is greater than in the beam and tail attacks. With a stability number of .75, the ratio of range to aircraft velocity

is less than 15 seconds before a solution is reached. For head-on attacks, the angular velocity of the controlled line becomes greater as the range decreases, and consequently the controlled-line error is large.

The effect of decreasing the initial range is demonstrated in Fig. III-29 through III-37 for a tail attack. With a stability number of .25, a long-period oscillation develops that requires nearly 20 seconds to damp to zero, taking less time with the higher gains. For this range, the optimum stability number is approximately .5, which is larger than required with a ratio of initial range to aircraft velocity of 40 seconds. These figures also show that the controlled-line error at a given range near the target depends on the initial conditions, even though the tracking time is several times the solution time.

For example at a range to aircraft velocity of 2 seconds the controlled-line error is 4.5 mils for an initial range to aircraft velocity of 20 seconds whereas it is only 3.0 mils for an initial range of 40 seconds. The reason is simply that the target angle is larger at all ranges in the first case than in the second. The increased target angle gives a larger angular velocity of the line of sight and consequently a larger forced error.

It can be seen from Fig. III-38 and III-39 that the signal modifier characteristic time does not affect the controlled-line error. From Fig. III-40, III-41 and III-42 it can be seen that when the prediction sensitivity ratio is 1 there is a controlled-line error at all ranges. Finally, from Fig. III-43, III-44, and III-45 it can be seen that with a ratio of initial range to aircraft velocity of 40 seconds and with an initial target angle of 90 degrees, a stability number of .35 gives optimum results.

The power spectral densities resulting from gust and radar interference are plotted as functions of frequency in Fig. III-47 through III-57. Were it not for a resonant effect at 4 radians per second, increasing the gain and increasing the stability number would have the effect of reducing the standard deviation of the controlled line resulting from gust interference and from radar interference. However, when the gain is 1.94 and the stability number is .75, the system is so close to instability that the effect of the interference in the region from 3 radians per second to six radians per second becomes appreciable in comparison with the interference at lower frequencies.

It can be seen from Fig. III-56, III-50, and III-57 that the characteristic time of the signal modifier has an appreciable effect on the standard deviation of the controlled line. In these three figures the characteristic

time is 0, .3, and .6 second, respectively, and the standard deviation of the controlled line resulting from gusts is 2.3, 2.9, and 3.4 mils. On the other hand, the standard deviation of the controlled line resulting from radar interference is maximum, with a signal modifier characteristic time of .3. It is felt that the results in Fig. III-56 represent nearly the optimum that can be obtained with a closed-loop tracking system with controlled-line prediction.

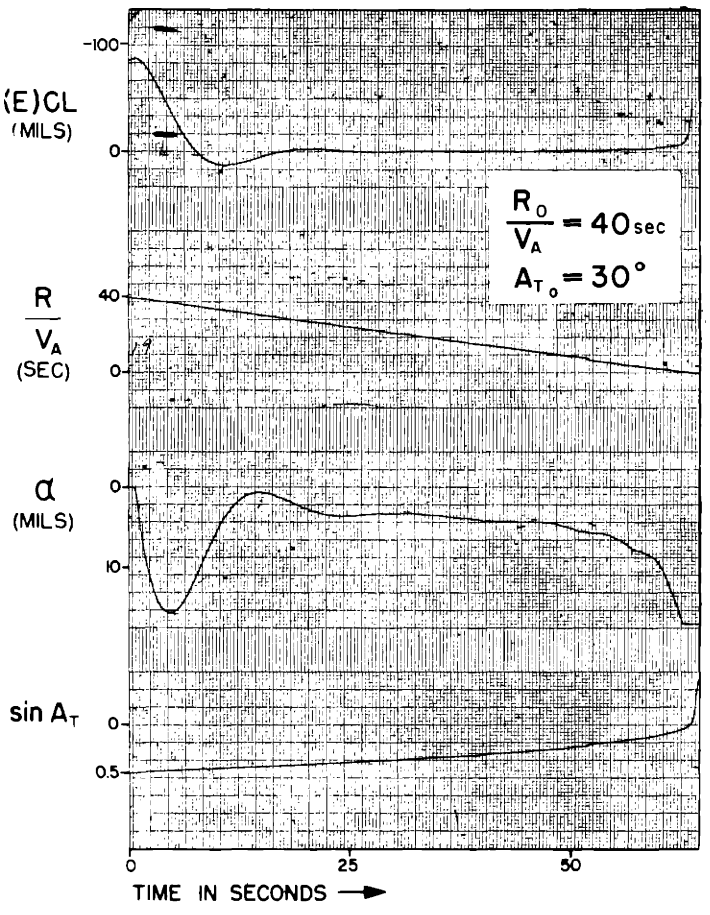

$S_{TID}\ S_{(sm)p}\ S_{(s,r)} = -1.00$ PSR = 1.11

$S_{TID}\ S_{(sm)i}\ S_{(s,r)} = 0$ SN = 0.25

$(CT)_{(sm)} = 0.30$ sec $(CT)_R = 0.15$ sec

AIRCRAFT CHARACTERISTICS OF APP B

FIG III - 2

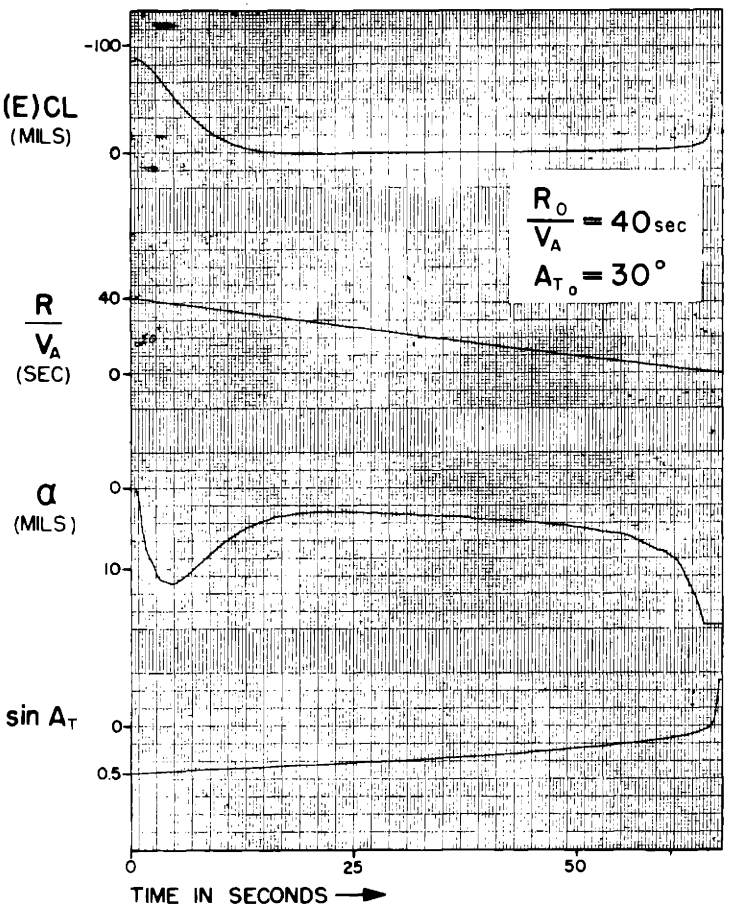

$S_{TID}\ S_{(sm)p}\ S_{(s,r)} = -1.00$ PSR = 1.11

$S_{TID}\ S_{(sm)i}\ S_{(s,r)} = 0$ SN = 0.50

$(CT)_{(sm)} = 0.30$ sec $(CT)_R = 0.15$ sec

AIRCRAFT CHARACTERISTICS OF APP B

FIG III - 3

RESPONSE OF CLOSED-LOOP TRACKING SYSTEM WITH CONTROLLED-LINE PREDICTION IN THE ABSENCE OF GUST AND RADAR INTERFERENCE

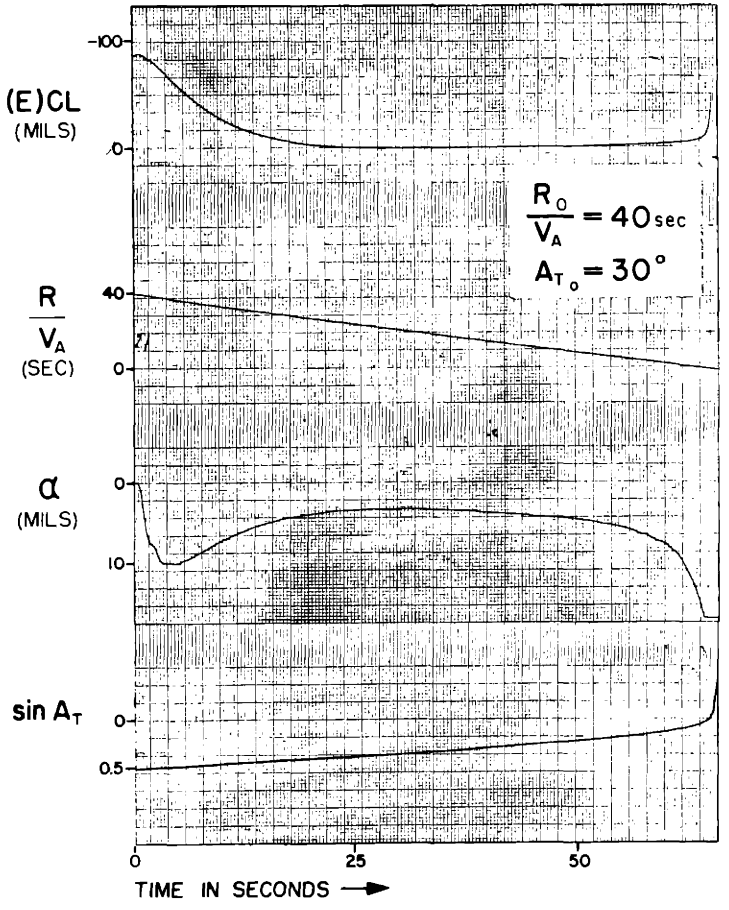

$S_{TID}\ S_{(sm)p}\ S_{(s,r)} = -1.00$ PSR = 1.11

$S_{TID}\ S_{(sm)i}\ S_{(s,r)} = 0$ SN = 0.75

$(CT)_{(sm)} = 0.30$ sec $(CT)_R = 0.15$ sec

AIRCRAFT CHARACTERISTICS OF APP B

FIG III - 4

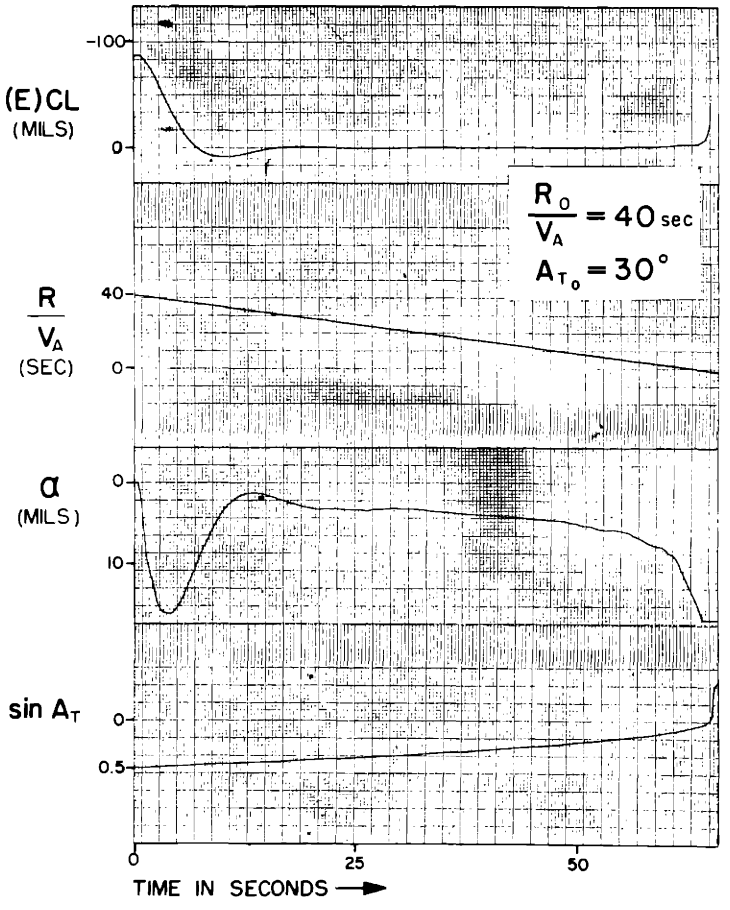

$S_{TID}\ S_{(sm)p}\ S_{(s,r)} = -1.50$ PSR = 1.11

$S_{TID}\ S_{(sm)i}\ S_{(s,r)} = 0$ SN = 0.25

$(CT)_{(sm)} = 0.30$ sec $(CT)_R = 0.15$ sec

AIRCRAFT CHARACTERISTICS OF APP B

FIG III - 5

RESPONSE OF CLOSED-LOOP TRACKING SYSTEM WITH CONTROLLED-LINE PREDICTION IN THE ABSENCE OF GUST AND RADAR INTERFERENCE

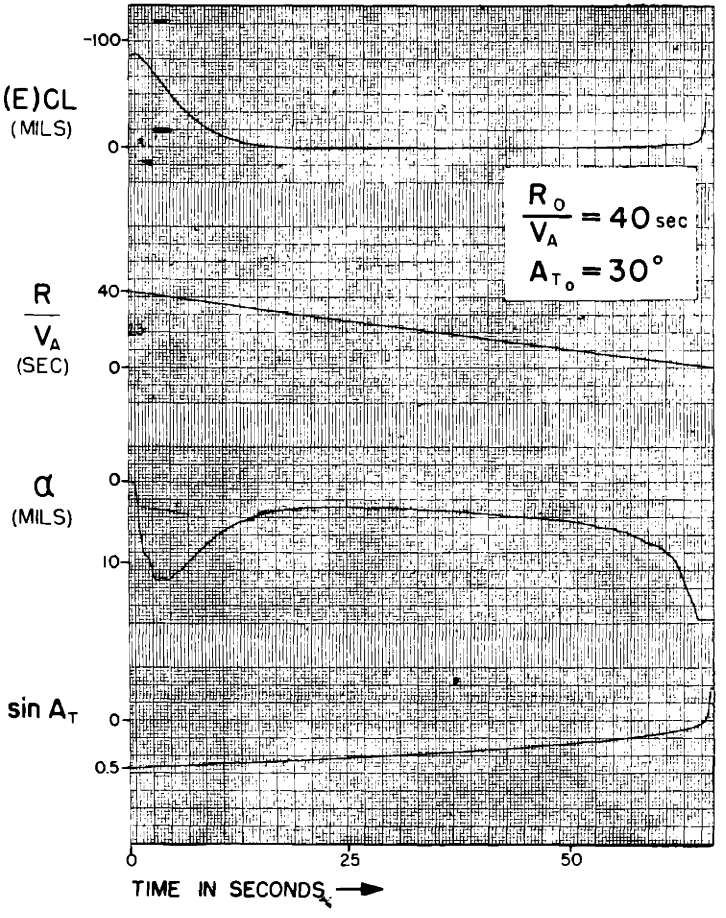

$S_{TID}\ S_{(sm)p}\ S_{(s,r)} = -1.50$ PSR = 1.11

$S_{TID}\ S_{(sm)i}\ S_{(s,r)} = 0$ SN = 0.50

$(CT)_{(sm)} = 0.30$ sec $(CT)_R = 0.15$ sec

AIRCRAFT CHARACTERISTICS OF APP B

FIG III - 6

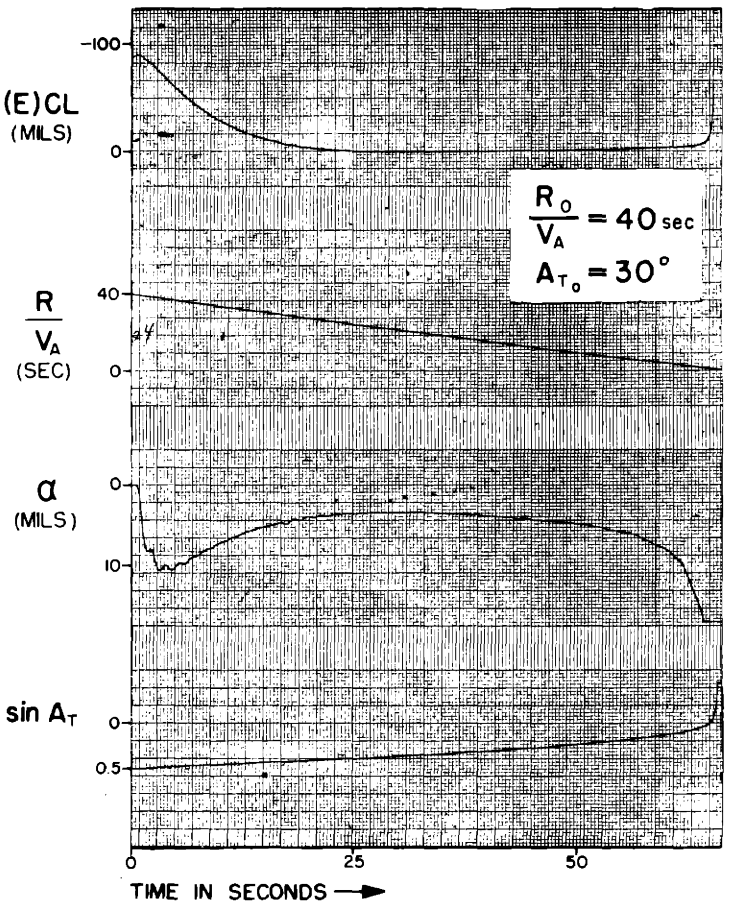

$S_{TID}\ S_{(sm)p}\ S_{(s,r)} = -1.50$ PSR = 1.11

$S_{TID}\ S_{(sm)i}\ S_{(s,r)} = 0$ SN = 0.75

$(CT)_{(sm)} = 0.30$ sec $(CT)_R = 0.15$ sec

AIRCRAFT CHARACTERISTICS OF APP B

FIG III - 7

RESPONSE OF CLOSED-LOOP TRACKING SYSTEM WITH CONTROLLED-LINE PREDICTION IN THE ABSENCE OF GUST AND RADAR INTERFERENCE

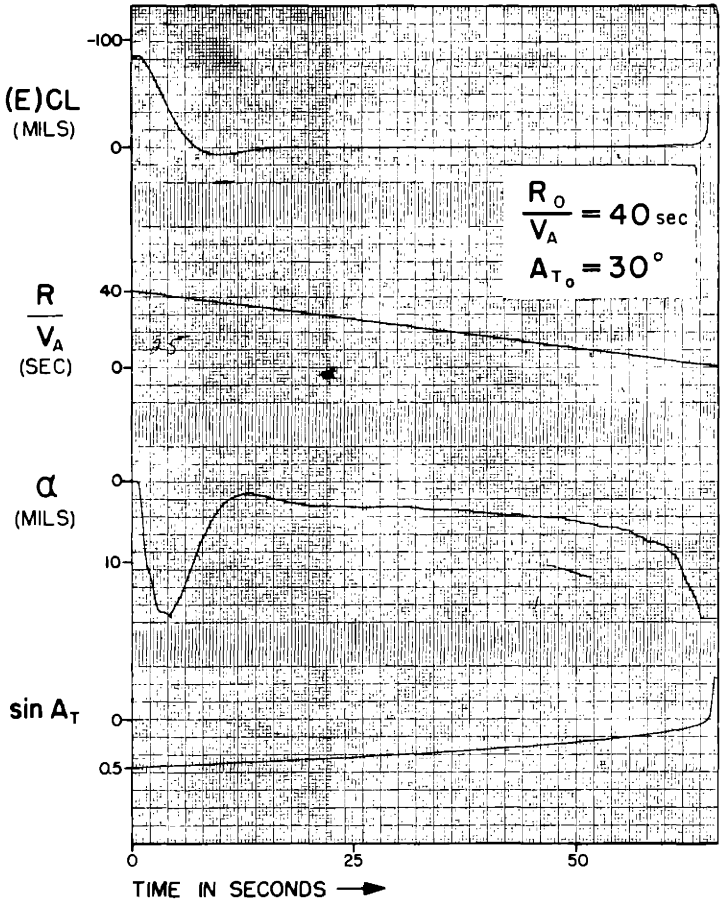

$S_{TID}\ S_{(sm)p}\ S_{(s,r)} = -1.94$ PSR = 1.11

$S_{TID}\ S_{(sm)i}\ S_{(s,r)} = 0$ SN = 0.25

$(CT)_{(sm)} = 0.30$ sec $(CT)_R = 0.15$ sec

AIRCRAFT CHARACTERISTICS OF APP B

FIG III - 8

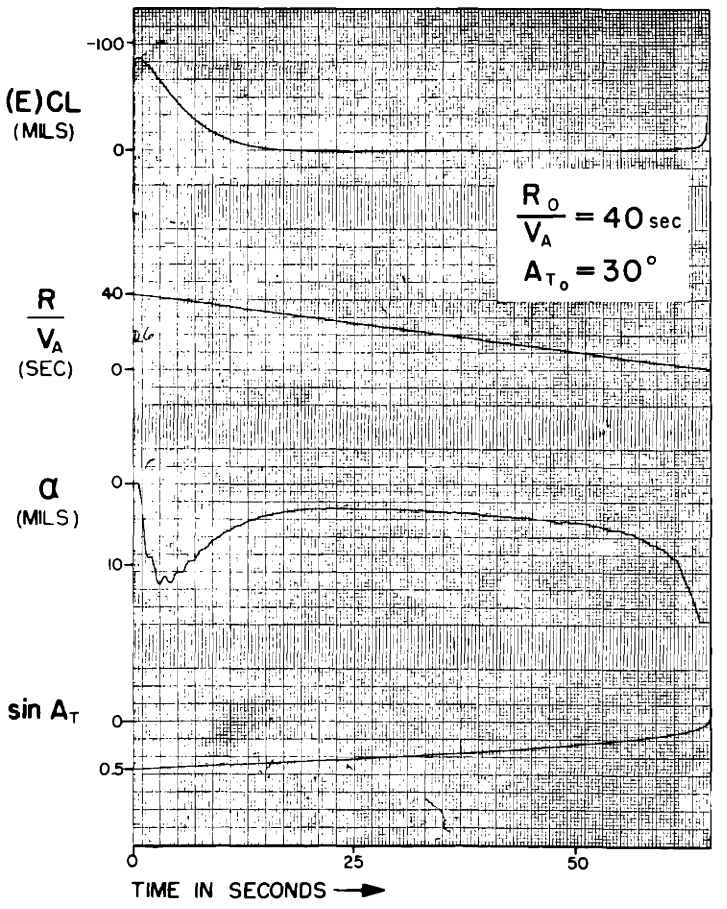

$S_{TID}\ S_{(sm)p}\ S_{(s,r)} = -1.94$ PSR = 1.11

$S_{TID}\ S_{(sm)i}\ S_{(s,r)} = 0$ SN = 0.50

$(CT)_{(sm)} = 0.30$ sec $(CT)_R = 0.15$ sec

AIRCRAFT CHARACTERISTICS OF APP B

FIG III - 9

RESPONSE OF CLOSED-LOOP TRACKING SYSTEM WITH CONTROLLED-LINE PREDICTION IN THE ABSENCE OF GUST AND RADAR INTERFERENCE

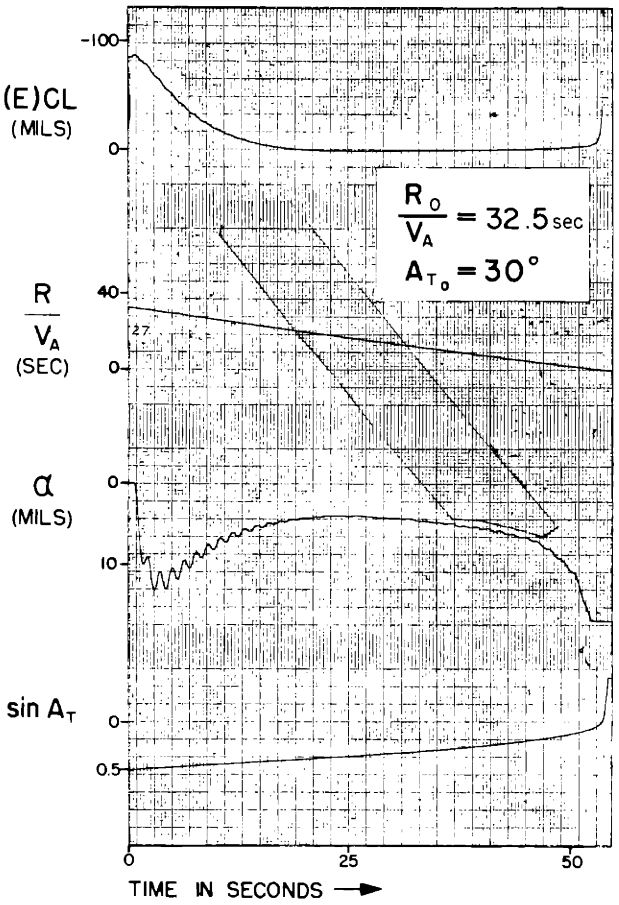

$S_{TID}\ S_{(sm)p}\ S_{(s,r)} = -1.94$ PSR = 1.11

$S_{TID}\ S_{(sm)i}\ S_{(s,r)} = 0$ SN = 0.75

$(CT)_{(sm)} = 0.30$ sec $(CT)_R = 0.15$ sec

AIRCRAFT CHARACTERISTICS OF APP B

FIG III - 10

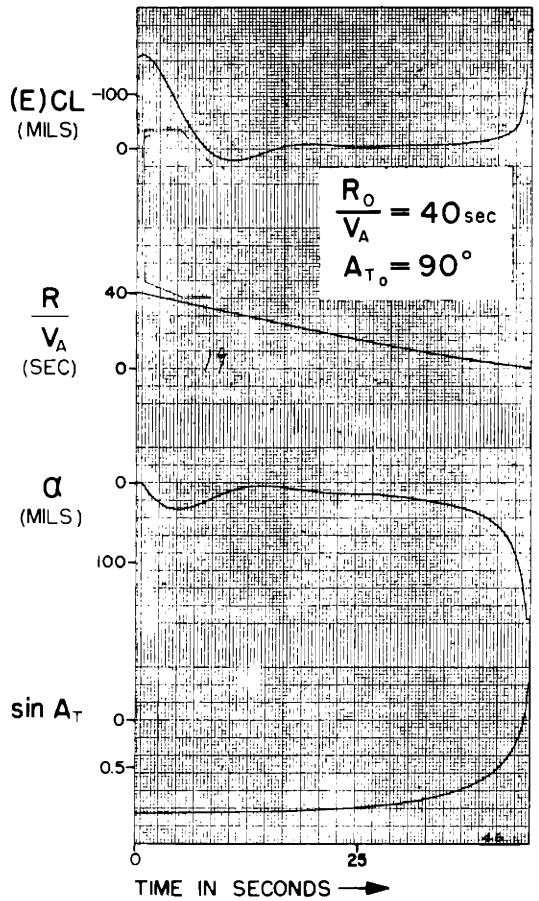

$S_{TID}\ S_{(sm)p}\ S_{(s,r)} = -1.00$ PSR = 1.11

$S_{TID}\ S_{(sm)i}\ S_{(s,r)} = 0$ SN = 0.25

$(CT)_{(sm)} = 0.30$ sec $(CT)_R = 0.15$ sec

AIRCRAFT CHARACTERISTICS OF APP B

FIG III - 11

RESPONSE OF CLOSED-LOOP TRACKING SYSTEM WITH CONTROLLED-LINE PREDICTION IN THE ABSENCE OF GUST AND RADAR INTERFERENCE

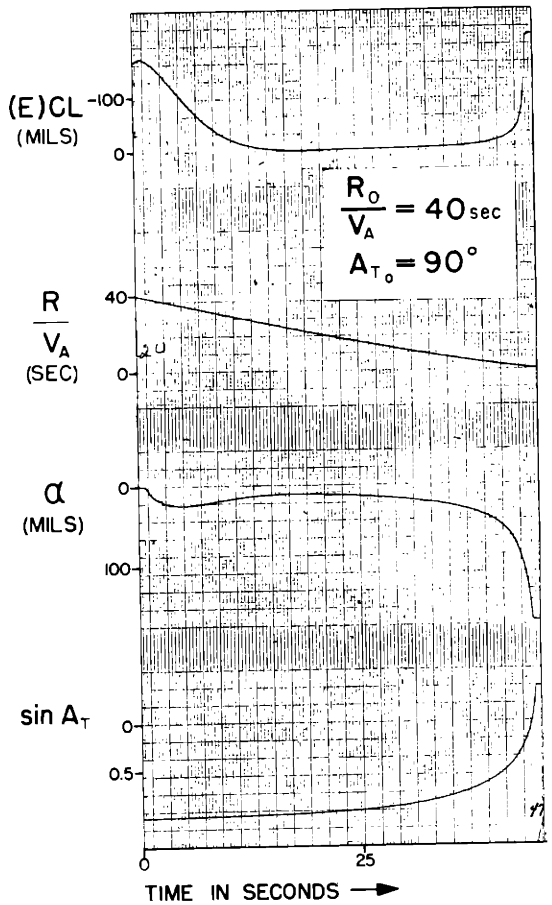

$S_{TID}\ S_{(sm)p}\ S_{(s,r)} = -1.00$ PSR = 1.11

$S_{TID}\ S_{(sm)i}\ S_{(s,r)} = 0$ SN = 0.50

$(CT)_{(sm)} = 0.30$ sec $(CT)_R = 0.15$ sec

AIRCRAFT CHARACTERISTICS OF APP B

FIG III - 12

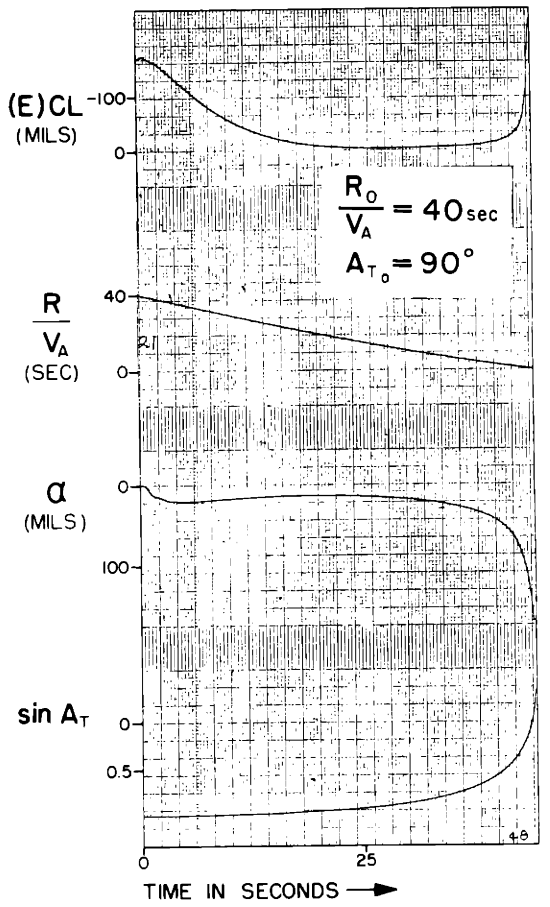

$S_{TID}\ S_{(sm)p}\ S_{(s,r)} = -1.00$ PSR = 1.11

$S_{TID}\ S_{(sm)i}\ S_{(s,r)} = 0$ SN = 0.75

$(CT)_{(sm)} = 0.30$ sec $(CT)_R = 0.15$ sec

AIRCRAFT CHARACTERISTICS OF APP B

FIG III - 13

RESPONSE OF CLOSED-LOOP TRACKING SYSTEM WITH CONTROLLED-LINE PREDICTION IN THE ABSENCE OF GUST AND RADAR INTERFERENCE

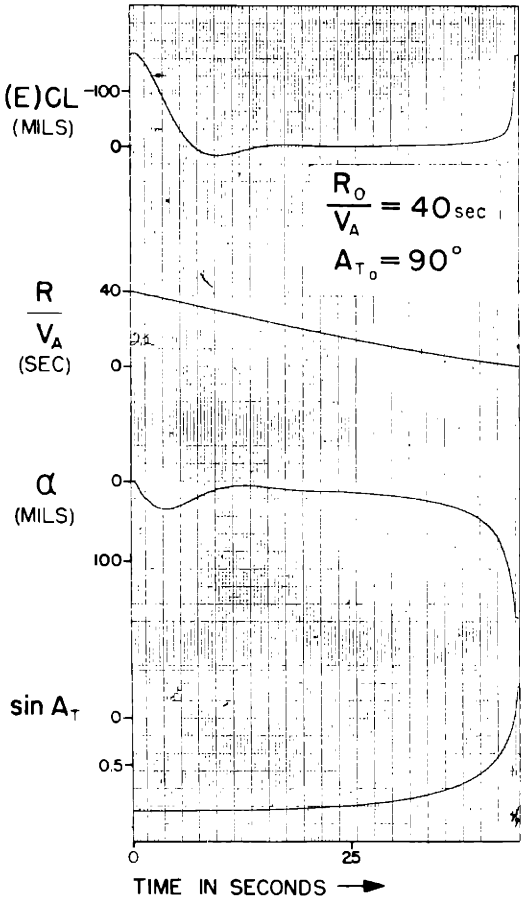

$S_{TID}\ S_{(sm)p}\ S_{(s,r)} = -1.50$ PSR = 1.11

$S_{TID}\ S_{(sm)i}\ S_{(s,r)} = 0$ SN = 0.25

$(CT)_{(sm)} = 0.30$ sec $(CT)_R = 0.15$ sec

AIRCRAFT CHARACTERISTICS OF APP B

FIG III - 14

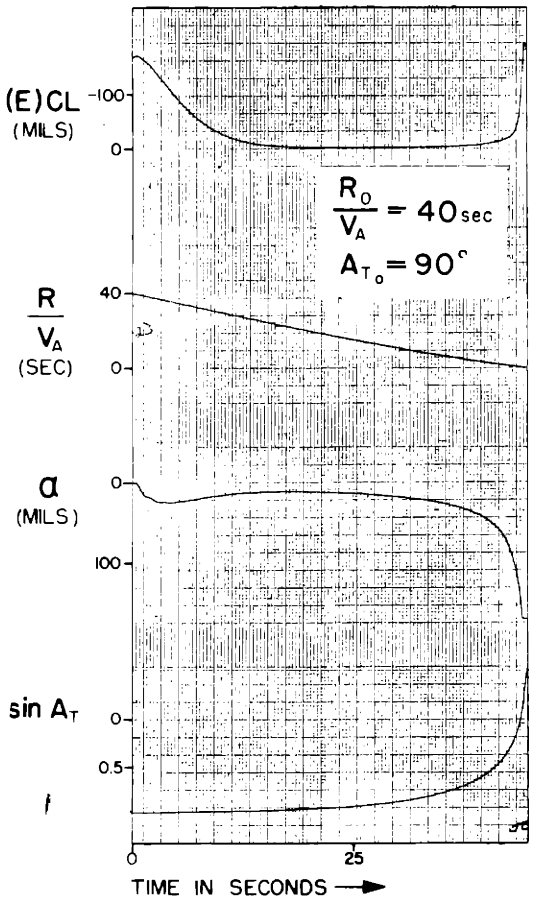

$S_{TID}\ S_{(sm)p}\ S_{(s,r)} = -1.50$ PSR = 1.11

$S_{TID}\ S_{(sm)i}\ S_{(s,r)} = 0$ SN = 0.50

$(CT)_{(sm)} = 0.30$ sec $(CT)_R = 0.15$ sec

AIRCRAFT CHARACTERISTICS OF APP B

FIG III - 15

RESPONSE OF CLOSED-LOOP TRACKING SYSTEM WITH CONTROLLED-LINE PREDICTION IN THE ABSENCE OF GUST AND RADAR INTERFERENCE

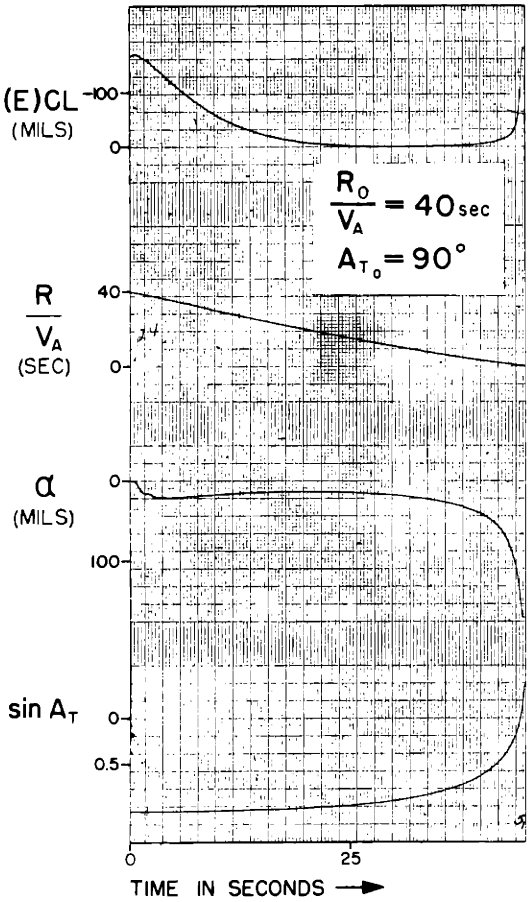

$S_{TID}\ S_{(sm)p}\ S_{(S,r)} = -1.50$ PSR = 1.11

$S_{TID}\ S_{(sm)i}\ S_{(S,r)} = 0$ SN = 0.75

$(CT)_{(sm)} = 0.30$ sec $(CT)_R = 0.15$ sec

AIRCRAFT CHARACTERISTICS OF APP B

FIG III - 16

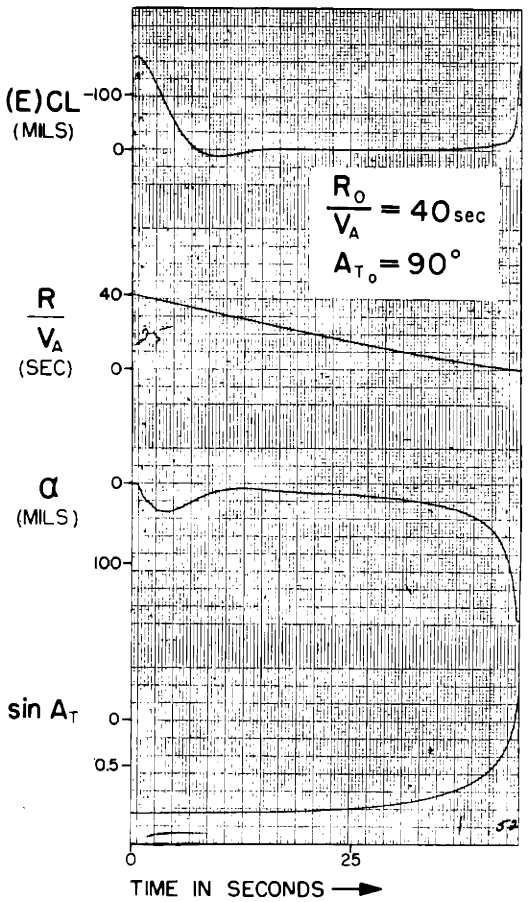

$S_{TID}\ S_{(sm)p}\ S_{(S,r)} = -1.94$ PSR = 1.11

$S_{TID}\ S_{(sm)i}\ S_{(S,r)} = 0$ SN = 0.25

$(CT)_{(sm)} = 0.30$ sec $(CT)_R = 0.15$ sec

AIRCRAFT CHARACTERISTICS OF APP B

FIG III - 17

RESPONSE OF CLOSED-LOOP TRACKING SYSTEM WITH CONTROLLED-LINE PREDICTION IN THE ABSENCE OF GUST AND RADAR INTERFERENCE

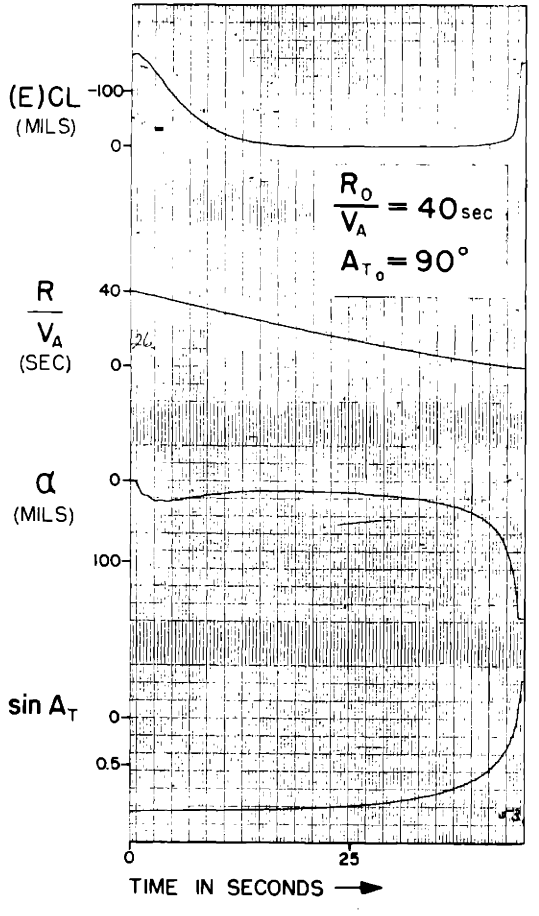

$S_{TID}\ S_{(sm)p}\ S_{(s,r)} = -1.94$ PSR = 1.11

$S_{TID}\ S_{(sm)i}\ S_{(s,r)} = 0$ SN = 0.50

$(CT)_{(sm)} = 0.30$ sec $(CT)_R = 0.15$ sec

AIRCRAFT CHARACTERISTICS OF APP B

FIG III - 18

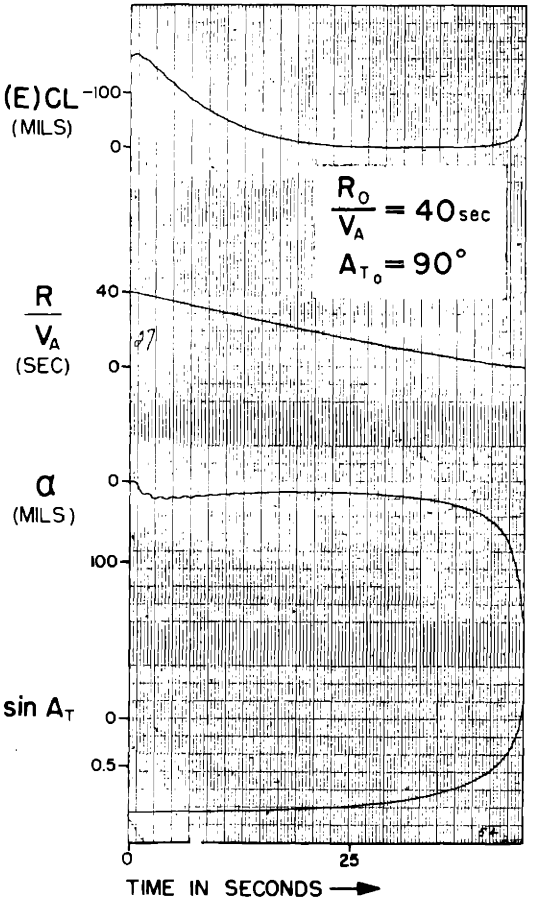

$S_{TID}\ S_{(sm)p}\ S_{(s,r)} = -1.94$ PSR = 1.11

$S_{TID}\ S_{(sm)i}\ S_{(s,r)} = 0$ SN = 0.75

$(CT)_{(sm)} = 0.30$ sec $(CT)_R = 0.15$ sec

AIRCRAFT CHARACTERISTICS OF APP B

FIG III - 19

RESPONSE OF CLOSED-LOOP TRACKING SYSTEM WITH CONTROLLED-LINE PREDICTION IN THE ABSENCE OF GUST AND RADAR INTERFERENCE

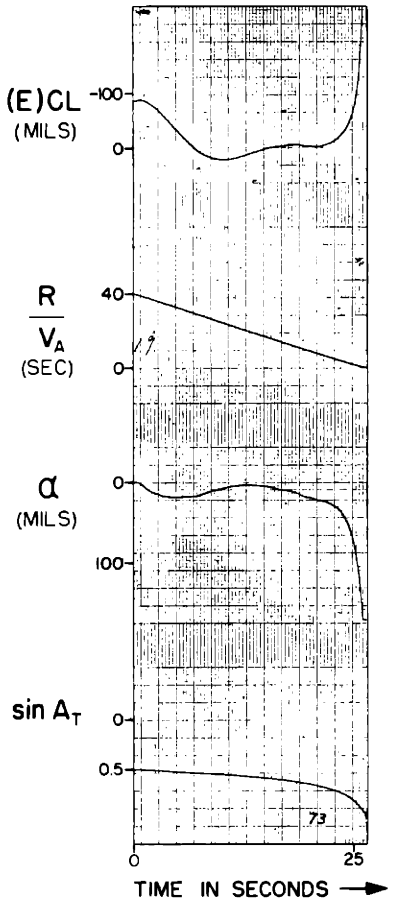

$\frac{R_0}{V_A} = 40$ sec

$A_{T_0} = 150°$

$S_{TID}\ S_{(sm)p}\ S_{(s,r)} = -1.00$ PSR = 1.11

$S_{TID}\ S_{(sm)i}\ S_{(s,r)} = 0$ SN = 0.25

$(CT)_{(sm)} = 0.30$ sec $(CT)_R = 0.15$ sec

AIRCRAFT CHARACTERISTICS OF APP B

FIG III - 20

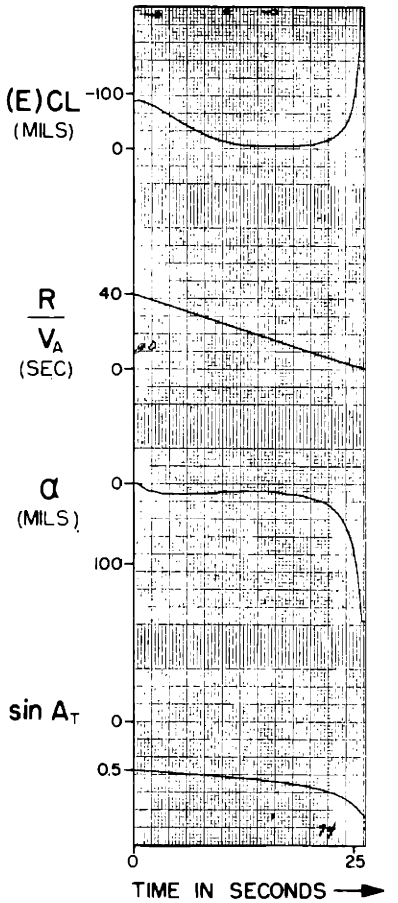

$\frac{R_0}{V_A} = 40$ sec

$A_{T_0} = 150°$

$S_{TID}\ S_{(sm)p}\ S_{(s,r)} = -1.00$ PSR = 1.11

$S_{TID}\ S_{(sm)i}\ S_{(s,r)} = 0$ SN = 0.50

$(CT)_{(sm)} = 0.30$ sec $(CT)_R = 0.15$ sec

AIRCRAFT CHARACTERISTICS OF APP B

FIG III - 21

RESPONSE OF CLOSED-LOOP TRACKING SYSTEM WITH CONTROLLED-LINE PREDICTION IN THE ABSENCE OF GUST AND RADAR INTERFERENCE

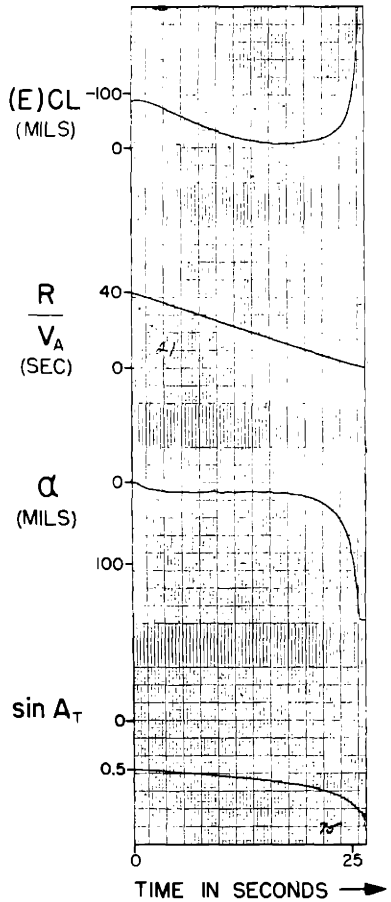

$\frac{R_0}{V_A} = 40$ sec

$A_{T_0} = 150°$

$S_{TID}\ S_{(sm)p}\ S_{(s,r)} = -1.00$ PSR = 1.11

$S_{TID}\ S_{(sm)i}\ S_{(s,r)} = 0$ SN = 0.75

$(CT)_{(sm)} = 0.30$ sec $(CT)_R = 0.15$ sec

AIRCRAFT CHARACTERISTICS OF APP B

FIG III - 22

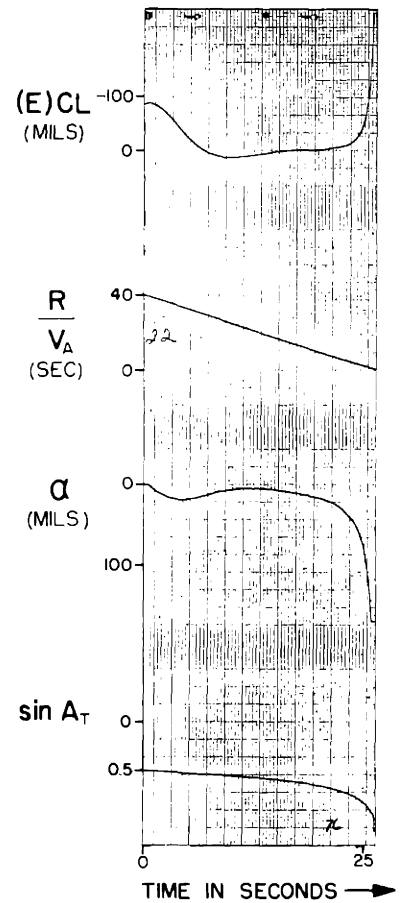

$\frac{R_0}{V_A} = 40$ sec

$A_{T_0} = 150°$

$S_{TID}\ S_{(sm)p}\ S_{(s,r)} = -1.50$ PSR = 1.11

$S_{TID}\ S_{(sm)i}\ S_{(s,r)} = 0$ SN = 0.25

$(CT)_{(sm)} = 0.30$ sec $(CT)_R = 0.15$ sec

AIRCRAFT CHARACTERISTICS OF APP B

FIG III - 23

RESPONSE OF CLOSED-LOOP TRACKING SYSTEM WITH CONTROLLED-LINE PREDICTION IN THE ABSENCE OF GUST AND RADAR INTERFERENCE

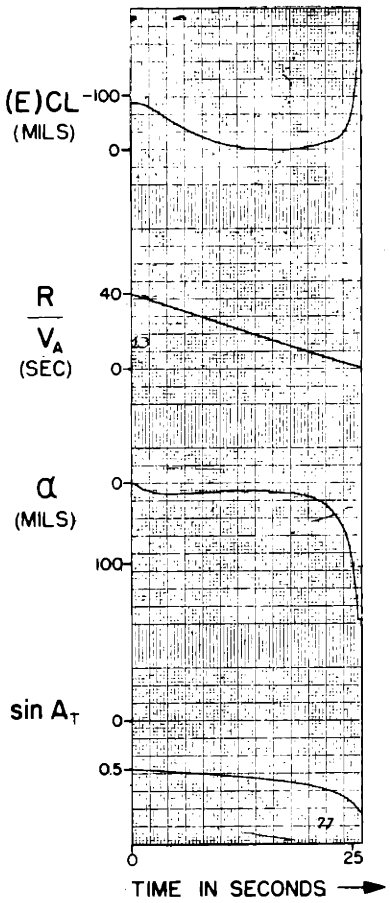

$\frac{R_0}{V_A} = 40$ sec

$A_{T_0} = 150°$

$S_{TID}\ S_{(sm)p}\ S_{(s,r)} = -1.50$ PSR = 1.11

$S_{TID}\ S_{(sm)i}\ S_{(s,r)} = 0$ SN = 0.50

$(CT)_{(sm)} = 0.30$ sec $(CT)_R = 0.15$ sec

AIRCRAFT CHARACTERISTICS OF APP B

FIG III - 24

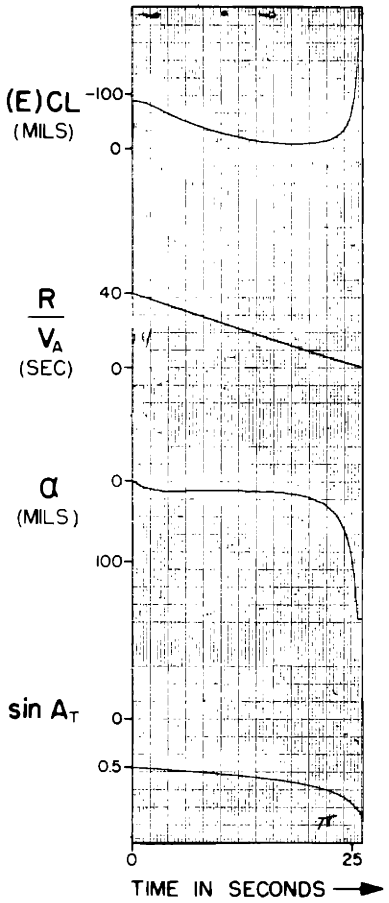

$\frac{R_0}{V_A} \doteq 40$ sec

$A_{T_0} = 150°$

$S_{TID}\ S_{(sm)p}\ S_{(s,r)} = -1.50$ PSR = 1.11

$S_{TID}\ S_{(sm)i}\ S_{(s,r)} = 0$ SN = 0.75

$(CT)_{(sm)} = 0.30$ sec $(CT)_R = 0.15$ sec

AIRCRAFT CHARACTERISTICS OF APP B

FIG III - 25

RESPONSE OF CLOSED-LOOP TRACKING SYSTEM WITH CONTROLLED-LINE PREDICTION IN THE ABSENCE OF GUST AND RADAR INTERFERENCE

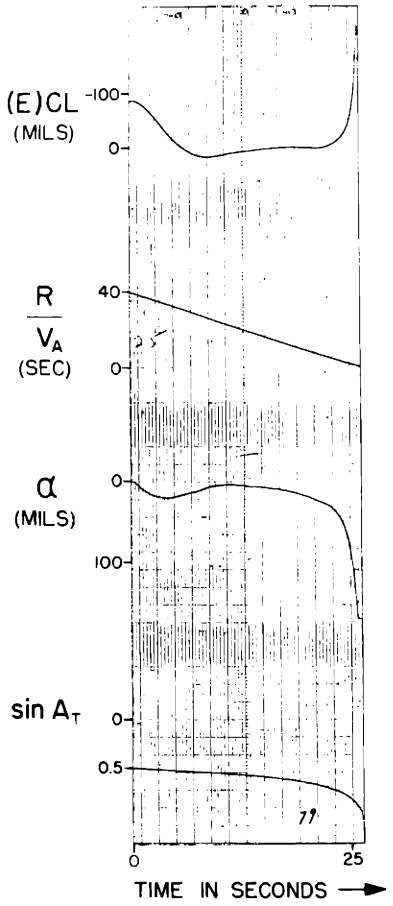

$\frac{R_0}{V_A} = 40$ sec

$A_{T_0} = 150°$

$S_{TID}\, S_{(sm)p}\, S_{(S,r)} = -1.94$ PSR = 1.11

$S_{TID}\, S_{(sm)i}\, S_{(S,r)} = 0$ SN = 0.25

$(CT)_{(sm)} = 0.30$ sec $(CT)_R = 0.15$ sec

AIRCRAFT CHARACTERISTICS OF APP B

FIG III - 26

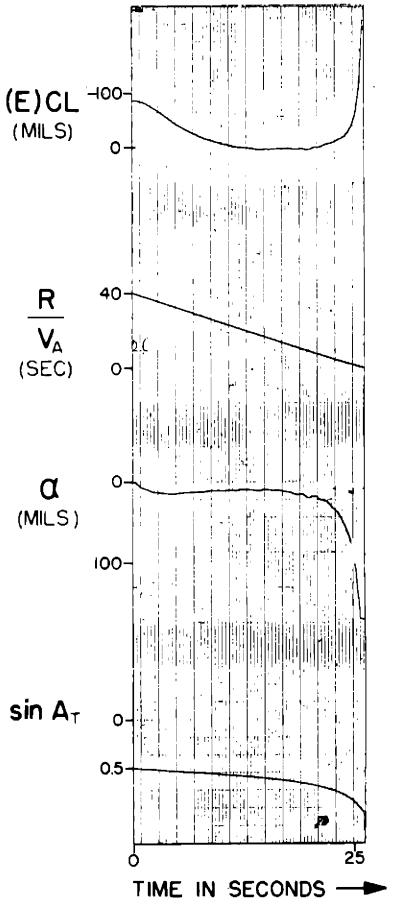

$\frac{R_0}{V_A} = 40$ sec

$A_{T_0} = 150°$

$S_{TID}\, S_{(sm)p}\, S_{(S,r)} = -1.94$ PSR = 1.11

$S_{TID}\, S_{(sm)i}\, S_{(S,r)} = 0$ SN = 0.50

$(CT)_{(sm)} = 0.30$ sec $(CT)_R = 0.15$ sec

AIRCRAFT CHARACTERISTICS OF APP B

FIG III - 27

RESPONSE OF CLOSED-LOOP TRACKING SYSTEM WITH CONTROLLED-LINE PREDICTION IN THE ABSENCE OF GUST AND RADAR INTERFERENCE

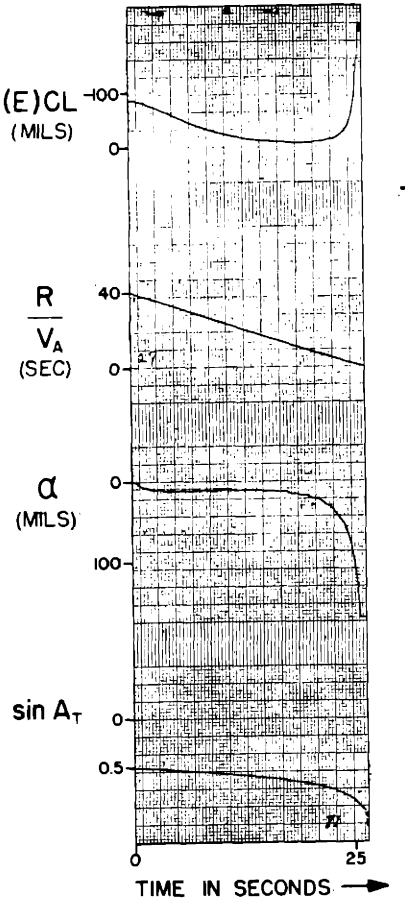

$\frac{R_0}{V_A} = 40$ sec

$A_{T_0} = 150°$

$S_{TID}\, S_{(sm)p}\, S_{(s,r)} = -1.94$ PSR = 1.11

$S_{TID}\, S_{(sm)i}\, S_{(s,r)} = 0$ SN = 0.75

$(CT)_{(sm)} = 0.30$ sec $(CT)_R = 0.15$ sec

AIRCRAFT CHARACTERISTICS OF APP B

FIG III - 28

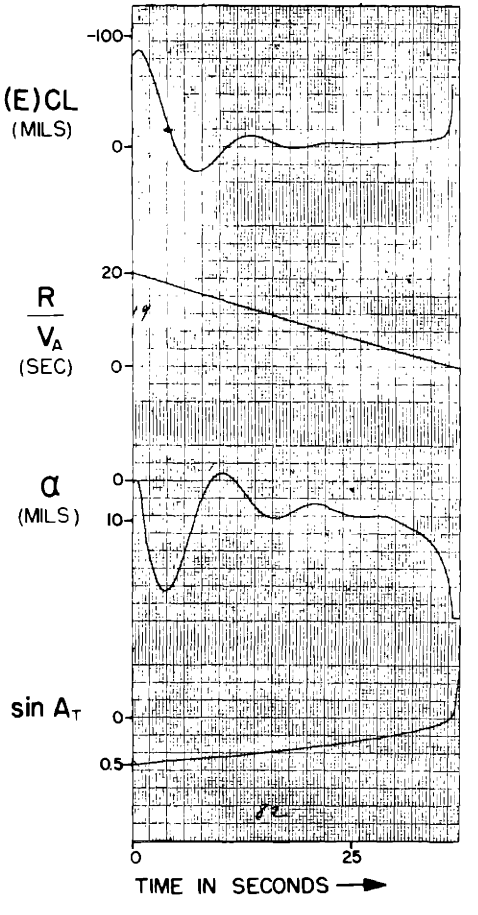

$\frac{R_0}{V_A} = 20$ sec

$A_{T_0} = 30°$

$S_{TID}\, S_{(sm)p}\, S_{(s,r)} = -1.00$ PSR = 1.11

$S_{TID}\, S_{(sm)i}\, S_{(s,r)} = 0$ SN = 0.25

$(CT)_{(sm)} = 0.30$ sec $(CT)_R = 0.15$ sec

AIRCRAFT CHARACTERISTICS OF APP B

FIG III - 29

RESPONSE OF CLOSED-LOOP TRACKING SYSTEM WITH CONTROLLED-LINE PREDICTION IN THE ABSENCE OF GUST AND RADAR INTERFERENCE

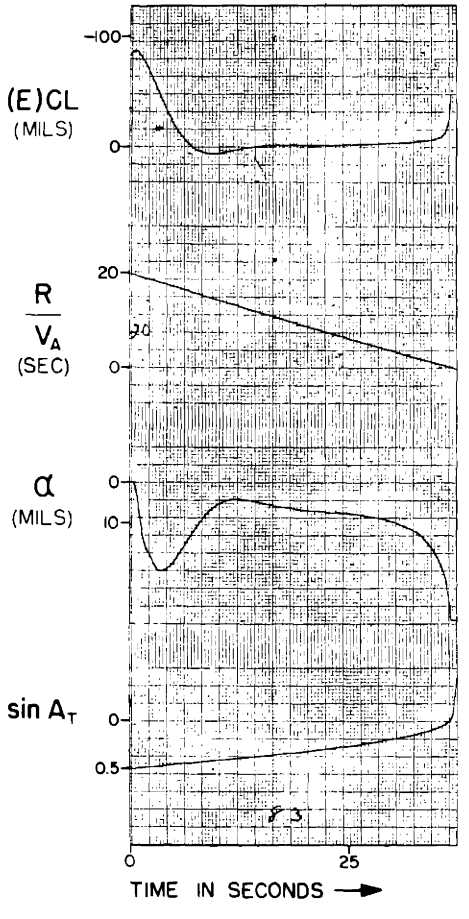

$\frac{R_0}{V_A} = 20$ sec

$A_{T_0} = 30°$

$S_{TID}\ S_{(sm)p}\ S_{(s,r)} = -1.00$ PSR = 1.11

$S_{TID}\ S_{(sm)i}\ S_{(s,r)} = 0$ SN = 0.50

$(CT)_{(sm)} = 0.30$ sec $(CT)_R = 0.15$ sec

AIRCRAFT CHARACTERISTICS OF APP B

FIG III - 30

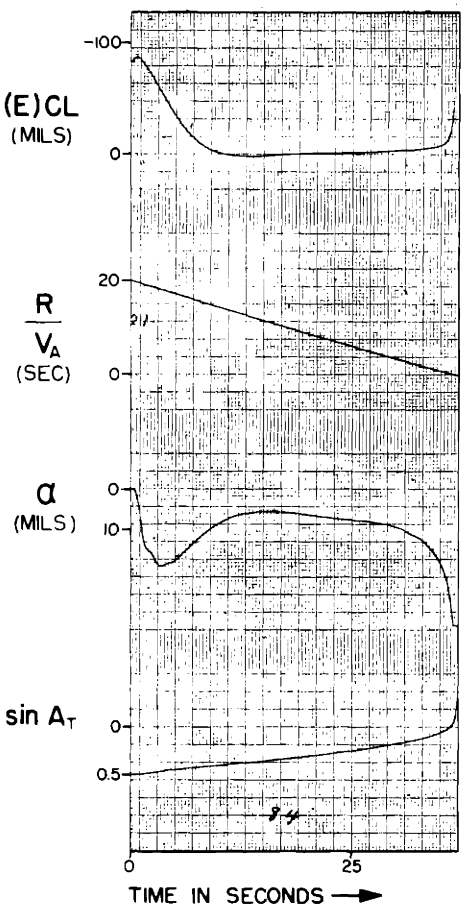

$\frac{R_0}{V_A} = 20$ sec

$A_{T_0} = 30°$

$S_{TID}\ S_{(sm)p}\ S_{(s,r)} = -1.00$ PSR = 1.11

$S_{TID}\ S_{(sm)i}\ S_{(s,r)} = 0$ SN = 0.75

$(CT)_{(sm)} = 0.30$ sec $(CT)_R = 0.15$ sec

AIRCRAFT CHARACTERISTICS OF APP B

FIG III - 31

RESPONSE OF CLOSED-LOOP TRACKING SYSTEM WITH CONTROLLED-LINE PREDICTION IN THE ABSENCE OF GUST AND RADAR INTERFERENCE

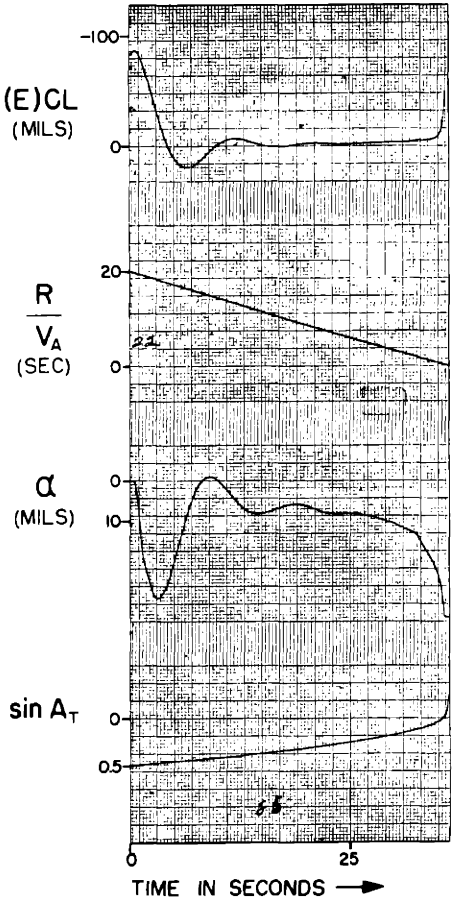

$\frac{R_0}{V_A} = 20$ sec

$A_{T_0} = 30°$

$S_{TID}\ S_{(sm)\rho}\ S_{(s,r)} = -1.50$ PSR = 1.11

$S_{TID}\ S_{(sm)i}\ S_{(s,r)} = 0$ SN = 0.25

$(CT)_{(sm)} = 0.30$ sec $(CT)_R = 0.15$ sec

AIRCRAFT CHARACTERISTICS OF APP B

FIG III - 32

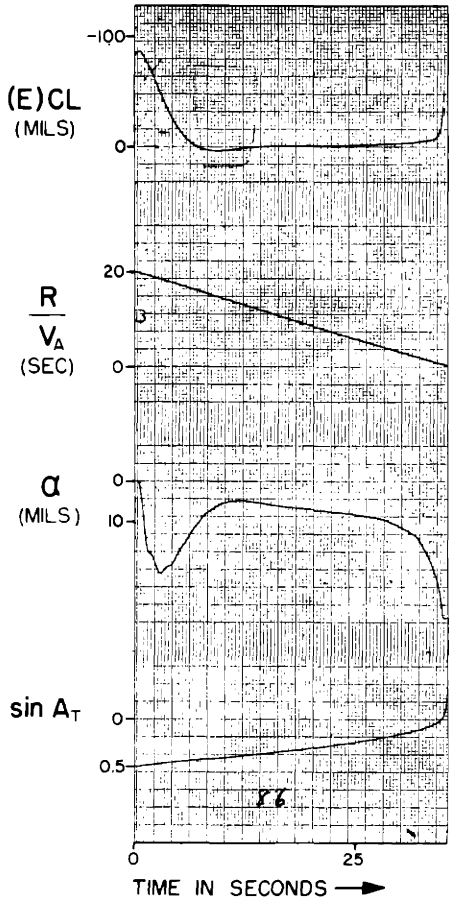

$\frac{R_0}{V_A} = 20$ sec

$A_{T_0} = 30°$

$S_{TID}\ S_{(sm)\rho}\ S_{(s,r)} = -1.50$ PSR = 1.11

$S_{TID}\ S_{(sm)i}\ S_{(s,r)} = 0$ SN = 0.50

$(CT)_{(sm)} = 0.30$ sec $(CT)_R = 0.15$ sec

AIRCRAFT CHARACTERISTICS OF APP B

FIG III - 33

RESPONSE OF CLOSED-LOOP TRACKING SYSTEM WITH CONTROLLED-LINE PREDICTION IN THE ABSENCE OF GUST AND RADAR INTERFERENCE

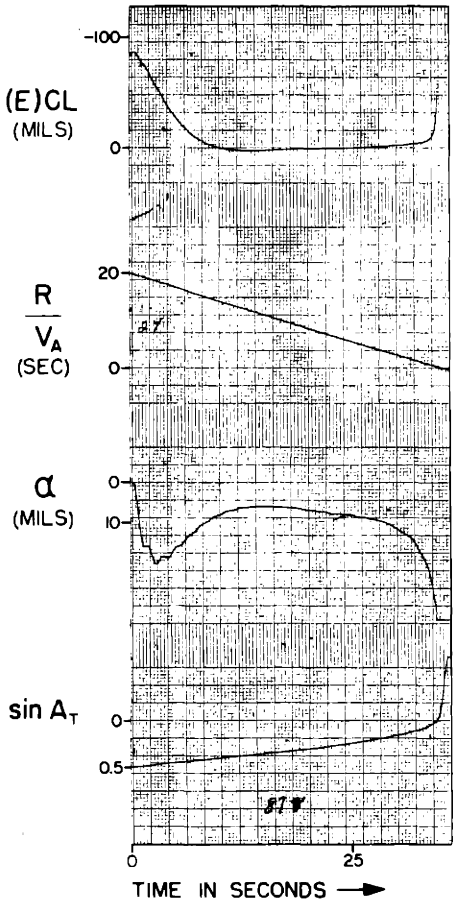

$\frac{R_0}{V_A} = 20$ sec

$A_{T_0} = 30°$

$S_{TID}\ S_{(sm)p}\ S_{(s,r)} = -1.50$ PSR = 1.11

$S_{TID}\ S_{(sm)i}\ S_{(s,r)} = 0$ SN = 0.75

$(CT)_{(sm)} = 0.30$ sec $(CT)_R = 0.15$ sec

AIRCRAFT CHARACTERISTICS OF APP B

FIG III - 34

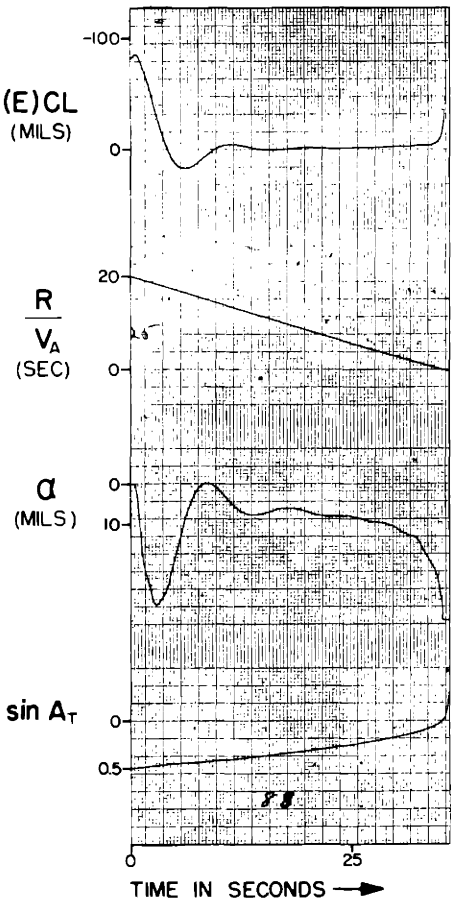

$\frac{R_0}{V_A} = 20$ sec

$A_{T_0} = 30°$

$S_{TID}\ S_{(sm)p}\ S_{(s,r)} = -1.94$ PSR = 1.11

$S_{TID}\ S_{(sm)i}\ S_{(s,r)} = 0$ SN = 0.25

$(CT)_{(sm)} = 0.30$ sec $(CT)_R = 0.15$ sec

AIRCRAFT CHARACTERISTICS OF APP B

FIG III - 35

RESPONSE OF CLOSED-LOOP TRACKING SYSTEM WITH CONTROLLED-LINE PREDICTION IN THE ABSENCE OF GUST AND RADAR INTERFERENCE

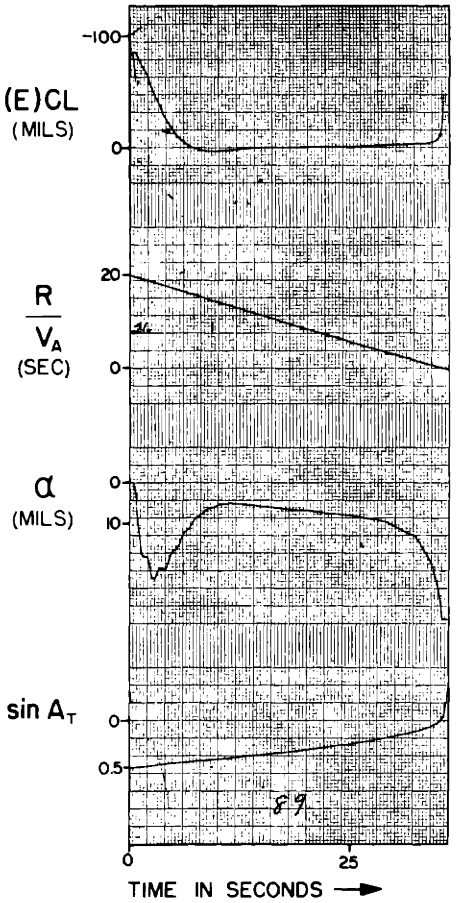

$\frac{R_0}{V_A} = 20$ sec

$A_{T_0} = 30°$

$S_{TID}\ S_{(sm)p}\ S_{(s,r)} = -1.94$ PSR = 1.11

$S_{TID}\ S_{(sm)i}\ S_{(s,r)} = 0$ SN = 0.50

$(CT)_{(sm)} = 0.30$ sec $(CT)_R = 0.15$ sec

AIRCRAFT CHARACTERISTICS OF APP B

FIG III - 36

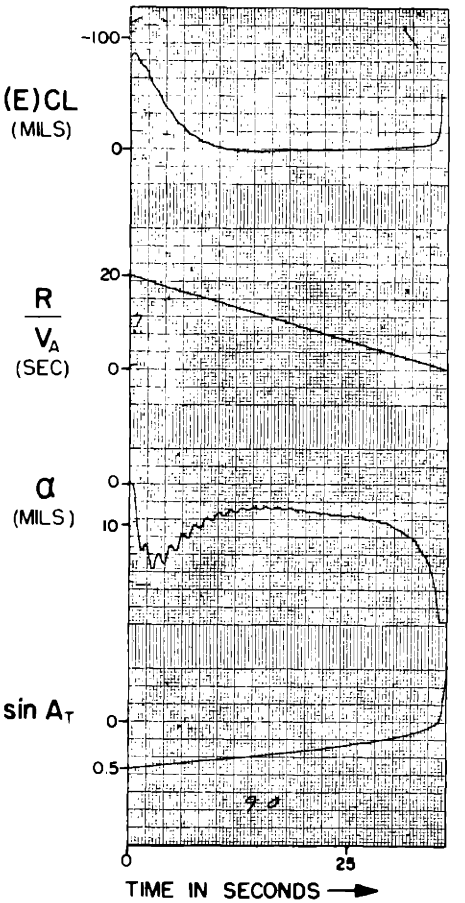

$\frac{R_0}{V_A} = 20$ sec

$A_{T_0} = 30°$

$S_{TID}\ S_{(sm)p}\ S_{(s,r)} = -1.94$ PSR = 1.11

$S_{TID}\ S_{(sm)i}\ S_{(s,r)} = 0$ SN = 0.75

$(CT)_{(sm)} = 0.30$ sec $(CT)_R = 0.15$ sec

AIRCRAFT CHARACTERISTICS OF APP B

FIG III - 37

RESPONSE OF CLOSED-LOOP TRACKING SYSTEM WITH CONTROLLED-LINE PREDICTION IN THE ABSENCE OF GUST AND RADAR INTERFERENCE

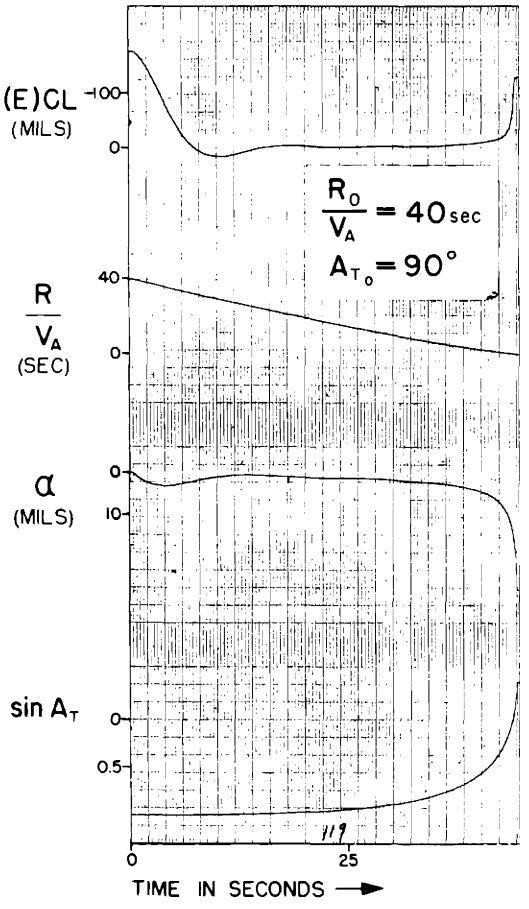

$S_{TID}\ S_{(sm)p}\ S_{(s,r)} = -1.50$ PSR = 1.11

$S_{TID}\ S_{(sm)i}\ S_{(s,r)} = 0$ SN = 0.25

$(CT)_{(sm)} = 0.0$ sec $(CT)_R = 0.15$ sec

AIRCRAFT CHARACTERISTICS OF APP B

FIG III - 38

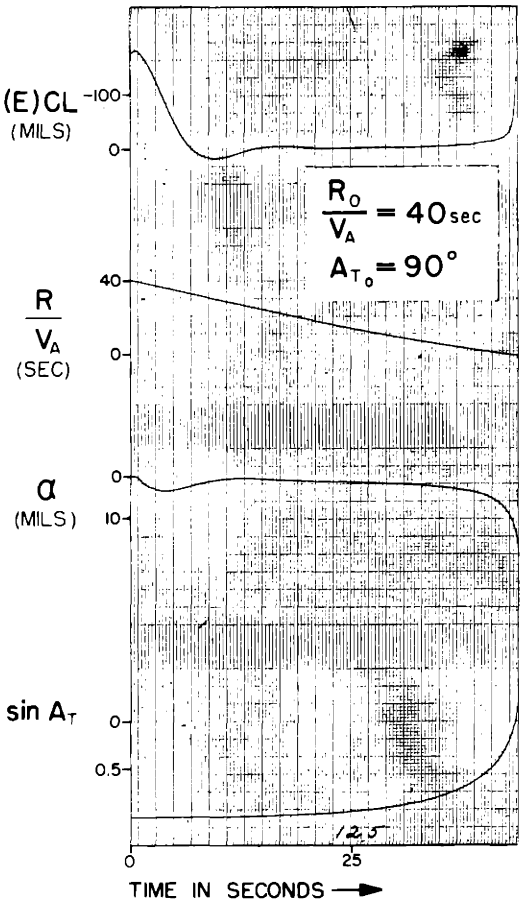

$S_{TID}\ S_{(sm)p}\ S_{(s,r)} = -1.50$ PSR = 1.11

$S_{TID}\ S_{(sm)i}\ S_{(s,r)} = 0$ SN = 0.25

$(CT)_{(sm)} = 0.6$ sec $(CT)_R = 0.15$ sec

AIRCRAFT CHARACTERISTICS OF APP B

FIG III - 39

RESPONSE OF CLOSED-LOOP TRACKING SYSTEM WITH CONTROLLED-LINE PREDICTION IN THE ABSENCE OF GUST AND RADAR INTERFERENCE

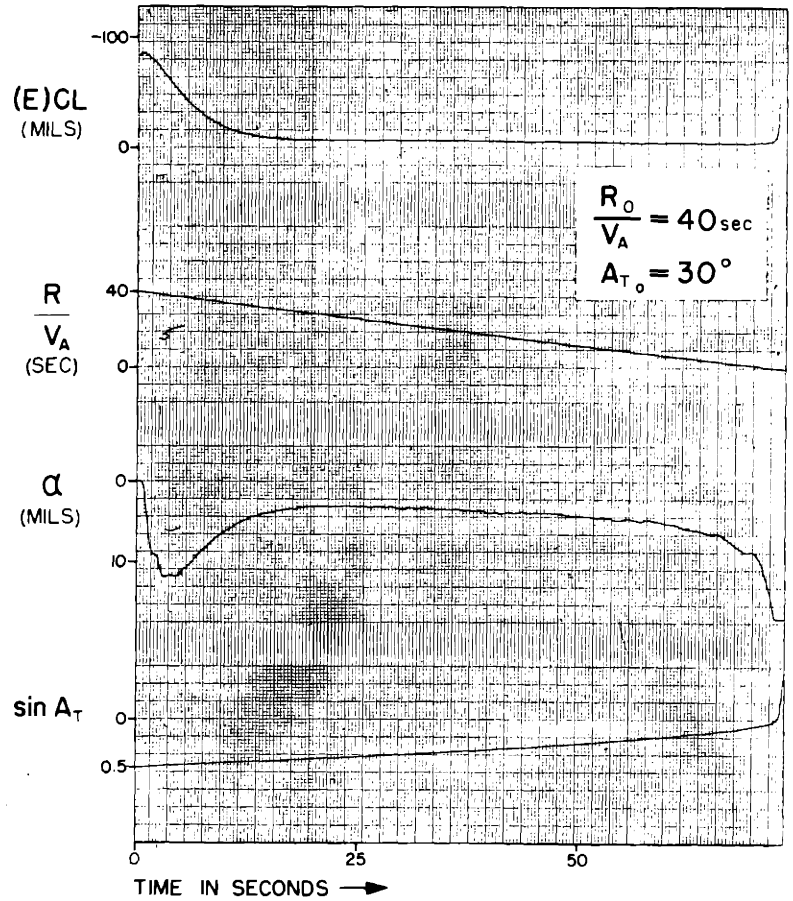

$S_{TID}\ S_{(Sm)P}\ S_{(S,r)} = -1.50$ PSR = 1.00

$S_{TID}\ S_{(Sm)i}\ S_{(S,r)} = 0$ SN = 0.50

$(CT)_{(sm)} = 0.30$ sec $(CT)_R = 0.15$ sec

AIRCRAFT CHARACTERISTICS OF APP B

FIG III - 40

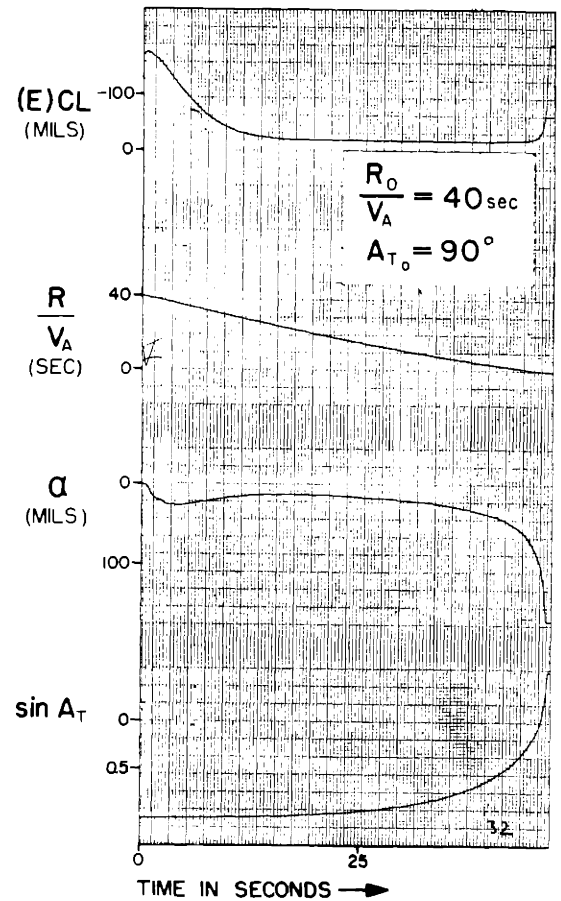

$S_{TID}\ S_{(Sm)P}\ S_{(S,r)} = -1.50$ PSR = 1.00

$S_{TID}\ S_{(Sm)i}\ S_{(S,r)} = 0$ SN = 0.50

$(CT)_{(sm)} = 0.30$ sec $(CT)_R = 0.15$ sec

AIRCRAFT CHARACTERISTICS OF APP B

FIG III - 41

RESPONSE OF CLOSED-LOOP TRACKING SYSTEM WITH CONTROLLED-LINE PREDICTION IN THE ABSENCE OF GUST AND RADAR INTERFERENCE

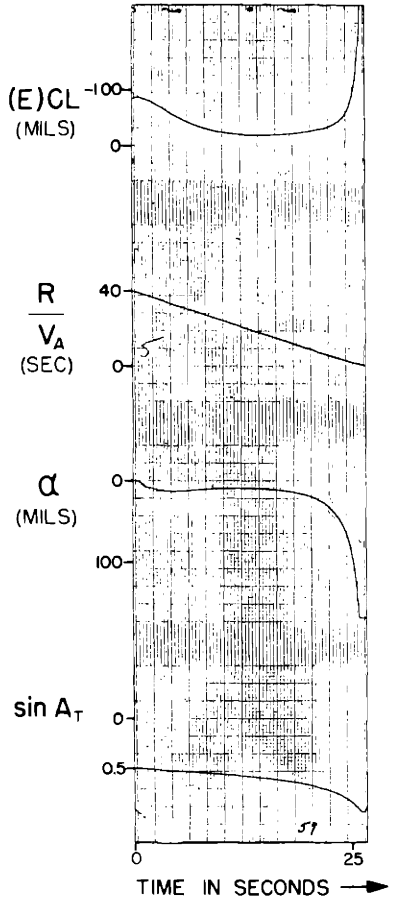

$\frac{R_0}{V_A} = 40$ sec

$A_{T_0} = 150°$

$S_{TID}\ S_{(sm)p}\ S_{(s,r)} = -1.50$ PSR = 1.00

$S_{TID}\ S_{(sm)i}\ S_{(s,r)} = 0$ SN = 0.50

$(CT)_{(sm)} = 0.30$ sec $(CT)_R = 0.15$ sec

AIRCRAFT CHARACTERISTICS OF APP B

FIG III-42

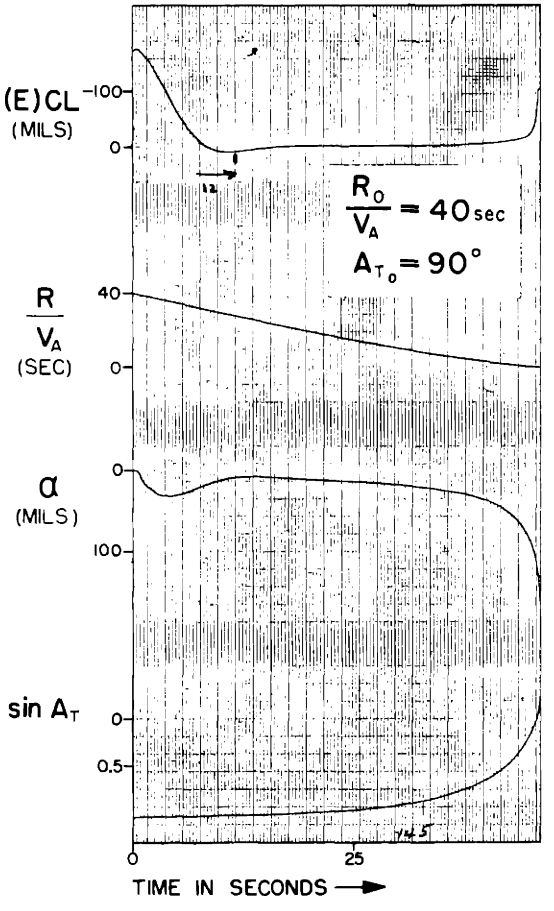

$\frac{R_0}{V_A} = 40$ sec

$A_{T_0} = 90°$

$S_{TID}\ S_{(sm)p}\ S_{(s,r)} = -1.50$ PSR = 1.11

$S_{TID}\ S_{(sm)i}\ S_{(s,r)} = 0$ SN = 0.30

$(CT)_{(sm)} = 0.30$ sec $(CT)_R = 0.15$ sec

AIRCRAFT CHARACTERISTICS OF APP B

FIG III-43

RESPONSE OF CLOSED-LOOP TRACKING SYSTEM WITH CONTROLLED-LINE PREDICTION IN THE ABSENCE OF GUST AND RADAR INTERFERENCE

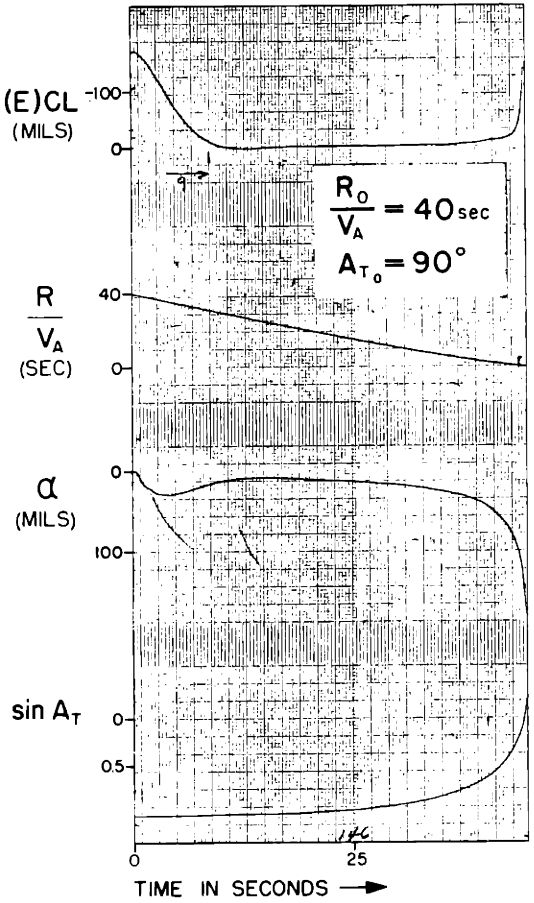

$S_{TID}\ S_{(sm)p}\ S_{(s,r)} = -1.50$ PSR = 1.11

$S_{TID}\ S_{(sm)i}\ S_{(s,r)} = 0$ SN = 0.35

$(CT)_{(sm)} = 0.30$ sec $(CT)_R = 0.15$ sec

AIRCRAFT CHARACTERISTICS OF APP B

FIG III - 44

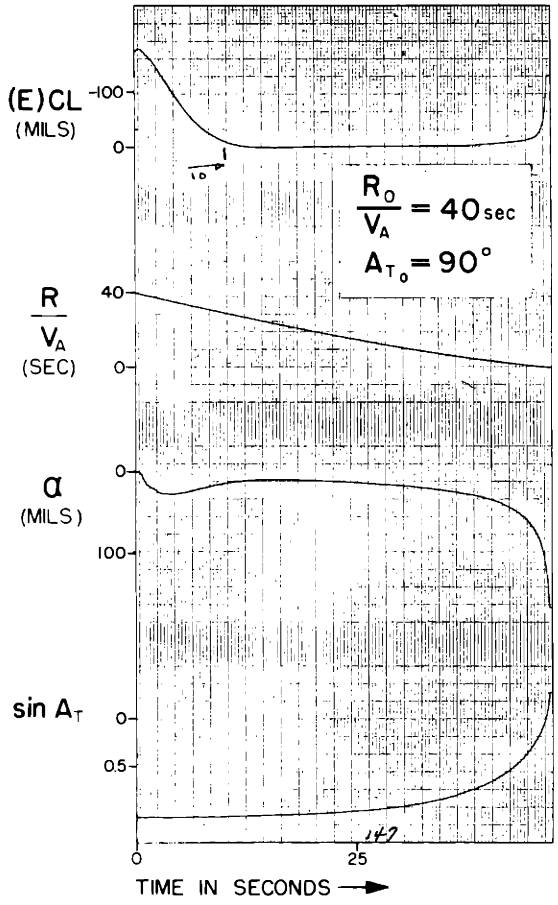

$S_{TID}\ S_{(sm)p}\ S_{(s,r)} = -1.50$ PSR = 1.11

$S_{TID}\ S_{(sm)i}\ S_{(s,r)} = 0$ SN = 0.40

$(CT)_{(sm)} = 0.30$ sec $(CT)_R = 0.15$ sec

AIRCRAFT CHARACTERISTICS OF APP B

FIG III - 45

RESPONSE OF CLOSED-LOOP TRACKING SYSTEM WITH CONTROLLED-LINE PREDICTION IN THE ABSENCE OF GUST AND RADAR INTERFERENCE

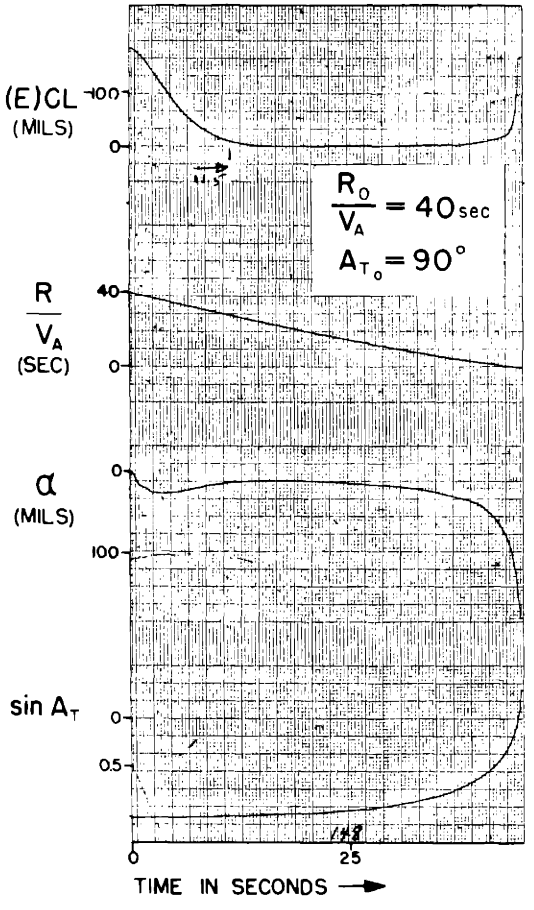

$S_{TID}\ S_{(sm)p}\ S_{(s,r)} = -1.50$ PSR = 1.11

$S_{TID}\ S_{(sm)i}\ S_{(s,r)} = 0$ SN = 0.45

$(CT)_{(sm)} = 0.30$ sec $(CT)_R = 0.15$ sec

AIRCRAFT CHARACTERISTICS OF APP B

FIG III - 46

RESPONSE OF CLOSED-LOOP TRACKING SYSTEM WITH CONTROLLED-LINE PREDICTION IN THE ABSENCE OF GUST AND RADAR INTERFERENCE

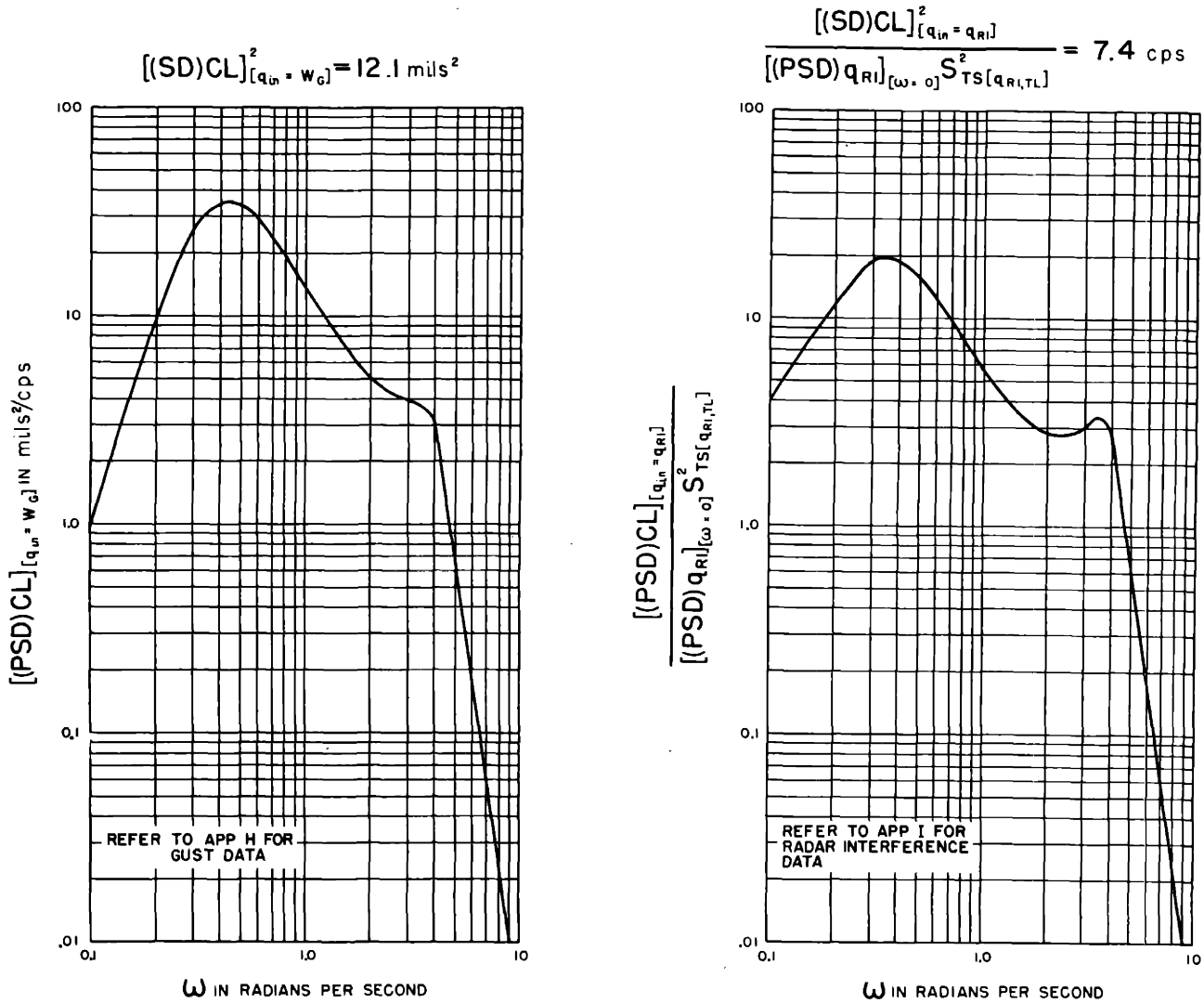

$S_{TID}\ S_{(sm)p}\ S_{(s,r)} = -1.00$ $\quad S_{P(\omega,P)} = 13.85$ sec

$S_{TID}\ S_{(sm)i}\ S_{(s,r)} = 0$ sec^{-1} $\quad SN = 0.25$

$(CT)_{(sm)} = 0.30$ sec $\quad (CT)_R = 0.15$ sec

AIRCRAFT CHARACTERISTICS OF APP B

FIG III-47 POWER SPECTRAL DENSITIES RESULTING FROM GUST AND RADAR INTERFERENCE OF CLOSED-LOOP TRACKING SYSTEM WITH THE CONTROLLED LINE PREDICTION

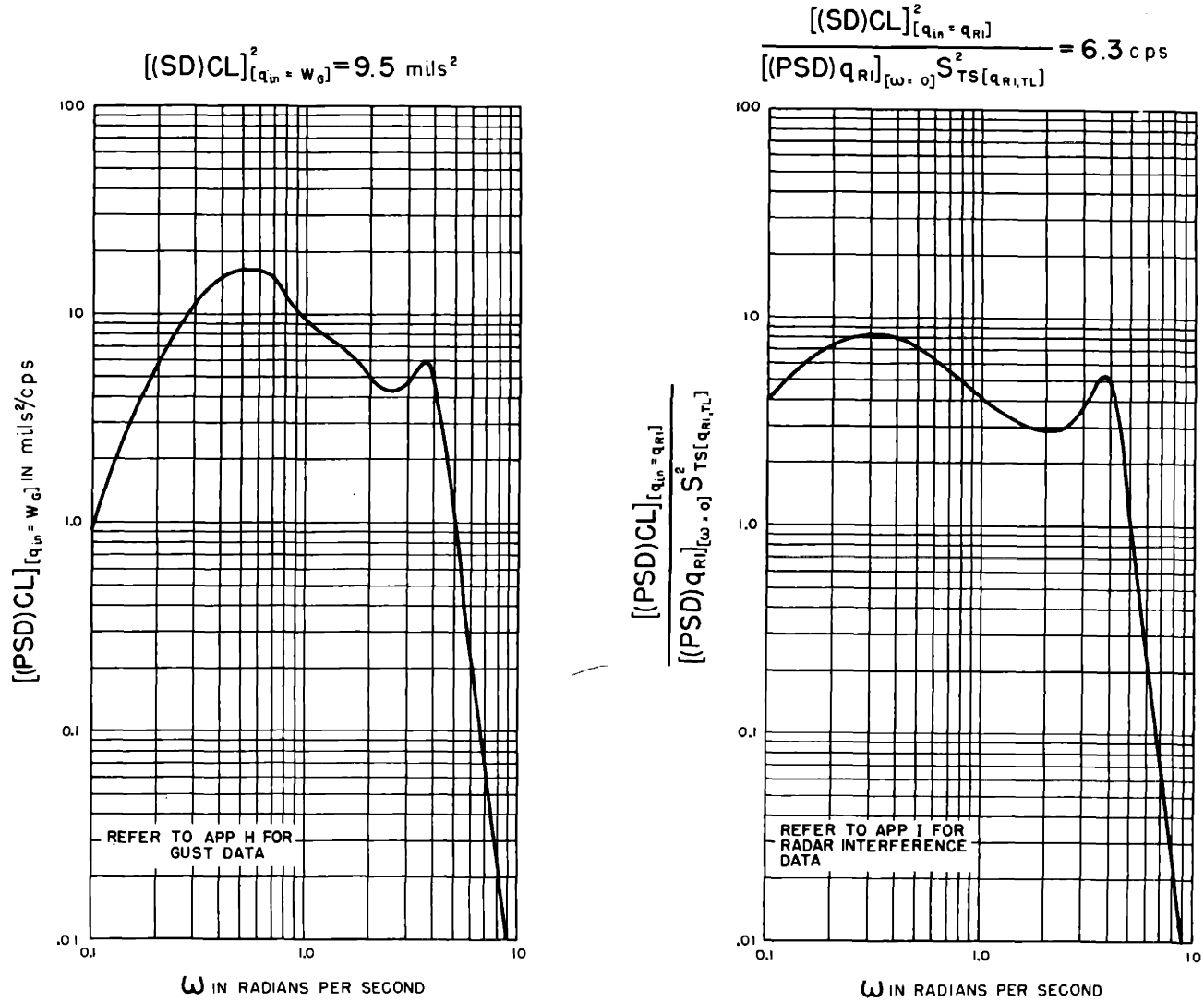

$S_{TID}\ S_{(sm)p}\ S_{(s,r)} = -1.00$ $\quad S_{P(\omega,P)} = 13.85$ sec

$S_{TID}\ S_{(sm)i}\ S_{(s,r)} = 0$ sec^{-1} $\quad SN = 0.50$

$(CT)_{(sm)} = 0.30$ sec $\quad (CT)_R = 0.15$ sec

AIRCRAFT CHARACTERISTICS OF APP B

FIG III-48 POWER SPECTRAL DENSITIES RESULTING FROM GUST AND RADAR INTERFERENCE OF CLOSED-LOOP TRACKING SYSTEM WITH THE CONTROLLED LINE PREDICTION

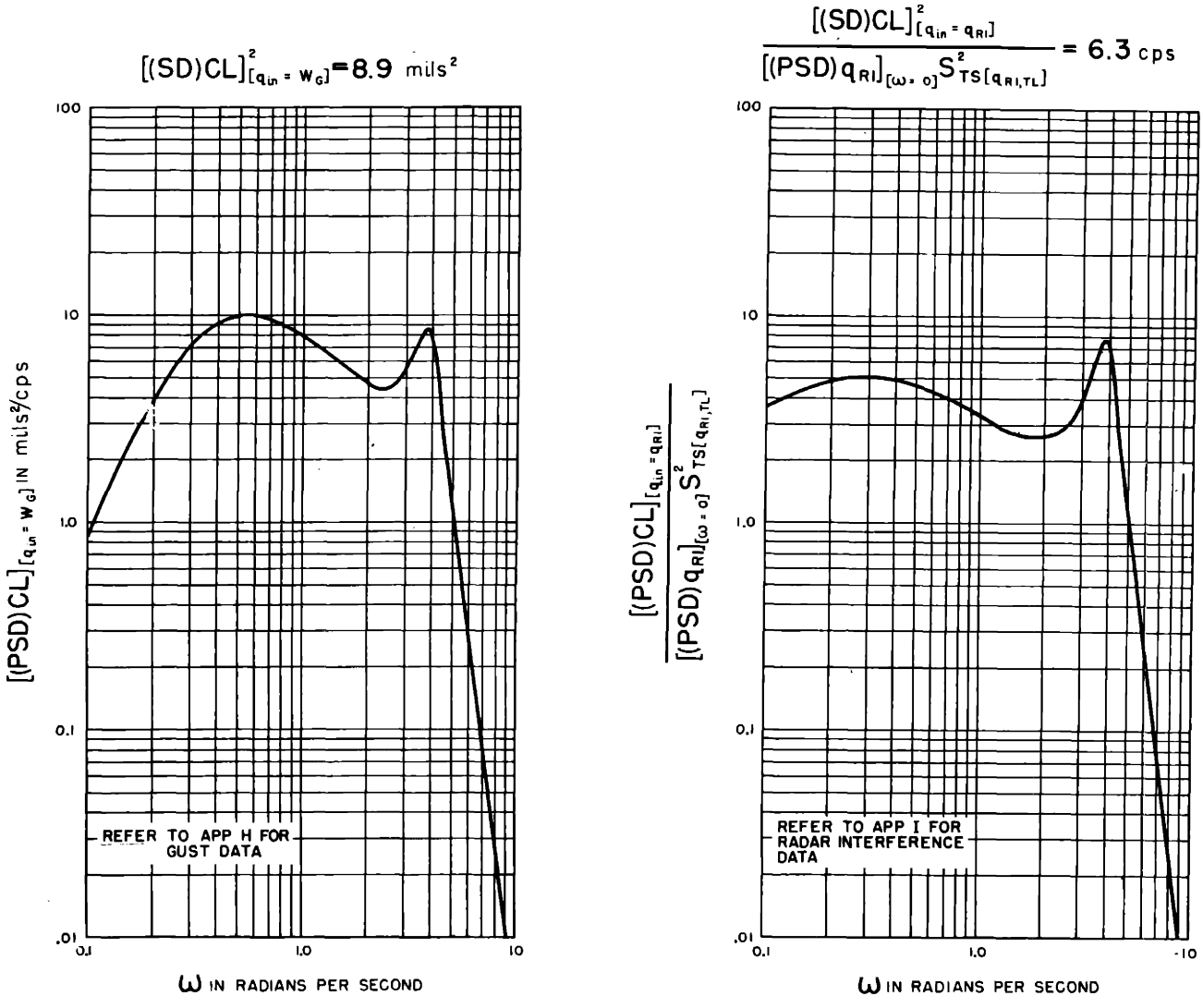

$S_{TID}\ S_{(sm)p}\ S_{(s,r)} = -1.00$ $\quad S_{P(\omega,P)} = 13.85$ sec

$S_{TID}\ S_{(sm)i}\ S_{(s,r)} = 0$ sec^{-1} $\quad SN = 0.75$

$(CT)_{(sm)} = 0.30$ sec $\quad (CT)_R = 0.15$ sec

AIRCRAFT CHARACTERISTICS OF APP B

FIG III-49 POWER SPECTRAL DENSITIES RESULTING FROM GUST AND RADAR INTERFERENCE OF CLOSED-LOOP TRACKING SYSTEM WITH THE CONTROLLED LINE PREDICTION

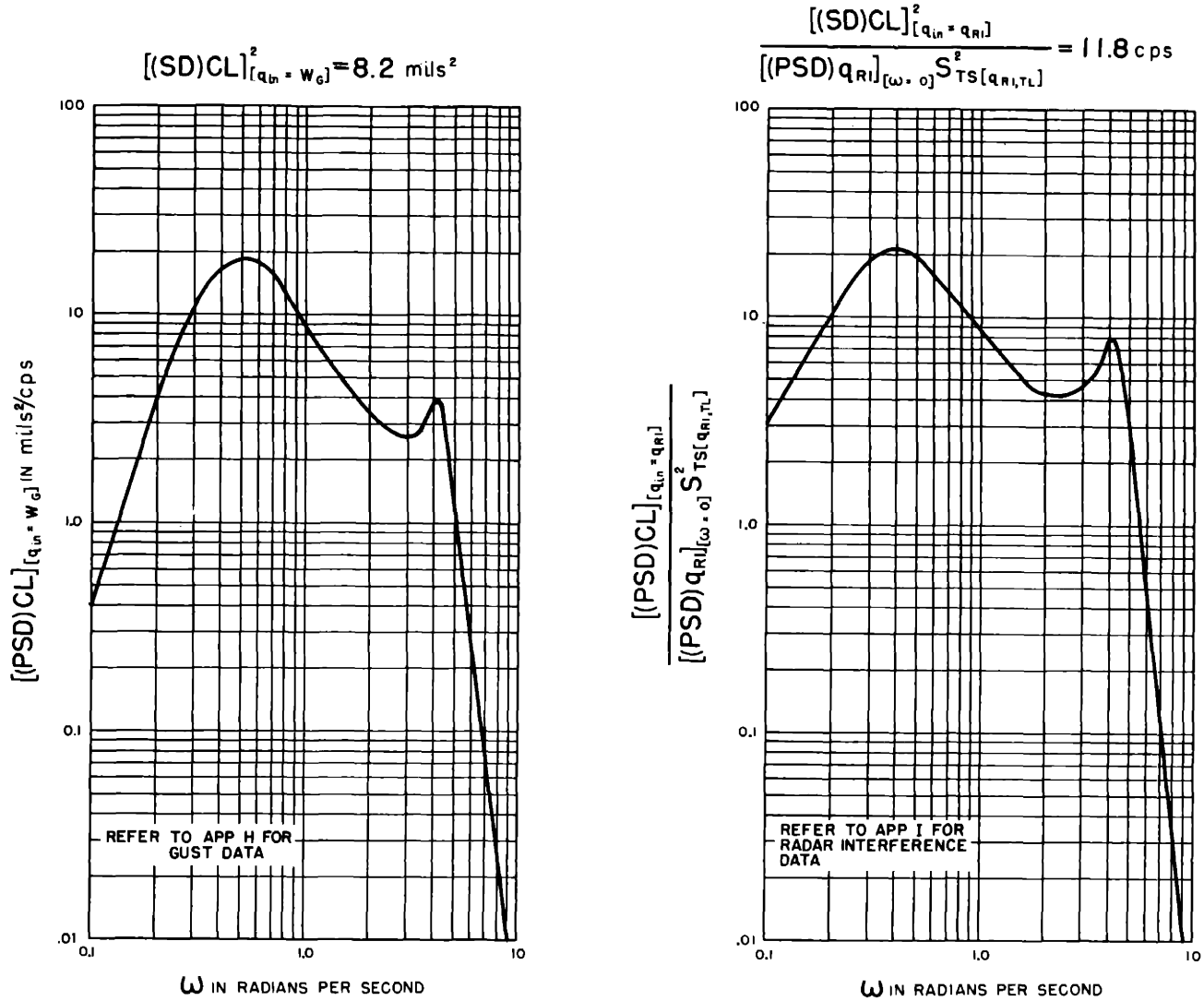

$S_{TID}\ S_{(Sm)p}\ S_{(S,r)} = -1.50$ $\quad S_{P(\omega,P)} = 13.85$ sec

$S_{TID}\ S_{(Sm)i}\ S_{(S,r)} = 0$ sec^{-1} $\quad SN = 0.25$

$(CT)_{(Sm)} = 0.30$ sec $\quad (CT)_R = 0.15$ sec

AIRCRAFT CHARACTERISTICS OF APP B

FIG III-50 POWER SPECTRAL DENSITIES RESULTING FROM GUST AND RADAR INTERFERENCE OF CLOSED-LOOP TRACKING SYSTEM WITH THE CONTROLLED LINE PREDICTION

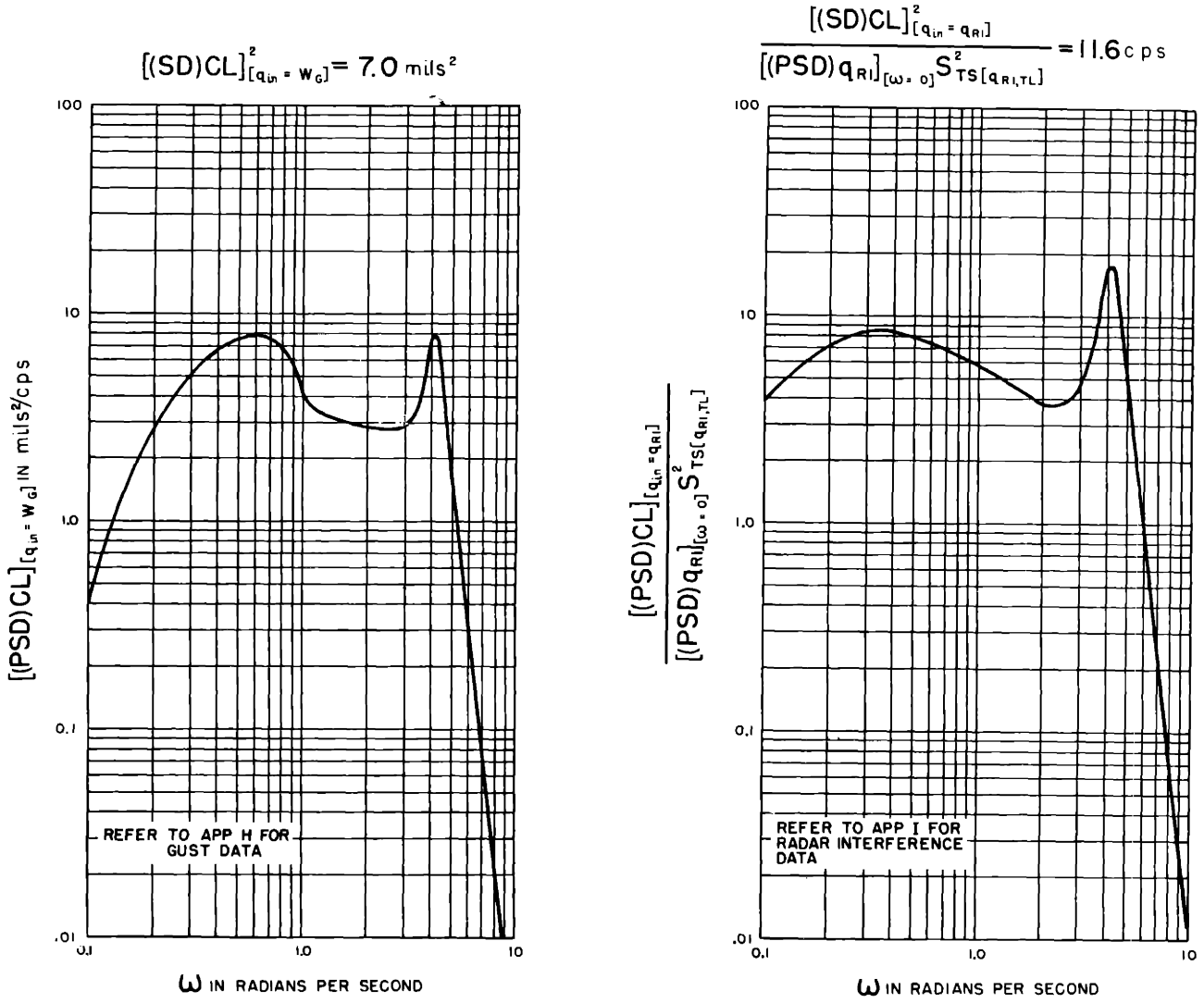

$S_{TID}\ S_{(sm)p}\ S_{(S,r)} = -1.50$ $\quad S_{P(\omega,P)} = 13.85$ sec

$S_{TID}\ S_{(sm)i}\ S_{(S,r)} = 0$ sec^{-1} $\quad SN = 0.50$

$(CT)_{(sm)} = 0.30$ sec $\quad (CT)_R = 0.15$ sec

AIRCRAFT CHARACTERISTICS OF APP B

FIG III-51 POWER SPECTRAL DENSITIES RESULTING FROM GUST AND RADAR INTERFERENCE OF CLOSED-LOOP TRACKING SYSTEM WITH THE CONTROLLED LINE PREDICTION

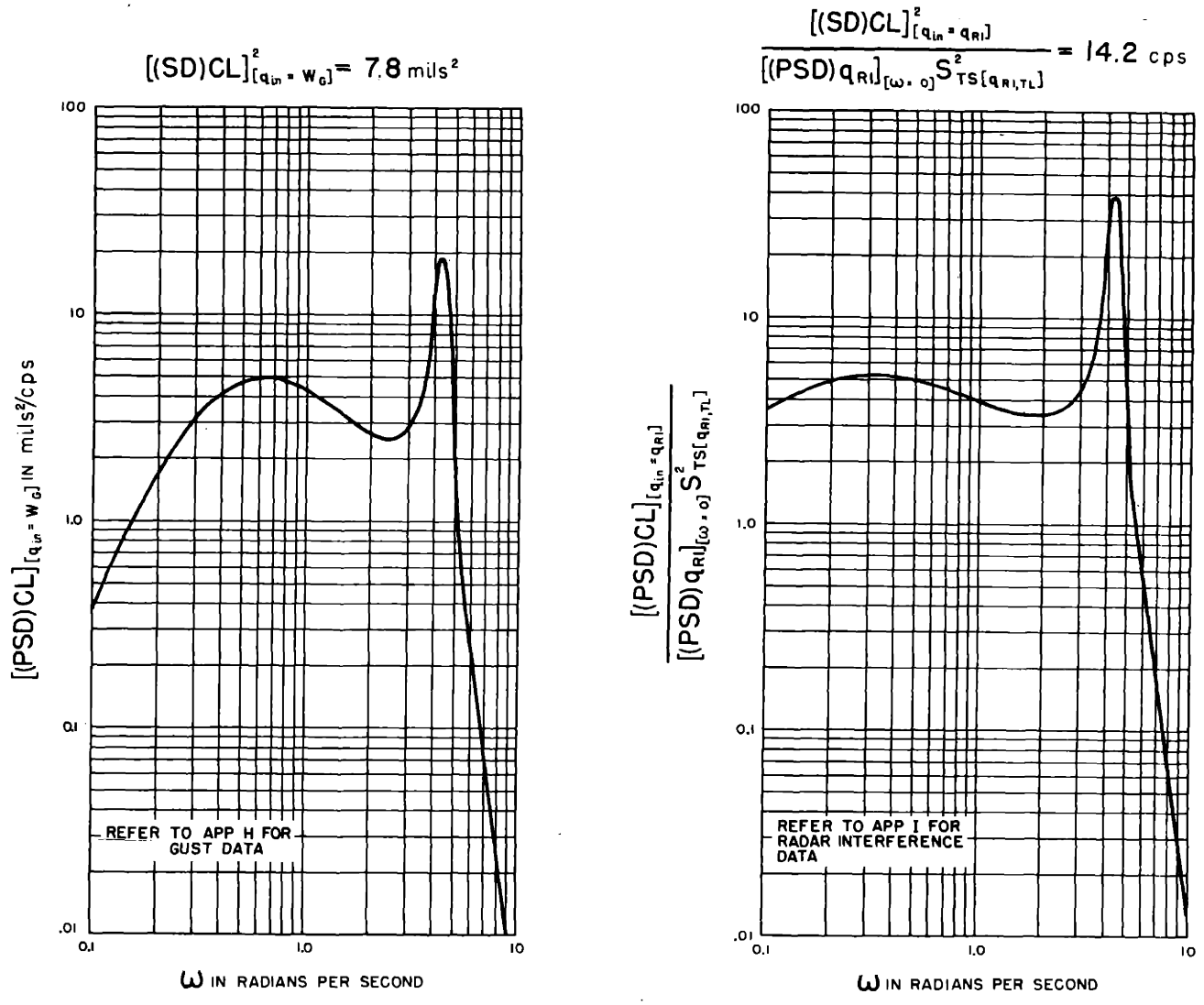

$S_{TID}\ S_{(sm)p}\ S_{(s,r)} = -1.50$ $\quad S_{P(\omega,P)} = 13.85$ sec

$S_{TID}\ S_{(sm)i}\ S_{(s,r)} = 0$ sec^{-1} $\quad SN = 0.75$

$(CT)_{(sm)} = 0.30$ sec $\quad (CT)_R = 0.15$ sec

AIRCRAFT CHARACTERISTICS OF APP B

FIG III-52 POWER SPECTRAL DENSITIES RESULTING FROM GUST AND RADAR INTERFERENCE OF CLOSED-LOOP TRACKING SYSTEM WITH THE CONTROLLED LINE PREDICTION

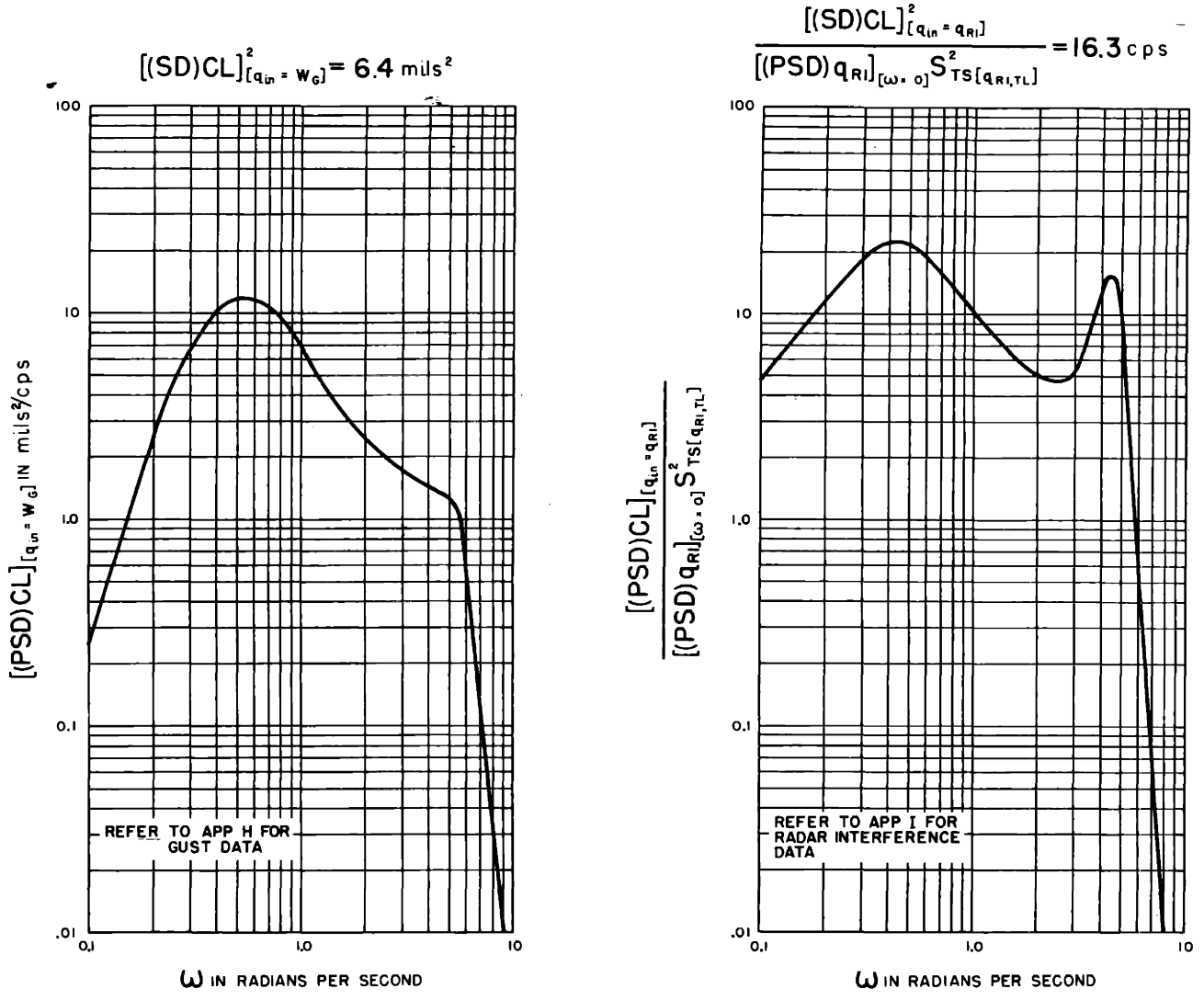

$S_{TID}\ S_{(Sm)p}\ S_{(S,r)} = -1.94$ $\quad S_{P(\omega,P)} = 13.85$ sec

$S_{TID}\ S_{(Sm)i}\ S_{(S,r)} = 0$ sec^{-1} $\quad SN = 0.25$

$(CT)_{(Sm)} = 0.30$ sec $\quad (CT)_R = 0.15$ sec

AIRCRAFT CHARACTERISTICS OF APP B

FIG III-53 POWER SPECTRAL DENSITIES RESULTING FROM GUST AND RADAR INTERFERENCE OF CLOSED-LOOP TRACKING SYSTEM WITH THE CONTROLLED LINE PREDICTION

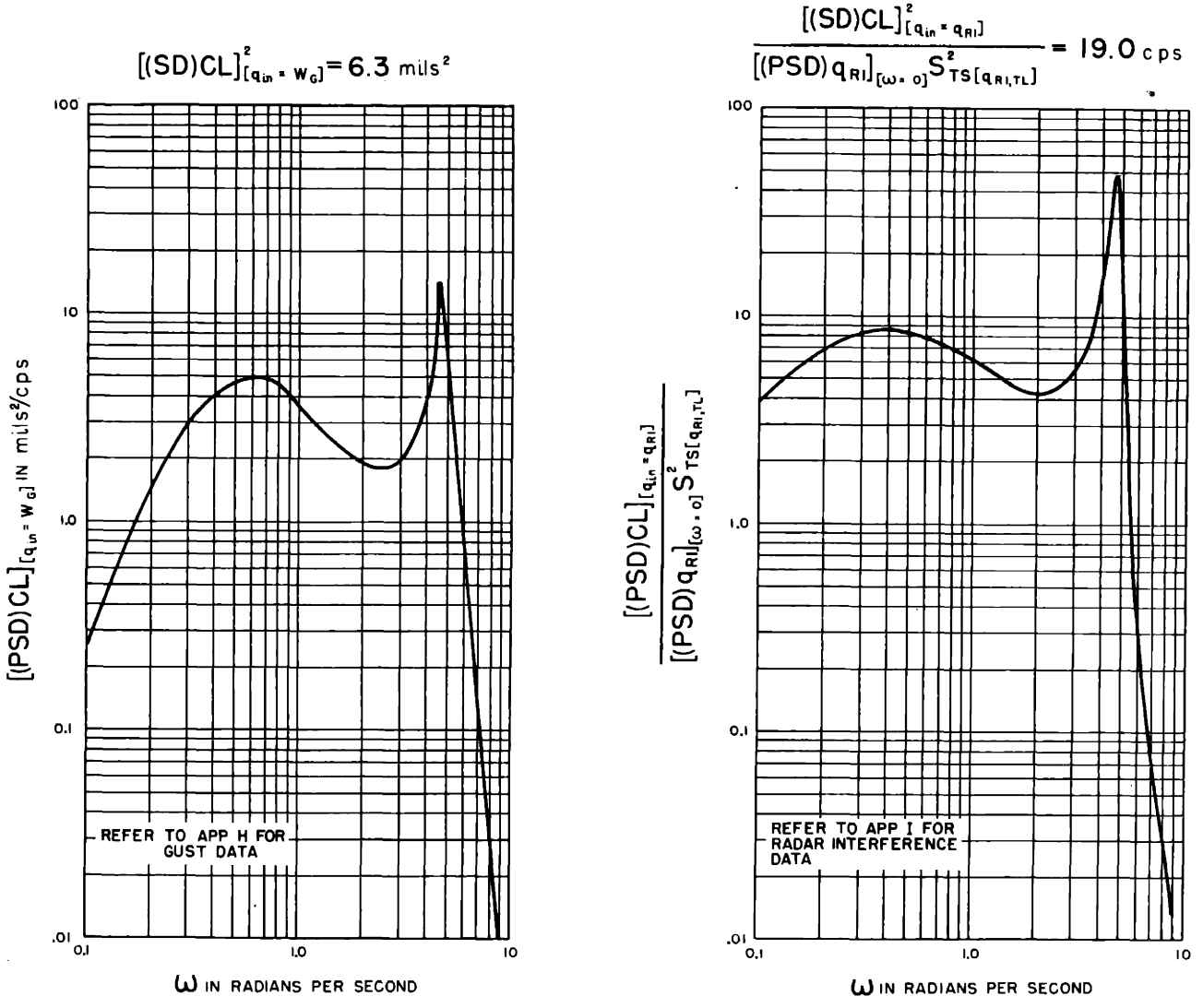

$S_{TID}\ S_{(sm)p}\ S_{(s,r)} = -1.94$ $\quad S_{P(\omega,P)} = 13.85$ sec

$S_{TID}\ S_{(sm)i}\ S_{(s,r)} = 0$ sec^{-1} $\quad SN = C.50$

$(CT)_{(Sm)} = 0.30$ sec $\quad (CT)_R = 0.15$ sec

AIRCRAFT CHARACTERISTICS OF APP B

FIG III-54 POWER SPECTRAL DENSITIES RESULTING FROM GUST AND RADAR INTERFERENCE OF CLOSED-LOOP TRACKING SYSTEM WITH THE CONTROLLED LINE PREDICTION

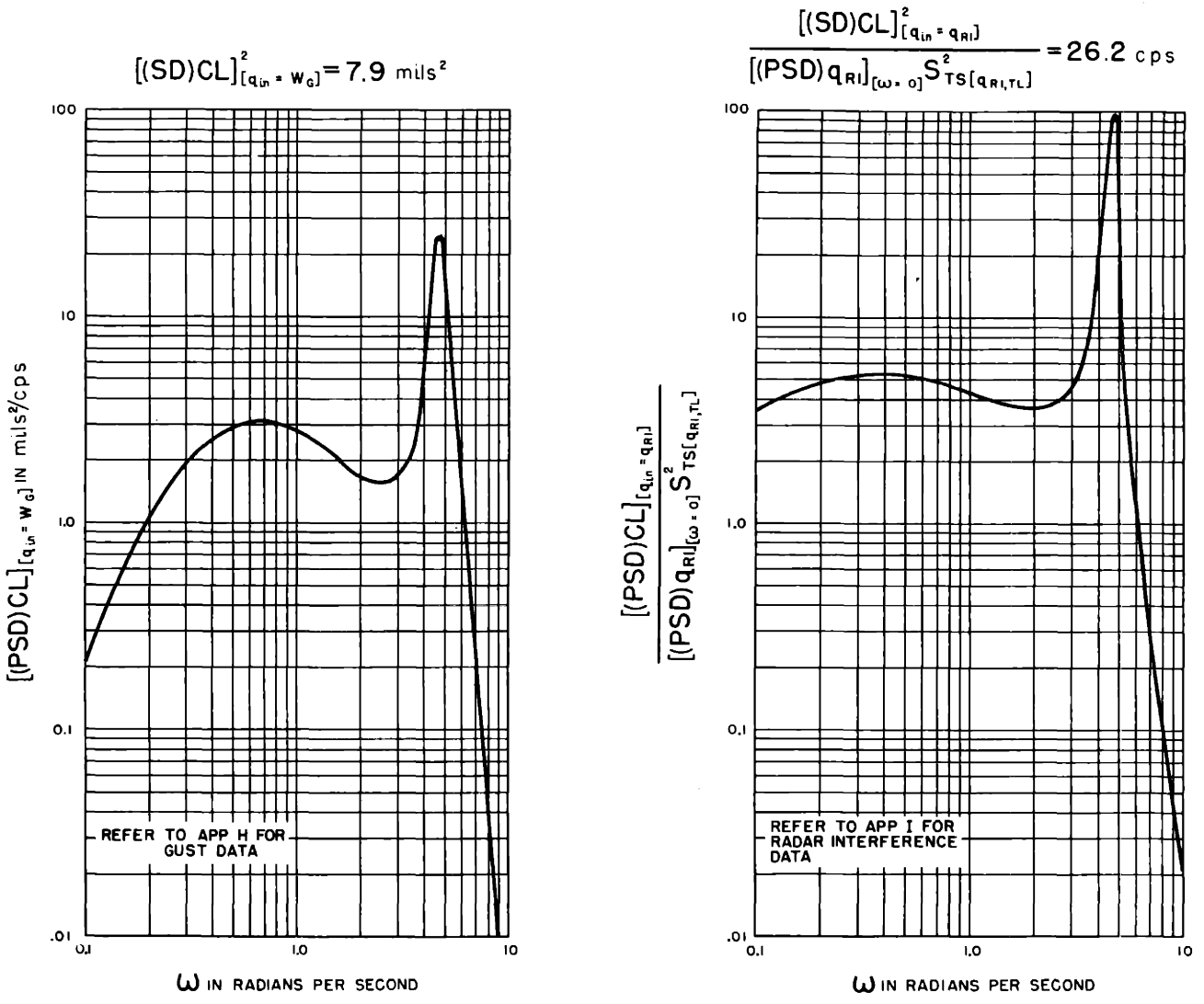

$S_{TID}\ S_{(sm)p}\ S_{(s,r)} = -1.94$ $\quad S_{P(\omega,P)} = 13.85$ sec

$S_{TID}\ S_{(sm)i}\ S_{(s,r)} = 0$ sec^{-1} $\quad SN = 0.75$

$(CT)_{(sm)} = 0.30$ sec $\quad (CT)_R = 0.15$ sec

AIRCRAFT CHARACTERISTICS OF APP B

FIG III-55 POWER SPECTRAL DENSITIES RESULTING FROM GUST AND RADAR INTERFERENCE OF CLOSED-LOOP TRACKING SYSTEM WITH THE CONTROLLED LINE PREDICTION

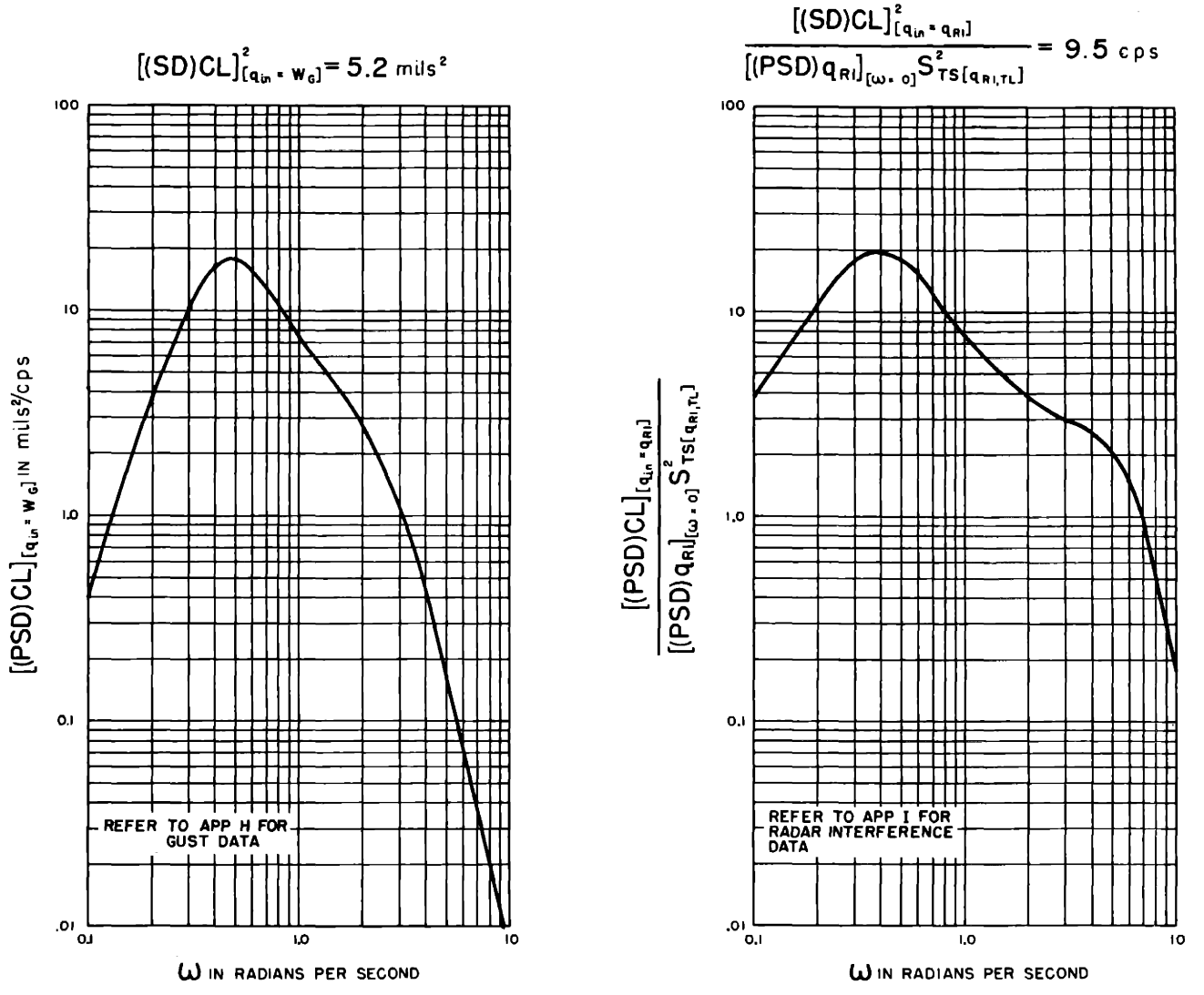

$S_{TID}\ S_{(sm)p}\ S_{(s,r)} = -1.50$ $\quad S_{P(\omega,P)} = 13.85$ sec

$S_{TID}\ S_{(sm)i}\ S_{(s,r)} = 0$ sec^{-1} $\quad SN = 0.25$

$(CT)_{(sm)} = 0$ sec $\quad (CT)_R = 0.15$ sec

AIRCRAFT CHARACTERISTICS OF APP B

FIG III-56 POWER SPECTRAL DENSITIES RESULTING FROM GUST AND RADAR INTERFERENCE OF CLOSED-LOOP TRACKING SYSTEM WITH THE CONTROLLED LINE PREDICTION

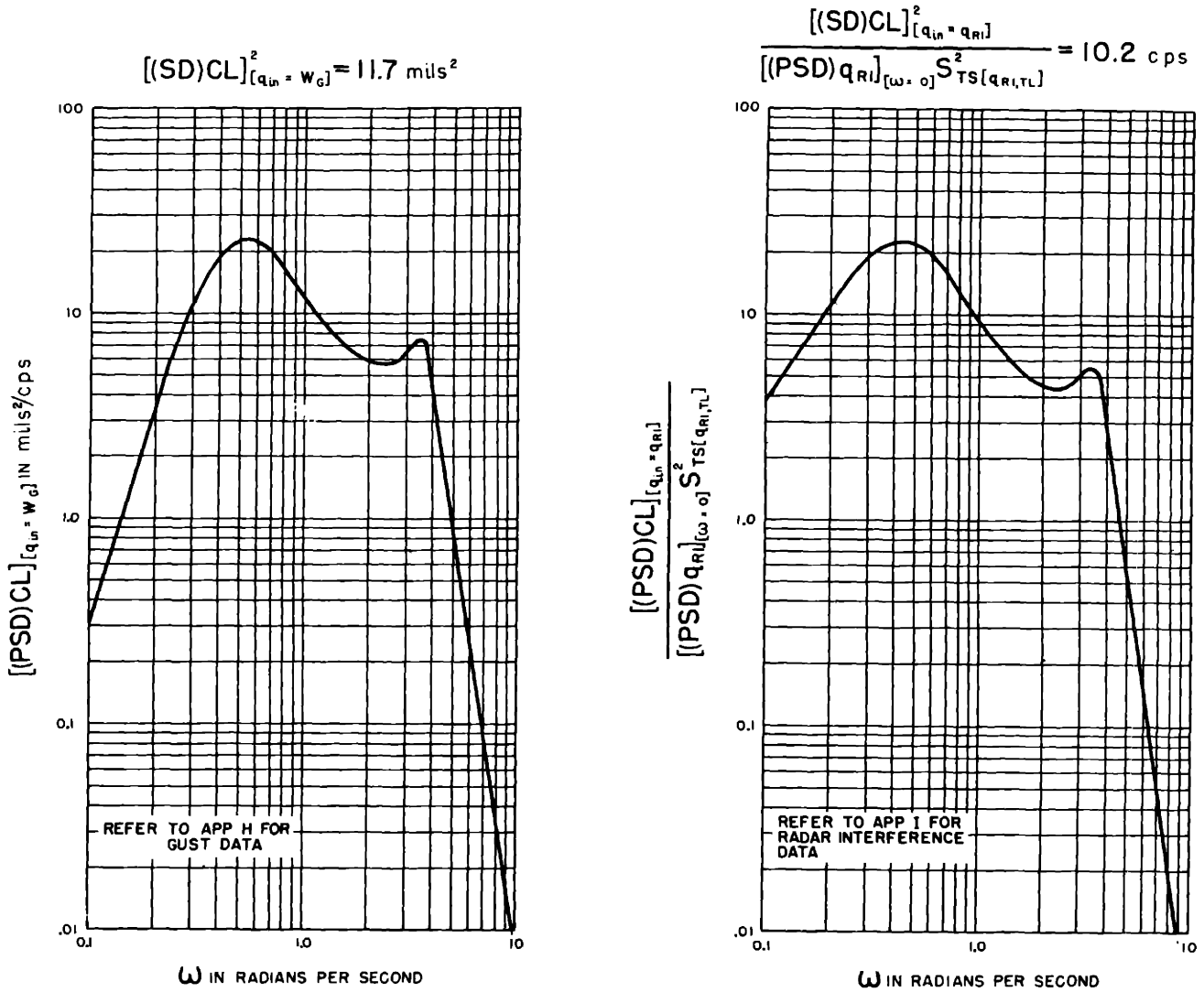

$S_{TID}\ S_{(sm)p}\ S_{(S,r)} = -1.00$ $\quad S_{P(\omega,P)} = 13.85$ sec

$S_{TID}\ S_{(sm)i}\ S_{(S,r)} = 0$ sec^{-1} $\quad SN = 0.25$

$(CT)_{(sm)} = 0.60$ sec $\quad (CT)_R = 0.15$ sec

AIRCRAFT CHARACTERISTICS OF APP B

FIG III-57 POWER SPECTRAL DENSITIES RESULTING FROM GUST AND RADAR INTERFERENCE OF CLOSED-LOOP TRACKING SYSTEM WITH THE CONTROLLED LINE PREDICTION

CHAPTER IV

CLOSED-LOOP TRACKING SYSTEM WITH CONTROLLED-LINE PREDICTION AND TIGHT-LOOP STABILIZATION OF THE INTERCEPTOR AIRCRAFT

A functional diagram of the closed-loop tracking system with controlled-line prediction and tight-loop stabilization of the aircraft is shown in Fig. IV-1. The responses of the system in the absence of gust and radar interference are presented in Fig. IV-2 through IV-11. Inasmuch as this system did not appear especially promising, the values of the power spectral density were not determined.

The results contained in this chapter were obtained by using Eq. B-8 and B-9 to represent the performance of the aircraft, supplemented with the following differential equations which are derived in Appendices C, D, and E:

For the prediction computer –

$$S_{p(W,P)}[1 + SN]S_{RAS}\dot{V}_{PC} + S_{RAS}V_{PC} = S_{p(W,P)}W_{CL} \qquad \text{IV-1}$$

where

$$S_{p(W,P)} = (PSR)\frac{R}{V_{p(av)} - V_A} \qquad \text{IV-2}$$

For the radar antenna servo –

$$(CT)_R \dot{P}_R + P_R = S_{RAS} V_{PC} \qquad \text{IV-3}$$

For the longitudinal control system, including the tracking inaccuracy detector –

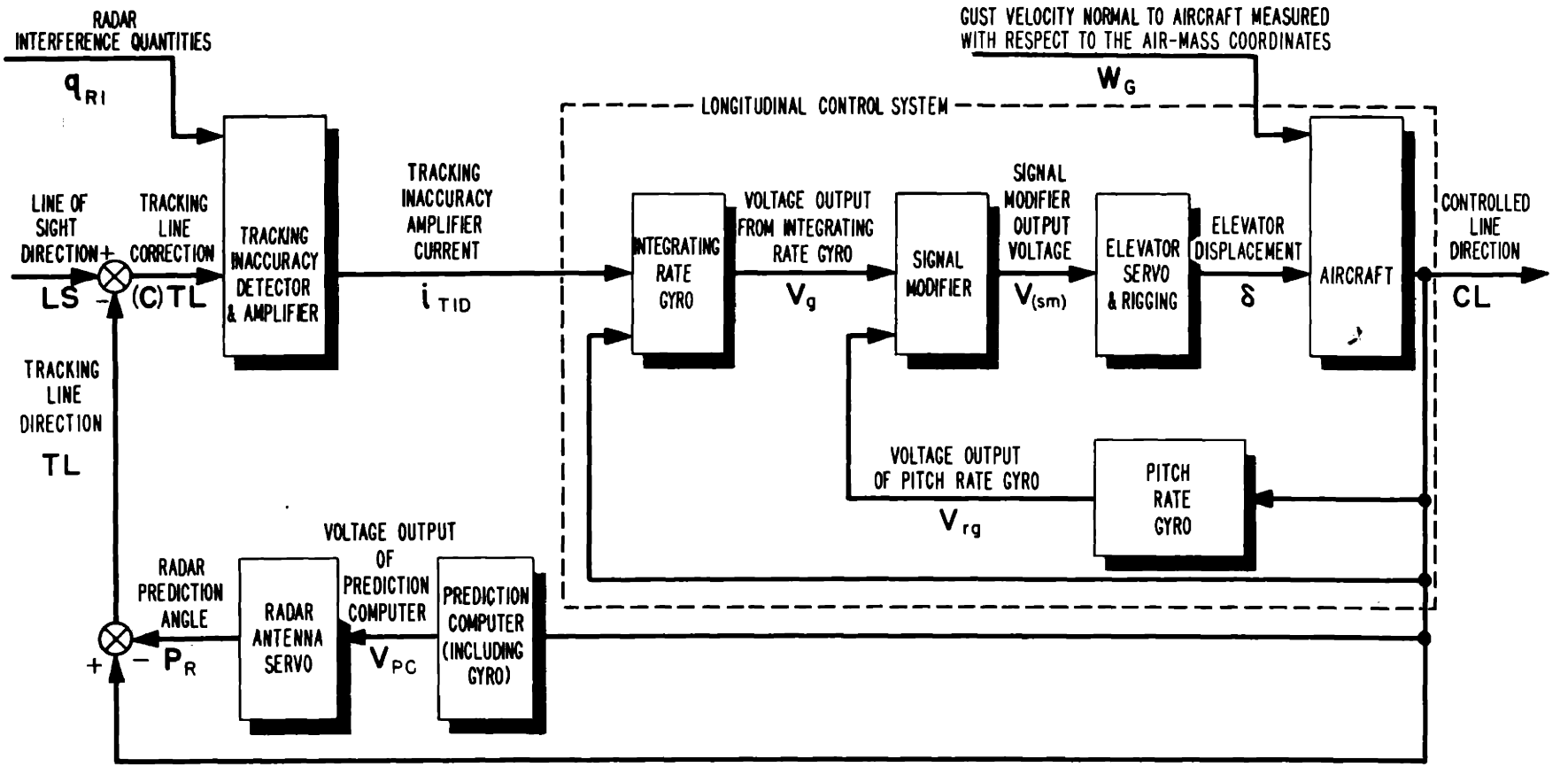

FIG IV-1 FUNCTIONAL DIAGRAM OF CLOSED-LOOP TRACKING SYSTEM WITH CONTROLLED LINE PREDICTION AND TIGHT-LOOP STABILIZATION OF THE AIRCRAFT

$$\delta = -[S_{g(CL,V)}S_{(sm)p}S_{(s,r)}][S_{TID}S_{LCS(i,W)}]\int[(C)TL]\,dt$$

$$+[S_{g(CL,V)}S_{(sm)p}S_{(s,r)}]CL + [S_{rg}S_{(sm)}\dot{\theta}\,S_{(s,r)}]W_{CL} \qquad \text{IV-4}$$

where

$$(C)TL = LS + P_R - CL \qquad \text{IV-5}$$

The prediction computer with radar antenna servo, the tracking inaccuracy detector, and their interconnections are the same in this tracking system as in the system analyzed in Chapter III.

It should be noted that in the systems described in Chapters I, II, and III changes in the stability derivatives of the interceptor aircraft change not only the aircraft lag but also the open-loop gain of the tracking system. The stability derivatives of the aircraft vary appreciably with speed and altitude; consequently, it is necessary to program the proportional sensitivity of the signal modifier as a function of altitude and speed when using the tracking systems of Chapters I, II, and III. Moreover, in system III the output from the tracking inaccuracy detector feeds through the signal modifier directly to the elevator servo. High frequency effects that may not disturb the aircraft controlled line may cause excessive elevator jitter, resulting in a structural failure of the tail. In an attempt to eliminate this difficulty and to minimize the effect of changes in the aircraft stability derivatives, an integrating rate gyro is used in the tracking system of this chapter and in the one of Chapter V. In this system the integrating gyro is used to stabilize the primary quantity, namely, the aircraft. Stabilizing the aircraft with an integrating gyro during tracking has the further advantage that this same gyro can be used to stabilize the aircraft during all phases of the interceptor operation, including take-off and landing.

It can be seen from Eq. IV-4 that the elevator is displaced an amount proportional to both the displacement of the controlled line and its angular velocity. The first term provides space stabilization; the second introduces damping additional to the aerodynamic damping of the aircraft. The aircraft is maneuvered by introducing a current to the torque generator in the integrating rate gyro. This results in an angular deflection of the gimbal frame, which changes the voltage output from the gyro and, as a result of action by the servo and elevator, the controlled line is displaced to a new position. The

current applied to the torque generator is proportional to the tracking line correction, as can be seen from Fig. IV-1. In a steady-state turn, it can be seen from Eq. IV-4 that the controlled line rotates at an angular velocity proportional to the tracking line correction.

The results of Fig. IV-2 through IV-10 are for a ratio of initial range to aircraft velocity of 40 seconds and a target angle of 30 degrees. The values of the stability number are .25, .50, and .75, with longitudinal control system open-loop gains of .50 and .75 mil elevator per mil displacement of the controlled line. Values are obtained for the ratio of controlled-line angular velocity to tracking line correction of 2 and 3 seconds^{-1}. Pitch rate feedback is used in all cases. It can be seen that the stability number is the dominant parameter and that for optimum performance it must have a value of approximately .6. However, even with this value the forced error is large at short range, and becomes even higher in the 90-degree beam attack, shown in Fig. IV-11. This result eliminates this tracking system from use in interceptor aircraft. The result is felt to be of quite general interest, however, since the dynamics of the complete longitudinal control system can be considered that of an aircraft with time lags greater than those of the F-94. Consequently, it can be seen that as the aircraft lags increase the stability number must also be increased, in order to eliminate long-period oscillations. Even more important is the fact that the tracking system with the long-period oscillation removed cannot be used effectively for gunfire or rocketfire, inasmuch as the controlled-line error is excessively large. The closed-loop tracking system of Chapter V permits tight-loop stabilization of the aircraft without introducing excessive dynamic lags in series with the computation.

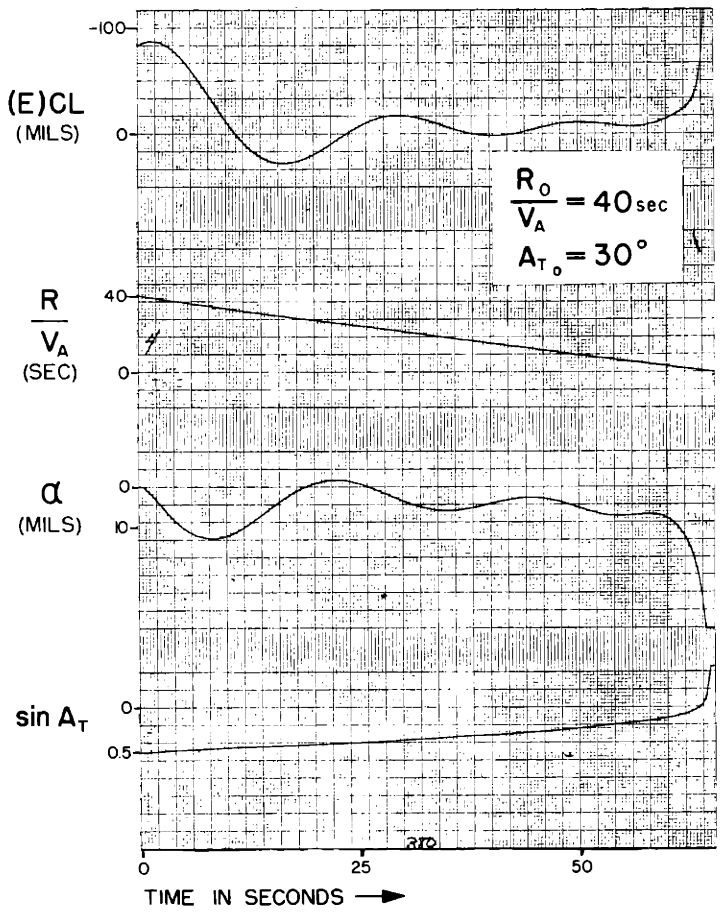

$S_{g(CL,V)}\, S_{(sm)p}\, S_{(s,r)} = 0.50$ PSR = 1.11

$S_{rg}\, S_{(sm)\dot{\theta}}\, S_{(s,r)} = .026$ SN = 0.25

$S_{TID}\, S_{LCS[i,\omega]} = 2.0\ \text{sec}^{-1}$ $(CT)_R = 0.15$ sec

$(CT)_{(sm)} = 0$

AIRCRAFT CHARACTERISTICS OF APP B

FIG IV - 2

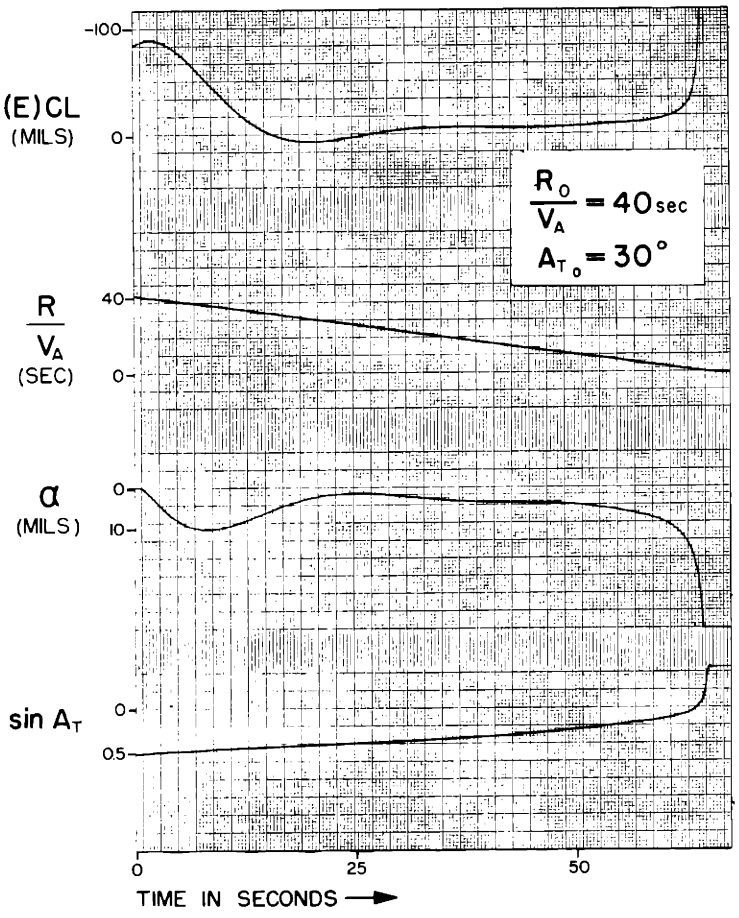

$S_{g(CL,V)}\, S_{(sm)p}\, S_{(s,r)} = 0.50$ PSR = 1.11

$S_{rg}\, S_{(sm)\dot{\theta}}\, S_{(s,r)} = .026$ SN = 0.50

$S_{TID}\, S_{LCS[i,\omega]} = 2.0\ \text{sec}^{-1}$ $(CT)_R = 0.15$ sec

$(CT)_{(sm)} = 0$

AIRCRAFT CHARACTERISTICS OF APP B

FIG IV - 3

RESPONSE OF CLOSED-LOOP TRACKING SYSTEM WITH CONTROLLED-LINE PREDICTION AND TIGHT-LOOP STABILILIZATION OF THE AIRCRAFT IN THE ABSENCE OF GUST AND RADAR INTERFERENCE

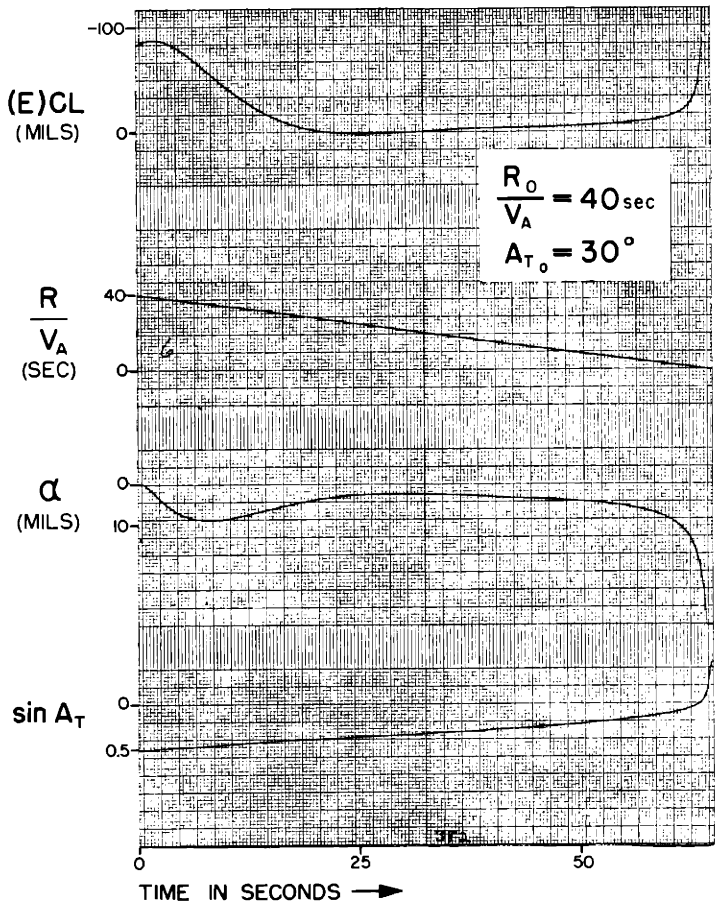

$S_{g(CL,V)}\, S_{(sm)p}\, S_{(s,r)} = 0.50$ PSR = 1.11

$S_{rg}\, S_{(sm)\dot{\theta}}\, S_{(s,r)} = .026$ SN = 0.75

$S_{TID}\, S_{LCS[i,\omega]} = 2.0\ \text{sec}^{-1}$ $(CT)_R = 0.15$ sec

$(CT)_{(sm)} = 0$

AIRCRAFT CHARACTERISTICS OF APP B

FIG IV – 4

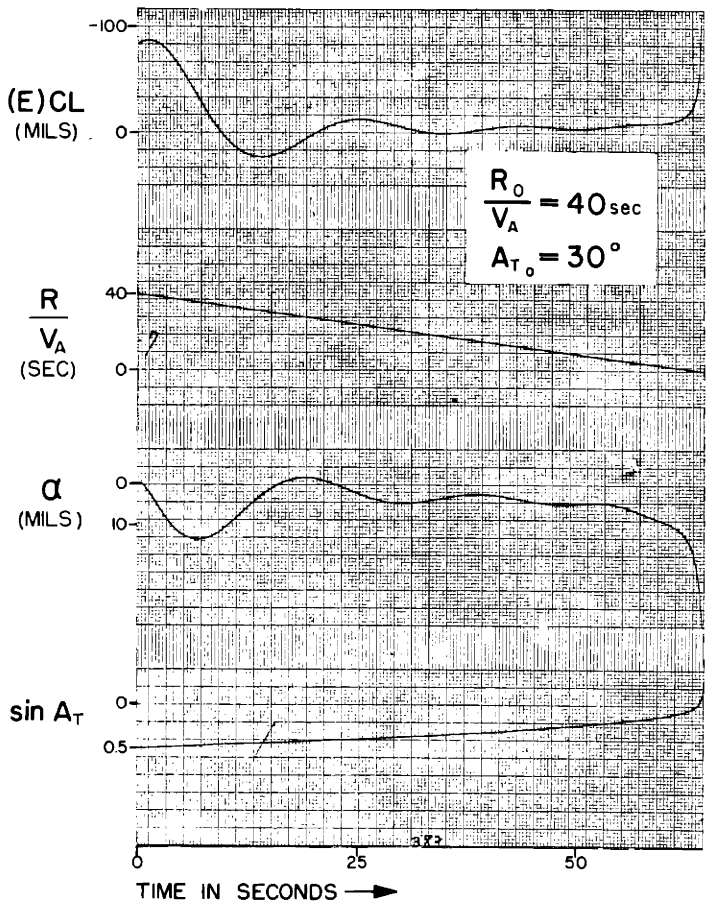

$S_{g(CL,V)}\, S_{(sm)p}\, S_{(s,r)} = 0.50$ PSR = 1.11

$S_{rg}\, S_{(sm)\dot{\theta}}\, S_{(s,r)} = .026$ SN = 0.25

$S_{TID}\, S_{LCS[i,\omega]} = 3.0\ \text{sec}^{-1}$ $(CT)_R = 0.15$ sec

$(CT)_{(sm)} = 0$

AIRCRAFT CHARACTERISTICS OF APP B

FIG IV – 5

RESPONSE OF CLOSED-LOOP TRACKING SYSTEM WITH CONTROLLED-LINE PREDICTION AND TIGHT-LOOP STABILILIZATION OF THE AIRCRAFT IN THE ABSENCE OF GUST AND RADAR INTERFERENCE

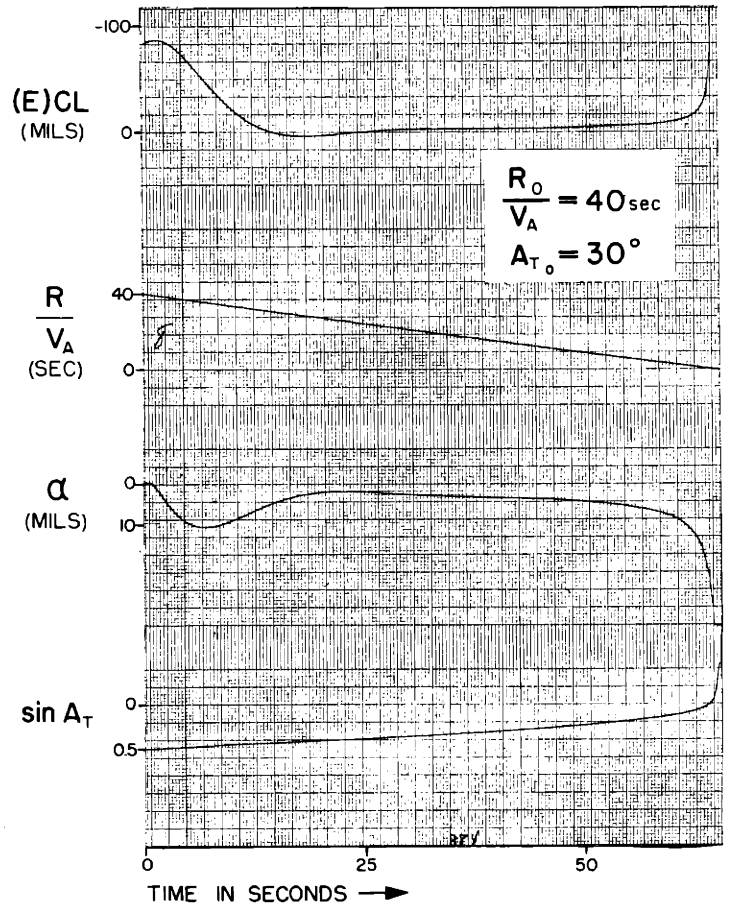

$S_{g(CL,V)}\, S_{(sm)p}\, S_{(s,r)} = 0.50$ PSR = 1.11

$S_{rg}\, S_{(sm)\dot{\theta}}\, S_{(s,r)} = .026$ SN = 0.50

$S_{TID}\, S_{LCS[i,\omega]} = 3.0\ sec^{-1}$ $(CT)_R = 0.15\ sec$

$(CT)_{(sm)} = 0$

AIRCRAFT CHARACTERISTICS OF APP B

FIG IV - 6

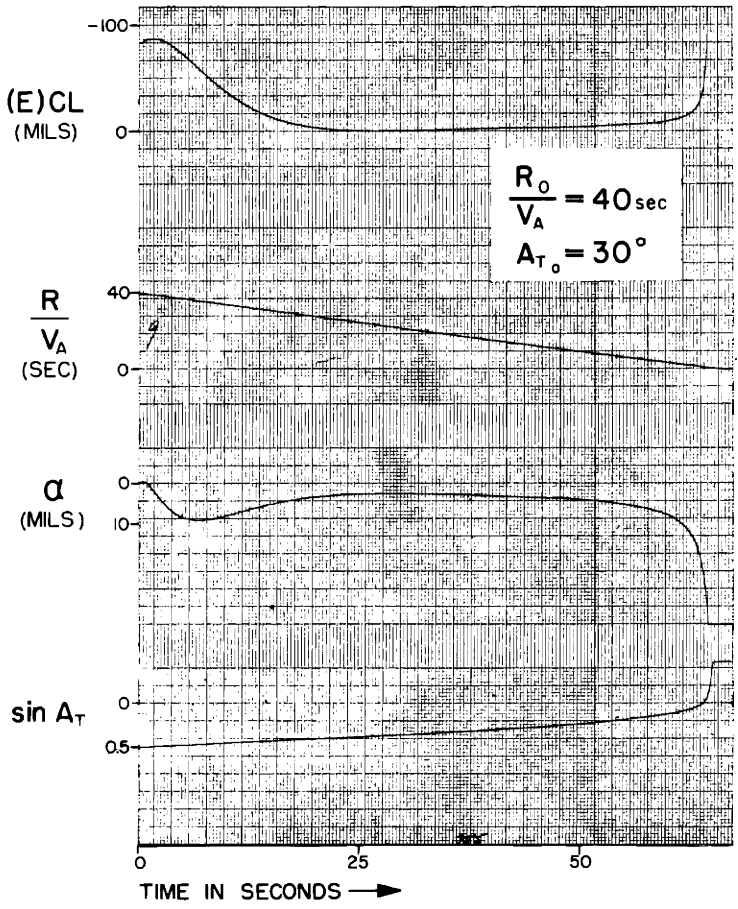

$S_{g(CL,V)}\, S_{(sm)p}\, S_{(s,r)} = 0.50$ PSR = 1.11

$S_{rg}\, S_{(sm)\dot{\theta}}\, S_{(s,r)} = .026$ SN = 0.75

$S_{TID}\, S_{LCS[i,\omega]} = 3.0\ sec^{-1}$ $(CT)_R = 0.15\ sec$

$(CT)_{(sm)} = 0$

AIRCRAFT CHARACTERISTICS OF APP B

FIG IV -7

RESPONSE OF CLOSED-LOOP TRACKING SYSTEM WITH CONTROLLED-LINE PREDICTION AND TIGHT-LOOP STABILILIZATION OF THE AIRCRAFT IN THE ABSENCE OF GUST AND RADAR INTERFERENCE

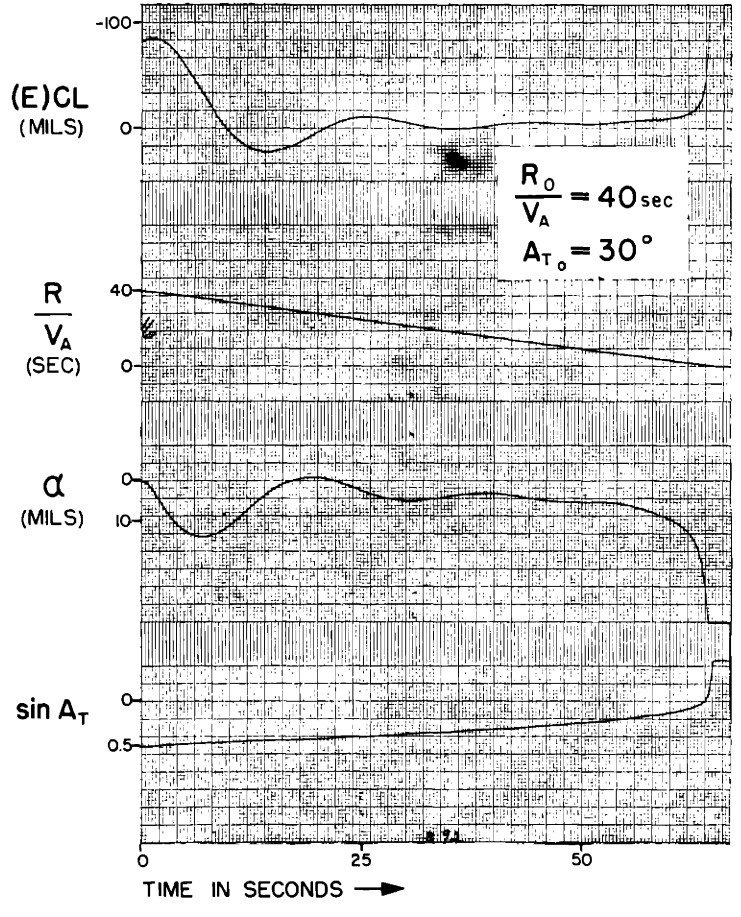

$S_{g(CL,V)}\, S_{(sm)p}\, S_{(s,r)} = 0.75$ PSR = 1.11

$S_{rg}\, S_{(sm)\dot{\theta}}\, S_{(s,r)} = .026$ SN = 0.25

$S_{TID}\, S_{LCS[i,\omega]} = 3.0\ \text{sec}^{-1}$ $(CT)_R = 0.15$ sec

$(CT)_{(sm)} = 0$

AIRCRAFT CHARACTERISTICS OF APP B

FIG IV-8

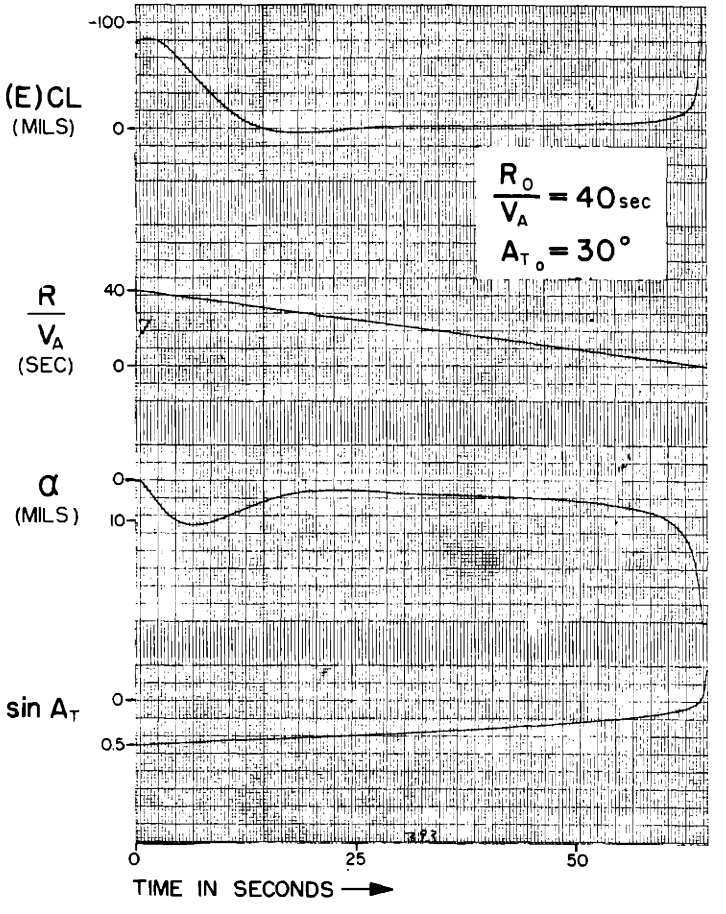

$S_{g(CL,V)}\, S_{(sm)p}\, S_{(s,r)} = 0.75$ PSR = 1.11

$S_{rg}\, S_{(sm)\dot{\theta}}\, S_{(s,r)} = .026$ SN = 0.50

$S_{TID}\, S_{LCS[i,\omega]} = 3.0\ \text{sec}^{-1}$ $(CT)_R = 0.15$ sec

$(CT)_{(sm)} = 0$

AIRCRAFT CHARACTERISTICS OF APP B

FIG IV-9

RESPONSE OF CLOSED-LOOP TRACKING SYSTEM WITH CONTROLLED-LINE PREDICTION AND TIGHT-LOOP STABILILIZATION OF THE AIRCRAFT IN THE ABSENCE OF GUST AND RADAR INTERFERENCE

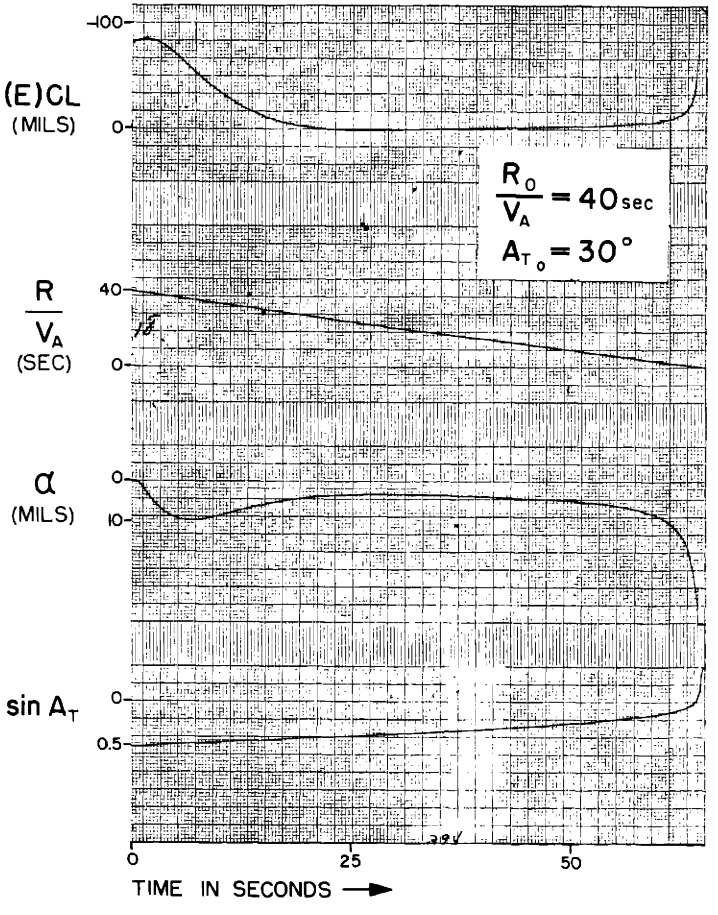

$S_{g(CL,V)}\, S_{(sm)p}\, S_{(s,r)} = 0.75$ PSR = 1.11

$S_{rg}\, S_{(sm)\dot{\theta}}\, S_{(s,r)} = .026$ SN = 0.75

$S_{TID}\, S_{LCS[i,\omega]} = 3.0\ \text{sec}^{-1}$ $(CT)_R = 0.15$ sec

$(CT)_{(sm)} = 0$

AIRCRAFT CHARACTERISTICS OF APP B

FIG IV - 10

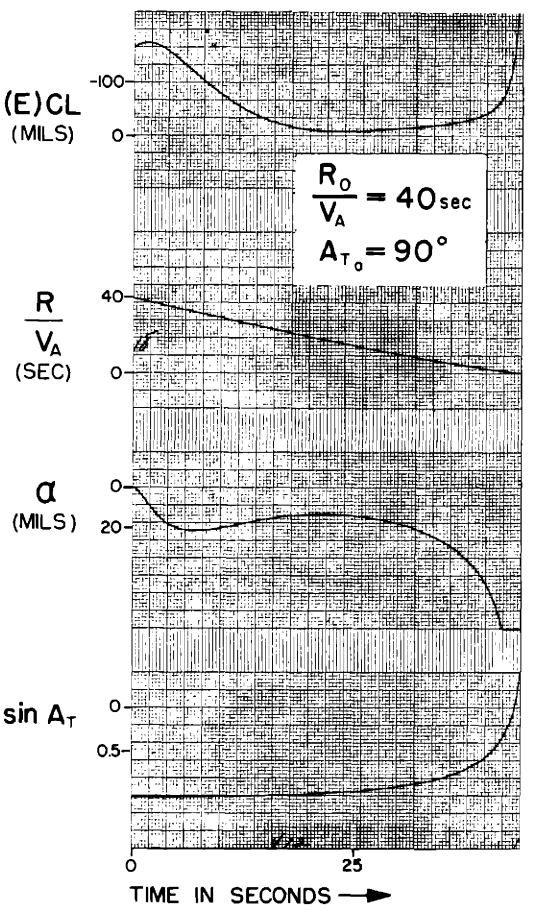

$S_{g(CL,V)}\, S_{(sm)p}\, S_{(s,r)} = 0.75$ PSR = 1.11

$S_{rg}\, S_{(sm)\dot{\theta}}\, S_{(s,r)} = .026$ SN = 0.75

$S_{TID}\, S_{LCS[i,\omega]} = 3.0\ \text{sec}^{-1}$ $(CT)_R = 0.15$ sec

$(CT)_{(sm)} = 0$

AIRCRAFT CHARACTERISTICS OF APP B

FIG IV - 11

RESPONSE OF CLOSED-LOOP TRACKING SYSTEM WITH CONTROLLED-LINE PREDICTION AND TIGHT-LOOP STABILILIZATION OF THE AIRCRAFT IN THE ABSENCE OF GUST AND RADAR INTERFERENCE

CHAPTER V

CLOSED-LOOP TRACKING SYSTEM WITH TRACKING INACCURACY PREDICTION AND TIGHT-LOOP STABILIZATION OF THE INTERCEPTOR AIRCRAFT

Figure V-1 is a functional diagram of the closed-loop tracking system, with tracking inaccuracy prediction and tight-loop stabilization of the interceptor aircraft. The response of the system in the absence of gust and radar interference is shown in Fig. V-2 through V-23, and the power spectral densities resulting from the gust and radar interferences are contained in Fig. V-24, V-25, and V-26. An alternate arrangement of components is shown in Fig. V-27. This arrangement requires one gyro and one integrator in place of the two gyros shown in Fig. V-1. However, the alternate arrangement and the arrangement of Fig. V-1 have the same performance and can be represented by the same differential equations.

The results contained in this chapter were obtained by using Eq. B-8 and B-9 to represent the performance of the aircraft and the following differential equations which are derived in Appendices C, D, and E.

For the prediction computer –

$$S_{p(W,P)}[1 + SN]\, S_{RAS}\dot{V}_{PC} + S_{RAS}V_{PC} = S_{p(W,P)}[S_{TID}S_{LCS(i,W)}][(C)TL] \qquad V\text{-}1$$

where

$$S_{p(W,P)} = (PSR)\frac{R}{V_{p\,(av)} - V_A} \qquad V\text{-}2$$

For the radar antenna servo –

$$(CT)_R\,\dot{P}_R + P_R = S_{RAS}V_{PC} \qquad V\text{-}3$$

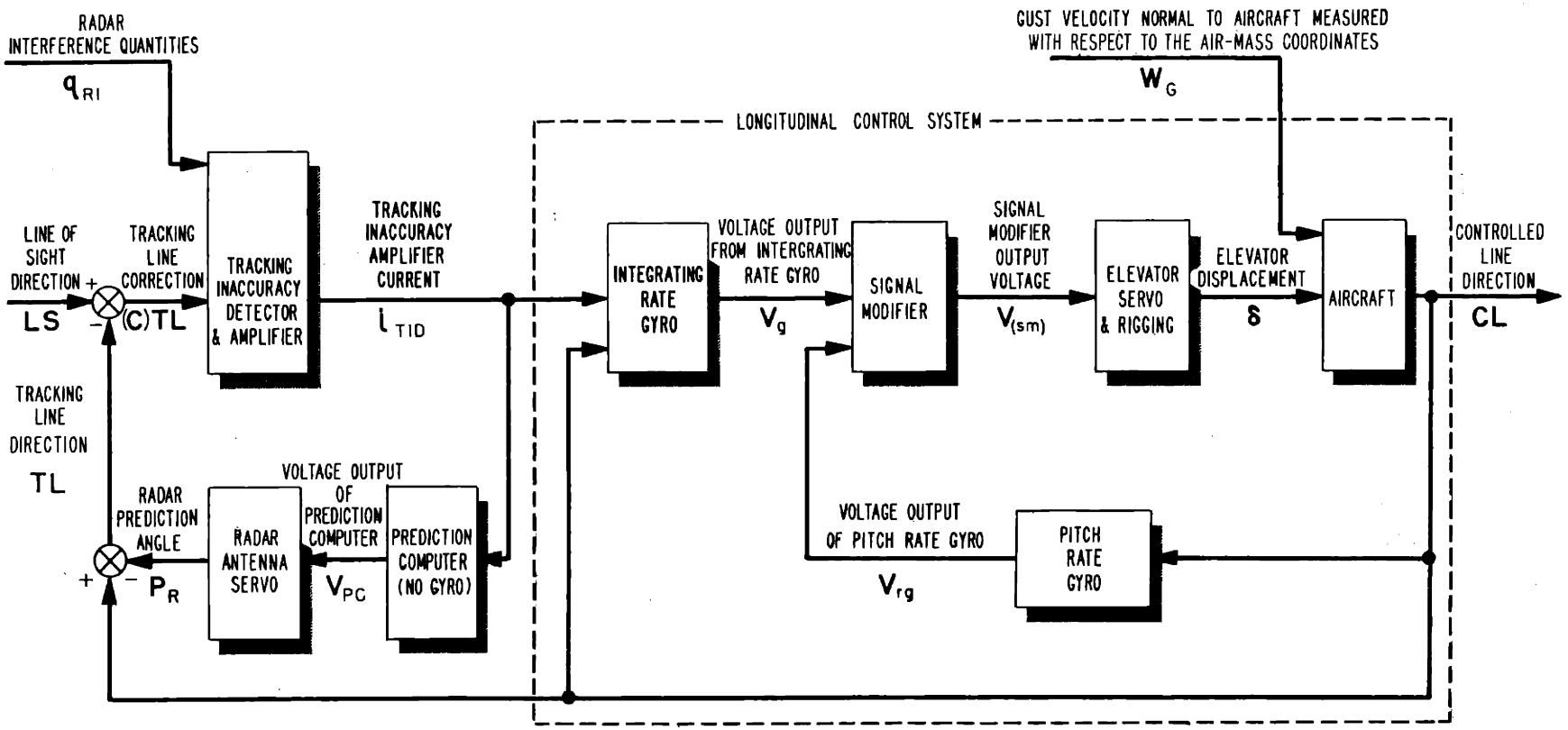

FIG V-1 FUNCTIONAL DIAGRAM OF CLOSED-LOOP TRACKING SYSTEM WITH TRACKING INACCURACY PREDICTION AND TIGHT-LOOP STABILIZATION OF THE AIRCRAFT

and for the tracking inaccuracy detector and the longitudinal control system —

$$\delta = -[S_{g(CL,V)}S_{(sm)p}S_{(s,r)}][S_{TID}S_{LCS(i,W)}]\int[(C)TL]dt$$

$$+ [S_{g(CL,V)}S_{(sm)p}S_{(s,r)}]CL + [S_{rg}S_{(sm)\dot{\theta}}S_{(s,r)}]W_{CL} \qquad V\text{-}4$$

in which

$$(C)TL = LS + P_R - CL \qquad V\text{-}5$$

It can be seen from Fig. V-1 that the aircraft is stabilized in a manner similar to that described in Chapter IV. However, the prediction computer receives as its primary input not the controlled-line angular velocity as in the system of Chapter IV, but rather the tracking inaccuracy amplifier current. It is mentioned in Chapter IV that, by means of the tight-loop stabilization, the controlled-line angular velocity is made proportional to the tracking inaccuracy amplifier current. Consequently, the current can be used as a measure of the controlled-line angular velocity in the prediction computer. In this manner, lags in the longitudinal control system are bypassed when developing the output from the prediction computer. The current introduced into the prediction computer is proportional to the tracking line correction, as indicated in Eq. V-1. The other equations are identical with those used in Chapter IV.

The improvement in performance over that obtained in Chapter IV can be noted by reference to Fig. V-2, V-3, and V-4, which were obtained for the respective initial target angles of 30, 90, and 150 degrees. The response for the nose attack with an initial target angle of 150 degrees is the best obtained with any tracking system. As stated in the Discussion of Results, at ranges less than 6,000 feet and for beam attacks, the controlled-line error is less for tracking system III than for the tracking system analyzed in this chapter. However, the fact that the system described in this chapter has the shortest solution time and appears to be the most insensitive to the direction of attack indicates that it should have the highest priority of any system under development for interceptor aircraft.

It is felt that integration in the tracking inaccuracy detector will further reduce the controlled-line error. Other types of compensation including the feedback of a signal proportional to thr rate of change of radar prediction angle may also prove beneficial.

The effect of changes in stability number, open-loop gain of the longitudinal control system, gain in the tracking inaccuracy system detector, and pitch rate feedback can be seen from Fig. V-6 through V-23. When the stability number and open-loop gain of the longitudinal control system are low, a long-period oscillation develops. With a stability number of .25 and an open-loop gain of the longitudinal control system of .50, the tracking system is unstable. The results with a stability number of .5 can be seen from Fig. V-5 and V-10. Incorporation of rate of pitch feedback improves the effective damping of the system but lowers the open-loop gain of the longitudinal control system. Hence, even with the stability number of .5 the tracking system is unstable, with a rate feedback of .026 mil elevator displacement per mil per second rate of pitch when the proportional gain is .50. Increasing the stability number to .75 stabilizes the system, as can be seen from Fig. V-20.

With an open-loop gain of the longitudinal control system of 1.0, a stable response can be obtained with a stability number of .25, as shown in Fig. V-7; but the response of Fig. V-8 with a stability number of .5 is better, since the long-period oscillation is not present.

With no pitch rate feedback, an open-loop gain of the longitudinal control system of 1.0, and a ratio of controlled-line angular velocity to tracking correction of 3, a one-cycle-per-second oscillation is present, as shown in Fig. V-12, V-13, and V-14. This oscillation is eliminated by the use of pitch rate feedback, as indicated by Fig. V-21, V-22, and V-23.

To summarize, the open-loop gain of the longitudinal control system must be high in order to obtain a satisfactory response with a stability number of .3. It is felt that by careful design, including the use of pitch rate feedback, a tight longitudinal control system can be achieved for a variety of flight conditions. This statement is borne out by the excellent performance indicated in Fig. V-2, V-3, and V-4.

The power spectral densities for the tracking system with the parameters of Fig. V-2, V-3, and V-4 are shown in the respective Fig. V-24, V-25, and V-26 for prediction sensitivities of 2.77, 8.33, and 13.85 seconds, respectively. An examination of these figures shows that the power spectral density of the controlled line resulting from radar interference has a peak value greater than 20 in each case that occurs at a frequency between .6 and 1.0 radian per second. This power spectral density equals the square of the line of sight to controlled-line amplitude ratio of the tracking system. The

fact that this amplitude ratio remains large in the frequency range around one radian per second permits the system to operate effectively in different tactical situations. The secondary peak at 5-1/2 radians per second can be eliminated by increasing the rate of pitch feedback. However, the standard deviation of the controlled line is increased only 10 percent by the presence of the peak.

In order to obtain an estimate of the optimum tracking system for interceptor aircraft, compare Fig. II-34, III-56, and V-26. These three figures represent the power spectral densities of the best results that were obtained with the systems described in Chapters II, III, and V. In each case, the power spectral density resulting from radar interference has a maximum greater than 19 occurring at a frequency between .4 and .6 radian per second. The system described in Chapter III minimizes the effect of gust interference, whereas the systems analyzed in Chapters II and V have slightly higher values for the standard deviation of the controlled line displacement. With the system of Chapter II the higher frequencies predominate, and with the system of Chapter V the lower frequency components largely contribute to the controlled-line deviations, caused by gust disturbances.

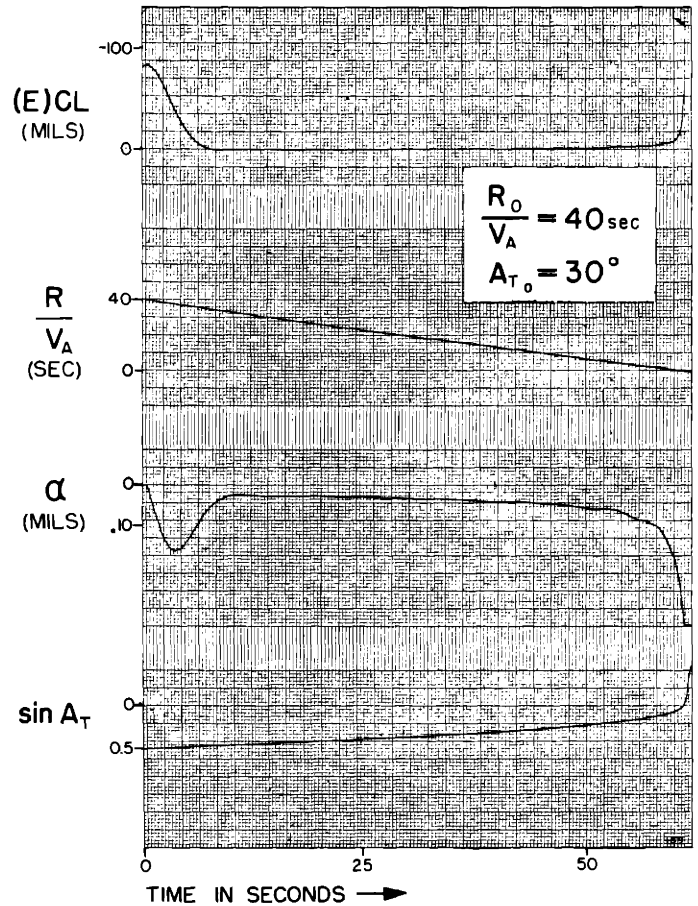

$S_{g(CL,V)} S_{(sm)p} S_{(s,r)} = 1.37$ PSR = 1.11

$S_{rg} S_{(sm)\dot{\theta}} S_{(s,r)} = .049$ SN = 0.30

$S_{TID} S_{LCS(i\omega)} = 3.0$ $(CT)_{(sm)} = 0$

$(CT)_R = 0.15$ sec

AIRCRAFT CHARACTERISTICS OF APP B

FIG V-2

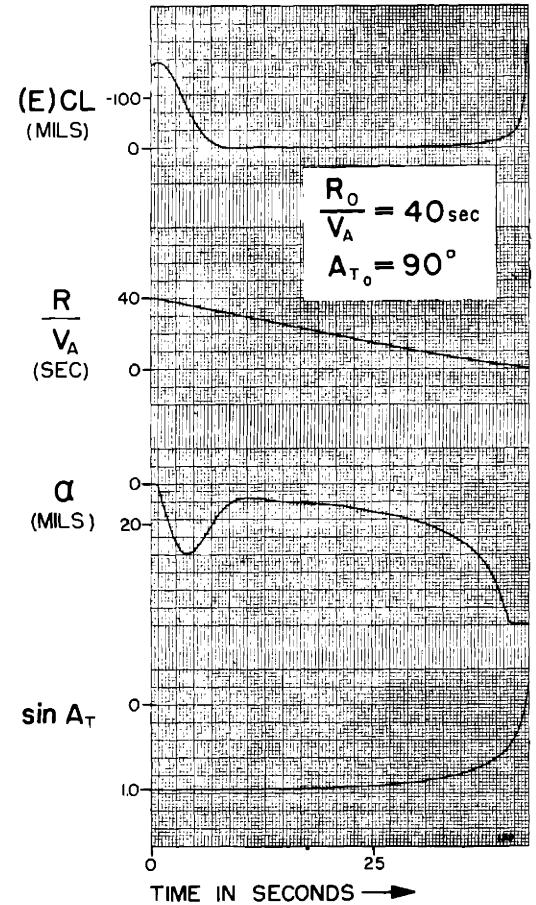

$S_{g(CL,V)} S_{(sm)p} S_{(s,r)} = 1.37$ PSR = 1.11

$S_{rg} S_{(sm)\dot{\theta}} S_{(s,r)} = .049$ SN = 0.30

$S_{TID} S_{LCS(i\omega)} = 3.0$ $(CT)_{(sm)} = 0$

$(CT)_R = 0.15$ sec

AIRCRAFT CHARACTERISTICS OF APP B

FIG V-3

RESPONSE OF CLOSED-LOOP TRACKING SYSTEM WITH TRACKING INACCURACY PREDICTION AND TIGHT-LOOP STABILIZATION OF THE AIRCRAFT IN THE ABSENCE OF GUST AND RADAR INTERFERENCE

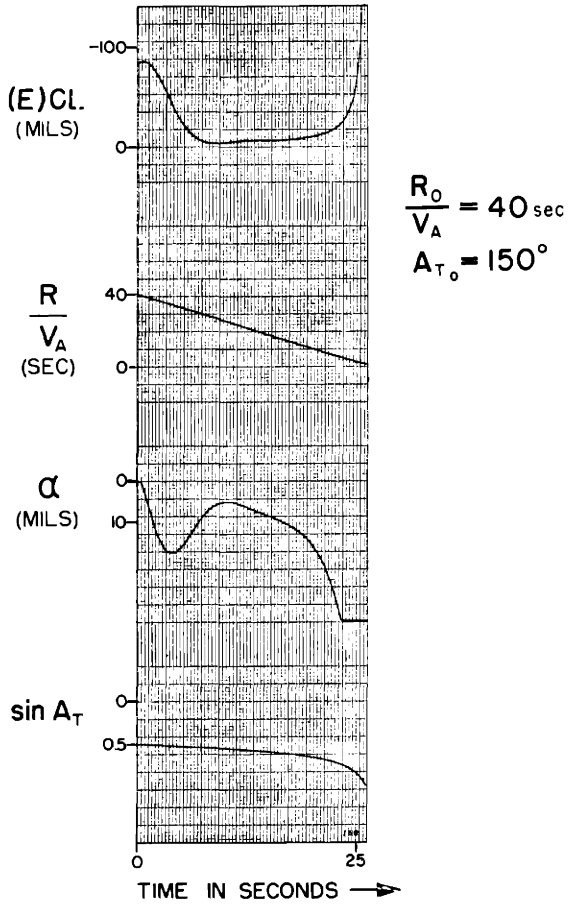

$S_{g(CL,V)} S_{(sm)p} S_{(s,r)} = 1.37$ PSR = 1.11

$S_{rg} S_{(sm)\dot{\theta}} S_{(s,r)} = .049$ SN = 0.30

$S_{TID} S_{LCS(i\omega)} = 3.0$ $(CT)_{(sm)} = 0$

$(CT)_R = 0.15$ sec

AIRCRAFT CHARACTERISTICS OF APP B

FIG V-4

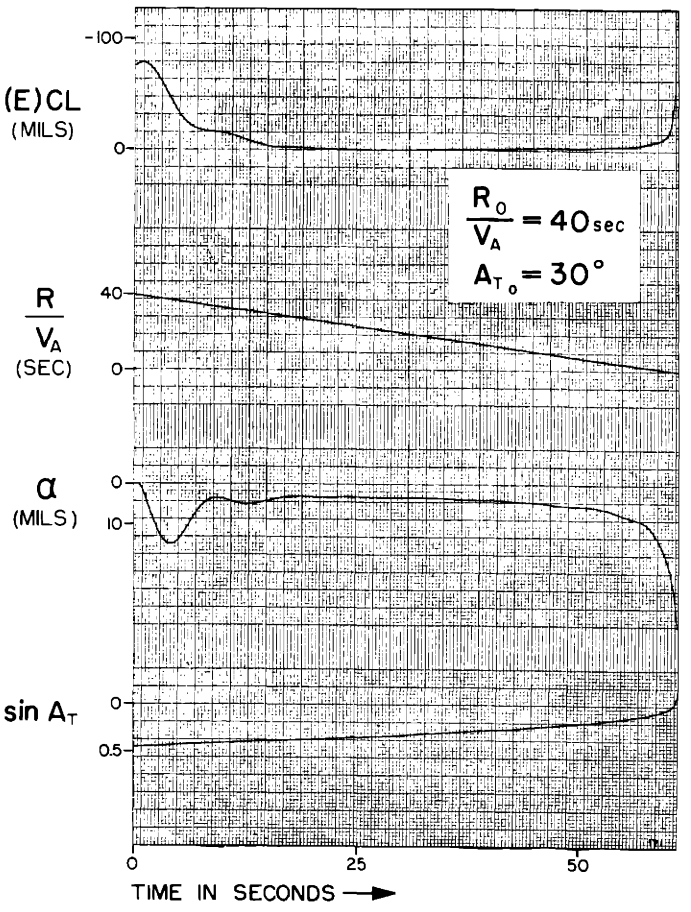

$S_{g(CL,V)} S_{(sm)p} S_{(s,r)} = 0.50$ PSR = 1.11

$S_{rg} S_{(sm)\dot{\theta}} S_{(s,r)} = 0$ SN = 0.50

$S_{TID} S_{LCS(i\omega)} = 2.0$ $(CT)_{(sm)} = 0$

$(CT)_R = 0.15$ sec

AIRCRAFT CHARACTERISTICS OF APP B

FIG V-5

RESPONSE OF CLOSED-LOOP TRACKING SYSTEM WITH TRACKING INACCURACY PREDICTION AND TIGHT-LOOP STABILIZATION OF THE AIRCRAFT IN THE ABSENCE OF GUST AND RADAR INTERFERENCE

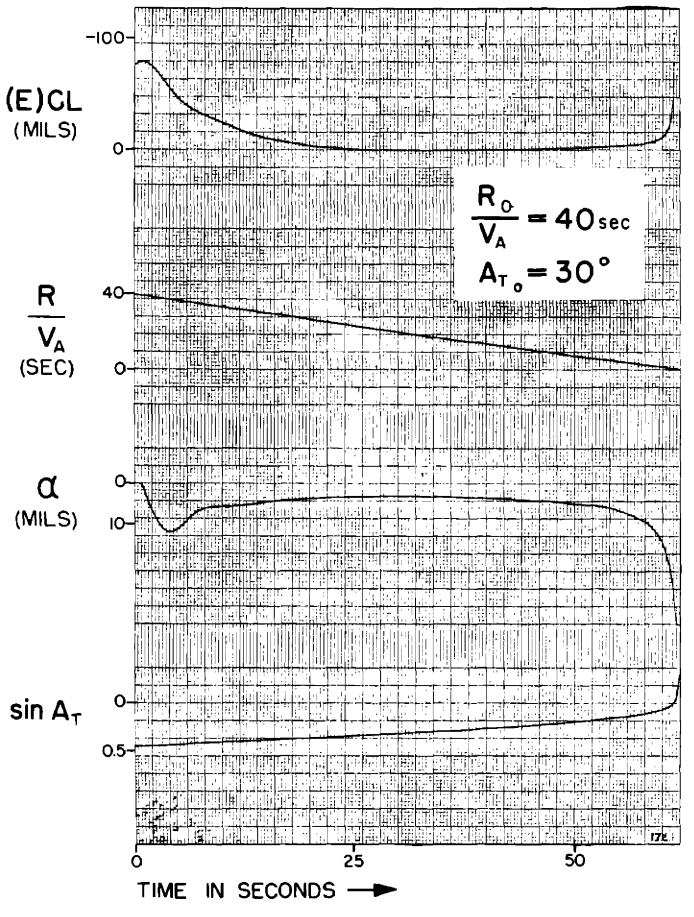

$S_{g(CL,V)} S_{(sm)p} S_{(s,r)} = 0.50$ PSR = 1.11

$S_{rg} S_{(sm)\dot{\theta}} S_{(s,r)} = 0$ SN = 0.75

$S_{TID} S_{LCS(i\omega)} = 2.0$ $(CT)_{(sm)} = 0$

$(CT)_R = 0.15$ sec

AIRCRAFT CHARACTERISTICS OF APP B

FIG V-6

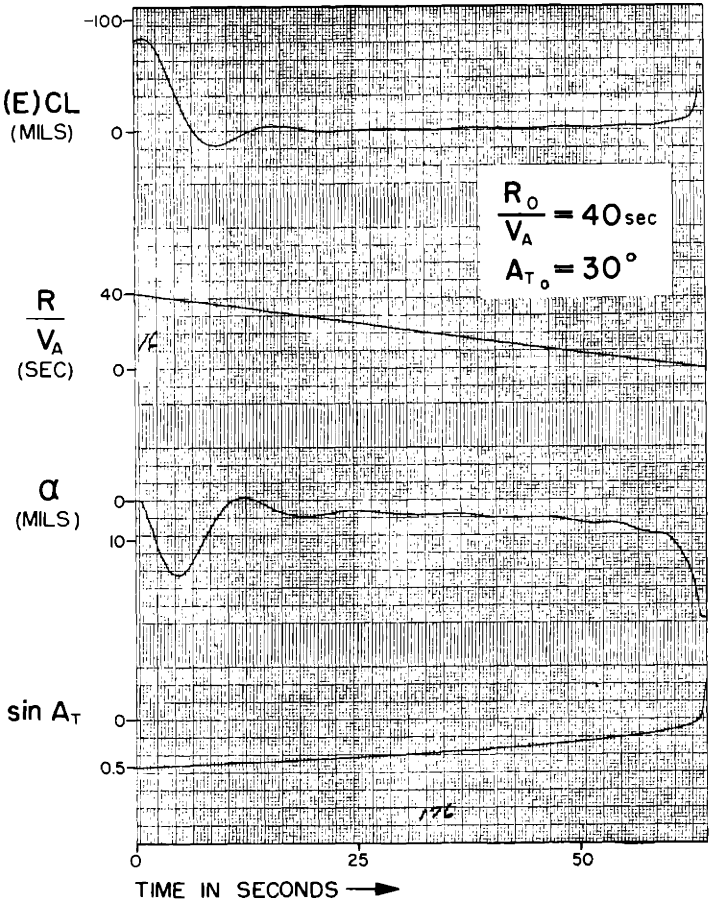

$S_{g(CL,V)} S_{(sm)p} S_{(s,r)} = 1.00$ PSR = 1.11

$S_{rg} S_{(sm)\dot{\theta}} S_{(s,r)} = 0$ SN = 0.25

$S_{TID} S_{LCS(i\omega)} = 2.0$ $(CT)_{(sm)} = 0$

$(CT)_R = 0.15$ sec

AIRCRAFT CHARACTERISTICS OF APP B

FIG V-7

RESPONSE OF CLOSED-LOOP TRACKING SYSTEM WITH TRACKING INACCURACY PREDICTION AND TIGHT-LOOP STABILIZATION OF THE AIRCRAFT IN THE ABSENCE OF GUST AND RADAR INTERFERENCE

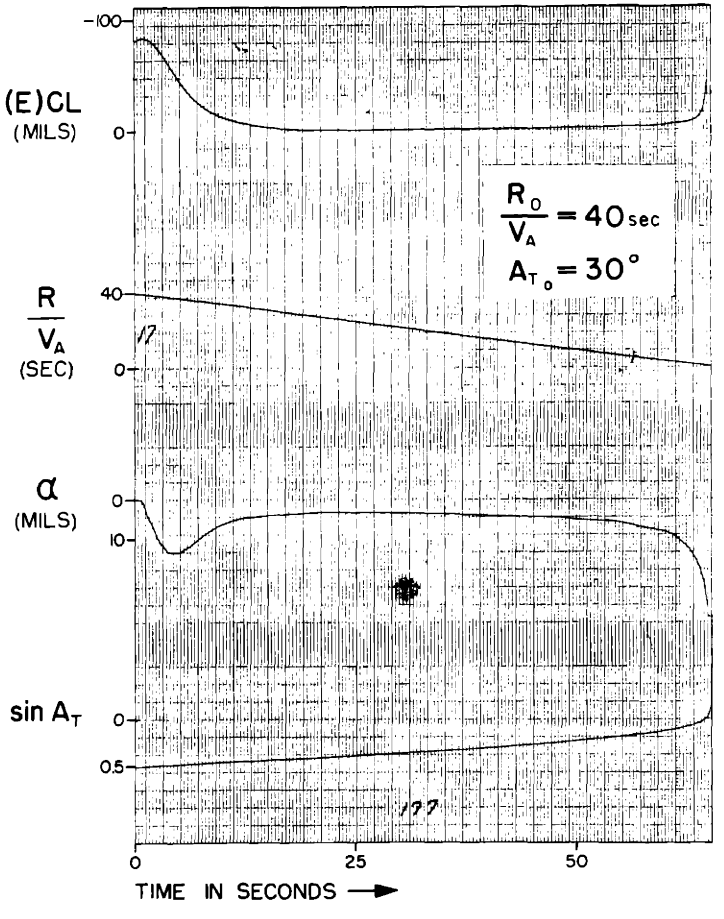

$S_{g(CL,V)} S_{(sm)p} S_{(s,r)} = 1.00$ PSR = 1.11

$S_{rg} S_{(sm)\dot{\theta}} S_{(s,r)} = 0$ SN = 0.50

$S_{TID} S_{LCS(i\omega)} = 2.0$ $(CT)_{(sm)} = 0$

$(CT)_R = 0.15$ sec

AIRCRAFT CHARACTERISTICS OF APP B

FIG V-8

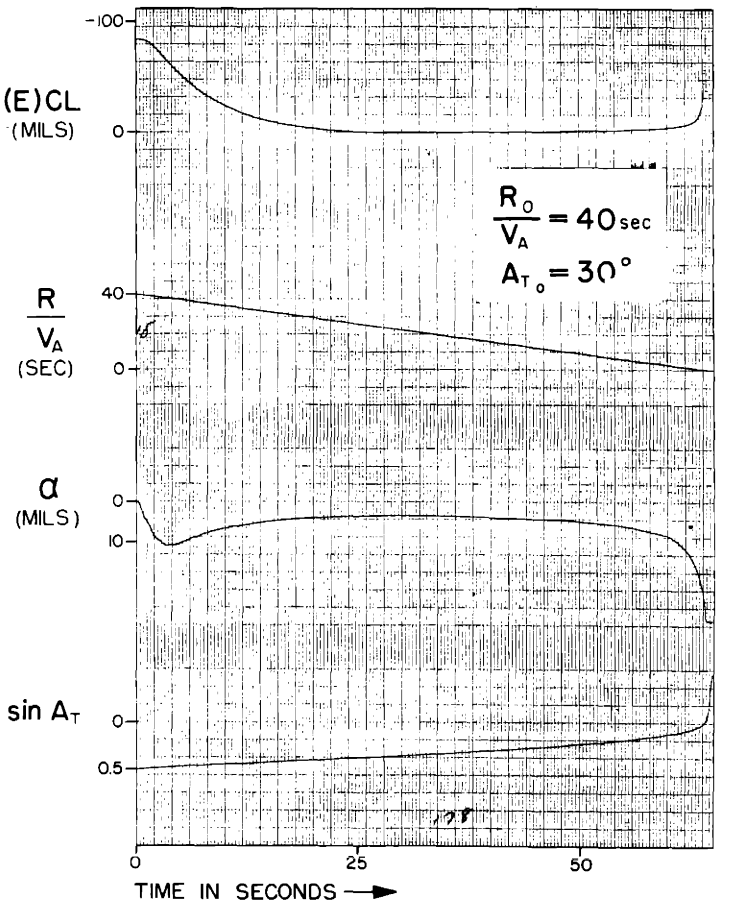

$S_{g(CL,V)} S_{(sm)p} S_{(s,r)} = 1.00$ PSR = 1.11

$S_{rg} S_{(sm)\dot{\theta}} S_{(s,r)} = 0$ SN = 0.75

$S_{TID} S_{LCS(i\omega)} = 2.0$ $(CT)_{(sm)} = 0$

$(CT)_R = 0.15$ sec

AIRCRAFT CHARACTERISTICS OF APP B

FIG V-9

RESPONSE OF CLOSED-LOOP TRACKING SYSTEM WITH TRACKING INACCURACY PREDICTION AND TIGHT-LOOP STABILIZATION OF THE AIRCRAFT IN THE ABSENCE OF GUST AND RADAR INTERFERENCE

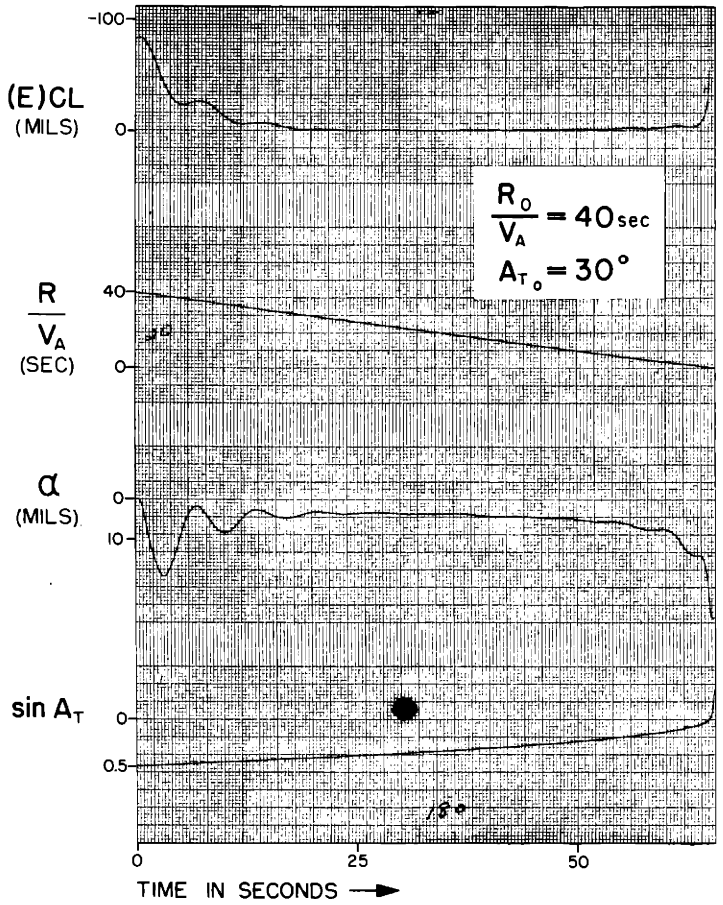

$S_{g(CL,V)} S_{(sm)p} S_{(s,r)} = 0.50$ PSR = 1.11

$S_{rg} S_{(sm)\dot{\theta}} S_{(s,r)} = 0$ SN = 0.50

$S_{TID} S_{LCS(i\omega)} = 3.0$ $(CT)_{(sm)} = 0$

$(CT)_R = 0.15$ sec

AIRCRAFT CHARACTERISTICS OF APP B

FIG V-10

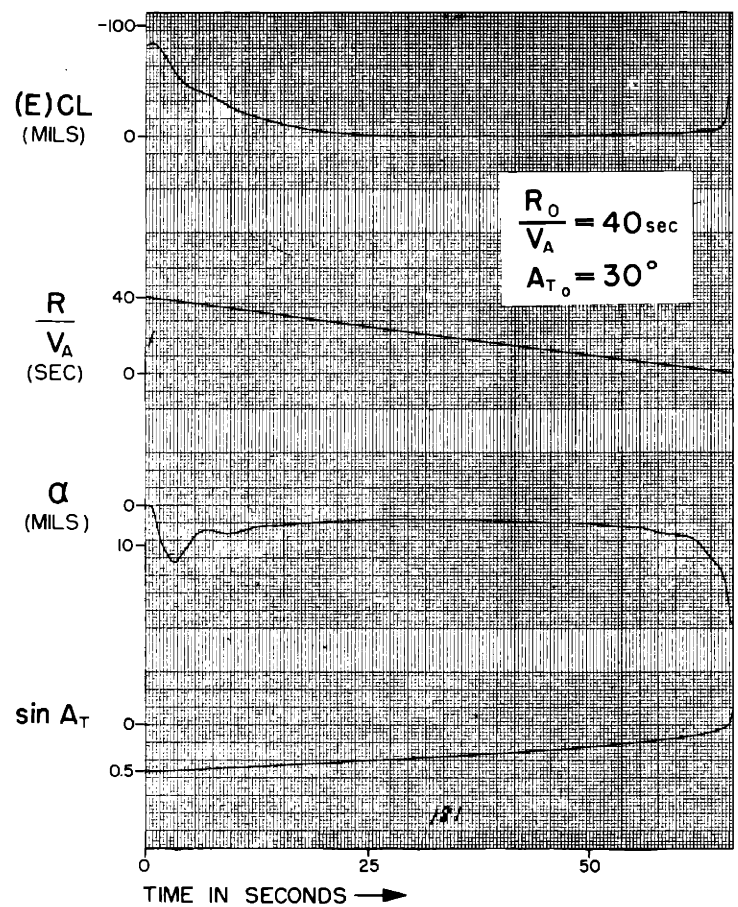

$S_{g(CL,V)} S_{(sm)p} S_{(s,r)} = 0.50$ PSR = 1.11

$S_{rg} S_{(sm)\dot{\theta}} S_{(s,r)} = 0$ SN = 0.75

$S_{TID} S_{LCS(i\omega)} = 3.0$ $(CT)_{(sm)} = 0$

$(CT)_R = 0.15$ sec

AIRCRAFT CHARACTERISTICS OF APP B

FIG V-11

RESPONSE OF CLOSED-LOOP TRACKING SYSTEM WITH TRACKING INACCURACY PREDICTION AND TIGHT-LOOP STABILIZATION OF THE AIRCRAFT IN THE ABSENCE OF GUST AND RADAR INTERFERENCE

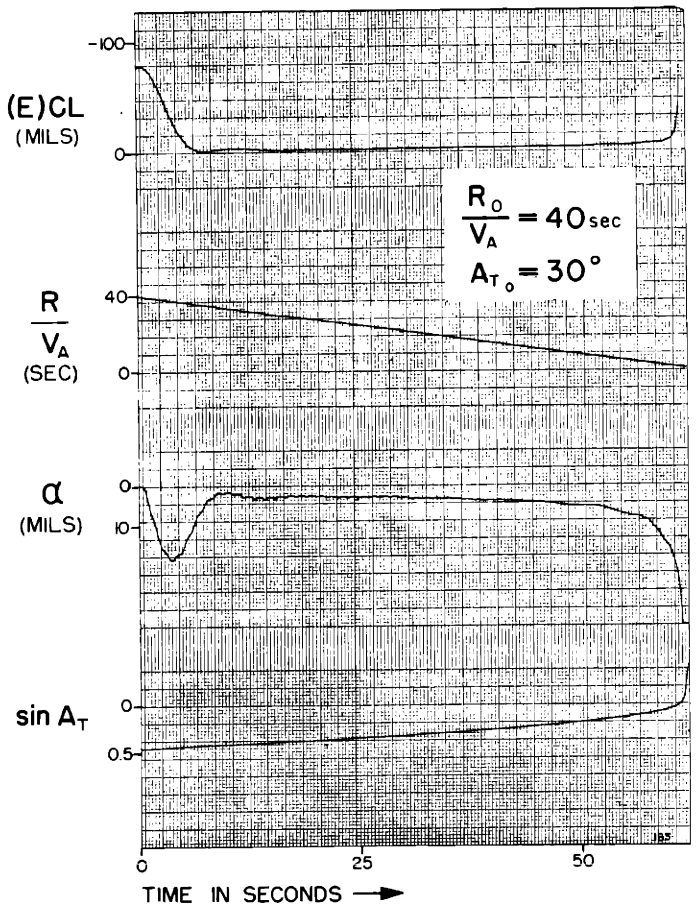

$S_{g(CL,V)} S_{(sm)p} S_{(s,r)} = 1.00$ PSR = 1.11

$S_{rg} S_{(sm)\dot{\theta}} S_{(s,r)} = 0$ SN = 0.25

$S_{TID} S_{LCS(i\omega)} = 3.0$ $(CT)_{(sm)} = 0$

$(CT)_R = 0.15$ sec

AIRCRAFT CHARACTERISTICS OF APP B

FIG V-12

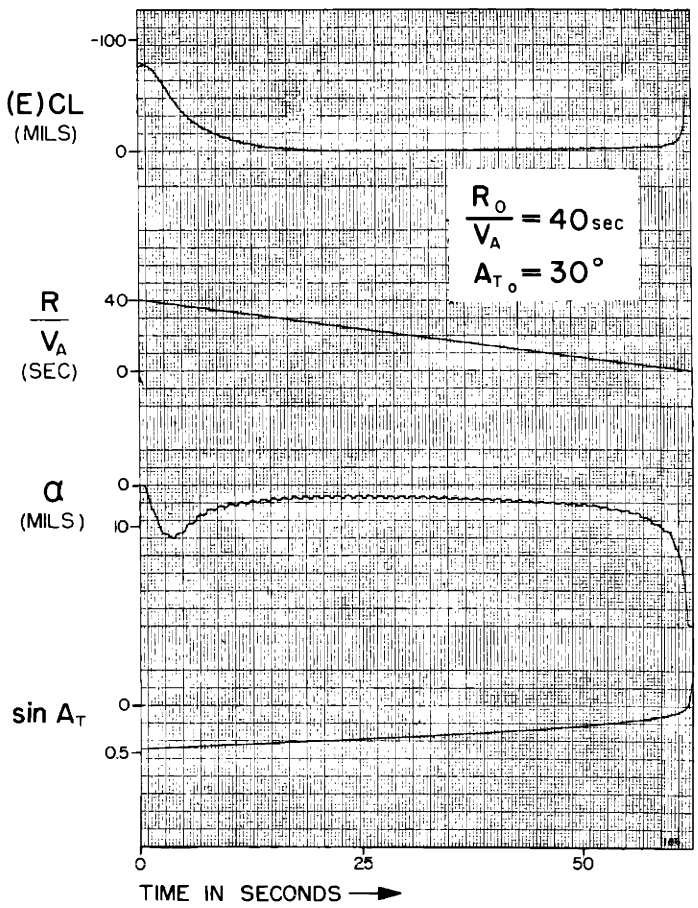

$S_{g(CL,V)} S_{(sm)p} S_{(s,r)} = 1.00$ PSR = 1.11

$S_{rg} S_{(sm)\dot{\theta}} S_{(s,r)} = 0$ SN = 0.50

$S_{TID} S_{LCS(i\omega)} = 3.0$ $(CT)_{(sm)} = 0$

$(CT)_R = 0.15$ sec

AIRCRAFT CHARACTERISTICS OF APP B

FIG V-13

RESPONSE OF CLOSED-LOOP TRACKING SYSTEM WITH TRACKING INACCURACY PREDICTION AND TIGHT-LOOP STABILIZATION OF THE AIRCRAFT IN THE ABSENCE OF GUST AND RADAR INTERFERENCE

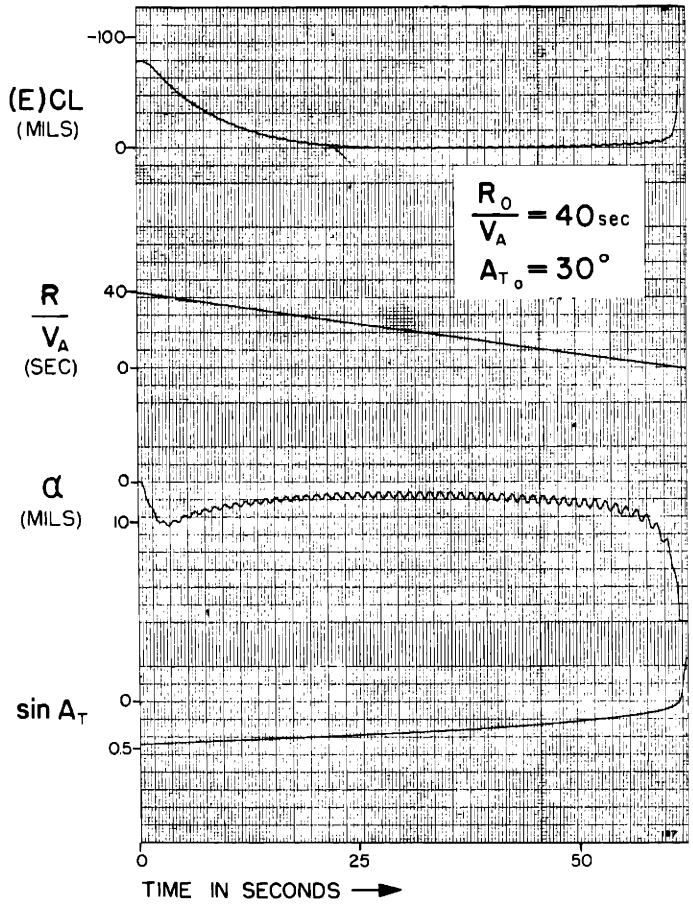

$S_{g(CL,V)} S_{(sm)p} S_{(s,r)} = 1.00$ PSR = 1.11

$S_{rg} S_{(sm)\dot{\theta}} S_{(s,r)} = 0$ SN = 0.75

$S_{TID} S_{LCS(i\omega)} = 3.0$ $(CT)_{(sm)} = 0$

$(CT)_R = 0.15$ sec

AIRCRAFT CHARACTERISTICS OF APP B

FIG V-14

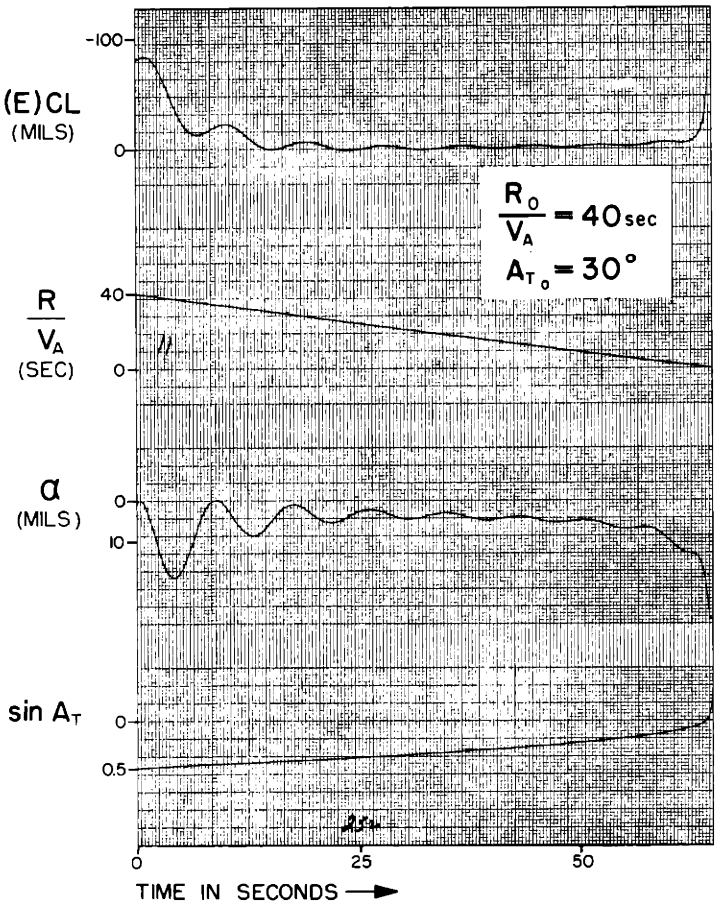

$S_{g(CL,V)} S_{(sm)p} S_{(s,r)} = 0.50$ PSR = 1.11

$S_{rg} S_{(sm)\dot{\theta}} S_{(s,r)} = .026$ SN = 0.50

$S_{TID} S_{LCS(i\omega)} = 2.0$ $(CT)_{(sm)} = 0$

$(CT)_R = 0.15$ sec

AIRCRAFT CHARACTERISTICS OF APP B

FIG V-15

RESPONSE OF CLOSED-LOOP TRACKING SYSTEM WITH TRACKING INACCURACY PREDICTION AND TIGHT-LOOP STABILIZATION OF THE AIRCRAFT IN THE ABSENCE OF GUST AND RADAR INTERFERENCE

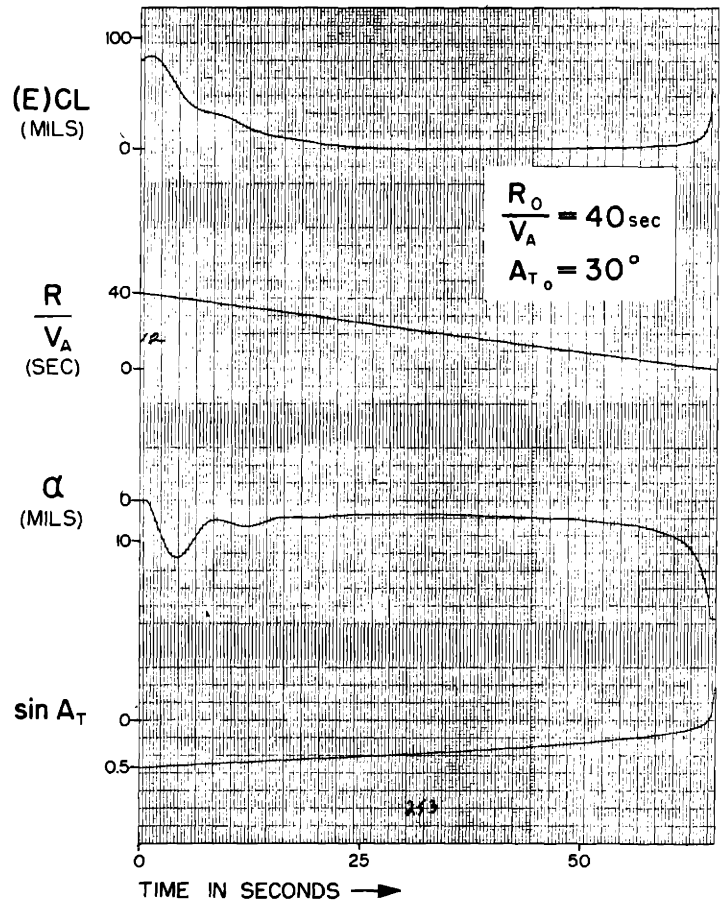

$S_{g(CL,V)} S_{(sm)p} S_{(s,r)} = 0.50$ PSR = 1.11

$S_{rg} S_{(sm)\dot{\theta}} S_{(s,r)} = .026$ SN = 0.75

$S_{TID} S_{LCS(i\omega)} = 2.0$ $(CT)_{(sm)} = 0$

$(CT)_R = 0.15$ sec

AIRCRAFT CHARACTERISTICS OF APP B

FIG V-16

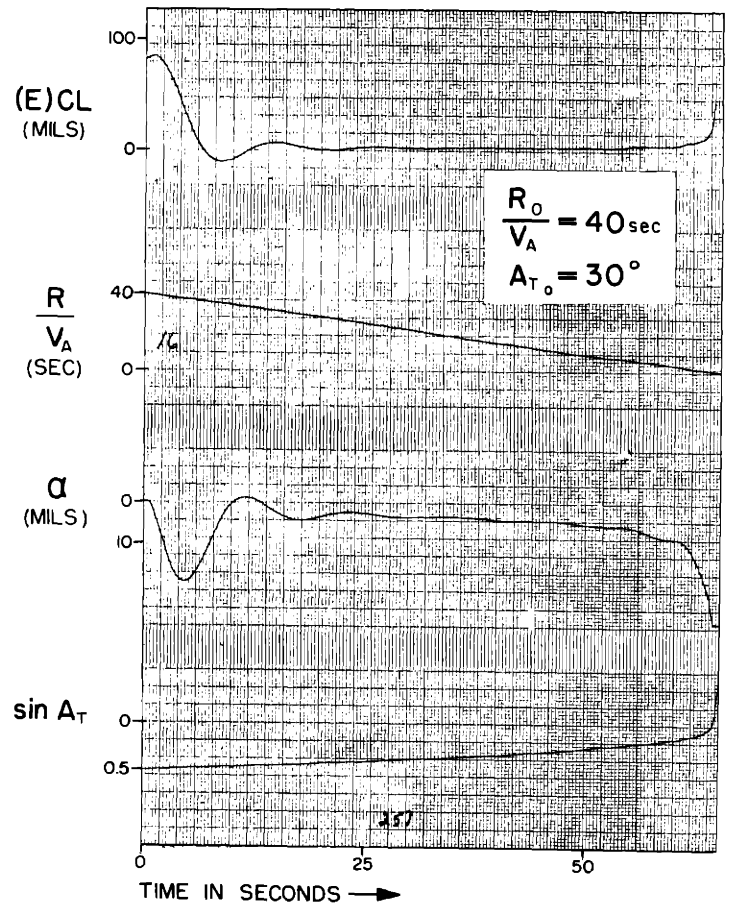

$S_{g(CL,V)} S_{(sm)p} S_{(s,r)} = 1.00$ PSR = 1.11

$S_{rg} S_{(sm)\dot{\theta}} S_{(s,r)} = .026$ SN = 0.25

$S_{TID} S_{LCS(i\omega)} = 2.0$ $(CT)_{(sm)} = 0$

$(CT)_R = 0.15$ sec

AIRCRAFT CHARACTERISTICS OF APP B

FIG V-17

RESPONSE OF CLOSED-LOOP TRACKING SYSTEM WITH TRACKING INACCURACY PREDICTION AND TIGHT-LOOP STABILIZATION OF THE AIRCRAFT IN THE ABSENCE OF GUST AND RADAR INTERFERENCE

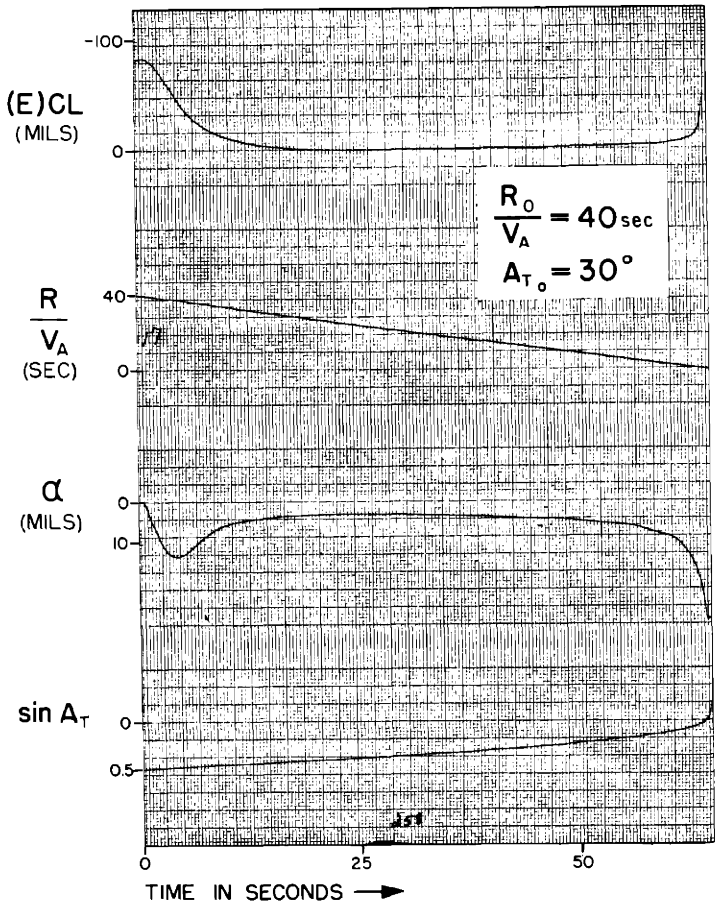

$S_{g(CL,V)} S_{(sm)p} S_{(s,r)} = 1.00$ PSR = 1.11

$S_{rg} S_{(sm)\dot{\theta}} S_{(s,r)} = .026$ SN = 0.50

$S_{TID} S_{LCS(i\omega)} = 2.0$ $(CT)_{(sm)} = 0$

$(CT)_R = 0.15$ sec

AIRCRAFT CHARACTERISTICS OF APP B

FIG V-18

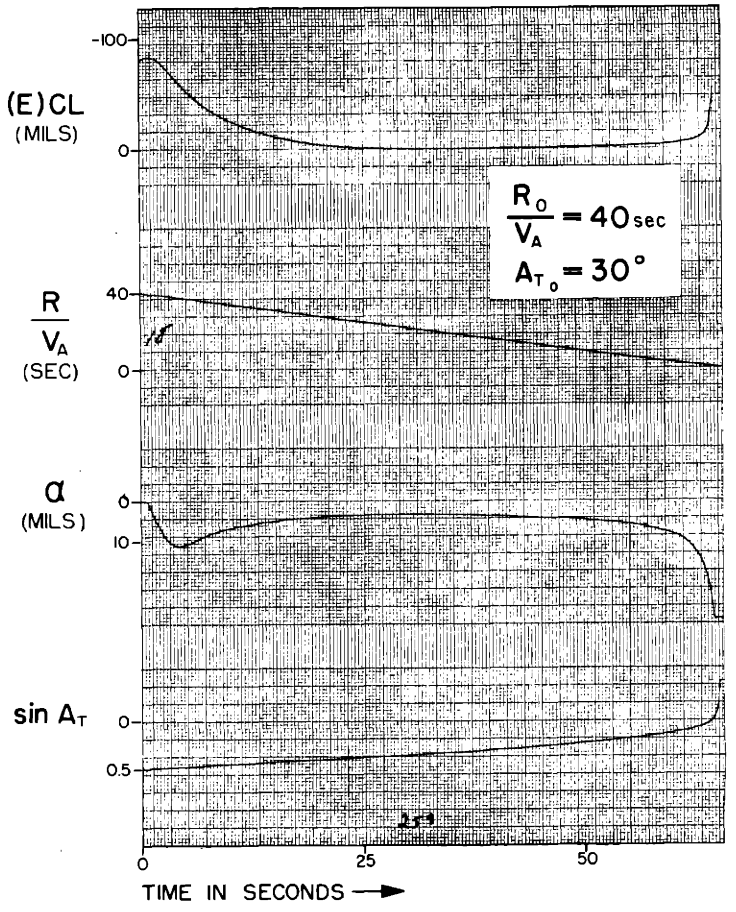

$S_{g(CL,V)} S_{(sm)p} S_{(s,r)} = 1.00$ PSR = 1.11

$S_{rg} S_{(sm)\dot{\theta}} S_{(s,r)} = .026$ SN = 0.75

$S_{TID} S_{LCS(i\omega)} = 2.0$ $(CT)_{(sm)} = 0$

$(CT)_R = 0.15$ sec

AIRCRAFT CHARACTERISTICS OF APP B

FIG V-19

RESPONSE OF CLOSED-LOOP TRACKING SYSTEM WITH TRACKING INACCURACY PREDICTION AND TIGHT-LOOP STABILIZATION OF THE AIRCRAFT IN THE ABSENCE OF GUST AND RADAR INTERFERENCE

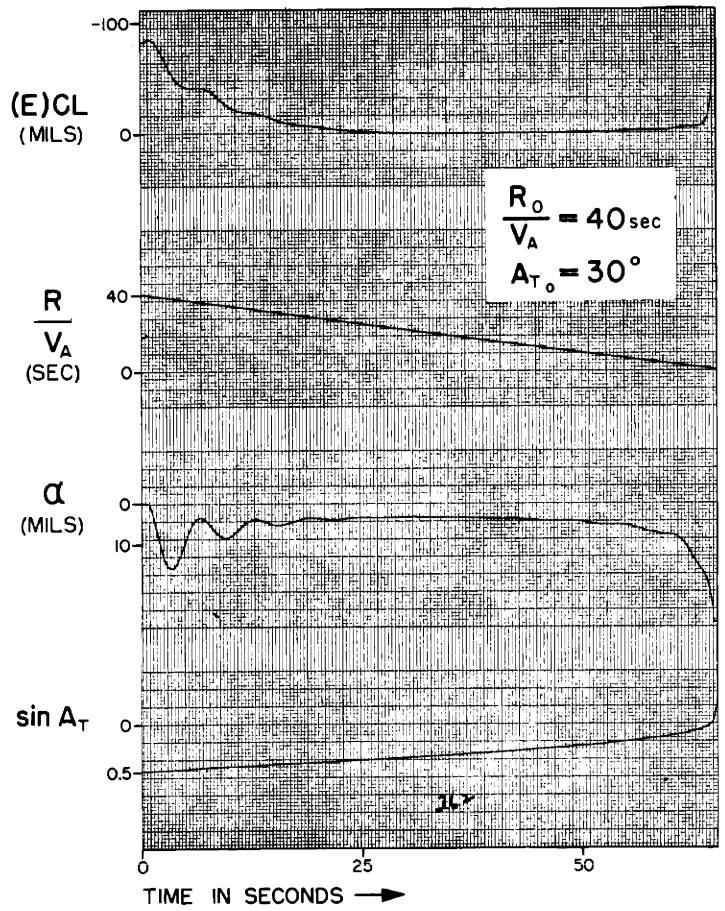

$S_{g(CL,V)} S_{(sm)p} S_{(s,r)} = 0.50$ PSR = 1.11

$S_{rg} S_{(sm)\dot{\theta}} S_{(s,r)} = .026$ SN = 0.75

$S_{TID} S_{LCS(i\omega)} = 3.0$ $(CT)_{(sm)} = 0$

$(CT)_R = 0.15$ sec

AIRCRAFT CHARACTERISTICS OF APP B

FIG V-20

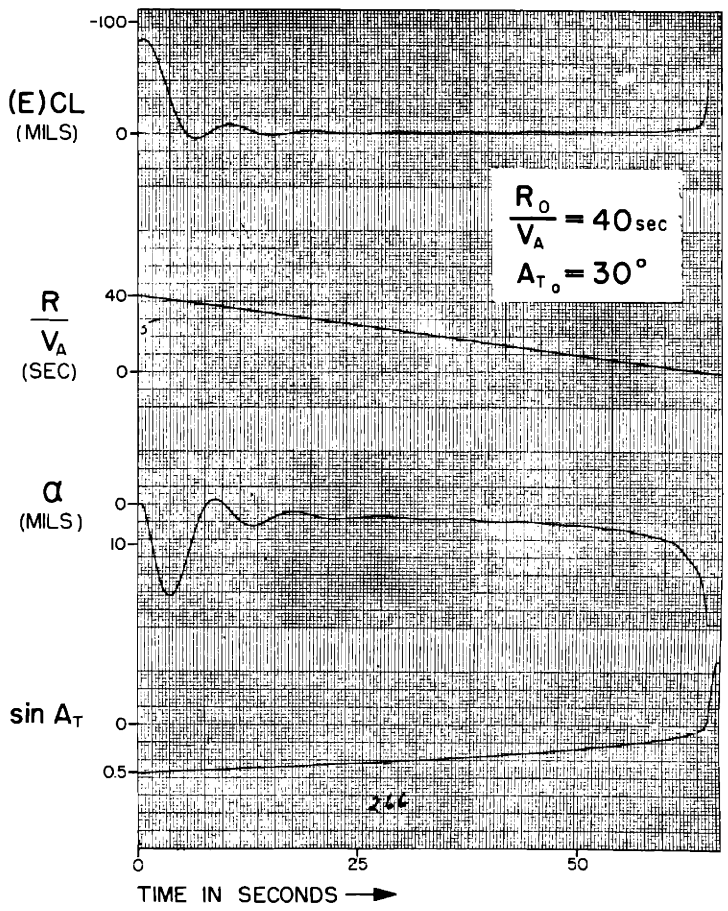

$S_{g(CL,V)} S_{(sm)p} S_{(s,r)} = 1.00$ PSR = 1.11

$S_{rg} S_{(sm)\dot{\theta}} S_{(s,r)} = .026$ SN = 0.25

$S_{TID} S_{LCS(i\omega)} = 3.0$ $(CT)_{(sm)} = 0$

$(CT)_R = 0.15$ sec

AIRCRAFT CHARACTERISTICS OF APP B

FIG V-21

RESPONSE OF CLOSED-LOOP TRACKING SYSTEM WITH TRACKING INACCURACY PREDICTION AND TIGHT-LOOP STABILIZATION OF THE AIRCRAFT IN THE ABSENCE OF GUST AND RADAR INTERFERENCE

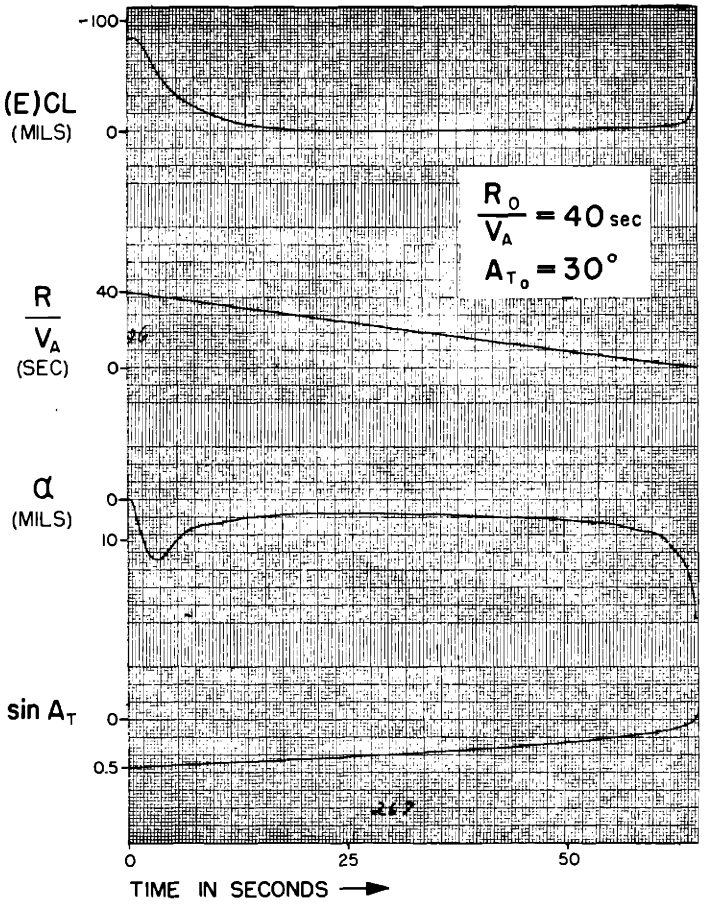

$S_{g(CL,V)} S_{(sm)p} S_{(s,r)} = 1.00$ PSR = 1.11

$S_{rg} S_{(sm)\dot{\theta}} S_{(s,r)} = .026$ SN = 0.50

$S_{TID} S_{LCS(i\omega)} = 3.0$ $(CT)_{(sm)} = 0$

$(CT)_R = 0.15$ sec

AIRCRAFT CHARACTERISTICS OF APP B

FIG V - 22

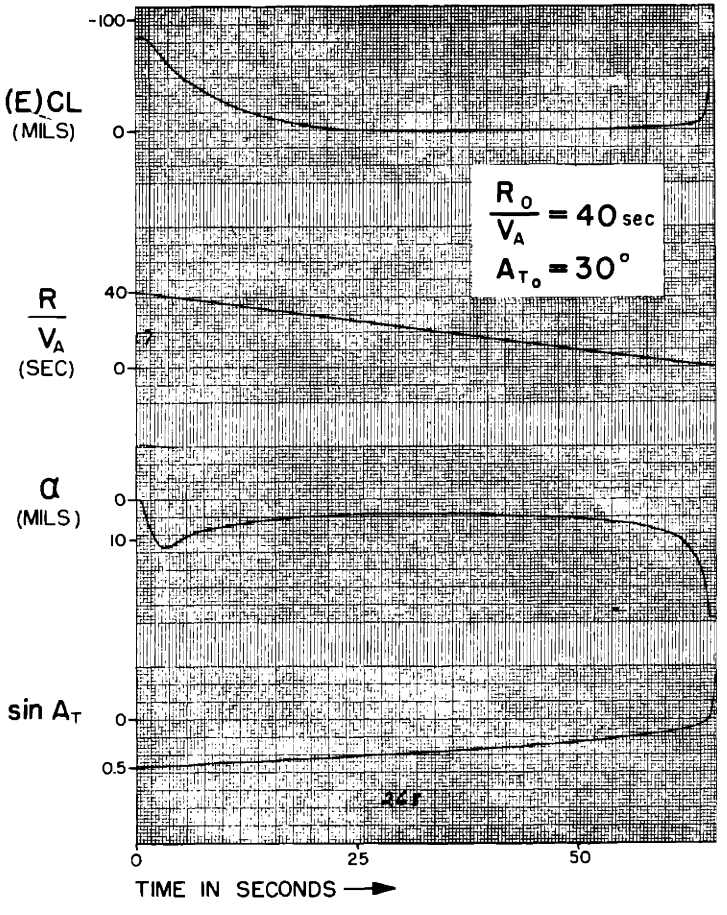

$S_{g(CL,V)} S_{(sm)p} S_{(s,r)} = 1.00$ PSR = 1.11

$S_{rg} S_{(sm)\dot{\theta}} S_{(s,r)} = .026$ SN = 0.75

$S_{TID} S_{LCS(i\omega)} = 3.0$ $(CT)_{(sm)} = 0$

$(CT)_R = 0.15$ sec

AIRCRAFT CHARACTERISTICS OF APP B

FIG V - 23

RESPONSE OF CLOSED-LOOP TRACKING SYSTEM WITH TRACKING INACCURACY PREDICTION AND TIGHT-LOOP STABILIZATION OF THE AIRCRAFT IN THE ABSENCE OF GUST AND RADAR INTERFERENCE

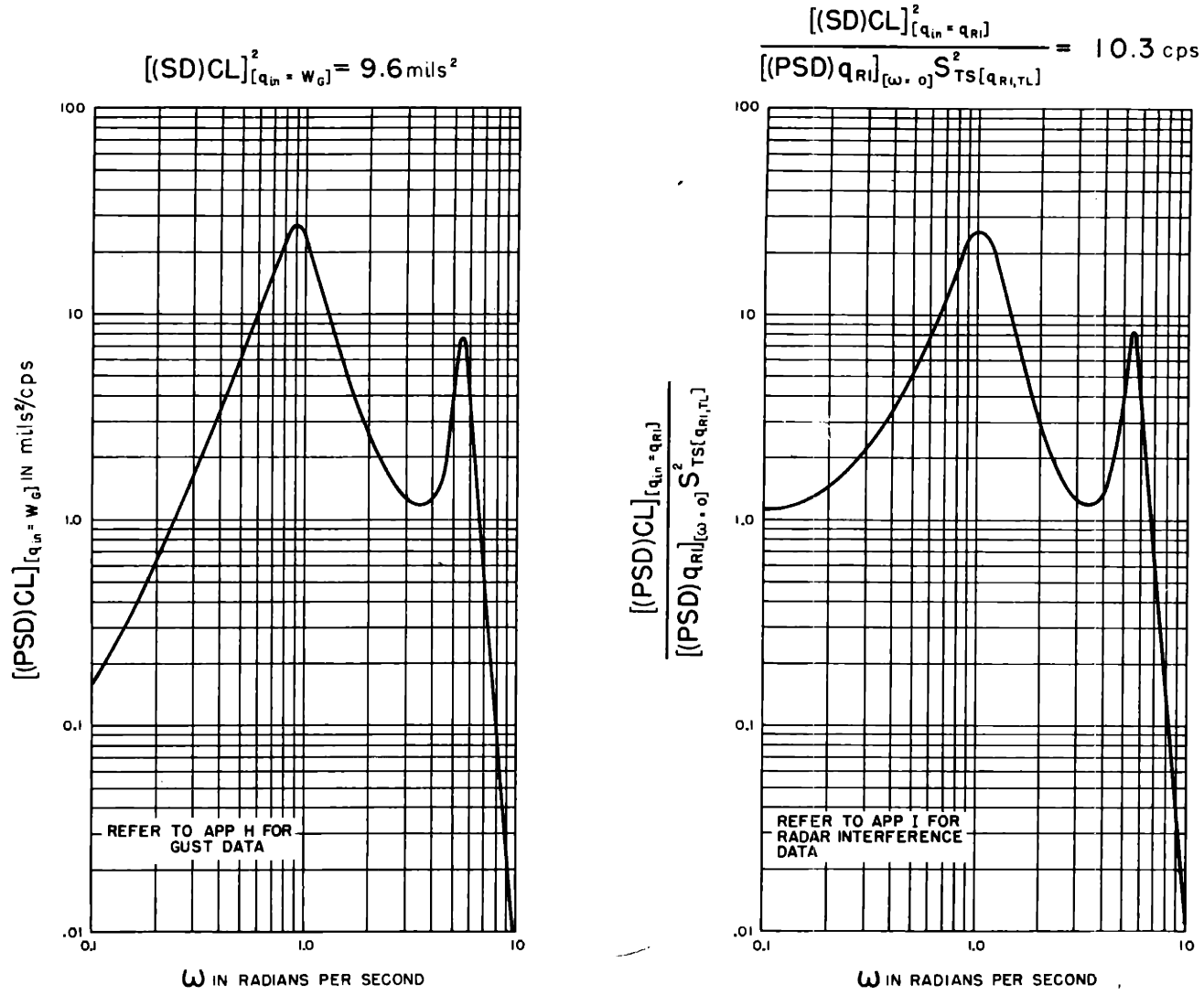

$S_{g(CL,V)}\ S_{(sm)p}\ S_{(S,r)} = 1.35$ $\qquad$ $S_{P(\omega,P)} = 2.77$ sec

$S_{rg}\ S_{(sm)\dot{\theta}}\ S_{(S,r)} = .05$ sec $\qquad$ $SN = 0.3$

$(CT)_{(sm)} = 0$ sec $\qquad$ $(CT)_R = 0.15$ sec

$S_{TID}\ S_{LCS(i,\omega)} = 3.0\ sec^{-1}$

AIRCRAFT CHARACTERISTICS OF APP B

FIG V-24 POWER SPECTRAL DENSITIES RESULTING FROM GUST AND RADAR INTERFERENCE OF CLOSED-LOOP TRACKING SYSTEM WITH TRACKING INACCURACY PREDICTION AND TIGHT-LOOP STABILIZATION OF THE INTERCEPTOR AIRCRAFT

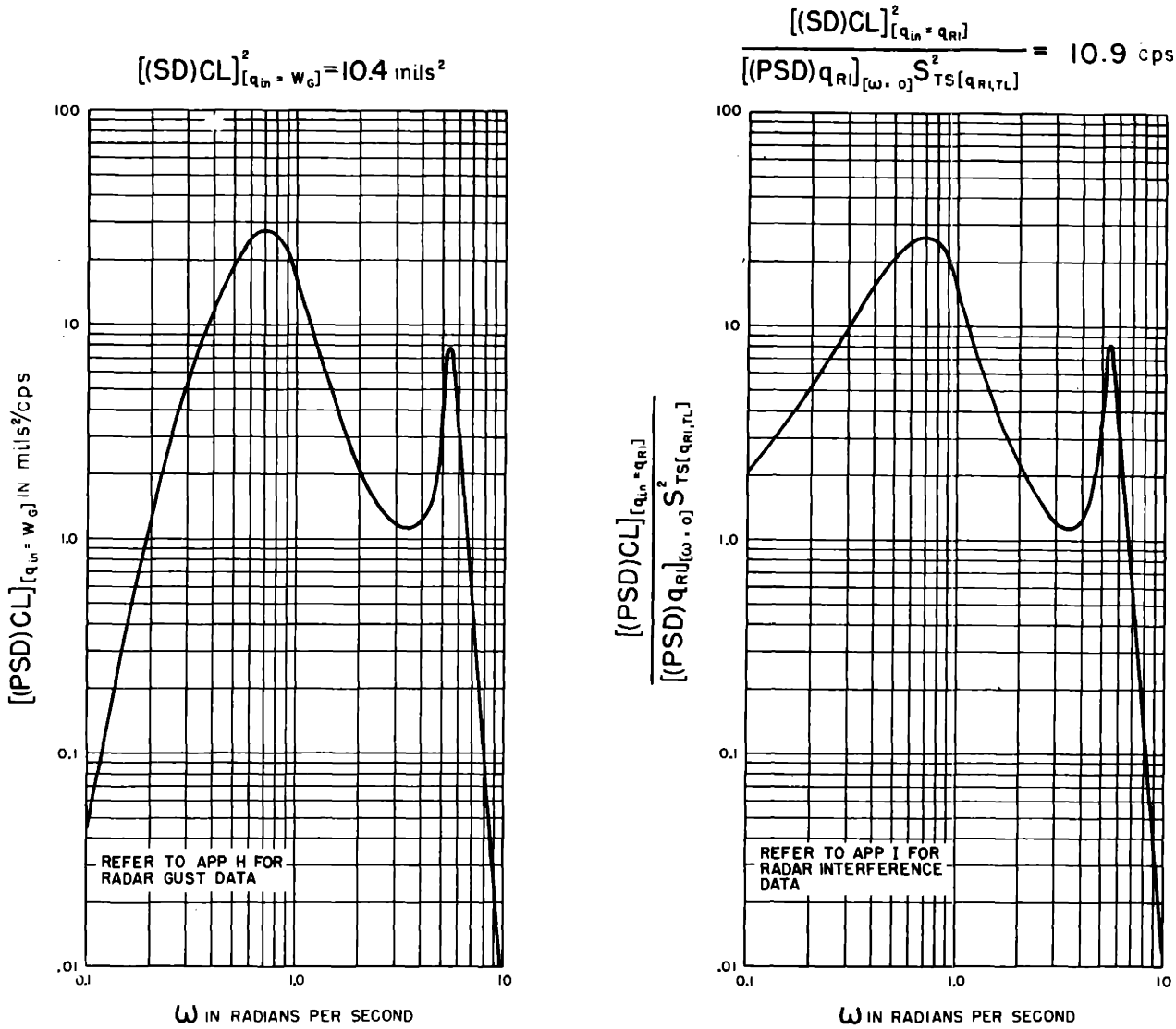

$S_{g(CL,V)}\, S_{(sm)p}\, S_{(S,r)} = 1.35$ $\qquad$ $S_{P(\omega,P)} = 8.33$ sec

$S_{rg}\, S_{(sm)\dot{\theta}}\, S_{(S,r)} = .05$ sec $\qquad$ $SN = 0.3$

$(CT)_{(sm)} = 0$ sec $\qquad$ $(CT)_R = 0.15$ sec

$S_{TID}\, S_{LCS(i,\omega)} = 3.0$ sec^{-1}

AIRCRAFT CHARACTERISTICS OF APP B

FIG V-25 POWER SPECTRAL DENSITIES RESULTING FROM GUST AND RADAR INTERFERENCE OF CLOSED-LOOP TRACKING SYSTEM WITH TRACKING INACCURACY PREDICTION AND TIGHT-LOOP STABILIZATION OF THE INTERCEPTOR AIRCRAFT

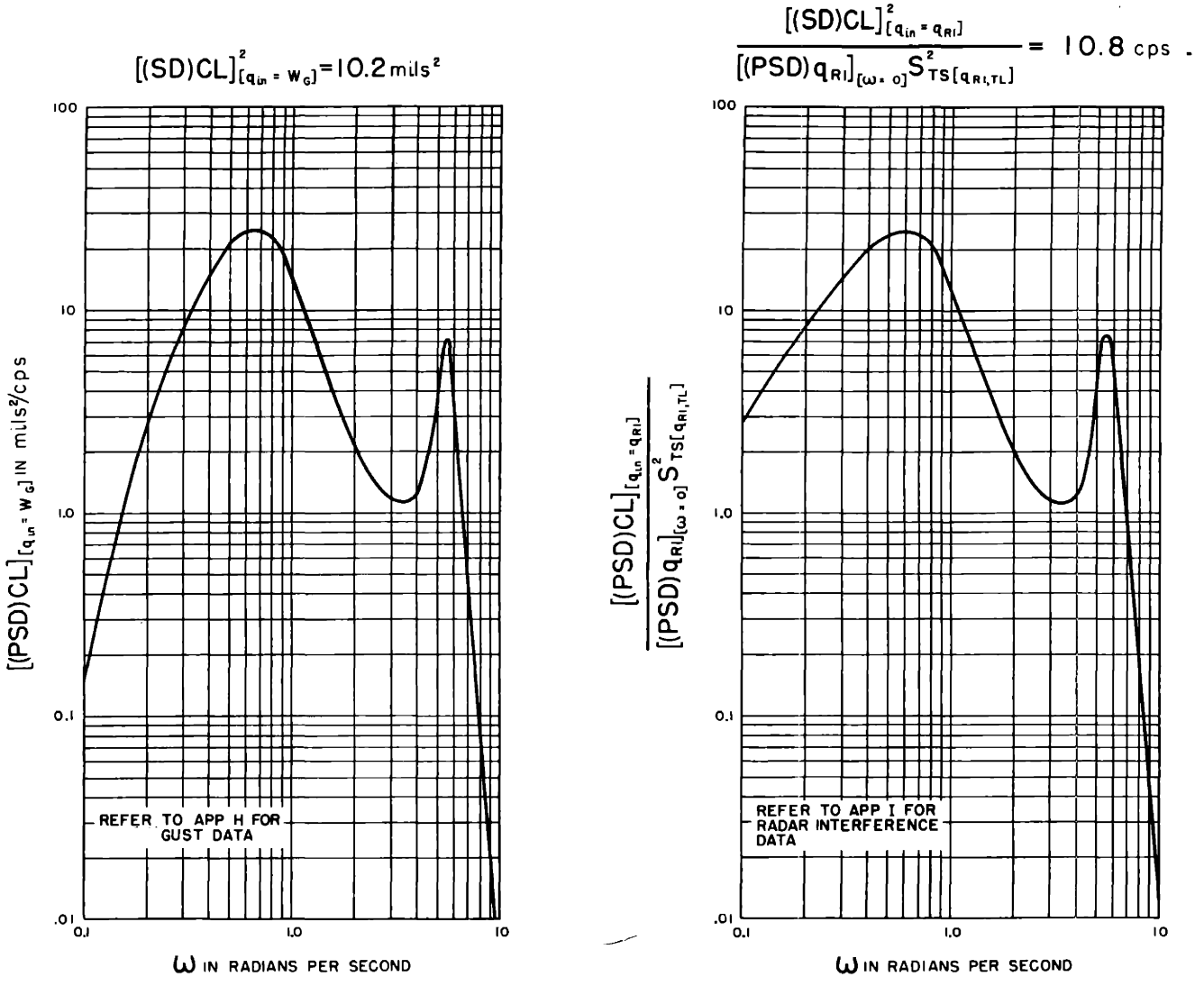

$S_{g(CL,V)}\, S_{(sm)p}\, S_{(S,r)} = 1.35$ $\qquad$ $S_{P(\omega,P)} = 13.85 \text{ sec}$

$S_{rg}\, S_{(sm)\dot{\theta}}\, S_{(S,r)} = .05 \text{ sec}$ $\qquad$ $SN = 0.3$

$(CT)_{(sm)} = 0 \text{ sec}$ $\qquad$ $(CT)_R = 0.15 \text{ sec}$

$S_{TID}\, S_{LCS(i,\omega)} = 3.0 \text{ sec}^{-1}$

AIRCRAFT CHARACTERISTICS OF APP B

FIG V - 26 POWER SPECTRAL DENSITIES RESULTING FROM GUST AND RADAR INTERFERENCE OF CLOSED-LOOP TRACKING SYSTEM WITH TRACKING INACCURACY PREDICTION AND TIGHT-LOOP STABILIZATION OF THE INTERCEPTOR AIRCRAFT

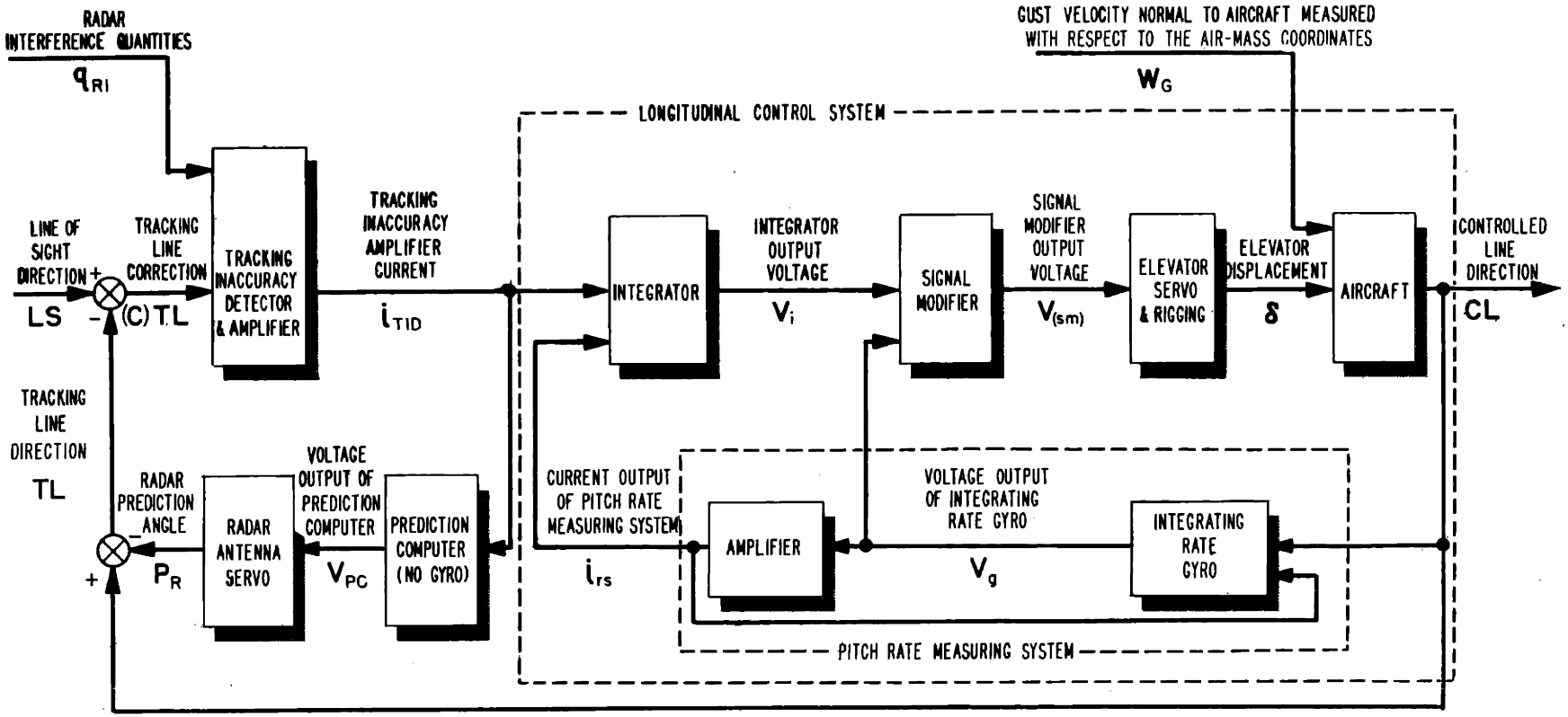

FIG V-27 FUNCTIONAL DIAGRAM OF CLOSED-LOOP TRACKING SYSTEM WITH TRACKING INACCURACY PREDICTION AND TIGHT-LOOP STABILIZATION OF THE AIRCRAFT USING AN INTEGRATING RATE GYRO AND AN INTEGRATOR

APPENDIX A

DEFINITION OF QUANTITIES REQUIRED IN THREE DIMENSIONAL ANALYSIS OF INTERCEPTOR AIRCRAFT

1. Definition of Coordinate Systems

When the performance of an interceptor aircraft is to be analyzed, a variety of coordinate systems is required. The interceptor is vectored to the target with information supplied from ground stations, and hence in Earth Coordinates. Once the target is acquired by the interceptor radar, the fire control problem must be solved with respect to Inertial Space since the gyroscopic elements used in the computer are sensitive to absolute angular velocities.

These angular velocities must be resolved along the gyroscopic input axes or computer axes. Closed-loop tracking systems have computer axes non-rotating with respect to the aircraft, whereas open-chain tracking systems have computer axes fixed with respect to the radar antenna. The computer coordinates are defined more completely in Appendix D.

When the heading of the aircraft is in error, corrections are applied by use of the elevator, rudder and ailerons, which provide moments about the airplane body axes. The most convenient airplane coordinates are those used by the NACA when supplying aerodynamic force and moment data. The Airplane axes, as well as Earth-Reference axes, Earth-Airplane axes, Earth-Plane of Symmetry axes, and Air Mass axes are defined as follows:

The Airplane Coordinate System, X_A, Y_A, Z_A, shown in Fig. A-1, has

its origin at the center of gravity of the airplane with Y_A normal to the plane of symmetry (positive along the right wing), X_A parallel to the projection of the velocity vector on the plane of symmetry in trimmed flight (positive forward), and Z_A forming a right-hand system. The velocity vector is a measure of the speed and direction of the airplane with respect to the air mass.

The Earth Coordinate System, X_E, Y_E, Z_E, has its origin at the airplane center of gravity, with Z_E along the vertical (positive downward), X_E in a convenient fixed geographic heading, and Y_E forming a right-hand system.

The Earth-Airplane Coordinate System, X_{EA}, Y_{EA}, Z_{EA}, has its origin at the airplane center of gravity, with Z_{EA} along the vertical (positive downward), X_{EA} in the vertical plane containing X_A (positive forward), and Y_{EA} forming a right-hand system.

The Earth-Plane of Symmetry Coordinate System, $X_{E(PS)}$, $Y_{E(PS)}$, $Z_{E(PS)}$, has its origin at the airplane center of gravity, with $Z_{E(PS)}$ along the vertical (positive downward), $X_{E(PS)}$ in the plane of symmetry (positive forward) and $Y_{E(PS)}$ forming a right-hand system.

The Air Mass Coordinate System, X_{AM}, Y_{AM}, Z_{AM}, is non-rotating with respect to the Earth Coordinate System, with X_{AM} along X_E, Y_{AM} along Y_E and Z_{AM} along Z_E. The origin of the air mass coordinates translates with the average velocity of the air and coincides with the center of gravity of the aircraft at the instant a projectile is fired.

2. Definition of the Airplane Orientation Angles

The coordinate systems of Section 1 are shown in Fig. A-1 in arbitrary positions. The airplane axes can be translated from coincidence with the earth axes in an infinite number of ways. One useful method involves yawing about the Z_E axis, banking about the $X_{E(PS)}$ axis, and pitching about the Y_A

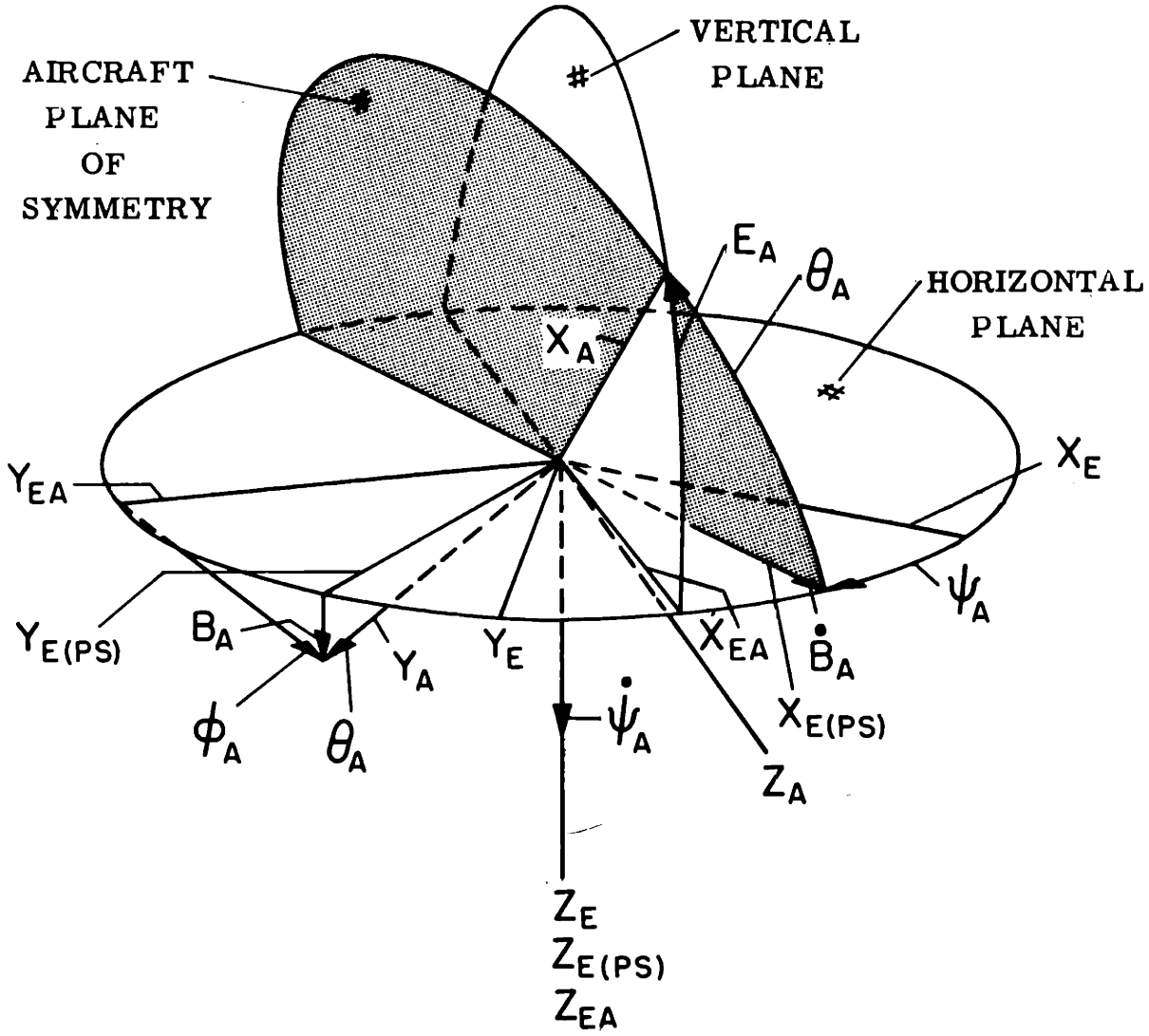

Fig. A-1.—Relationships among the coordinate systems used in an analysis of interceptor aircraft.

axis, giving rise to angles

Ψ_A = angle heading measured from X_E to $X_{E(PS)}$

$= A[X_E - X_{E(PS)}]$

B_A = airplane bank angle

$= A[Y_{E(PS)} - Y_A]$

and

Θ_A = airplane pitch angle

$= A[X_{E(PS)} - X_A]$

By the use of angles Ψ_A, B_A and Θ_A, the angular orientation of the airplane is fixed with respect to the earth. It must be remembered that since large angles cannot be treated as vectors, the angles must be used in the proper order. Two other useful angles are

Φ_A = airplane roll angle

$= A[Y_{EA} - Y_A]$

and

E_A = airplane elevation angle

$= A[X_{EA} - X_A]$

3. Relationship Between the Orientation Angles and the Angular Velocity of the Airplane with Respect to the Earth

The maneuvering airplane has components of angular velocity about all three body axes. The vector sum of these components is the angular

velocity of the airplane, which is noted by the symbol $\overline{W}_{EA}$ when measured with respect to the earth. The airplane angular velocity gives rise to rates of change of the orientation angles. It can be seen from Fig. A-1 that

1. $\dot{\Psi}_A$ is about Z_E

2. $\dot{B}_A$ is about $X_{E(PS)}$

3. $\dot{\theta}_A$ is about Y_A

and consequently these angular velocities are not mutually orthogonal. However, these angular velocities are independent, and hence their vector sum must equal $\overline{W}_{EA}$. Projecting these angular velocities onto airplane axes gives

$$W_{(EA)X_A} = \dot{B}_A \cos\theta_A - \dot{\Psi}_A \cos B_A \sin\theta_A \qquad \text{A-1}$$

$$W_{(EA)Y_A} = \dot{\theta}_A + \dot{\Psi}_A \sin B_A \qquad \text{A-2}$$

$$W_{(EA)Z_A} = \dot{\Psi}_A \cos B_A \cos\theta_A + \dot{B}_A \sin\theta_A \qquad \text{A-3}$$

Solving Eq. A-1, A-2, and A-3 for $\dot{\Psi}_A$, $\dot{B}_A$, and $\dot{\theta}_A$ leads to

$$\dot{\Psi}_A = -\frac{\sin\theta_A}{\cos B_A} W_{(EA)X_A} + \frac{\cos\theta_A}{\cos B_A} W_{(EA)Z_A} \qquad \text{A-4}$$

$$\dot{B}_A = \cos\theta_A W_{(EA)X_A} + \sin\theta_A W_{(EA)Z_A} \qquad \text{A-5}$$

$$\dot{\theta}_A = \tan B_A \sin\theta_A W_{(EA)X_A} + W_{(EA)Y_A} - \tan B_A \cos\theta_A W_{(EA)Z_A} \qquad \text{A-6}$$

The integration of Eq. A-4, A-5, and A-6 yields the airplane orientation, given its angular velocity about the airplane axes.

4. Differentiation With Respect to Fixed and Moving Axes

It is frequently convenient to relate the time variation of a vector viewed from a moving coordinate system with the time variation of the same vector viewed from a reference coordinate system. For example, an airplane performing a loop appears to be moving in a straight direction, as viewed by the pilot, whereas his path is curved as seen by a spectator on the ground. In this case, the moving system is fixed to the airplane, the reference system is fixed to the ground, and the vector quantity is the velocity of the airplane.

A general vector $\bar{R}$ is shown in Fig. A-2 at time, t, and at an instant later at time t + dt. The vector has changed an amount $(d\bar{R})_r$ with respect to the reference system, whereas the variation observed from the moving system is $(d\bar{R})_m$. The difference arises from the angular velocity of the moving coordinates, $\bar{W}_{rm}$. It can be seen that the total change in $(d\bar{R})_r$ is a result of the change with respect to the moving system, $(d\bar{R})_m$, and the change caused by the angular velocity, $(d\bar{R})_W$, and hence that

$$(d\bar{R})_r = (d\bar{R})_W + (d\bar{R})_m \qquad \text{A-7}$$

However, the magnitude of $(d\bar{R})_W$,

$$\left|(d\bar{R})_W\right| = [W_{rm}\, dt][R_t \sin A[W_{rm} - R_t]] \qquad \text{A-8}$$

so that

$$(d\bar{R})_W = [\bar{W}_{rm} \times \bar{R}_t]\, dt \qquad \text{A-9}$$

and consequently

$$\left(\frac{d\bar{R}}{dt}\right)_r = \left(\frac{dR}{dt}\right)_m + \bar{W}_{rm} \times \bar{R}_t \qquad \text{A-10}$$

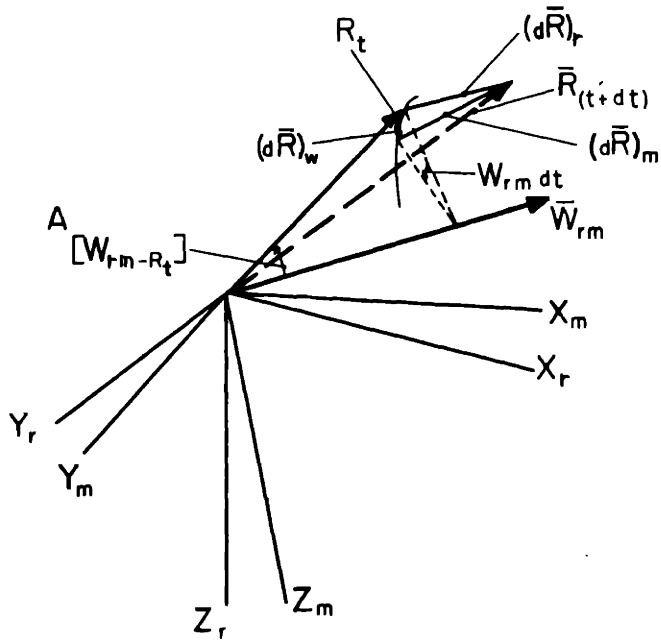

X_r, Y_r, Z_r ARE COORDINATES OF THE REFERENCE SYSTEM.

$X_m\ Y_m\ Z_m$ ARE COORDINATES OF THE MOVING SYSTEM.

$\bar{W}_{rm}$ IS THE ANGULAR VELOCITY OF THE MOVING SYSTEM WITH RESPECT TO THE REFERENCE SYSTEM.

$\bar{R}_t$ SPECIFIES THE MAGNITUDE AND DIRECTION OF THE QUANTITY R AT TIME, t.

$\bar{R}_{(t+dt)}$ SPECIFIES THE QUANTITY R AT TIME, $t+dt$

Fig. A-2.–Geometric factors involved in differentiation with respect to fixed and moving axes.

Equation A-10 is useful not only when analyzing the performance of an airplane, but also when investigating the dynamics of computing systems.

5. Acceleration of an Airplane with Respect to the Air Mass

The forces applied to an airplane result from a summation of gravitational and aerodynamic effects. The gravitational force is the weight of the airplane, acting downward along the vertical. The aerodynamic effects can not be as simply expressed, but are functions of the linear and angular velocities of the airplane with respect to the air mass. In general, the air is not stationary, as it may translate both linearly and angularly. It is convenient to use the Air Mass Coordinate System, X_{AM}, Y_{AM}, Z_{AM}, of Section 1, which is non-rotating with respect to Earth Coordinates but translates at the average velocity of the air mass. Changes in the air mass velocity from the average are a function of the atmospheric turbulence, and vary with the terrain, the altitude, and the weather. The amount of turbulence can be measured in terms of the velocity of the gusts, V_G. This effect is discussed more fully in Appendix H.

When $\bar{a}_A$ is the acceleration of the airplane with respect to the air mass, and $\bar{V}_A$ is the velocity of the airplane with respect to the air mass,

$$\bar{a}_A = \left[\frac{d\bar{V}_A}{dt}\right]_{AM} \qquad \text{A-11}$$

Making use of Eq. A-10, Eq. A-11 becomes

$$\bar{a}_A = \left(\frac{d\bar{V}_A}{dt}\right)_A + \bar{W}_{(AM)A} \times \bar{V}_A \qquad \text{A-12}$$

However, since the air mass reference system is moving at constant velocity and non-rotating with respect to the earth, the acceleration, $\bar{a}_A$, is also the acceleration with respect to the earth; and the angular velocity of

the airplane with respect to the air mass, $\bar{W}_{(AM)A}$, equals the angular velocity with respect to the earth, $\bar{W}_{EA}$.

Taking $\bar{i}$, $\bar{j}$, $\bar{k}$ as unit vectors along X_A, Y_A, and Z_A, respectively, Eq. A-12 can be expanded into the form

$$\bar{a}_A = \bar{i}\,\dot{V}_{AX_A} + \bar{j}\,\dot{V}_{AY_A} + \bar{k}\,\dot{V}_{AZ_A}$$

$$+[\bar{i}W_{(EA)X_A} + \bar{j}W_{(EA)Y_A} + \bar{k}\,W_{(EA)Z_A}]\,X[\bar{i}V_{AX_A} + \bar{j}\,V_{AY_A} + \bar{k}\,V_{AZ_A}] \qquad \text{A-12A}$$

Equating the X_A, Y_A, Z_A components of Eq. A-12A gives

$$a_{AX_A} = \dot{V}_{AX_A} + W_{(EA)Y_A}\,V_{AZ_A} - W_{(EA)Z_A}\,V_{AY_A} \qquad \text{A-13}$$

$$a_{AY_A} = \dot{V}_{AY_A} + W_{(EA)Z_A}\,V_{AX_A} - W_{(EA)X_A}\,V_{AZ_A} \qquad \text{A-14}$$

$$a_{AZ_A} = \dot{V}_{AZ_A} + W_{(EA)X_A}\,V_{AY_A} - W_{(EA)Y_A}\,V_{AX_A} \qquad \text{A-15}$$

Equations A-13, A-14, and A-15 are kinematic relationships, which can be used in conjunction with a summation of component forces to establish three equations of motion of the airplane. An additional set of three equations is obtained by equating the applied moment to the rate of change of angular momentum.

6. Moment Required for Angular Acceleration of the Airplane

Before discussing the complete airplane, it is convenient to consider a particle, P, situated at distance, $\bar{R}_{(IP)}$, from an Inertial Space Coordinate System, X_I, Y_I, Z_I, as shown in Fig. A-3. By the definition of inertial space,

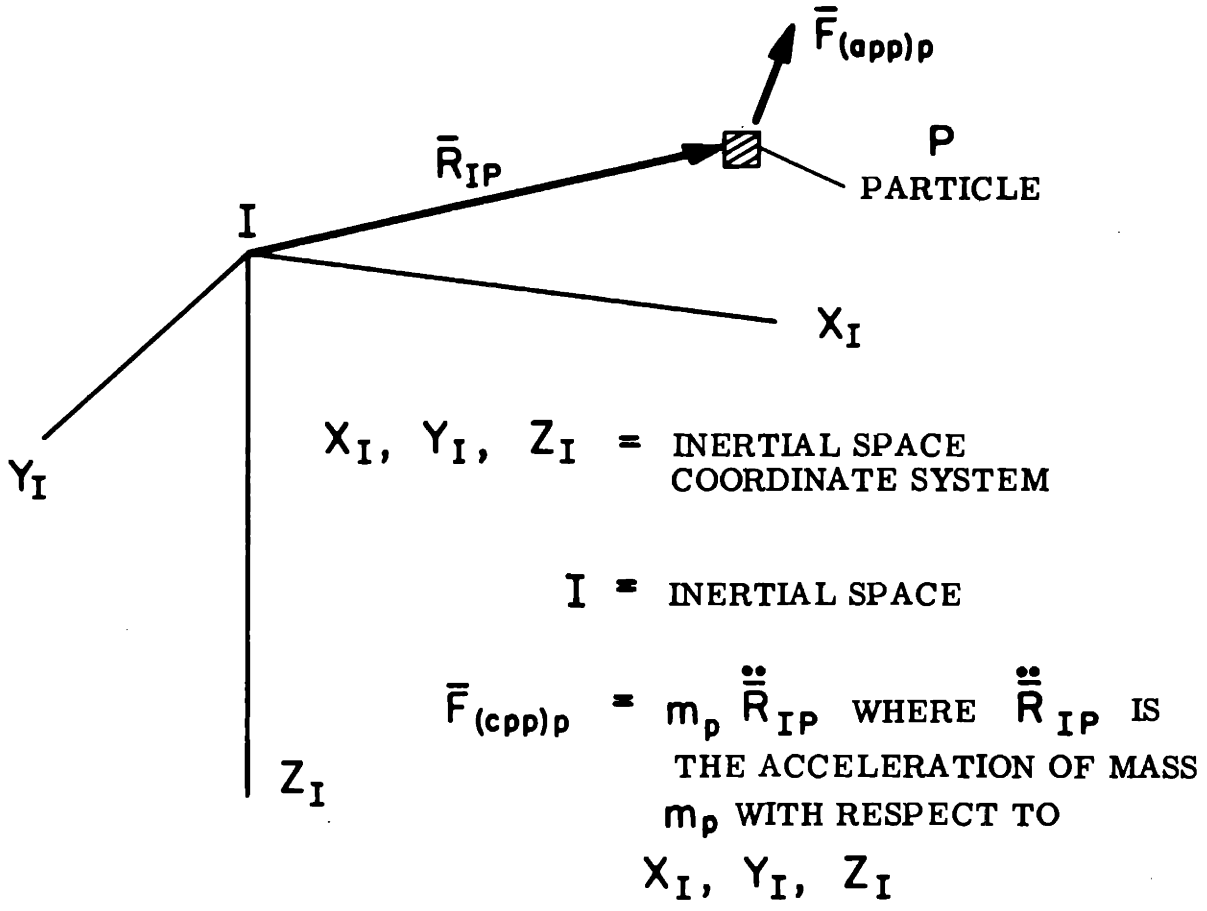

Fig. A-3.–Location of a particle with respect to inertial space.

$$\bar{F}_{(app)P} = m_P \ddot{\bar{R}}_{IP} \qquad \text{A-16}$$

and, consequently,

$$\bar{M}_{(app)P} = \bar{R}_{IP} \times [m_P \ddot{\bar{R}}_{IP}]$$

$$= \bar{R}_{IP} \times [m_P \ddot{\bar{R}}_{IP}] + \dot{\bar{R}}_{IP} \times [m_P \dot{\bar{R}}_{IP}]$$

$$= [\frac{d}{dt} (\bar{R}_{IP} \times m_P \dot{\bar{R}}_{IP})]_I \qquad \text{A-17}$$

The quantity appearing in the last term of Eq. A-17 is called the angular momentum of the particle P, or $\bar{H}_P$, so that

$$\bar{M}_{(app)P} = \left[\frac{d \bar{H}_P}{dt}\right]_I \qquad \text{A-18}$$

where

$$\bar{H}_P = \bar{R}_{IP} \times m_P \dot{\bar{R}}_{IP}$$

$$= \bar{R}_{IP} \times [m_P (\bar{W}_{IP} \times \bar{R}_{IP})] \qquad \text{A-19}$$

The linear velocity of the particle, $\dot{\bar{R}}_{IP}$, equals the cross product of the angular velocity $\bar{W}_{IP}$ and $\bar{R}_{IP}$, as shown in Eq. A-19. The vector distance, $\bar{R}_{IP}$, has components X_{IP}, Y_{IP}, and Z_{IP}; hence Eq. A-19 can be expanded to give

$$\bar{H}_P = \bar{u}_{X_I} [(Y_{IP}^2 + Z_{IP}^2) W_{(IP)X_I} - X_{IP} Y_{IP} W_{(IP)Y_I} - X_{IP} Z_{IP} W_{(IP)Z_I}] m_P$$

$$+ \bar{u}_{Y_I} [-X_{IP} Y_{IP} W_{(IP)X_I} + (X_{IP}^2 + Z_{IP}^2) W_{(IP)Y_I} - Y_{IP} Z_{IP} W_{(IP)Z_I}] m_P$$

$$+ \bar{u}_{Z_I} [-X_{IP} Z_{IP} W_{(IP)Y_I} - Y_{IP} Z_{IP} W_{(IP)Z_I} + (X_{IP}^2 + Y_{IP}^2) W_{(IP)Z_I}] m_P \qquad \text{A-20}$$

In Eq. A-20, $\bar{u}_{X_I}$, $\bar{u}_{Y_I}$, and u_{Z_I} are unit vectors along X_I, Y_I, and Z_I, respectively. Equation A-20 is comprised of terms involving both the moments of inertia and products of inertia. For example, the moment of inertia about X_I is $m_P[Y_{IP}^2 + Z_{IP}^2]$ and is given the symbol $I_{P[X_IX_I]}$. Two product of inertia terms constitute torques about the X_I axis, namely, $I_{P[X_IY_I]}$ and $I_{P[X_IZ_I]}$ equal to $-[m_P I_{IP} Y_{IP}]$ and $-[m_P X_{IP} Z_{IP}]$.

The airplane may be considered a summation of particles, in which case

$$\bar{M}_{(app)} = \Sigma\, \bar{M}_{(app)P} = \Sigma\left(\frac{d\bar{H}_P}{dt}\right)_I = \left[\frac{d}{dt}\,\Sigma\,\bar{H}_P\right]_I = \left(\frac{d\bar{H}_A}{dt}\right)_I \qquad \text{A-21}$$

making

$$\begin{aligned}\bar{H}_A = {} & \bar{u}_{X_I}\left[I_{A[X_IX_I]}{}^{W}{}_{[IA]X_I} + I_{A[X_IY_I]}{}^{W}{}_{(IA)Y_I} + I_{A[X_IZ_I]}{}^{W}{}_{(IA)Z_I}\right] \\ & + \bar{u}_{Y_I}\left[I_{A[X_IY_I]}{}^{W}{}_{[IA]X_I} + I_{A[Y_IY_I]}{}^{W}{}_{(IA)Y_I} + I_{A(Y_IZ_I)}{}^{W}{}_{(IA)Z_I}\right] \\ & + \bar{u}_{Z_I}\left[I_{A[X_IZ_I]}{}^{W}{}_{[IA]X_I} + I_{A[Y_IZ_I]}{}^{W}{}_{(IA)Y_I} + I_{A[Z_IZ_I]}{}^{W}{}_{(IA)Z_I}\right]\end{aligned} \qquad \text{A-22}$$

However, the moments and products of inertia are not constant but vary with time as the airplane maneuvers. Therefore, it is convenient to express the angular momentum in airplane coordinates and then, by the use of Eq. A-10, Eq. A-21 becomes

$$\bar{M}_{(app)} = \left[\frac{d\bar{H}_A}{dt}\right]_A + \bar{W}_{IA} \times \bar{H}_A \qquad \text{A-23}$$

and the angular momentum of the airplane can be written

$$\bar{H}_A = \bar{i}[I_{A(XX)}{}^{W}{}_{(IA)X_A} + I_{A(XY)}{}^{W}{}_{(IA)Y_A} + I_{A(XZ)}{}^{W}{}_{(IA)Z_A}]$$

$$+ \bar{j}[I_{A(XY)}{}^{W}{}_{(IA)X_A} + I_{A(YY)}{}^{W}{}_{(IA)Y_A} + I_{A(YZ)}{}^{W}{}_{(IA)Z_A}]$$

$$+ \bar{k}[I_{A(XZ)}{}^{W}{}_{(IA)X_A} + I_{A(YZ)}{}^{W}{}_{(IA)Y_A} + I_{A(ZZ)}{}^{W}{}_{(IA)Z_A}] \qquad \text{A-24}$$

When using an arbitrary set of body coordinates, all nine terms of Eq. A-24 must be used to evaluate the angular momentum of the airplane. A set of axes, called principal axes, always exists, causing the product of inertia terms to vanish. The X_A and Z_A axes cannot always be principal axes, since their direction varies with the trim angle of attack. Usually, as shown by Eckhardt[2], one principal axis is below X_A due to the mass distribution of the tail. However, the Y_A axis is a principal axis, so that all products of inertia terms involving Y are zero. Making use of this fact, Eq. A-23 and A-24 yield

$$\begin{aligned}\bar{M}_{app} = \bar{i}\Big\{ & I_{A(XX)}\dot{W}_{(IA)X_A} + I_{A(XZ)}\dot{W}_{(IA)Z_A} + I_{A(XZ)}{}^{W}{}_{(IA)X_A}{}^{W}{}_{(IA)Y_A} \\ & + [I_{A(ZZ)} - I_{A(YY)}]{}^{W}{}_{(IA)Y_A}{}^{W}{}_{(IA)Z_A}\Big\} \\ + \bar{j}\Big\{ & I_{A(YY)}\dot{W}_{(IA)Y_A} + I_{A(XZ)}[W^2_{(IA)Z_A} - W^2_{(IA)X_A}] \\ & + [I_{A(XX)} - I_{A(ZZ)}]\, W_{(IA)X_A} W_{(IA)Z_A}\Big\} \\ + \bar{k}\Big\{ & I_{A(ZZ)}\dot{W}_{(IA)Z_A} + I_{A(XZ)}\dot{W}_{(IA)X_A} - I_{A(XZ)}{}^{W}{}_{(IA)Y_A}{}^{W}{}_{(IA)Z_A} \\ & + [I_{A(YY)} - I_{A(XX)}]\, W_{(IA)X_A} W_{(IA)Y_A}\Big\}\end{aligned} \qquad \text{A-25}$$

Differentiation in Eq. A-25 is with respect to airplane coordinates. The

applied moments result from aerodynamic, gravitational, and gyroscopic effects. When these effects are resolved in X_A, Y_A, Z_A axes, three equations are obtained from Eq. A-25 which, combined with equations from Section 5, give six equations necessary when determining the motion of the airplane. In order to determine the airplane position in earth coordinates, the equations for Ψ_A, B_A, and θ_A developed in Section 3 must also be used.

APPENDIX B

AIRPLANE DYNAMICS

The target interception investigated in this thesis has been restricted to a vertical plane. Therefore, it is reasonable to assume that the angular velocity of the airplane is entirely about the Y_A axis; that is, $w_{(EA)X_A}$ and $w_{(EA)Z_A}$ equal zero. Furthermore, for the relatively short-period effects under analysis in this thesis, the earth is assumed fixed with respect to inertial space. When greater accuracy is required, refer to Appendix VI of Reference 14.

With the restrictions of the preceding paragraph, Eq. A-6, A-15, and A-25 become

$$\dot{\theta}_A = w_{(EA)Y_A} \qquad \text{B-1}$$

$$a_{AZ_A} = \dot{V}_{AZ_A} - \dot{\theta}_A V_{AX_A} \qquad \text{B-2}$$

$$M_{(app)Y_A} = I_{A(YY)} \ddot{\theta}_A \qquad \text{B-3}$$

In NACA notation, the velocity along X_A is u, the velocity along Z_A is w, and the resultant velocity is u_o. For small changes in angle of attack, α, the velocity component along X_A is substantially equal to u_o. Consequently,

$$\dot{w} - \dot{\theta}_A u_o = \frac{F_{(app)Z_A}}{m_A} \qquad \text{B-4}$$

$$\ddot{\theta}_A = \frac{M_{(app)Y_A}}{I_{A(YY)}} \qquad \text{B-5}$$

Equation B-4 is based on Eq. B-2 and Newton's second law, which states that the applied force equals the product of the mass and the acceleration when the mass is independent of time.

By definition, the center of gravity is at the origin, so that the only applied moment arises from aerodynamic effects. Furthermore, only changes in the force of gravity need be considered in Eq. B-4, due to the selection of airplane coordinates. For equilibrium conditions, the lift resulting from trim angle of attack is just sufficient to balance the weight of the airplane along Z_A. It is true that deviations from trim lead to incremental changes in the airplane's weight along Z_A, but this effect has been found secondary by Van Meter[3].

The forces along Z_A and moments about Y_A acting on the airplane depend upon the velocity of the airplane with respect to the local air mass or gusts, $\overline{V}_{A[G-A]}$. The velocity of the airplane, $\overline{V}_A$, equals the sum of $\overline{V}_{A[G-A]}$ and the velocity of the gusts with respect to the air mass, $\overline{V}_G$, or

$$\overline{V}_A = \overline{V}_G + \overline{V}_{A[G-A]} \qquad \text{B-6}$$

Making use of NACA notation, Eq. B-6 can be written for the velocities along Z_A as

$$w_{A[G-A]} = w - w_G \qquad \text{B-7}$$

The forces along Z_A and the moments about Y_A are functions not only of $w_{A[G-A]}$ but also of the elevator displacement, δ, and the pitch rate, $\dot{\theta}$, so that a partial expansion of the forces and moments in Eq. B-4 and B-5 yields

$$-u_o \dot{\theta}_A + \dot{w} - wZ_w = \delta Z_\delta - w_G Z_w \qquad \text{B-8}$$

and

$$\ddot{\theta}_A - \dot{\theta}_A M_{\dot{\theta}} - \dot{w}M_{\dot{w}} - wM_w = \delta M_\delta - w_G M_w - \dot{w}_G M_{\dot{w}} \qquad \text{B-9}$$

The effect of changes in the forward velocity of the airplane is not included in Eq. B-8 and B-9. This effect was found to be negligible by Rea[15] for short-period responses with frequency greater than 0.5 rad/sec. Aerodynamic terms involving $\dot{\theta}_A$ and $\dot{w}_{A(G-A)}$ were omitted from Eq. B-8, because they are known to be unimportant. For a more complete treatment of the derivation of Eq. B-8 and B-9 refer to Durand[16].

Equations B-8 and B-9 are used for the aiming error studies conducted on the REAC, as described in Appendix E, and also for the interference studies discussed in Appendix J. The REAC solves Eq. B-8 and B-9 simultaneously but,for the interference analysis, it is necessary to express the performance of the airplane in operational form. This form, called the performance function, (PF), is defined in an article by Seamans, Blasingame, and Clementson[17].

The performance functions of the airplane are obtained by expressing the elevator displacement and the gust velocity as complex exponentials. In this manner,

$$\delta = \delta_a e^{j[\omega t + (PA)_\delta]} \qquad \text{B-10}$$

and

$$w_G = w_{Ga} e^{j[\omega t + (PA)_w]} \qquad \text{B-11}$$

The steady-state solution of Eq. B-8 and B-9 for the inputs of Eq. B-10 and B-11 gives

$$w = (PF)_{A(\delta,w)}\delta + (PF)_{A(w_G,w)} w_G \qquad \text{B-12}$$

$$\dot{\theta}_A = (PF)_{A(\delta,\dot{\theta})}\,\delta + (PF)_{A(w_G,\dot{\theta})}\,w_G \qquad \text{B-13}$$

where

$$(PF)_{A(\delta,w)} = S_{A(\delta,w)(ref)}\,\frac{1 + j(FR)_A\,\omega_{nA}\,(CT)_{A(\delta,w)}}{1 - (FR)_A^2 + j2(DR)_A(FR)_A} \qquad \text{B-14}$$

$$(PF)_{A(w_G,w)} = \frac{1 + j(FR)_A\,\omega_{nA}(CT)_{A(w_G,w)}}{1 - (FR)_A^2 + j2(DR)_A(FR)_A} \qquad \text{B-15}$$

$$(PF)_{A(\delta,\dot{\theta})} = S_{A(\delta,\dot{\theta})(ref)}\,\frac{1 + j(FR)_A\,\omega_{nA}(CT)_{A(\delta,\dot{\theta})}}{1 - (FR)_A^2 + j2(DR)_A(FR)_A} \qquad \text{B-16}$$

$$(PF)_{A(w_G,\dot{\theta})} = S_{A(w_G,\theta)(ref)}\,\frac{[j(FR)_A\,\omega_{nA}][1 + j(FR)_A\,\omega_{nA}(CT)_{A(w_G,\theta)}]}{1 - (FR)_A^2 + j2(DR)_A(FR)_A} \qquad \text{B-17}$$

In Eq. B-14, B-15, B-16, and B-17 it has been found useful to define the following characteristic parameters:

$$\omega_{nA} = \sqrt{Z_w M_{\dot{\theta}} - u_o M_w} \qquad \text{B-18}$$

$$(DR)_A = \frac{-[M_{\dot{\theta}} + Z_w + u_o Z_{\dot{w}}]}{2\sqrt{Z_w M_{\dot{\theta}} - u_o M_w}} \qquad \text{B-19}$$

$$(FR)_A = \frac{\omega}{\omega_{nA}} \qquad \text{B-20}$$

$$S_{A(\delta,w)(ref)} = \frac{u_o M_\delta - M_{\dot{\theta}} Z_\delta}{\omega_{nA}^2} \qquad \text{B-21}$$

$$(CT)_{A(\delta,w)} = \frac{Z_\delta}{u_o M_\delta - M_{\dot\theta} Z_\delta} \qquad \text{B-22}$$

$$(CT)_{A(w_G,w)} = -\frac{Z_w + u_o M_{\dot w}}{\omega_{nA}^2} \qquad \text{B-23}$$

$$S_{A(\delta,\dot\theta)(ref)} = \frac{Z_\delta M_w - Z_w M_\delta}{\omega_{nA}^2} \qquad \text{B-24}$$

$$(CT)_{A(\delta,\dot\theta)} = \frac{M_\delta + Z_\delta M_{\dot w}}{Z_\delta M_w - Z_w M_\delta} \qquad \text{B-25}$$

$$S_{A(w_G,\theta)(ref)} = -\frac{M_w}{\omega_{nA}^2} \qquad \text{B-26}$$

$$(CT)_{A(w_G,\theta)} = \frac{M_{\dot w}}{M_w} \qquad \text{B-27}$$

Equations B-14 and B-15 involve linear velocity along the Z_A axis, which is a difficult output quantity to instrument. A more convenient quantity to measure in flight is normal acceleration, n_Z. Equations B-12 and B-13 can be combined to give performance functions in terms of normal acceleration, since from Eq. B-8

$$n_Z = \frac{(\dot w - u_o \dot\theta)}{g} = \delta \frac{Z_\delta}{g} + w \frac{Z_w}{g} - w_G \frac{Z_w}{g} \qquad \text{B-28}$$

and hence

$$n_Z = \left[\frac{Z_\delta}{g} + \frac{Z_w}{g}(PF)_{A(\delta,w)}\right]\delta + \left[-\frac{Z_w}{g} + \frac{Z_w}{g}(PF)_{A(w_G,w)}\right] w_g$$

$$= (PF)_{A(\delta,n)}\ \delta + (PF)_{A(w_G,n)}\ w_G \qquad \text{B-29}$$

Comparison of Eq. B-29 with Eq. B-14 and B-15 shows that

$$(PF)_{A(\delta, n)} = \frac{Z_\delta}{g} + \frac{Z_w}{g}(PF)_{A(\delta, w)} \qquad \text{B-30}$$

and

$$(PF)_{A(w_G,n)} = S_{A(w_G, \int n\, dt)}[j(FR)_A\, \omega_{nA}]\ \frac{1 + j(FR)_A \omega_{nA}(CT)_{A(w_G,n)}}{1 - (FR)_A^2 + j2(DR)_A(FR)_A} \qquad \text{B-31}$$

where

$$S_{A(w_G, \int n\, dt)(ref)} = \frac{Z_w}{g}\ \frac{M_{\dot\theta}}{\omega_{nA}^2} \qquad \text{B-32}$$

$$(CT)_{A(w_G,n)} = -\frac{1}{M_{\dot\theta}} \qquad \text{B-33}$$

Equations B-14, B-15, B-16, B-17, B-30, and B-31 can be used to calculate the theoretical performance functions of an airplane. The theoretical responses of the airplane to radar and gust interference are based on these equations, with the following F-94 data. These data were extrapolated from the flight test results of an F-80[18], taking into account the increased tail length and area of the F-94.

Computed Stability Derivations

Mach Number = 0.7, C. G. at 27% MAC, 20,000 ft. Pressure Altitude

$M_\delta = -20.69\ (1/sec^2)$

$Z_\delta = -76.44\ (ft/sec^2)$

$M_w = -.0121\ (1/ft\ sec)$

$Z_w = -1.468\ (1/sec)$

$M_{\dot w} = -7.36 \times 10^{-4}(1/ft)$

$M_{\dot\theta} = -.957\ (1/sec)$

$u_o = 727\ (ft/sec)$

Characteristic Parameters

$\omega_{nA} = 3.19$ rad/sec from Eq. B-18

$(DR)_A = .47$ from Eq. B-19

$\frac{1}{u_o} S_{A(\delta,w)(ref)} = 2.04$ mil/mil from Eq. B-21

$(CT)_{A(\delta,w)} = .005$ sec from Eq. B-22

$(CT)_{A(w_G w)} = .20$ sec from Eq. B-23

$S_{A(\delta,\dot{\theta})(ref)} = -2.88 \frac{\text{mil/sec}}{\text{mil}}$ from Eq. B-24

$(CT)_{A(w_G,\theta)} = .06$ sec from Eq. B-27

$S_{A(w_G\sqrt{ndt})} = 4.30 \times 10^{-3} \frac{\text{sec}^2}{\text{ft}}$ from Eq. B-32

$(CT)_{A(w_G,n)} = 1.05$ sec from Eq. B-33

$(CT)_{A(\delta,\dot{\theta})} = .70$ sec from Eq. B-25

$S_{A(w_G,\theta)} = 1.19 \frac{\text{mil}}{\text{ft/sec}}$ from Eq. B-26

APPENDIX C

FACTORS INVOLVED IN GUNFIRE AND ROCKETFIRE

The interceptor aircraft of today is usually equipped with guns and rockets. Against an airborne target, guns are the most probable weapon, rockets being used primarily for ground or sea attack. Other methods for killing a target involve either bombs or guided missiles. Bombs have the disadvantage of a long time of flight and present a difficult storage problem. Guided missiles for air-to-air combat offer the hope of greater kill probability per pound of armament, with greater safety to the interceptor aircraft. Much remains to be done before guided missiles are operational; in the meantime, guns and rockets must be used. However, it is anticipated that several guided missiles under development, for example, Meteor[5], will have launching requirements similar to those for gunfire and rocketfire. Therefore, it is expected that much of the analysis in this thesis can be applied to this newer weapon when it is more completely developed.

Figure C-1 shows the geometrical relationship between the interceptor aircraft and the target. The target direction is established by the line of sight, LS: the line along which the pilot sees the target when it is visible. When the target is not visible, or whenever the target tracking is automatic, radar must be used to detect the target location. The radar tracking line, TL,fixed to the radar antenna, indicates the target direction. Since ideal radar does not exist, the tracking line is never perfectly aligned with the line of sight, and consequently a tracking line inaccuracy, (I)TL, exists.

The tracking line inaccuracy is measured from the correct position of the tracking line, which is the line of sight, to the actual position of the tracking line, so that

$$(I)TL = TL - LS \qquad C\text{-}1$$

In order to correct for the inaccuracy of the tracking line, the tracking line is moved towards the line of sight, so that the tracking line correction, (C)TL, is related to the inaccuracy simply as

$$(C)TL = -(I)TL = LS - TL \qquad C\text{-}2$$

The aiming of guns and rockets involves a consideration of target motion and ballistic effects, and consequently it is necessary to head the aircraft in a direction away from the line of sight. The angular amount by which the aircraft is aimed "ahead" of the target involves a prediction of events after firing, and is called the prediction angle, P. The prediction angle is measured from the line of sight LS to the controlled line CL. The controlled line is a boresight reference fixed in the airplane parallel to the X_A axis under the most likely combat conditions. The best indication of the actual prediction angle is the angle set forth by the radar tracking line, and is called the radar prediction angle, P_R.

The controlled line has a correct position, $(CL)_{(corr)}$, for a hit to be scored. The inaccuracy of aiming the controlled line, (I)CL, is the basis for comparison of the tracking systems discussed in this thesis. It can be seen from Fig. C-1 that

$$(I)CL = CL - (CL)_{(corr)} \qquad C\text{-}3$$
$$= P - P_{(corr)}$$

The inaccuracy is composed of errors and uncertainties – the errors being completely predictable, whereas the uncertainties must be treated statistically.

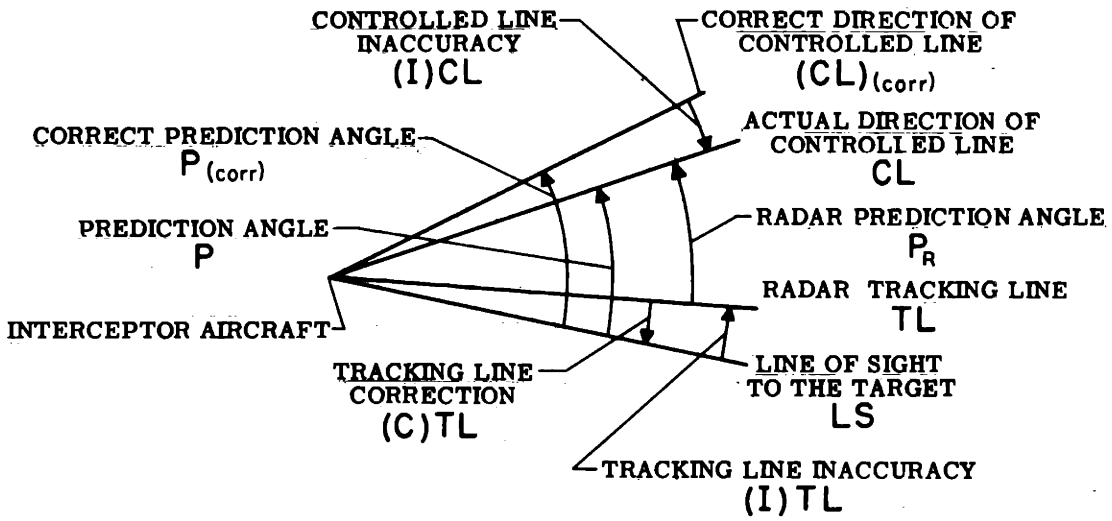

FIG. C-1 GEOMETRICAL RELATIONSHIP BETWEEN THE INTERCEPTOR AIRCRAFT AND TARGET

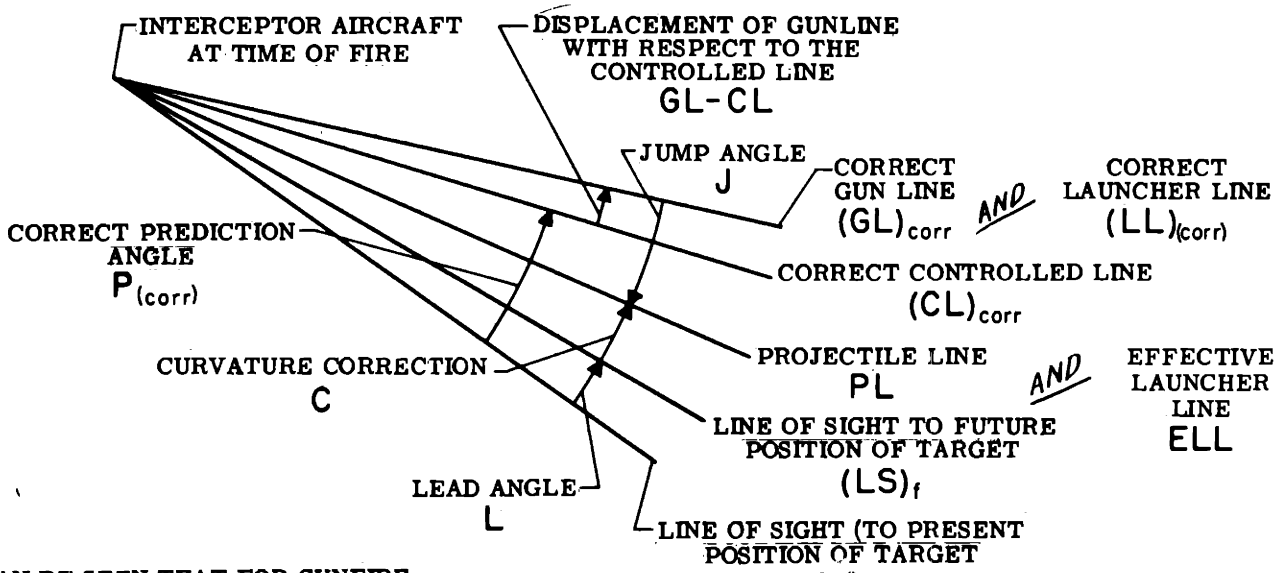

IT CAN BE SEEN THAT FOR GUNFIRE,

$$\bar{P}_{(corr)} = \bar{C} + \bar{L} - \bar{J} + [\overline{CL} - \overline{GL}]$$

THIS SUMMATION MUST BE VECTORIAL SINCE LS, $(LS)_f$, PL, CL, and GL ARE IN GENERAL NOT CONFINED TO A SINGLE PLANE.

Fig. C-2.—Geometrical factors involved in correctly aiming an interceptor aircraft for gunfire or rocketfire.

As previously stated, the aiming of the interceptor aircraft must depend upon the target motion and the ballistics of the projectile. These two effects are defined in Fig. C-2. During the time of flight of the projectile, the target moves from its "present" position at the time of fire to its "future" position. The line of sight LS and the line of sight to future position $(LS)_f$ pass respectively through these two target positions, and eminate from the position of the interceptor aircraft at firing. The lead angle, L, is measured from the present to the future line of sight, so that

$$L = (LS)_f - LS \qquad C-4$$

The projectile travels along a curved trajectory, since side forces due to gravity and windage are acting during the time of flight. Gravity is the important cause of curvature in forward-firing fixed gun installations. The amount of trajectory curvature is measured from the future line of sight to the projectile line, PL, or

$$C = PL - (LS)_f \qquad C-5$$

the projectile line being a line parallel to the projectile velocity with respect to the air mass the instant after firing.

The initial projectile velocity differs from the direction in which the projectile is aimed. The difference depends upon the angle of attack of the interceptor aircraft. The effect is independent of range and, since it is instantaneous for gunfire and nearly instantaneous for rocketfire, it is called the projectile jump.

Bullets are aimed in the direction of the gun bore, which defines the gun line, GL. Rockets are held either in stores or on zero-length rails under the wing of the interceptor. The initial orientation of the rocket defines the launcher line, LL. The jump angle, J, for gunfire is measured from the gun line to the projectile line, whereas for rocketfire the jump

angle is measured from the launcher line. The projectile line for rocketfire is often called the effective launcher line, ELL. Consequently,

$$J = PL - GL \quad \text{for gunfire} \qquad \text{C-6}$$

and

$$J = ELL - LL \quad \text{for rocketfire}$$

The gun line and the launcher line are shown in Fig. C-2 displaced with respect to the controlled line. The harmonization procedure, when using computers of the A-1 Sight type, calls for as close alignment as possible. For gunfire, the harmonization is achieved by "firing in" against a ground target, with the aircraft secured. Rockets need not be harmonized as precisely as guns. With 5.0" HVAR, the zero-length launching rails are adjusted using a gunner's quadrant to determine the direction of the rocket case with respect to the controlled line.

The correct prediction angle, $P_{(corr)}$, depends upon the target lead, the trajectory curvature, the projectile jump, and variations in harmonization. It can be seen from Fig. C-2 that

$$\bar{P}_{(corr)} = \bar{C} + \bar{L} - \bar{J} + [\overline{CL - GL}] \quad \text{for gunfire} \qquad \text{C-7}$$

and

$$\bar{P}_{(corr)} = \bar{C} + \bar{L} - \bar{J} + [\overline{CL - LL}] \quad \text{for rocketfire} \qquad \text{C-8}$$

The angles in Eq. C-7 and C-8 are expressed as vectors, since they are not necessarily measured about a common axis, and their directions must be considered as well as their magnitudes.

Although the prediction computer must correct for the trajectory curvature, it is not considered in detail in this thesis, since its effect on the dynamic performance of a tracking system can be made negligibly small. The lead angle is the most important consideration. Figure C-3 shows the target

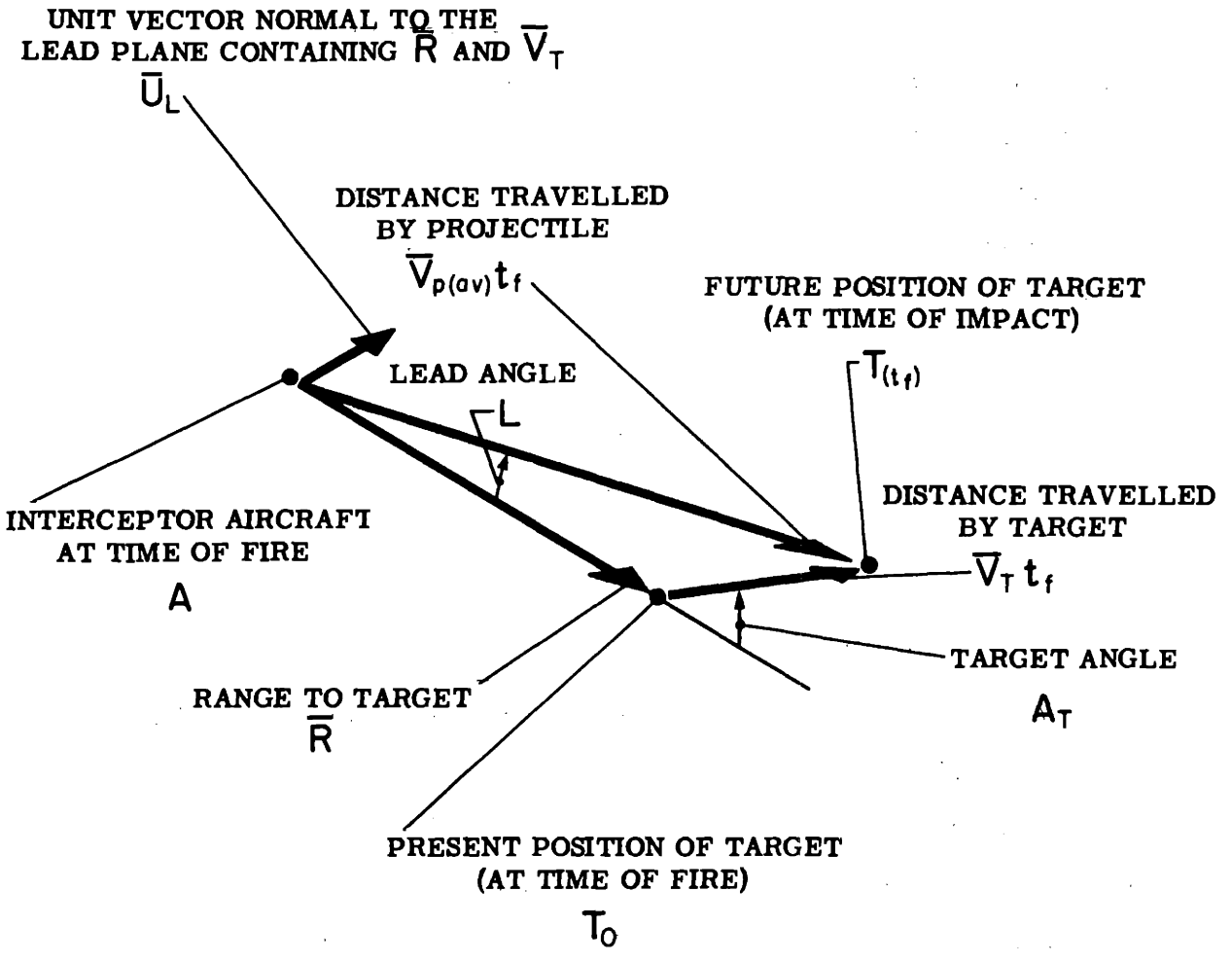

IT CAN BE SEEN THAT

$$\text{SIN } L = \frac{V_T}{V_{p(av)}} \text{SIN } A_T$$

$$\cong L$$

Fig. C-3.–Factors determining the lead angle required to hit a moving target.

travelling at velocity, $\bar{V}_T$, in a direction displaced from the line of sight (range vector) by the angle A_T. The distance travelled by the target during the time of flight of the projectile is $\bar{V}_T t_f$, and the distance travelled by the projectile is $\bar{V}_{p(av)} t_f$. For a hit to be scored, these vectors must meet at the point of impact, and hence the magnitude of the lead angle, determined by the use of the law of sines, is

$$\sin L = \frac{V_T}{V_{p(av)}} \sin A_T \cong L \qquad \text{C-9}$$

The lead angle can be expressed in vector form by defining a unit vector, $\bar{u}_L$, normal to the plane containing the range vector, $\bar{R}$, and the target velocity vector, $\bar{V}_T$. Then

$$\bar{L} = \left[\frac{R}{V_{p(av)}}\right] \left[\frac{\bar{R} \times \bar{V}_T}{R^2}\right] \qquad \text{C-10}$$

Equation C-10 is useful when developing a relation between the lead angle and the angular velocity of the line of sight.

The jump angle for gunfire can be determined simply by considering the relative and absolute velocities of a bullet for the instant just after firing. The bullet has a muzzle velocity $\bar{V}_m$, with respect to the gun barrel, but the gun barrel is travelling with the aircraft at a velocity, $\bar{V}_A$. The vector sum of these velocities is the initial projectile velocity, $\bar{V}_{po}$. Figure C-4 shows the relationship of these velocities assuming the sideslip of the interceptor aircraft to be zero. In this case the jump occurs about the pitch, or elevation, axis. Since the gun line is measured with respect to the airplane no-lift line, it is necessary to consider both the trim angle of attack α_{tr}, and the deviation from trim, α. For small angles, the relation between the elevation jump angle, J_e, and the angle of attack is

$$J_e = -\frac{V_A}{V_{p_o}} [\alpha + \alpha_{tr} + I_{(GL)_e}]$$

$$= -(JF)_g [\alpha + \alpha_{tr} + I_{(GL)_e}] \qquad \text{C-11}$$

α = CHANGE IN ANGLE OF ATTACK FROM TRIM

α_{tr} = TRIM ANGLE OF ATTACK

α_{GL} = INCLINATION OF THE GUN LINE WITH RESPECT TO THE AIRCRAFT NO-LIFT LINE

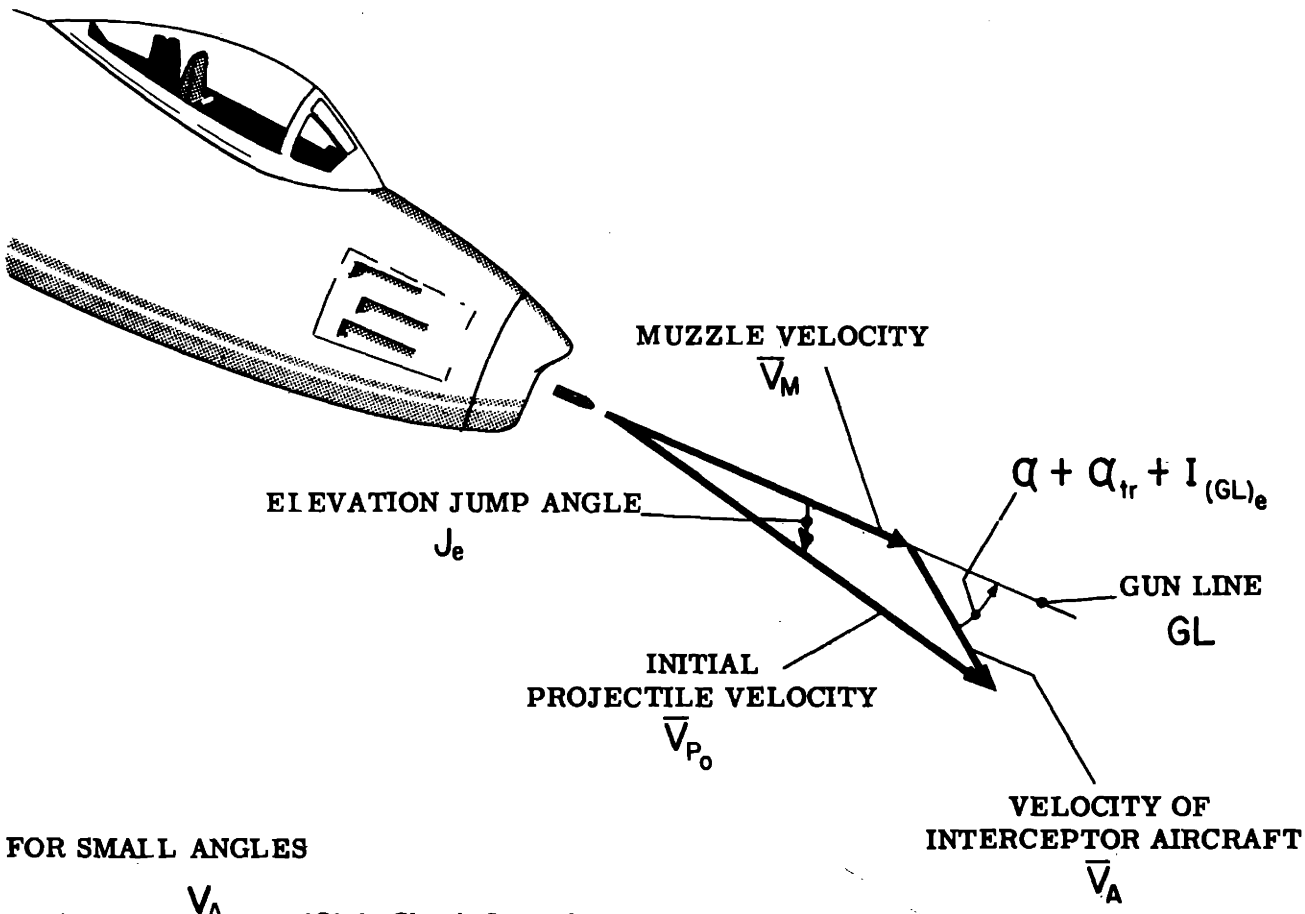

FOR SMALL ANGLES

$$J_e = -\frac{V_A}{V_M + V_A}(\alpha + \alpha_{tr} + I_{(GL)_e})$$

$$= -\frac{V_A}{V_{P_o}}(\alpha + \alpha_{tr} + I_{(GL)_e})$$

$$= -(JF)_g(\alpha + \alpha_{tr} + I_{(GL)_e}) \quad \text{WHERE} \quad (JF)_g = \text{GUN JUMP FACTOR}$$

Fig. C-4.—Factors affecting the elevation jump angle of a bullet when fired from an interceptor aircraft.

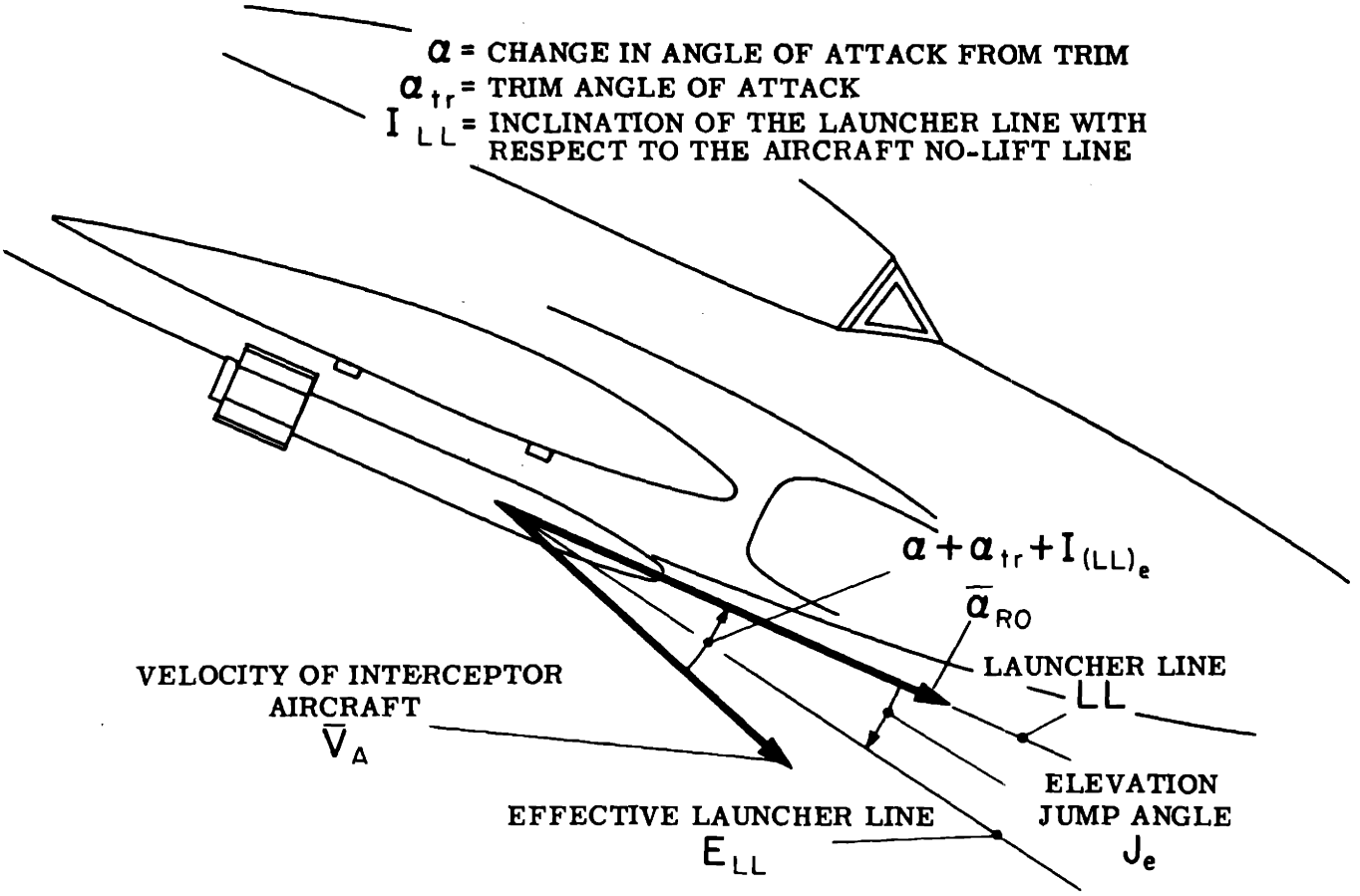

$$J_e = -(JF)_R (\alpha + \alpha_{tr} + I_{(LL)_e})$$

WHERE $(JF)_R$ = ROCKET JUMP FACTOR

THE ROCKET DIRECTION AFTER THE FIRST INSTANT OF FLIGHT IS ALONG THE EFFECTIVE LAUNCHER LINE

Fig. C-5.—Factors affecting the elevation jump angle of a rocket when fired from an interceptor aircraft.

where $(JF)_g$ is the jump factor of the gun.

The jump angle of a rocket (Fig. C-5) depends upon certain of its characteristics. Just after leaving the rocket rails, the rocket travels with the velocity of the aircraft; but it accelerates along the launcher line, due to the thrust of its motor. Its direction of travel at the end of burning is a function of the magnitude of the acceleration and the speed at which it weathercocks into the relative wind. Since rockets are aerodynamically quite stable, their acceleration normal to the aircraft velocity vector is small, and hence the effective launcher line is nearly parallel to the flight path of the airplane. The elevation jump angle is equal to the displacement of the launcher line with respect to the aircraft velocity vector, modified by the rocket jump factor, $(JF)_R$, or

$$J_e = - (JF)_R \left(\alpha + \alpha_{tr} + I_{(LL)_e} \right) \qquad C\text{-}12$$

An analysis of the trajectory of a rocket, including the effect of gravity, is contained in Appendix XVIII of Reference 14.

APPENDIX D

COMPUTER CHARACTERISTICS FOR CLOSED-LOOP AND OPEN-CHAIN TRACKING SYSTEMS

1. Relationship between the Lead Angle and the Angular Velocity of the Line of Sight.

The computation of the lead must be based on measurements of the line of sight angular velocity and the range, since the target velocity is seldom known accurately enough for fire control purposes. Figure D-1 shows the line of sight drawn from the interceptor aircraft to the target. Expressed vectorially, this line is the range, $\bar{R}$. The line of sight rotates when either the target or the interceptor has a velocity component normal to $\bar{R}$, unless the velocity components of the target and the interceptor are in the same direction and of equal magnitude.

If the target were stationary, the line of sight would have an angular velocity equal to the aircraft velocity component normal to the line of sight divided by the range. The direction of rotation would be about an axis perpendicular to the plane of $\bar{V}_A$ and $\bar{R}$, with a negative sense. Similarly, if the interceptor aircraft were stationary, the line of sight would rotate about an axis perpendicular to the plane of $\bar{R}$ and $\bar{V}_T$, with positive sense and a magnitude equal to the normal component of the target velocity divided by the range. Actually, neither target nor aircraft is stationary, and the resulting angular velocity of the line of sight, $\bar{W}_{LS}$, is the vector sum of the effect of each, so that

$$\bar{W}_{LS} = \frac{\bar{R} \times \bar{V}_T}{R^2} - \frac{\bar{R} \times \bar{V}_A}{R^2} \qquad \text{D-1}$$

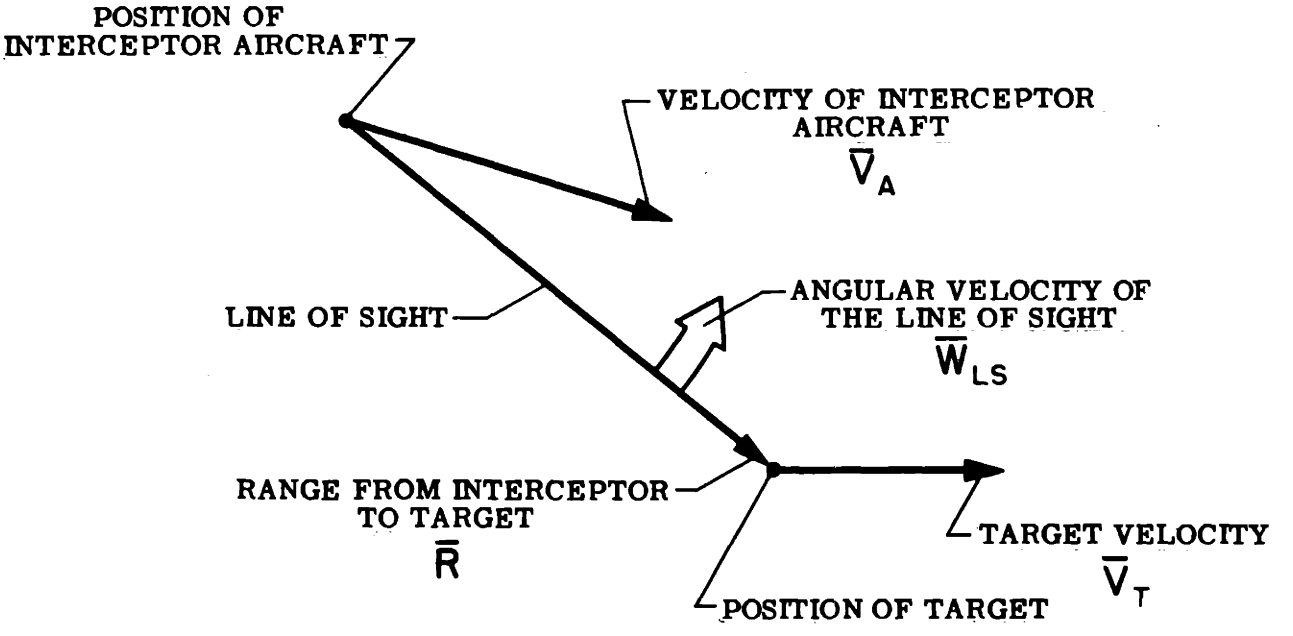

THIS DIAGRAM SHOWS THAT:

$$\bar{W}_{LS} = \frac{\bar{R} \times \bar{V}_T}{R^2} - \frac{\bar{R} \times \bar{V}_A}{R^2}$$

$$\dot{R} = \frac{\bar{R} \cdot \bar{V}_T}{R} - \frac{\bar{R} \cdot \bar{V}_A}{R}$$

Fig. D-1.–Geometrical factors affecting the angular velocity of the line of sight and the range rate.

Reference to Eq. C-10 shows that

$$L = \frac{R}{V_{p(av)}} \left[\bar{W}_{LS} + \frac{\bar{R} \times \bar{V}_A}{R^2} \right] \qquad \text{D-2}$$

The lead angle is equal to the sum of two terms, one proportional to the sight line angular velocity and the other accounting for the velocity of the interceptor aircraft. Actually, the second term is not unwanted, since it partially compensates for the projectile jump angle.

2. The Correct Prediction Angle for Closed-Loop Tracking Systems.

In a closed-loop tracking system, the tracking line is maintained along the line of sight by proper control of the aircraft. The tracking inaccuracy is detected by the radar, and a tracking correction signal is transmitted to the controls. The prediction is based on the motion required of the aircraft in the process of tracking. The output signal from the prediction computer is used to displace the tracking line with respect to the aircraft.

The computer axes for a closed-loop system are fixed to the aircraft with the controlled line forward, the elevation axis, EA, along the Y_A axis and the deflection axis, DA, forming a right-hand system. The controlled line is not always aligned with the X_A axis, for at different speeds and altitudes the trim angle of attack varies and, as a result, the X_A axis is reoriented with respect to the aircraft. However, for the purpose of this analysis, it is assumed that the aircraft is operating at the conditions of speed and altitude for which it is boresighted, thereby aligning the controlled line with the X_A axis, and the deflection axis with Z_A, as shown in Fig. D-2. Therefore,

$$\alpha_{tr} + I_{(CL)e} = 0 \qquad \text{D-3}$$

Furthermore, ideal harmonization is assumed, in which case

$$\alpha_{tr} + I_{(GL)e} = 0 \qquad \text{D-4}$$

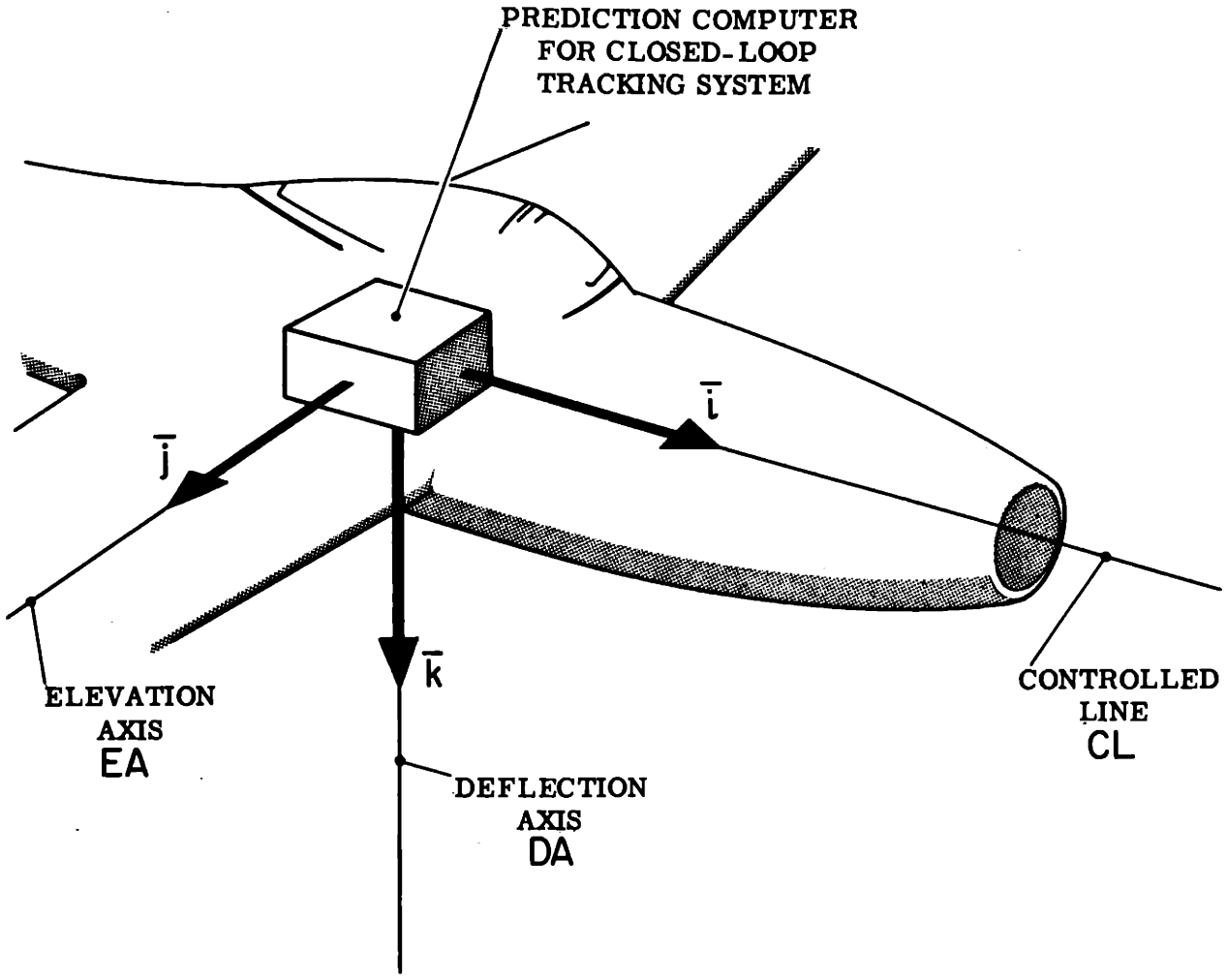

FOR THE PURPOSES OF THIS ANALYSIS IT IS ASSUMED THAT THE COMPUTER COORDINATE SYSTEM CL, EA AND DA IS ALIGNED WITH THE AIRCRAFT COORDINATE SYSTEM X_A, Y_A AND Z_A WITH CL ALONG $\bar{i}$, EA ALONG $\bar{j}$ AND DA ALONG $\bar{k}$

Fig. D-2.–Relationship between computer and aircraft coordinates for a closed-loop tracking system.

and

$$\alpha_{tr} + I_{(LL)e} = 0 \qquad \text{D-5}$$

thereby permitting Eq. C-11 and C-12 to be written

$$J_e = -(JF)\alpha \qquad \text{D-6}$$

The jump angle about the deflection axis, J_d, is similar to J_e in both gunfire and rocketfire, with the angle of aerodynamic yaw, β, replacing the angle of attack. Consequently,

$$J_d = -(JF)\beta \qquad \text{D-7}$$

Positive aerodynamic yaw occurs when the nose of the aircraft turns about the Z_A axis, away from the velocity vector.

The angular velocity of the line of sight, the target range, and the aircraft velocity can all be expressed in terms of X_A, Y_A, Z_A components as

$$\bar{W}_{LS} = \bar{i}\, W_{(LS)c} + \bar{j}\, W_{(LS)e} + \bar{k}\, W_{(LS)d} \qquad \text{D-8}$$

$$\bar{R} = \bar{I}\, R_{X_A} + \bar{j}\, R_{Y_A} + \bar{k}\, R_{Z_A} \qquad \text{D-9}$$

and

$$\bar{V}_A = \bar{I}\, V_A + \bar{j}(-V_A\beta) + \bar{k}\, V_A\alpha \qquad \text{D-10}$$

It can be seen from Eq. D-10 that the angles of attack and yaw have been assumed sufficiently small so that their cosines are unity and their sines equal to the angle. Substitution of Eq. D-8, D-9, and D-10 in Eq. D-2 gives for the elevation and deflection components of the lead angle

$$L_e = \frac{R}{V_{p(av)}} W_{(LS)e} + \left(\frac{V_A}{V_{p(av)}}\right)\frac{R_{Z_A}}{R} - \left(\frac{V_A}{V_{p(av)}}\right)\frac{R_{X_A}}{R}\alpha \qquad \text{D-11}$$

$$L_d = \frac{R}{V_{p(av)}} W_{(LS)d} - \left(\frac{V_A}{V_{p(av)}}\right)\frac{R_{Y_A}}{R} - \left(\frac{V_A}{V_{p(av)}}\right)\frac{R_{X_A}}{R}\beta \qquad \text{D-12}$$

Under the boresighting assumptions of Eq. D-3, D-4, and D-5, Eq. C-7 and C-8 become respectively

$$P_{e(corr)} = L_e + C_e - J_e \qquad \text{D-13}$$

$$P_{d(corr)} = L_d + C_d - J_d \qquad \text{D-14}$$

It is obvious from Fig. D-3 that

$$\frac{R_{Y_A}}{R} = - \tan P_d \cos P \qquad \text{D-15}$$

$$\frac{R_{Z_A}}{R} = \tan P_e \cos P \qquad \text{D-16}$$

Equations D-15 and D-16 are for any value of the prediction angle, whether this value is correct or not. For the correct conditions of fire, and assuming relatively small angles, these equations become simply

$$\frac{R_{Y_A}}{R} = - P_{d(corr)} \qquad \text{D-17}$$

$$\frac{R_{Z_A}}{R} = P_{e(corr)} \qquad \text{D-18}$$

Substitution Eq. D-6, D-7, D-11, D-12, D-17, and D-18 into Eq. D-13 and D-14 gives for the correct elevation and deflection prediction angles:

$$P_{e(corr)} = \left[\frac{R}{V_{p(av)} - V_A}\right] W_{(LS)e} + \left[\frac{(JF)V_{p(av)} - V_A}{V_{p(av)} - V_A}\right]\alpha + \left[\frac{V_{p(av)}}{V_{p(av)} - V_A}\right] C_e \qquad \text{D-19}$$

$$P_{d(corr)} = \left[\frac{R}{V_{p(av)} - V_A}\right] W_{(LS)d} + \left[\frac{(JF)V_{p(av)} - V_A}{V_{p(av)} - V_A}\right] \beta + \left[\frac{V_{p(av)}}{V_{p(av)} - V_A}\right] C_d \qquad \text{D-20}$$

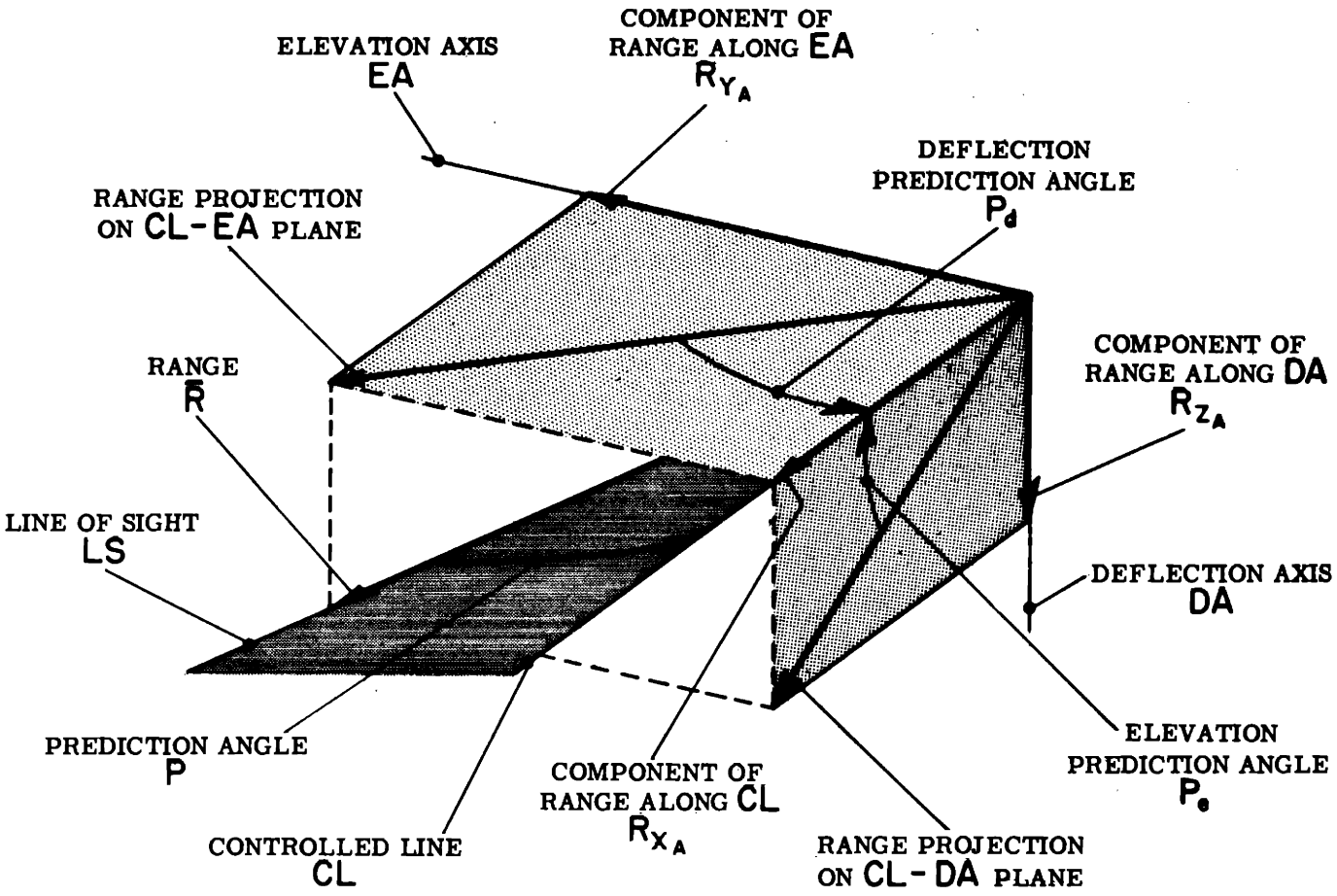

IN THE DIAGRAM:

$$\tan P_e = \frac{R_{Z_A}}{R_{X_A}}; \quad \tan P_d = -\frac{R_{Y_A}}{R_{X_A}}; \quad \cos P = \frac{R_{X_A}}{R}$$

SO THAT $$\frac{R_{Z_A}}{R} = -\tan P_d \cos P$$

AND $$\frac{R_{Z_A}}{R} = \tan P_e \cos P$$

Fig. D-3.--Diagram showing the prediction angle components and their relation to range in X_A, Y_A, Z_A coordinates.

For comparative purposes, the correct prediction angle for open-loop tracking systems is discussed in Section 3. The design for prediction computers for these two types of systems is described in Sections 4 and 5.

3. The Correct Prediction Angle for Open-Chain Tracking Systems.

In an open-chain tracking system, an attempt is made to separate the functions of tracking and computing. Signals from the tracking inaccuracy detector are transmitted directly to the radar antenna drive to bring the tracking line into coincidence with the line of sight, thus providing a self-tracking radar set.

The prediction computer receives signals proportional to the angular velocity of the tracking line, which with ideal radar equals the angular velocity of the line of sight. The output of the computer is a measure of the desired prediction angle, which is compared with the actual prediction angle as determined by the radar antenna position. The difference between the prediction signals is a measure of the heading error of the aircraft, and consequently is transmitted to the servo system in order that the control surfaces may be appropriately displaced.

The radar tracking line can rotate with respect to the aircraft about two axes. The first, and outer, axis is along Z_A; the second, and inner, axis is normal to both the Z_A axis and the tracking line. These axes are shown in Fig. D-4, together with the input axes for the prediction computer. The elevation input axis is along the second antenna axis, and the deflection input axis is normal to both the elevation input axis and the tracking line. Unit vectors $\bar{f}$, $\bar{g}$, $\bar{h}$ are selected along the tracking line, the elevation input axis, and the deflection input axis, respectively.

The components of the prediction angle, P_g and P_h, measured about the respective $\bar{g}$ and $\bar{h}$ axes, are shown in Fig. D-5. For comparative pur-

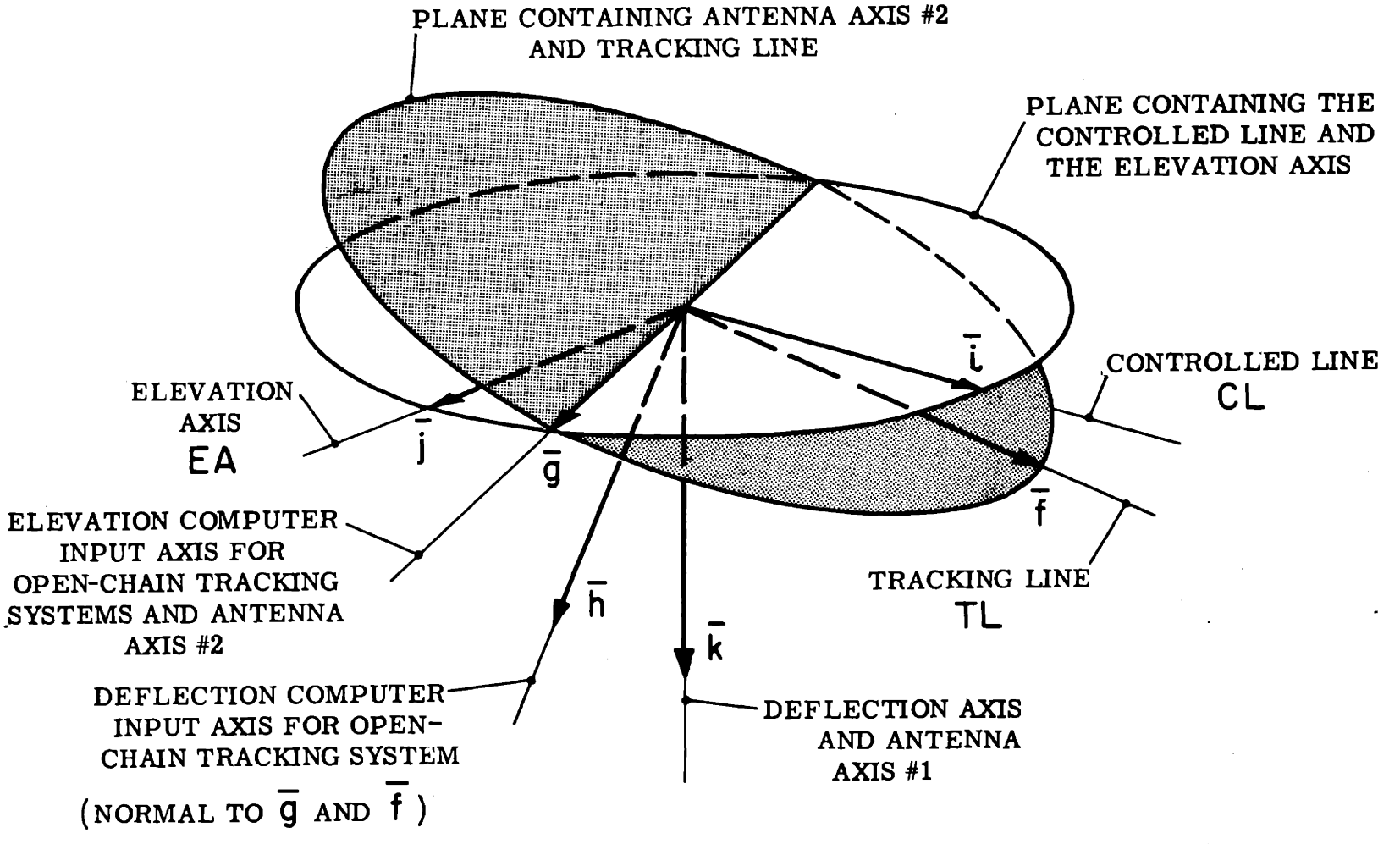

Fig. D-4.–Relationship between computer and aircraft coordinates in an

poses the elevation and deflection components developed for closed-loop tracking are shown in Fig. D-6.

It can be seen that the radar antenna rotates about $\bar{g}$, the elevation axis of an open-chain system, and $\bar{k}$, the deflection axis of a closed-loop system. For this reason, when the prediction angle components are large, trigonometric corrections must be applied about the elevation axis of a closed-loop system, and about the deflection axis of an open-chain system. However, once the correction is made in a closed-loop system, indications are available about aircraft axes. With an open-chain system, further corrections must be made to transform the data into aircraft coordinates. For example, when a deflection prediction angle exists a correction about the $\bar{g}$ axis involves both pitching and rolling of the interceptor aircraft.

Expressions for the correct components of the prediction angle, $P_{g(corr)}$, and $P_{h(corr)}$, can be developed by first referring to Fig. C-3 and noting that

$\bar{T}(o)$ = position of the target at zero time

$$= \bar{A} + \bar{R} \qquad \text{D-21}$$

and

$\bar{T}(t_f)$ = position of the target at projectile impact

$$= \bar{T}(o) + t_f \bar{V}_T \qquad \text{D-22}$$

However,

$$\bar{V}_T = \left[\frac{d(\bar{T}(o))}{dt} \right]_I$$

$$= \left(\frac{d\bar{A}}{dt} \right)_I + \left(\frac{d\bar{R}}{dt} \right)_I \qquad \text{D-23}$$

For the purposes of the analysis in this thesis, the air mass coordinates of Appendix A have been assumed synonymous with inertial space. Consequently, the differentiations of Eq. D-23 are made with respect to

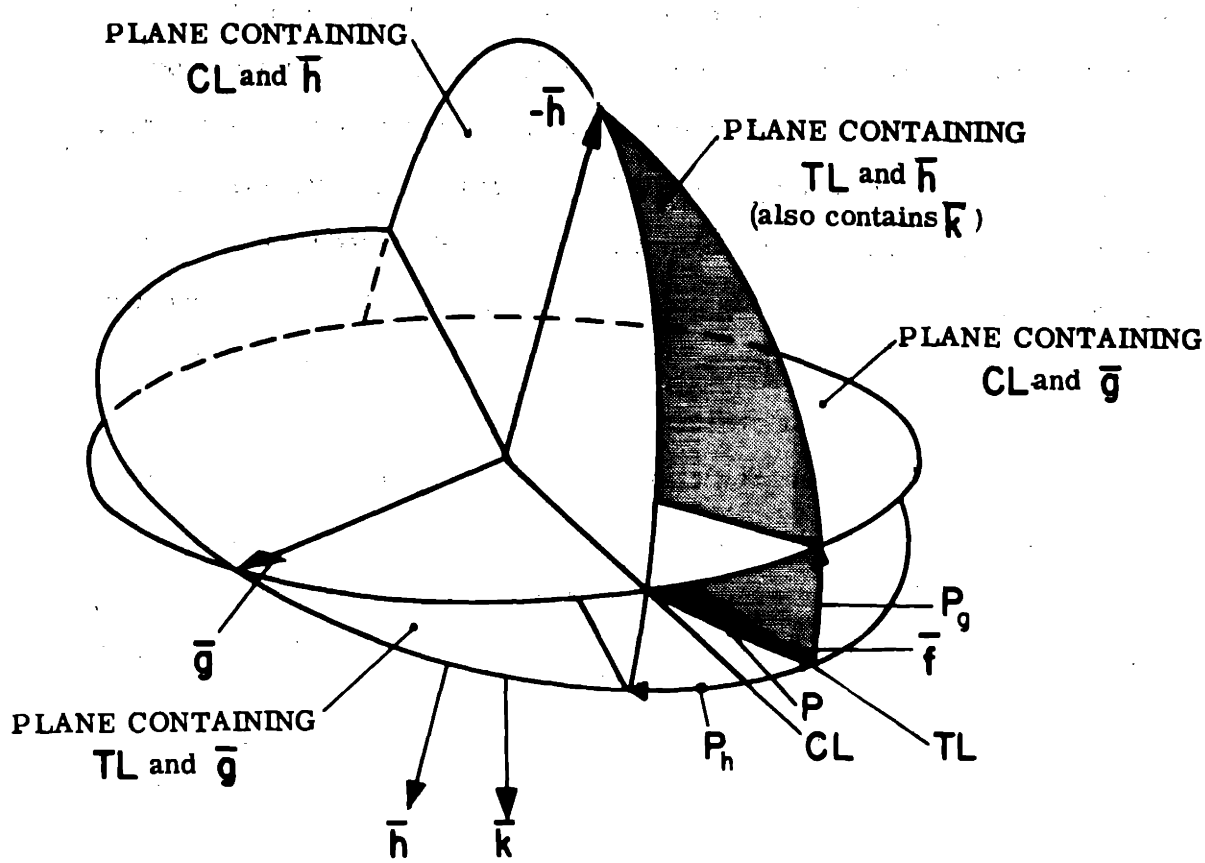

$\bar{f}$ $\bar{g}$ AND $\bar{h}$ ARE MUTUALLY ORTHOGONAL UNIT VECTORS. THE ELEVATION AND DEFLECTION AXES OF THE OPEN-CHAIN TRACKING SYSTEMS ARE ALONG $\bar{g}$ AND $\bar{h}$. THE UNIT VECTOR $\bar{k}$ IS ALONG THE DEFLECTION AXIS OF THE CLOSED-LOOP TRACKING SYSTEM

Fig. D-5.--Prediction angle components for open-chain tracking systems.

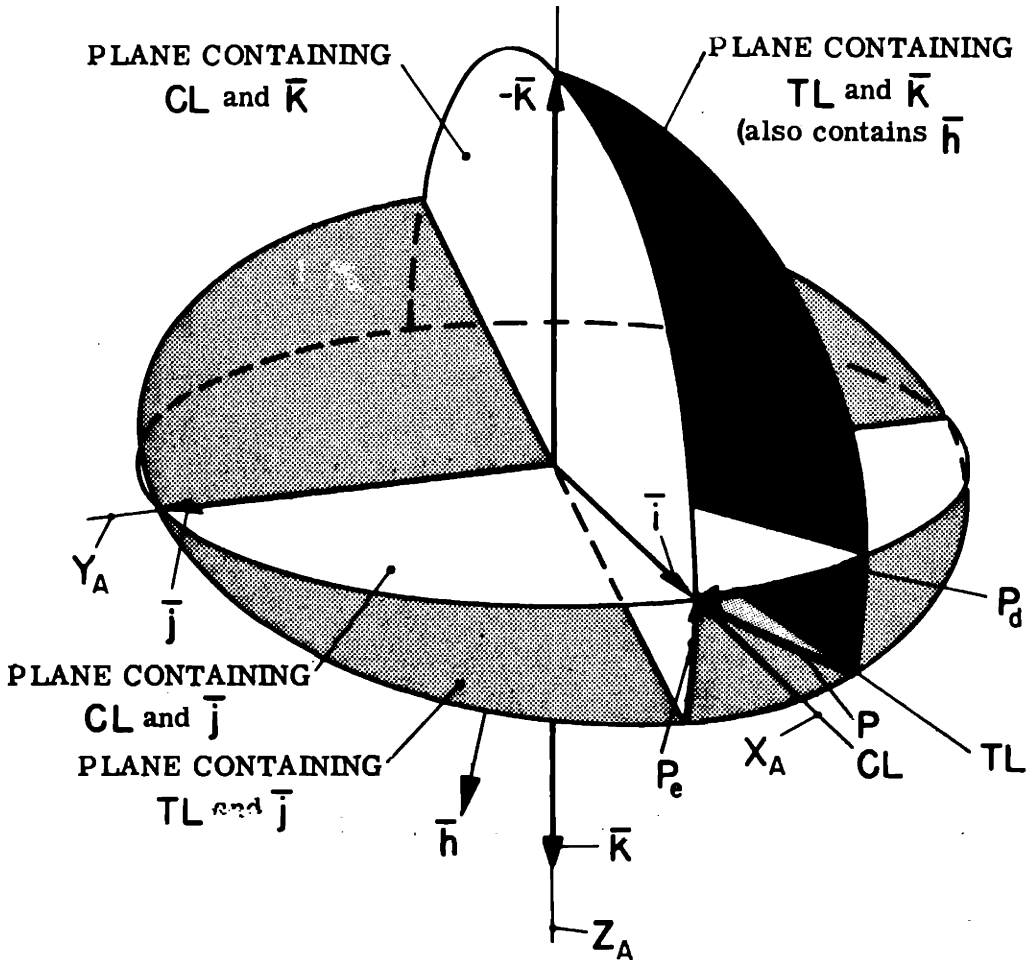

$\bar{i}$ $\bar{j}$ AND $\bar{K}$ ARE UNIT VECTORS ALONG THE RESPECTIVE AXES X_A, Y_A, AND Z_A. THE ELEVATION AND DEFLECTION AXES OF THE CLOSED-LOOP TRACKING SYSTEM ARE ALONG $\bar{j}$ AND $\bar{K}$. THE UNIT VECTOR $\bar{h}$ IS ALONG THE DEFLECTION AXIS OF THE OPEN-CHAIN TRACKING SYSTEM

Fig. D-6.–Prediction angle components for closed-loop tracking systems.

air mass coordinates. Furthermore, zero time is taken as the instant of fire, so that by definition of the air mass coordinates, $\bar{A} = 0$, and Eq. D-21, D-22, and D-23 can be combined to

$$\bar{T}(t_f) = \bar{R} + t_f \bar{V}_A + t_f \left[\frac{d\bar{R}}{dt} \right]_{[AM]} \qquad \text{D-24}$$

In order to express the future target position, $\bar{T}_{(t_f)}$, in component form, the aircraft velocity is written

$$\bar{V}_A = \bar{f}\, V_{Af} + \bar{g}\, V_{Ag} + \bar{h}\, V_{Ah} \qquad \text{D-25}$$

Then, for the ideal conditions of this section, the tracking line is taken along the line of sight so that

$$\bar{R} = \bar{f}R \qquad \text{D-26}$$

and

$$\bar{W}_{LS} = \bar{g}\, W_{(LS)g} + \bar{h}\, W_{(LS)h} \qquad \text{D-27}$$

Finally, making use of Eq. D-25, D-26, D-27 and A-10, Eq. D-24 yields

$$\begin{aligned} \bar{T}(t_f) = {} & \bar{f}\,[R_o + t_f\,(\dot{R} + V_{Af})] \\ & + \bar{g}[R\, W_{(LS)h} + V_{Ag}]\, t_f \\ & + \bar{h}\,[-RW_{(LS)g} + V_{Ah}]\, t_f \end{aligned} \qquad \text{D-28}$$

However, for a hit to be scored, the projectile must intersect the target at $\bar{T}(t_f)$ so that

$$\bar{T}\,(t_f) = \bar{V}_{p(av)}\, t_f \qquad \text{D-29}$$

The average projectile velocity is directed along the future line of sight offset from the projectile line by the trajectory curvature. The curvature is a result of side forces due to gravity, which translate the projectile normal to the projectile line by an amount $S_{(gr)}$. Consequently, for gunfire

$$\bar{T}(t_f) = \frac{V_{p(av)}}{V_{P_o}} [\bar{V}_{m(corr)} + \bar{V}_A] t_f + \bar{S}_{(gr)} \qquad \text{D-30}$$

Equation D-30 is the condition for a hit, and hence the gun muzzle must be aimed correctly, as indicated. The distance travelled by the projectile under the influence of gravity is equal to the product of the future range, $V_{p(av)}t_f$, and the curvature correction, so that in component form

$$\bar{T}(t_f) = \bar{f} \left[\frac{V_{mf(corr)} + V_{Af}}{V_{P_o}} \right] V_{p(av)} t_f$$

$$+ \bar{g} \left[\frac{V_{mg(corr)} + V_{Ag}}{V_{P_o}} + C_g \right] V_{p(av)} t_f \qquad \text{D-31}$$

$$+ \bar{h} \left[\frac{V_{mh(corr)} + V_{Ah}}{V_{P_o}} + C_h \right] V_{p(av)} t_f$$

Equations D-28 and D-31 can be equated and solutions obtained for the components of the correct muzzle velocity in the $\bar{f}$, $\bar{g}$, $\bar{h}$ directions. However, the muzzle velocity is harmonized with the controlled line; hence, once the components of the correct muzzle velocity are determined, the correct prediction angle is established. It is apparent from Fig. D-5 that

$$\tan P_{g(corr)} = - \frac{V_{mh(corr)}}{V_{mf(corr)}} \qquad \text{D-32}$$

and

$$\tan P_{h(corr)} = \frac{V_{mg(corr)}}{V_{mf(corr)}} \qquad \text{D-33}$$

Combining Eq. D-28, D-31, D-32, and D-33 leads to the following expressions for the correct prediction angle:

$$\tan P_{g(corr)} = \frac{W_{(LS)g} R - [\,1 - \frac{V_{p(av)}}{V_{P_o}}\,] V_{Ah} + V_{p(av)} C_g}{\frac{R}{t_f} + \dot{R} + [1 - \frac{V_{p(av)}}{V_{P_o}}\,] V_{Af}} \qquad \text{D-34}$$

and

$$\tan P_{h(corr)} = \frac{W_{(LS)h} R + [\,1 - \frac{V_{p(av)}}{V_{P_o}}\,] V_{Ag} + V_{p(av)} C_h}{\frac{R}{t_f} + \dot{R} + [\,1 - \frac{V_{p(av)}}{V_{P_o}}\,] V_{Af}} \qquad \text{D-35}$$

Equations D-34 and D-35 are the bases for the design of an automatic gun-laying turret[4], and might be used as performance equations for the prediction computer in an interceptor aircraft with open-chain tracking. The computer in the X5A turret requires as inputs not only the range and tracking line angular velocities, but also the range rate and the velocity of the aircraft along $\bar{f}$, $\bar{g}$, and $\bar{h}$. The time of flight, t_f, is computed by a mechanism similar to the fuze computer for antiaircraft shells.

The mechanization of the prediction computer for fixed gun interceptor aircraft with open-chain tracking can be considerably simplified by introducing the following assumptions. For small angles, the components of aircraft velocity can be readily expressed in terms of the prediction angle com-

ponents, the angle of attack, and the angle of aerodynamic yaw. From Fig. D-5 it can be seen that for small angles

$$\tan\left[\left(P_{h(corr)} - \beta\right)\right] \cong \frac{V_{Ag}}{V_{Af}} \cong P_{h(corr)} - \beta \qquad \text{D-36}$$

and

$$\tan\left[\left(P_{g(corr)} - \alpha\right)\right] \cong -\frac{V_{Ah}}{V_{Af}} \cong P_{g(corr)} - \alpha \qquad \text{D-37}$$

Furthermore, the distance travelled by the projectile during its time of flight, $V_{p(av)}t_f$, can be related to the initial range and target motion by the equation

$$V_{p(av)}t_f = \sqrt{\left[R + V_{Tf}\,t_f\right]^2 + \left[V_{Tg}\,t_f\right]^2 + \left[V_{Th}\,t_f\right]^2}$$

$$\cong R + V_{Tf}t_f \qquad \text{D-38}$$

Finally, remembering that the derivative of range, R, is taken with respect to the aircraft, and with ideal tracking

$$\dot{R} = V_{Tf} - V_{Af} \qquad \text{D-39}$$

Using the approximations of Eq. D-36, D-37, and D-38 in Eq. D-34 and D-35 gives

$$P_{g(corr)} = \frac{R}{V_{p(av)} - V_A} W_{(LS)g} + \frac{\left(\frac{V_A}{V_{P_o}}\right)V_{p(av)} - V_A}{V_{p(av)} - V_A}\alpha + \frac{V_{p(av)}}{V_{p(av)} - V_A}C_g \qquad \text{D-40}$$

$$P_{h(corr)} = \frac{R}{V_{p(av)} - V_A} W_{(LS)h} + \frac{\left(\frac{V_A}{V_{P_o}}\right)V_{p(av)} - V_A}{V_{p(av)} - V_A}\beta + \frac{V_{p(av)}}{V_{p(av)} - V_A}C_h \qquad \text{D-41}$$

Inasmuch as small angle approximations were used in deriving Eq. D-40 and D-41, it is assumed that the tangents of the prediction angle components occurring in Eq. D-34 and D-35 are equal to their respective angles. A comparison of Eq. D-40 and D-41 with the performance equations for the computer of a closed-loop system, Eq. D-19 and D-20, indicates their similarity. Equations D-40 and D-41 are developed exclusively for gunfire, in which case the ratio, $[V_A/V_{po}]$, becomes the jump factor of Eq. D-19 and D-20.

Assumptions were made in the derivation of the ideal performance equations for the prediction computers of both the closed-loop and the open-chain tracking systems. The effect of these assumptions on the aiming accuracy of the weapon systems is not included in this thesis.

4. The prediction Computer for Closed-Loop Tracking Systems.

In a closed-loop tracking system, the gyro elements detect the angular velocity of the aircraft about the computer input axes. However, the fundamental rate input is the line of sight angular velocity, which is indicated by the direction of the tracking line. Reference to Fig. C-1 shows that the angular velocity of the controlled line and the angular velocity of the tracking line are related by the expression

$$\overline{W}_{CL} = \overline{W}_{TL} + \left(\frac{d\overline{P}_R}{dt}\right)_I \qquad \text{D-42}$$

or, in component form,

$$W_{(CL)e} = W_{(TL)e} + \left(\frac{dP_{Re}}{dt}\right)_I \qquad \text{D-43}$$

and

$$W_{(CL)d} = W_{(TL)d} + \left(\frac{dP_{Rd}}{dt}\right)_I \qquad \text{D-44}$$

In this analysis, the angular components of the prediction angle are treated as vectors. Since appreciable errors are introduced for large angles, additional terms developed by Wrigley[7] must be included when these angles are both greater than 15 degrees.

In addition to the controlled line angular velocity inputs, the prediction computer must have indications of the angle of attack, the angle of yaw, and the projection of gravity along the elevation and deflection axes. Also, the prediction computer must compensate for the rates of change of the prediction angle found in Eq. D-43 and D-44.

The actual computation can result from a summation of torques on a shaft, the summation of voltages, or the summation of currents. A mechanical torque summing computer is described in this appendix for ready comparison with the description of the A-1 Sight in reference 14. However, future computers may incorporate electronic computing.

The computer includes gyro elements, elastic restraint generators, viscous dampers, and torque generators. The torque generators apply moments proportional to the angle of attack, angle of yaw, elevation cross-roll correction, and curvature correction. Equating these moments about the elevation computer shaft gives

$$C_{ce}\dot{A}_{ce} + Kce\ Ace = HW_{(CL)e} + M_{(tg)\alpha} + M_{(tg)(cr)e} + M_{(tg)}C_e \qquad D\text{-}45$$

A signal generator provides a modulated voltage, $V_{(Pc)e}$, with amplitude proportional to the computer displacement, A_{ce}. This voltage is used as the input to the radar antenna servo, which drives the tracking line a comparable amount. Neglecting dynamic lags in the radar antenna servo (these lags are not neglected in the planar analysis described in Chapters I to V):

$$P_{Re} = S_{(RAS)} V_{PC_e} = S_{(sg)(A,V)} S_{(RAS)} A_{Ce} \qquad \text{D-46}$$

making

$$\left(\frac{C_{ce}}{k_{ce}}\right)\left(\dot{P}_{Re}\right)_A + P_{Re} = \left[\frac{H}{k_{ce}} S_{(sg)(A,V)} S_{(RAS)}\right]\left[W_{(CL)e}\right.$$

$$\left. + \frac{M_{(tg)\alpha}}{H} + \frac{M_{(tg)(cr)e}}{H} + \frac{M_{(tg)C_e}}{H}\right] \qquad \text{D-47}$$

Equation D-47 shows that in steady-state conditions, the amount of prediction is proportional to the product of the angular velocity input and a term involving the gyro angular momentum, H; the signal generator sensitivity, $S_{(sg)(A,V)}$; the radar antenna servo sensitivity, S_{RAS}; and the stiffness of the computer elastic restraint generator, k_{ce}. This term is called the elevation angular velocity — prediction angle sensitivity, $S_{p(W,P)e}$ so that

$$S_{p(W,P)e} = \frac{H}{k_{ce}} S_{(sg)(A,V)} S_{RAS} \qquad \text{D-48}$$

Angle of attack can be measured either directly with a vane or Prandtl tube, or indirectly by taking into account normal acceleration and dynamic pressure[10]. In order to obtain the angle of attack input for the prediction computer, the output of the instrument must be transmitted to the angle-of-attack torque generator, thus providing a torque on the computer shaft, $M_{(tg)\alpha}$. The change in prediction angle for a given change in angle of attack is called the angle of attack - prediction angle sensitivity, $S_{p(\alpha,P)}$, which is related to the angle-of-attack torque generator output in the form

$$\frac{M_{(tg)\alpha}}{H} = \frac{S_{p(\alpha, P)}}{S_{p(W,P)e}} \alpha \qquad \text{D-49}$$

Finally, the rate of change of the radar prediction angle in Eq. D-47 is with respect to the airplane, whereas in Eq. D-43 its derivative is with respect to inertial space. In order to express both derivatives on a common basis, use is made of Eq. A-10, giving

$$\left[\frac{d\bar{P}_R}{dt}\right]_I = \left[\frac{d\bar{P}_R}{dt}\right]_A + \bar{W}_{EA} \times \bar{P}_R \qquad \text{D-50}$$

Expanding Eq. D-50 and equating components yields

$$\left[\frac{dP_{Re}}{dt}\right]_I = \left[\frac{dP_{Re}}{dt}\right]_A - P_{Rd}W_{(EA)}X_A \qquad \text{D-51}$$

and

$$\left[\frac{dP_{Rd}}{dt}\right]_I = \left[\frac{dP_{Rd}}{dt}\right]_A + P_{Re}W_{(EA)}X_A \qquad \text{D-52}$$

Substituting Eqs. D-43, D-48, D-49, and D-51 into Eq. D-47 leads to the expression

$$S_{p(W,P)e}(SN)_e[\dot{P}_{Re}]_I + P_{Re} = S_{p(W,P)e}W_{(TL)e} + S_{p(\alpha,P)}\alpha + S_{p(W,P)e}\left[\frac{M_{(tg)(cr)e}}{H} - (1 + (SN)_e)P_{Rd}W_{(EA)}X_A\right] + S_{p(W,P)e}\frac{M_{(tg)}C_e}{H} \qquad \text{D-53}$$

The term $(SN)_e$ contained in Eq. D-53 is the elevation stability number. The sense of the stability number determines the direction in which the tracking line moves with respect to inertial space. When the stability number is positive, positive motion of the aircraft about the pitch axis induces a downward motion of the tracking line with respect to the aircraft, but an upward displacement of the tracking line in inertial space coordinates, thus permitting a stable weapon system. When the stability number is negative, positive pitching forces the tracking line down with respect to the aircraft,

also with respect to inertial space; consequently, a stable system is impossible. The stability number is related to the prediction computer coefficients in the form

$$(SN)_e = \frac{C_{ce}}{S_{(sg)(A,V)} S_{RAS} \bar{H}} - 1 \qquad \text{D-54}$$

Equation D-53 is the performance equation for the elevation prediction computer, wheras Eq. D-19 gives an expression for correct, or ideal, performance. Correct settings for the prediction computer can be obtained by equating similar terms in Eq. D-19 and D-53, yielding

$$S_{p(W,P)e(corr)} = \frac{R}{V_{p(av)} - V_A} (PSR)_e \qquad \text{D-55}$$

$$S_{p(\alpha,P)(corr)} = \frac{(JF)V_{p(av)} - V_A}{V_{p(av)} - V_A} \qquad \text{D-56}$$

$$\left(\frac{M_{(tg)} C_e}{\bar{H}} \right)_{(corr)} = \left[\frac{V_{p(av)}}{V_{p(av)} - V_A} \right] \frac{C_e}{S_{p(W,P)e}} \qquad \text{D-57}$$

and

$$\left(\frac{M_{(tg)(cr)e}}{\bar{H}} \right)_{(corr)} = [1 + (SN)_e] P_{Rd} W_{(EA)} X_A \qquad \text{D-58}$$

The correct prediction sensitivity, $S_{p(W,P)e(corr)}$, is set equal to the product of $\left[\frac{R}{V_{p(av)} - V_A} \right]$ and the elevation prediction sensitivity ratio, $(PSR)_e$. This ratio provides a compensation for the dynamic error caused by the rate of change of prediction angle, and for the fact that the tracking is never ideal. Simulator studies indicate that a constant value for 1.1 for $(PSR)_e$ gives satisfactory results.

An analysis of the deflection prediction computer shows that

$$S_{p(W,P)d}(SN)_d[\dot{P}_{Rd}]_I + P_{Rd} = S_{p(W,P)d}\, W_{(TL)d} + S_{p(\beta,P)}\,\beta$$

$$+ S_{p(W,P)d}\left[\frac{M_{(tg)(cr)d}}{H} + (1 + (SN)_d)P_{Re}W_{(EA)}X_A\right]$$

$$+ S_{p(W,P)d}\,\frac{M_{(tg)}C_d}{H} \qquad \text{D-59}$$

and that the ideal computer characteristics are

$$S_{p(W,P)d(corr)} = \frac{R}{V_{p(av)} - V_A}\,(PSR)_d \qquad \text{D-60}$$

$$S_{p(\beta\ ,P)(corr)} = \frac{(JF)\,V_{p(av)} - V_A}{V_{p(av)} - V_A} \qquad \text{D-61}$$

$$\left(\frac{M_{(tg)}C_d}{H}\right)_{(corr)} = \left[\frac{V_{p(av)}}{V_{p(av)} - V_A}\right]\frac{C_d}{S_{p(W,P)d}} \qquad \text{D-62}$$

and

$$\left(\frac{M_{(tg)(cr)d}}{H}\right)_{(corr)} = -\left[1 + (SN)_d\right]P_{Re}\,W_{(EA)}X_A \qquad \text{D-63}$$

5. The Prediction Computer for Open-Chain Tracking Systems.

A comparison of the expressions for the correct prediction angle components for open-chain tracking systems, Eq. D-40 and D-41, with those for closed-loop systems, Eq. D-19 and D-20, shows that with a change in coordinates the expressions are identical. Consequently, the prediction computer used in a closed-loop system can also be used in an open-chain system, with a minor modification. The modification arises from the fact that the gyro sensing elements are carried on the radar antenna and, consequently,

measure the angular velocity of the tracking line directly. For this reason, the viscous damping and the cross-roll correction are less in an open-chain system than in a closed loop but, for comparable accuracy, cannot be omitted.

The output from the prediction computer is a voltage signal, V_{PC}, which in an open-chain system is compared with the voltage, V_{PR}, from a signal generator on the radar antenna that indicates the angular displacement of the tracking line. This comparison results in a correction voltage, (C)V, which is transmitted to the aircraft controls. The correction voltage is defined in this thesis (ref. Figs. I-1 and II-1) as the sum of the two signals, so that

$$(C)V = V_{PC} + V_{PR}$$

$$= V_{PC} + S_{(sg)(P,V)}P_R \qquad \text{D-64}$$

Ideally, the correction voltage is zero, so that

$$P_{R(ideal)} = \left[- \frac{1}{S_{(sg)(P,V)}} \right] V_{PC} \qquad \text{D-64a}$$

In this thesis, the sensitivity of the signal generator on the radar antenna carries a negative sign, so that the bracketed term in Eq. D-64a is positive. As a result, a positive voltage from the prediction computer leads to a positive radar prediction angle.

An analysis similar to Section 4, but for the prediction computer in an open-chain tracking system, shows that, with (C)V = 0,

$$S_{p(W,P)g}(SN)_g[\dot{P}_{Rg}]_I + P_{Rg} = S_{p(W,P)g}W_{(TL)g} + S_{p(\alpha,P)}\alpha + S_{p(W,P)g}\frac{M_{(tg)}C_g}{H} \qquad \text{D-65}$$

and

$$S_{p(W,P)h}(SN)_h[\dot{P}_{Rh}]_I + P_{Rh} = S_{p(W,P)h}W_{(TL)h} + S_{p(\beta,P)}\beta + S_{p(W,P)h}\frac{M_{(tg)}C_h}{H} \qquad \text{D-66}$$

where

$$(SN)_g = \frac{C_{cg}}{H}\frac{|S_{(sg)(P,V)g}|}{S_{(sg)(A,V)g}} \qquad \text{D-67}$$

and

$$(SN)_h = \frac{C_{ch}}{H}\frac{|S_{(sg)(P,V)h}|}{S_{(sg)(A,V)h}} \qquad \text{D-68}$$

provided

$$\frac{M_{(tg)(cr)g}}{H} = (SN)_g P_{Rh} W_{(EA)f} \qquad \text{D-69}$$

and

$$\frac{M_{(tg)(cr)h}}{H} = -(SN)_h P_{Rg} W_{(EA)f} \qquad \text{D-70}$$

A comparison of Eq. D-40 and D-41 with Eq. D-65 and D-66 reveals that the correct expressions for the prediction sensitivities and torque generator outputs are

$$S_{p(W,P)g(corr)} = \frac{R}{V_{p(av)} - V_A}(PSR)_g \qquad \text{D-71}$$

$$S_{p(W,P)h(corr)} = \frac{R}{V_{p(av)} - V_A}(PSR)_h \qquad \text{D-72}$$

$$S_{p(\alpha,P)(corr)} = S_{p(\beta,P)(corr)} = \frac{(JF)V_{p(av)} - V_A}{V_{p(av)} - V_A} \qquad \text{D-73}$$

$$\left[\frac{M_{(tg)cg}}{H}\right]_{(corr)} = \left[\frac{V_{p(av)}}{V_{p(av)}-V_A}\right] \frac{C_g}{S_{p(W,P)g}} \qquad \text{D-74}$$

and

$$\left[\frac{M_{(tg)}C_h}{H}\right]_{(corr)} = \left[\frac{V_{p(av)}}{V_{p(av)}-V_A}\right] \frac{C_h}{S_{p(W,P)h}} \qquad \text{D-75}$$

APPENDIX E

DETERMINATION OF THE CONTROLLED-LINE ERROR

The controlled-line inaccuracy defined in Appendix C, and shown in Fig. C-1 is composed of two parts: namely that which is predictable, called error, and that which must be treated statistically, called uncertainty. Both errors and uncertainties may arise because of imperfections in the tracking system or they may arise from external causes. In the investigation of this thesis, the errors are assumed to result entirely from the dynamics involved in tracking a target, and only the uncertainties arising from gust and radar interference are considered. The errors were determined for various approach angles and initial ranges by solving the kinematic and system performance equations on the REAC, as described in this appendix. The evaluation of gust and radar interference is discussed in Appendices H, I, and J.

The REAC shown in Fig. E-9 is an analogue computer manufactured by the Reeves Instrument Co. and described in the Maintenance Instructions[8]. The equipment available for this thesis was purchased by the USAF for use in the Instrumentation Laboratory at M.I.T. The components employed in this analysis were:

Servo Power Supply Unit	PS101
Servo Chassis	S101
Auxiliary Cabinet	S-101
Computer Chassis	C101

Power Unit	P101
Input-Output Function Generator	FG101
Multi Channel Recorder	R102

In the computer chassis there are:

a. 7 integrators numbered 1, 3, 5, 7, 9, 11, and 13 each with 3 gains of 1, 2 gains of 4, and 2 gains of 10.

b. 7 amplifiers numbered 14, 15, 16, 17, 18, 19, and 20 each with 3 gains of 1, 2 gains of 4, and 2 gains of 10.

c. 6 amplifiers numbered 2, 4, 6, 8, 10, and 12 with 3 gains of 1.

d. 24 coefficient potentiometers.

e. 6 initial condition potentiometers for six integrators.

The servo chassis contains 4 servos. Servo # 1 has 1 multiplying potentiometer and three resolvers, servo #4 has 3 multiplying potentiometers, 1 resolver, and 1 non-linear potentiometer, and servos #2 and #3 each have 3 multiplying potentiometers and 2 resolvers.

The auxiliary cabinet contains limiters, relays, passive networks, modulators, and demodulators.

Figures E-1 through E-7 are functional diagrams for the target-aircraft kinematics and the tracking system investigated in this thesis.

In these diagrams solid arrows designate electrical connections, and dashed lines are shaft connections. The quantity represented electrically or mechanically is written symbolically above the arrow or line and the scale factor is written below.

1. Target-Aircraft Kinematics.

The cabling of Fig. E-1 was used to solve the target-aircraft kinematics for all solutions except those involving the "Open-Chain Tracking System with

Tracking Inaccuracy Prediction, Tight-Loop Stabilization of the Radar Antenna, and Integration in the Signal Modifier." The kinematic section was changed for these solutions in order to economize on components, as shown in Fig. E-4.

The target-aircraft kinematics account for the motion of the target relative to the interceptor aircraft, and generate as outputs the direction of the line of sight, LS, the range expressed in R/V_A units, and the controlled line error, (E)CL. The inputs are the elevation of the target flight path, E_{V_T}, the direction of the controlled line, CL, and the angle of attack of the aircraft, α.

Equation D-1 is a general expression for the angular velocity of the line of sight, W_{LS}. It has previously been stated that the tracking line error analyzed in this thesis results from target-aircraft motion in a vertical plane. With this simplification, Eq. D-1 leads to the following expression for the line of sight direction,

$$LS = \int W_{LS} dt$$

$$= (LS)_0 + \int_0^t \frac{\left(\frac{V_T}{V_A}\right) \sin A_T - \sin [CL - \alpha - LS]}{\frac{R}{V_A}} dt \qquad E\text{-}1$$

where

$$A_T = E_{V_T} - LS \qquad E\text{-}2$$

The rate of change of range depends upon the aircraft and target velocities projected along the line of sight, as shown in Fig. D-1. The integral of this rate is the target range which, for the restriction of planar motion, may be written

$$\frac{R}{V_A} = \left(\frac{R}{V_A}\right)_0 + \int_0^t \left\{\frac{V_T}{V_A} \cos A_T - \cos [CL - \alpha - LS]\right\} dt \qquad E\text{-}3$$

The controlled-line error equals the controlled line inaccuracy for the assumed conditions of zero uncertainty in this section. Hence from Eq. C-3,

$$\begin{aligned}(E)CL &= P - P_{(corr)} \\ &= CL - LS - P_{(corr)}\end{aligned} \qquad \text{E-4}$$

and using Eq. C-9, D-6, and D-13

$$(E)CL = CL - LS - (JF)\alpha - \frac{V_T}{V_{p(av)}} \sin A_T \qquad \text{E-5}$$

As solved by the REAC, Eq. E-5 was in the form

$$(E)CL = [CL - \alpha - LS] + [1 - (JF)]\alpha - \frac{V_T}{V_{p(av)}} \sin A_T \qquad \text{E-6}$$

It should be noted that the trajectory curvature is omitted in Eq. E-6. Although the curvature correction is an important quantity in gunfire and rocketfire, it need not effect the dynamic performance of automatic tracking systems, and hence is neglected in this analysis.

Figure E-1 shows the REAC interconnections required to solve Eq. E-1, E-2, E-3, and E-6. The initial heading conditions are summarized in Fig. E-8. Initial target angles of 30, 90, and 150 degrees were used in all cases. The controlled line was initially along the line of sight and the initial angle of attack was zero. The solutions presented in this thesis were confined to initial ranges of 20 and 40 seconds although a few solutions were obtained for 60 seconds.

The controlled-line error, range, and the sine of the target angle were recorded continuously along with the angle of attack. The results are shown in Chapters I, II, III, IV, and V, for the five different tracking systems.

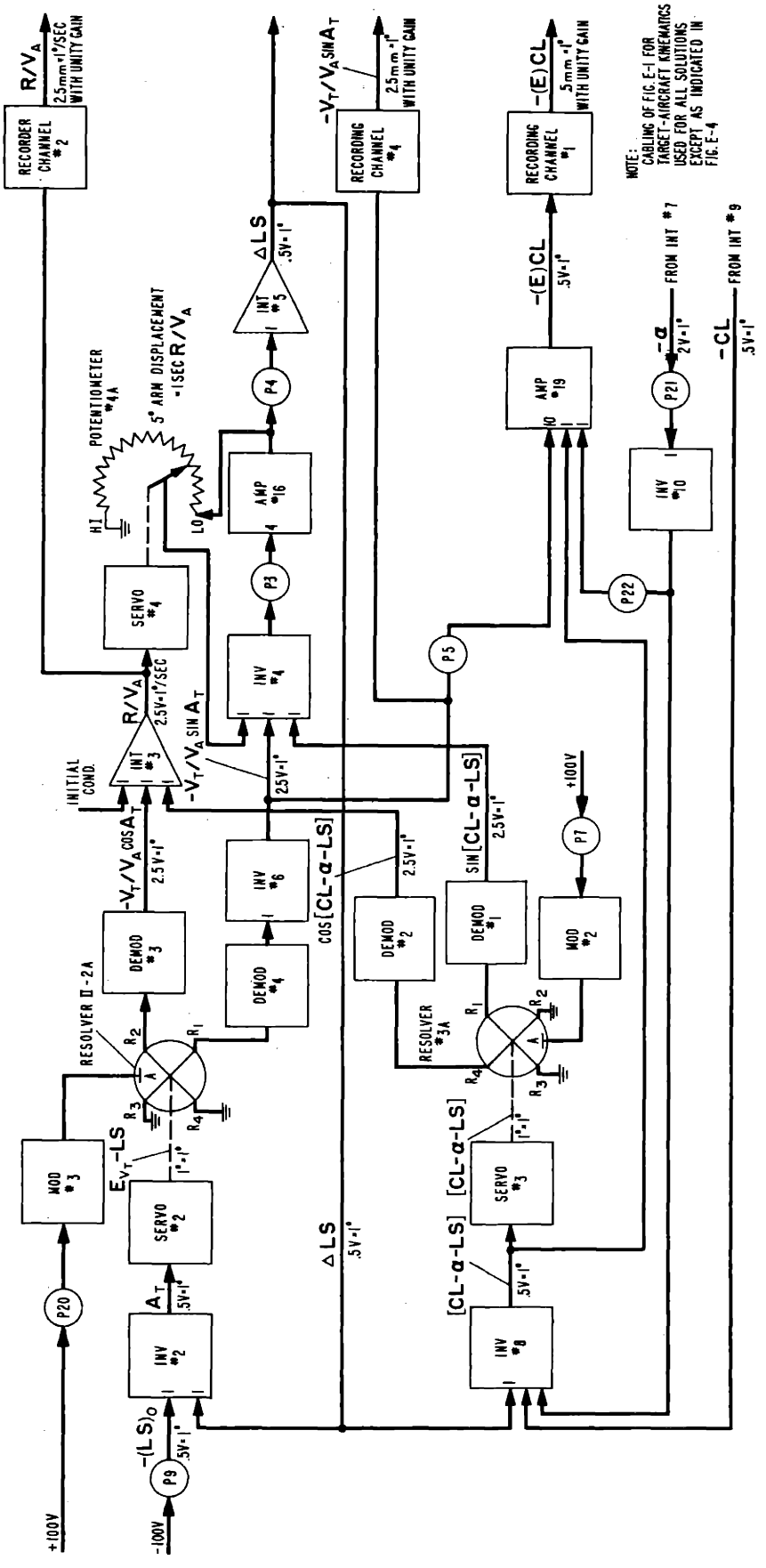

Fig. E-1.–Reac functional diagram for target-aircraft kinematics.

2. Open-Chain Tracking System with Tracking Line Prediction.

The prediction computer output is a voltage signal which is matched against the output from a signal generator indicating the displacement of the radar tracking line. Performance Eq. D-65 assumes that the aircraft flies in such a manner that the correction voltage is zero. In general, the correction voltage is not zero, so that from Eq. D-64

$$\frac{(C)V}{S_{(sg)(P,V)}} = P_R + S_{(sg)(V,P)}V_{PC} \qquad E\text{-}7$$

and Eq. D-65 becomes

$$S_{p(W,P)}(SN)[-S_{(sg)(V,P)}]\dot{V}_{PC} + [-S_{(sg)(V,P)}]V_{PC} = S_{p(W,P)}W_{TL} + S_{p(\alpha,P)}\alpha \qquad E\text{-}8$$

The input for the curvature correction has been omitted, as previously noted. Furthermore, the subscript g has been dropped inasmuch as all computing is about the g-axis in the planar problem, and there is no danger of ambiguity.

Setting the prediction sensitivity, $S_{p(W,P)}$ equal to the correct value of Eq. D-71, and making use of Eq. D-42

$$S_{(sg)(V,P)}V_{PC} = \frac{P_R - CL}{SN} - \left[\frac{V_{p(av)}}{V_A} - 1\right]\frac{1}{(SN)(PSR)}\int \frac{S_{(sg)(V,P)}V_{PC} + S_{p(\alpha,P)}\alpha}{\frac{R}{V_A}}dt \qquad E\text{-}9$$

In this analysis the average projectile velocity, $V_{p(av)}$ is assumed to be constant.

The self-tracking radar responds to motions of the line of sight and the controlled line. Reference to Fig. I-1 shows that when lags in the tracking inaccuracy detector and in the radar antenna drive are neglected

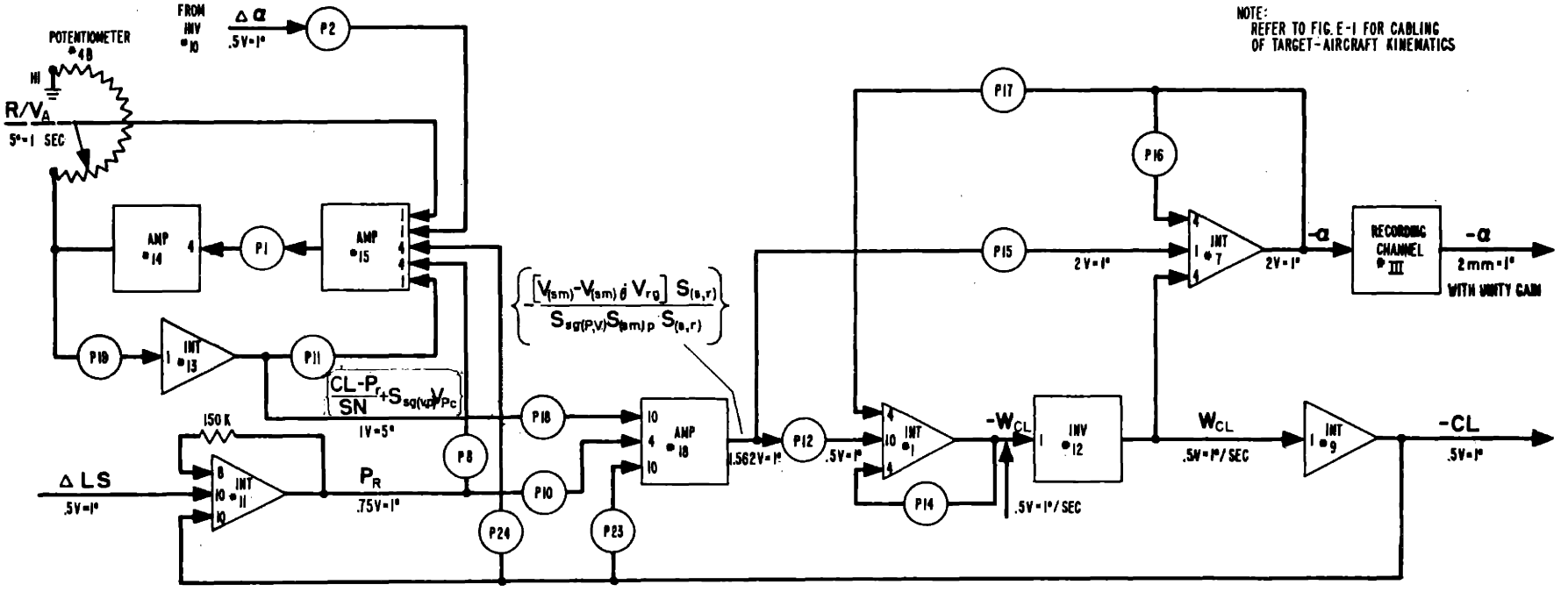

Fig. E–2.–Reac functional diagram for open-chain tracking system with tracking line prediction.

$$\dot{P}_R = S_{R(V,\dot{P})} V_{TID}$$

$$= S_{TID} S_{R(V,\dot{P})} [LS + P_R - CL] \qquad \text{E-10}$$

or

$$(CT)_R \dot{P}_R + P_R = CL - LS \qquad \text{E-11}$$

where

$$(CT)_R = \frac{-1}{S_{TID} S_{R(V,\dot{P})}} \qquad \text{E-12}$$

The sum of the radar prediction angle of Eq. E-11 and the prediction computer output of Eq. E-9 provides the correction voltage of Eq. E-7. This voltage is transmitted to the signal modifier along with a voltage signal from a pitch rate gyro. The output from the signal modifier energizes the elevator servo which when displaced actuates the elevator through the control rigging. Lags[9] in the servo and rigging are omitted, or

$$\delta = S_{(s,r)} V_{(sm)} \qquad \text{E-12A}$$

The sensitivity of the servo and rigging $S_{(s,r)}$ is not the simple product of the two individual sensitivities because of the effect of the elevator hinge moment on the elevator servo and rigging.

It is convenient to expand Eq. E-12A in the form

$$\delta = S_{(s,r)} [V_{(sm)} - S_{(sm)} \dot{\theta} \; V_{rg}] + S_{rg} S_{(sm)} \dot{\theta} S_{(s,r)} W_{CL} \qquad \text{E-12B}$$

It should be remembered that in this analysis the rate of change of pitch angle, $\dot{\theta}_A$ equals the angular velocity of the controlled line as shown by Eq. B-1. In Eq. E-12B, the sum of the terms within the braces represents the signal modifier output resulting from the correction voltage input. The term involving W_{CL} provides the tracking system with damping in addition

to the aerodynamic damping of the aircraft.

The response of the aircraft to an applied elevator displacement can be found by solving Eq. B-8 and B-9. The velocity, W, in these equations equals the product of the forward aircraft velocity and the angle of attack, or

$$W = V_A \alpha = \mu_o \alpha \qquad \text{E-12C}$$

Substitution of Eq. E-12B and E-12C into B-8 and B-9 gives for zero gust interference [$w_G = o$]

$$W_{CL} = \int \Big\{ \alpha [M_w + M_{\dot{w}} Z_w] V_A + W_{CL} [M_{\dot{\theta}} + V_A M_{\dot{w}} + S_{rg} S_{(sm)\dot{\theta}} S_{(s,r)} M_\delta] + [V_{sm} - S_{(sm)\dot{\theta}} V_{rg}] S_{(s,r)} M_\delta \Big\} dt \qquad \text{E-12D}$$

and

$$\alpha = \int \Big\{ \alpha Z_w + W_{CL} + [V_{(sm)} - S_{(sm)\dot{\theta}} V_{rg}] S_{(s,r)} \frac{Z_\delta}{V_A} \Big\} dt \qquad \text{E-13}$$

The term $S_{rg} S_{(sm)\dot{\theta}} S_{(s,r)} \dfrac{Z_\delta}{V_A} W_{CL}$ is omitted in Eq. E-13, since it is negligibly small.

The output from the signal modifier when the pitch rate gyro signal is zero is proportional to the correction voltage, so that utilizing Eq. E-7

$$[V_{(sm)} - V_{(sm)\dot{\theta}} V_{rg}] S_{(s,r)} = [S_{(sg)(P,V)} S_{(sm)p} S_{(s,r)}][P_R + S_{(sg)(P,V)} V_{PC}] \qquad \text{E-14}$$

Equations E-9, E-11, E-12D, E-13, and E-14 represent the performance of the open-chain tracking system with tracking line prediction as investigated. The REAC interconnections are shown in Fig. E-2. The potentiometer sensitivities are related to the system parameters in the following manner:

$$S_{P1} = .500 + C_4$$

$$S_{P2} = .20\, S_{P(\alpha,P)} + C_1$$

$$S_{P3} = .500 + C_4$$

$$S_{P4} = \frac{180}{\pi} \times \frac{1}{400} + C_1$$

$$S_{P5} = \frac{180}{\pi} \left(\frac{V_T}{V_{p(av)}} \right) \frac{1}{25} + C_{10}$$

P_6 not used

$$S_{P7} = .025 + C_1$$

$$S_{P8} = \frac{.025}{.750} \left(\frac{1}{SN} \right) + C_4$$

$$S_{P9} = \frac{A_{To}}{200} + C_1$$

$$S_{P10} = .350 + C_4$$

$$S_{P11} = .640 + C_1$$

$$S_{P12} = -\frac{.500}{1.563} \left[\frac{M_\delta}{10} \right] \left(\frac{1 + SN}{SN} \right) S_{(sg)(P,V)} S_{(sm)p} S_{(s,r)} + C_{10}$$

P_{13} not used

$$S_{P14} = -\left[M_{\dot{\theta}} + V_A M_{\dot{w}} + S_{rg} S_{(sm)\dot{\theta}} S_{(s,r)} M_\delta \right] \frac{1}{4} + C_4$$

$$S_{P15} = -\frac{2.00}{1.563} \frac{Z_\delta}{V_A} \left(\frac{1 + SN}{SN} \right) S_{(sg)\,(P,V)} S_{(sm)p} S_{(s,r)} + C_1$$

$$S_{P16} = -Z_w/4 + C_4$$

$$S_{P17} = -V_A [M_w + Z_w M_{\dot{w}}]/16 + C_4$$

$$S_{P18} = \frac{SN}{1 + SN} + C_{10}$$

$$S_{P19} = \frac{1.563}{200} \left[\frac{V_{p(av)}}{V_A} - 1 \right]_{(SN)(PSR)} \frac{2.5}{} + C_1$$

$$S_{P20} = .025\left(\frac{V_T}{V_A}\right) + C_1$$

$$S_{P21} = .250 + C_1$$

$$S_{P22} = 1 - (JF) + C_1$$

All sensitivities must be positive and less than unity. The corrections C_1, C_4, and C_{10} account for the impedance match between the potentiometer and the electronic unit to which it is connected. The corrections vary with the potentiometer setting, and are relatively small and can be readily determined from a prepared chart.

3. Open-Chain Tracking System with Tracking Inaccuracy Prediction and Tight-Loop Stabilization of the Radar Antenna.

In this system integrating rate gyros are mounted on the radar antenna with input axes normal to the tracking line along g and h. The output from the elevation gyro is the input for the elevation channel of the radar antenna drive. Neglecting inertia and electronic lags in the drive, the tracking line rotates at a rate proportional to the gyro voltage, so that

$$\dot{P}_R = S_{R(V,\dot{P})} V_g \qquad \text{E-15}$$

The integrating rate gyro consists of a gyro element mounted in a gimbal frame which can rotate through small angles about an axis normal to the gyro angular momentum vector. The gyro element is sealed in a cylindrical case fastened to the gimbal frame. In this manner the case of the gyro can be filled with liquid which unloads the gimbal frame pivots, and also provides a restraining moment proportional to rate of rotation of the gimbal. A signal generator converts the gimbal frame displacement into the voltage, V_g. The inputs to the gyro are the gyro moment resulting from an angular velocity about the input axis, and a moment from a torque generator proportional

to its input current. In this system the input current is provided by the tracking inaccuracy detector, and consequently

$$\dot{V}_g = S_{g(TL,V)} W_{TL} + S_{g(i,\dot{V})}\, i_{TID} \qquad \text{E-16}$$

With a steady-state current, i_{TID}, the gyro voltage increases until the radar antenna drive rotates the tracking line at a rate such that the moments from the torque generator and the gyro element are equal and opposite. Then the gyro voltage is constant, and hence in this steady-state condition.

$$W_{TL} = -\frac{S_{g(i,\dot{V})}}{S_{g(TL,V)}}\, i_{TID} = S_{RSS(i,W)} i_{TID} \qquad \text{E-17}$$

It can be seen from Eq. E-17 that the sensitivity of the radar antenna stabilization system, $S_{RSS(i,W)}$ equals the ratio of torque generator sensitivity to gyro wheel sensitivity. Using sensitivity $S_{RSS(i,W)}$, Eq. E-17 may be written

$$S_{g(V,TL)} \dot{V}_g = W_{TL} - S_{RSS(i,W)}\, i_{TID}$$

$$= W_{TL} - S_{TID}\, S_{RSS(i,W)} [(C)TL] \qquad \text{E-18}$$

Equations E-15 and E-18 can be written in integral form as

$$S_{g(V,TL)} V_g = CL - P_R - S_{TID}\, S_{RSS(i,W)} \int [LS + P_R - CL]\, dt \qquad \text{E-19}$$

and

$$P_R = [S_{g(TL,V)} S_{R(V,\dot{P})}] \int [S_{g(V,TL)} V_g]\, dt \qquad \text{E-20}$$

The integrating rate gyro used to stabilize the radar antenna is used indirectly to provide rate signals for the prediction computer. It is shown in Eq. E-17 that for steady-state conditions the tracking line angular velocity is proportional to the current from the tracking inaccuracy detector. As a result this same current can be used as the input to a torque generator in the

prediction computer. With this torque generator replacing the gyro element in the prediction computer of the Open-Chain Tracking System with Tracking Line Prediction, Eq. E-8 shows that

$$S_{p(W,P)}(SN)[-S_{(sg)(V,P)}]\dot{V}_{PC} + [-S_{(sg)(V,P)}]V_{PC} =$$

$$S_{p(W,P)}S_{TID}S_{RSS(i,W)}[LS + P_R - CL] + S_{p(\alpha,P)}\alpha \qquad \text{E-21}$$

or in integral form

$$S_{(sg)(V,P)}V_{PC} = -\frac{S_{TID}S_{RSS(i,W)}}{SN}\int[LS + P_R - CL]\,dt$$

$$-\left[\frac{V_{p(av)}}{V_A} - 1\right]\frac{1}{(SN)(PSR)}\int\frac{S_{(sg)(V,P)}V_{PC}+S_{p(\alpha,P)}\alpha}{R/V_A}\,dt \qquad \text{E-22}$$

As in the Open-Chain Tracking System with Tracking Line Prediction,

$$\frac{(C)V}{S_{(sg)(P,V)}} = P_R + S_{(sg)(V,P)}V_{PC} \qquad \text{E-23}$$

So that with both proportional and integral control in the signal modifier

$$[V_{(sm)} - V_{(sm)\dot{\theta}}\dot{V}_{rg}]S_{(s,r)} = [S_{(sg)(P,V)}S_{(sm)p}S_{(s,r)}][P_R + S_{(sg)(P,V)}V_{PC}]$$

$$+[S_{(sg)(P,V)}S_{(sm)i}S_{(s,r)}]\int[P_R + S_{(sg)(P,V)}V_{PC}]dt \qquad \text{E-24}$$

The aircraft equations with pitch rate stabilization are the same for this tracking system as for the system with tracking line prediction. Therefore Eq. E-12D, E-13, E-19, E-20, E-22, and E-24 represent the performance

of the Open-Chain Tracking System with Tracking Inaccuracy Prediction. The REAC cabling is shown functionally in Fig. E-3 for the system with no integration in the signal modifier.

It should be noticed that amplifier #17 is converted into an integrator for these solutions. In order to include integration in the signal modifier, it is necessary to rewire the REAC as indicated in Fig. E-4. For this latter series of solutions the controlled line error was obtained by recording the quantities in Eq. E-6 separately. The summation was then carried out manually.

The potentiometer sensitivities for use with Fig. E-3, the REAC functional diagram of the system with no integration in the signal modifier, are as follows:

$$S_{P1} = .500 + C4$$

$$S_{P2} = .2\, S_{p\,(\alpha,P)} + C_1$$

$$S_{P3} = .500 + C_4$$

$$S_{P4} = .143 + C_1$$

$$S_{P5} = \frac{180}{\pi} \left(\frac{V_T}{V_{p(av)}} \right) \frac{1}{25} + C_{10}$$

$$S_{P6} = \frac{.05}{.50} S_{g(TL,V)} S_{R(V,\dot{P})} + C_4$$

$$S_{P7} = .025 + C_1$$

$$S_{P8} = .350 + C_4$$

$$S_{P9} = \frac{A_{To}}{200} + C_1$$

$$S_{P10} = .100\, S_{g(TL,V)} S_{R(V,\dot{P})} + C_{10}$$

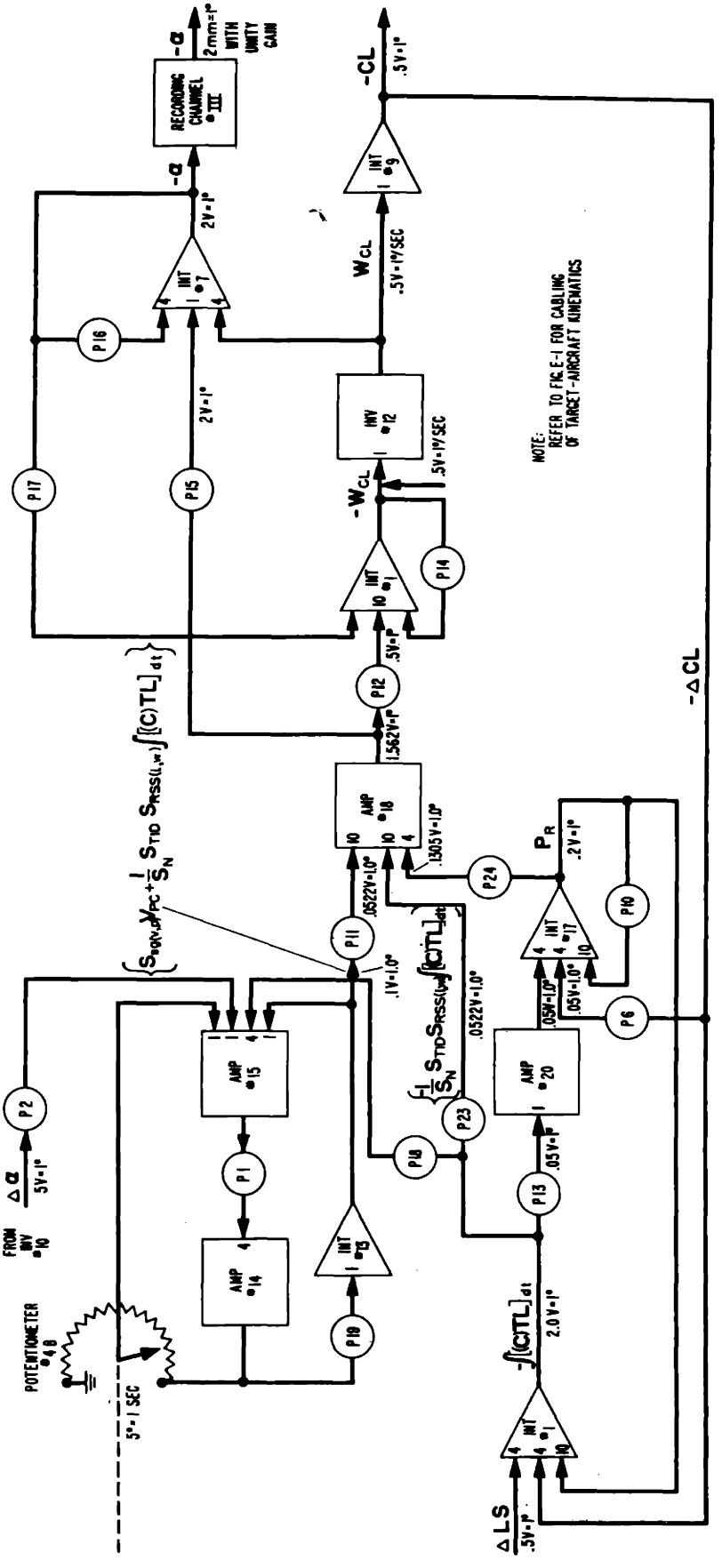

Fig. E–3.–Reac functional diagram for open-chain tracking system with tracking inaccuracy prediction and tight-loop stabilization of the radar antenna.

$$S_{P11} = .522 + C_{10}$$

$$S_{P12} = -\frac{.500}{.522}\left(\frac{M_\delta}{10}\right) S_{(sg)(P,V)} S_{(sm)p} S_{(s,r)} + C_{10}$$

$$S_{P13} = \frac{.050}{2.00}\left[S_{TID} S_{RSS(i,w)}\right]\left[S_{g(TL,V)} S_{R(V,\dot{P})}\right] + C_1$$

$$S_{P14} = -\left[M_{\dot{\theta}} + V_A M_{\dot{w}} + S_{rg} S_{(sm)\dot{\theta}} S_{(s,r)} M_\delta\right]\frac{1}{4} + C_4$$

$$S_{P15} = -\frac{2.0}{.522}\,\frac{Z_\delta}{V_A}\, S_{(sg)(P,V)} S_{(sm)p} S_{(s,r)} + C_1$$

$$S_{P16} = -\frac{Z_w}{4} + C_4$$

$$S_{P17} = -V_A\left[\frac{M_w + Z_w M_{\dot{w}}}{16}\right] + C_4$$

$$S_{P18} = \frac{.025}{2.00}\left(\frac{1}{SN}\right) S_{TID} S_{RSS(i,w)} + C_4$$

$$S_{P19} = \left(\frac{.96}{200}\right)\left[\frac{V_{p(av)}}{V_A} - 1\right]\frac{2.5}{(PSR)SN} + C_1$$

$$S_{P20} = .025\,\frac{V_T}{V_A} + C_1$$

$$S_{P21} = .250 + C_1$$

$$S_{P22} = 1 - (JF) + C_1$$

$$S_{P23} = \frac{.0522}{2.00}\left(\frac{1}{SN}\right) S_{TID} S_{RSS(i,w)} + C_{10}$$

$$S_{P24} = \frac{.1305}{.200} + C_4$$

The potentiometer sensitivities for use with Fig. E-4, the REAC functional diagram of the system with integration in the signal modifier, are as follows:

$$S_{P1} = .50 + C_4$$

$$S_{P2} = .2S_{p(\alpha,P)} + C_1$$

$$S_{P3} = \frac{.125}{.721} + C_4 \text{ with } S_{rg}S_{(sm)\dot{\theta}}S_{(s,r)} = 0$$

$$= \frac{.125}{.483} + C_4 \text{ with } S_{rg}S_{(sm)\dot{\theta}}S_{(s,r)} = 0.05$$

$$S_{P4} = .2865 + C_1$$

$$S_{P5} = \frac{.500}{.721} \times .6812 + C_1 \text{ with } S_{rg}S_{(sm)\dot{\theta}}S_{(s,r)} = 0$$

$$= \frac{.500}{.483} \times .6812 + C_1 \text{ with } S_{rg}S_{(sm)\dot{\theta}}S_{(s,r)} = 0.05$$

$$S_{P6} = \frac{.05}{.50} S_{g(TL,V)}S_{R(V,\dot{P})} + C_4$$

$$S_{P7} = \frac{.25}{.10} S_{sg(P,V)}S_{(sm)i}S_{(s,r)} + C_4$$

P8 not used

$$S_{P9} = \frac{A_{To}}{200} + C_1$$

$$S_{P10} = .100\, S_{g(TL,V)}S_{R(V,\dot{P})} + C_{10}$$

$$S_{P11} = \frac{.25}{.10} S_{sg(P,V)}S_{(sm)p}S_{(s,r)} + C_4$$

$$S_{P12} = \frac{.25}{.10} S_{sg(P,V)}S_{(sm)i}S_{(s,r)} + C_4$$

$$S_{P13} = \frac{.050}{2.00} [S_{TID}S_{RSS(i,w)}][S_{g(TL,V)}S_{R(V,\dot{P})}] + C_1$$

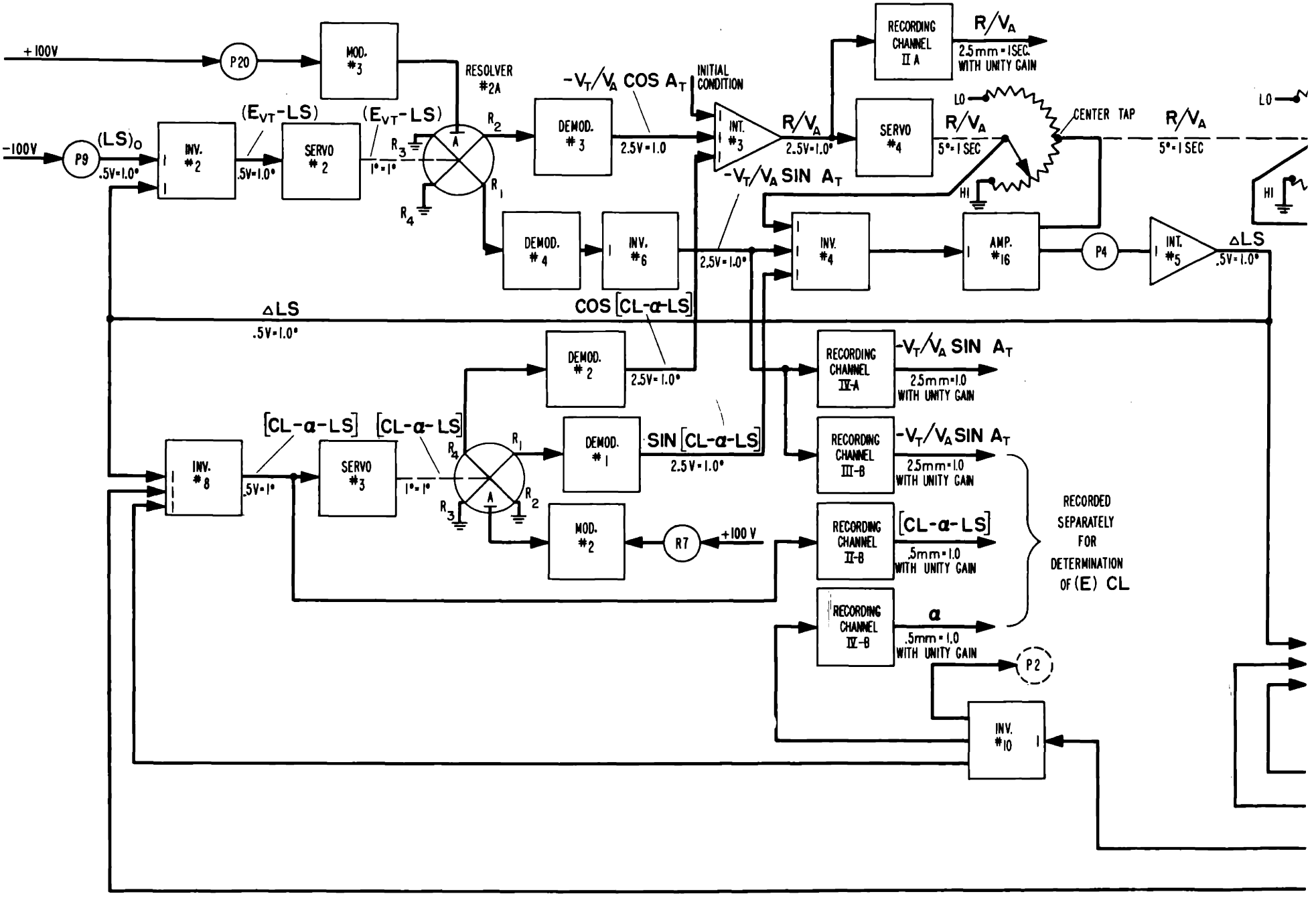

Fig. E–4.–Reac functional diagram for open-chain tracking sy
and inte

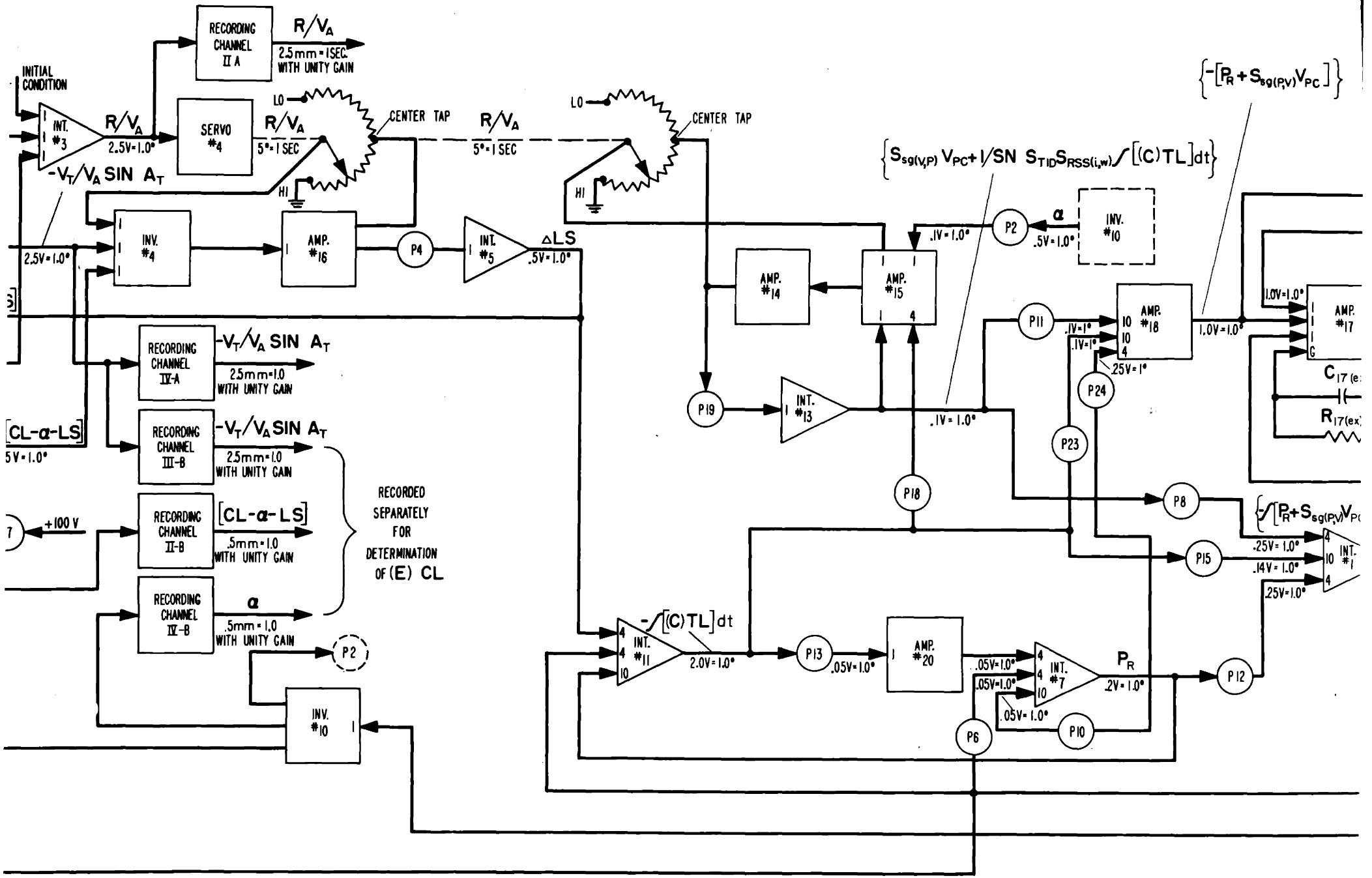

Fig. E–4.–Reac functional diagram for open-chain tracking system with tracking inaccuracy prediction, tight-loop stabilization of the radar antenna, and integration in the signal modifier.

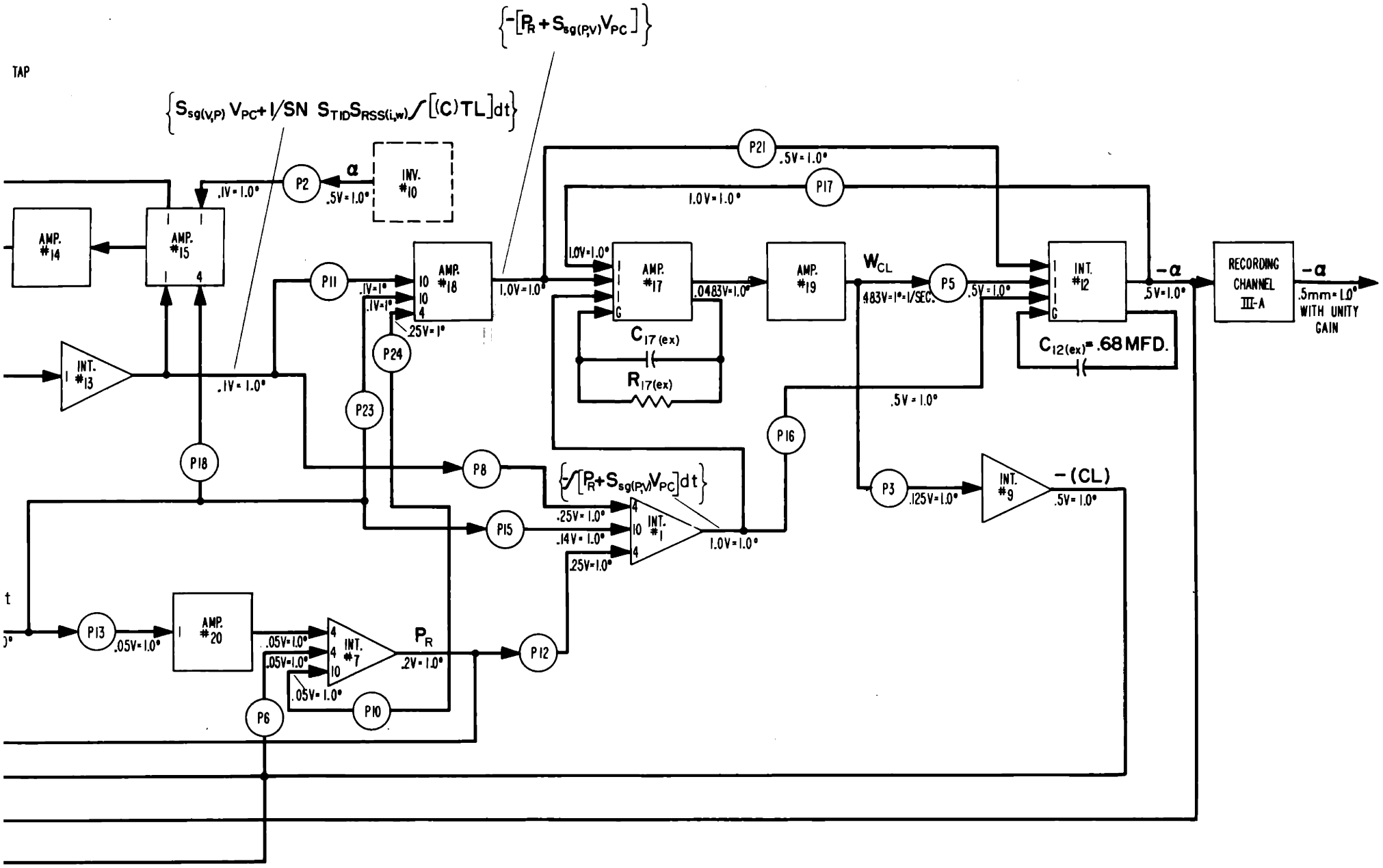

; inaccuracy prediction, tight-loop stabilization of the radar antenna,
ıal modifier.

$$S_{P14} = -\left[M_{\dot{\theta}} + V_A M_{\dot{w}} + S_{rg} S_{(sm)\dot{\theta}}\, S_{(s,r)} M_{\delta}\right] \frac{1}{4} + C_4$$

$$S_{P15} = \frac{.10}{2.0}\left(\frac{1}{SN}\right)\left[S_{TID} S_{RSS(i,w)}\right]\left[S_{sg(P,V)} S_{(sm)i} S_{(s,r)}\right] + C_{10}$$

$$S_{P16} = .0716 \times \frac{.50}{1.00} + C_1$$

$$S_{P17} = \frac{1.00}{.50} \times .3872 + C_{10}$$

$$S_{P18} = \frac{.025}{2.00}\left(\frac{1}{SN}\right) S_{TID} S_{RSS(i,W)} + C_4$$

$$S_{P19} = \frac{1}{100}\left[\frac{V_{p(av)}}{V_A} - 1\right] \frac{2.5}{(PSR)(SN)} + C_1$$

$$S_{P20} = .025\left(\frac{V_T}{V_A}\right) + C_1$$

$$S_{P21} = .0716 \times \frac{.50}{1.00} + C_1$$

$$S_{P22} = 1 - (JF) + C_1$$

$$S_{P23} = \frac{.10}{2.00}\left(\frac{1}{SN}\right)\left[S_{TID} S_{RSS[i,W]}\right] S_{(sg)(P,V)} S_{(sm)p} S_{(s,r)} + C_{10}$$

$$S_{P24} = \frac{.25}{.20}\, S_{(sg)(P,V)} S_{(sm)p} S_{(s,r)} + C_4$$

In addition

$R_{(17)ex}$ = 0 with $S_{rg} S_{(sm)\dot{\theta}}\, S_{(s,r)} = 0$

= 651,500 with $S_{rg} S_{(sm)\dot{\theta}}\, S_{(s,r)} = 0.05$

$C_{(17)ex}$ = .67 μfd with $S_{rg}\, S_{(sm)\dot{\theta}}\, S_{(s,r)} = 0$

= 1.00 μfd with $S_{rg}\, S_{(sm)\dot{\theta}}\, S_{(s,r)} = 0.05$

4. Closed-Loop Tracking System with Controlled-Line Prediction.

The prediction computer includes a gyro with the input axis fixed to the

aircraft along the elevation axis. Performance equations for this type of computer are developed in Appendix D assuming negligible lag in the radar antenna servo. In order to include the effect of dynamics in this servo, the torque summation equation of the prediction computer, Eq. D-45, is utilized. Using this equation, and Eq. D-48, D-49, D-54, and remembering that

$$V_{PC} = S_{(sg)(A,V)}A_c$$

yields

$$S_{p(W,P)}[1 + SN][S_{RAS}\dot{V}_{PC}] + [S_{RAS}V_{PC}] = S_{p(W,P)}W_{CL} + S_{p(\alpha,P)}\alpha \quad \text{E-25}$$

In order to obtain Eq. E-25, it is necessary to multiply all terms in Eq. D-45 by the sensitivity of the radar antenna servo, S_{RAS}. Replacing the prediction sensitivity $S_{p(W,P)}$ in Eq. E-25 with the correct value of Eq. D-55 and then integrating gives

$$S_{RAS}V_{PC} = \frac{CL}{1 + SN} - \left[\frac{V_{p(av)}}{V_A} - 1\right] \frac{1}{[1 + SN][PSR]} \int \frac{S_{RAS}V_{PC} - S_{p(\alpha,P)}\alpha}{R/V_A}\, dt \quad \text{E-26}$$

A complete analysis of the radar antenna servo[11] includes the inertia of the antenna, the gearing, and the drive motor. In addition, the dynamics of the electronic amplifiers must be included. However, these factors are secondary to this investigation in which only the drive motor back e.m.f. and other damping effects are considered, so that

$$(CT)_R \dot{P}_R + P_R = S_{RAS} V_{PC} \quad \text{E-27}$$

The radar antenna servo positions the tracking line with respect to the aircraft according to Eq. E-27. The tracking line is kept along the line of sight by properly aiming the aircraft. The tracking line correction is de-

tected by the radar receiver, which transmits a voltage proportional to the signal modifier.

The effect of lags in the forward actuating chain is analyzed in this tracking system by including a first-order filter in the signal modifier with characteristic time, $(CT)_{sm}$. The elevator displacement resulting from a tracking inaccuracy $[V_{sm} - S_{(sm)\dot{\theta}} V_{rg}]S_{(s,r)}$ can then be expressed as

$$(CT)_{sm} \frac{d}{dt}[V_{sm} - S_{(sm)\dot{\theta}} V_{rg}]S_{(s,r)} + [V_{sm} - S_{(sm)\dot{\theta}} V_{rg}]S_{(s,r)} =$$

$$S_{TID} S_{(sm)p} S_{(s,r)}[LS + P_R - CL] \quad \text{E-28}$$

Equations E-26, E-27, and E-28 along with E-12D and E-13 are used to represent the performance of the Closed-Loop Tracking System with Controlled-Line Prediction. The REAC is cabled to solve these equations as indicated in Fig. E-5. The potentiometer sensitivities are set as follows:

$$S_{P1} = .500 + C_4$$

$$S_{P2} = .050\, S_{p(\alpha,P)} + C_1$$

$$S_{P3} = .500 + C_4$$

$$S_{P4} = \frac{180}{\pi} \times \frac{1}{400} + C_1$$

$$S_{P5} = \frac{180}{\pi} \left(\frac{V_T}{V_{p(av)}}\right) \frac{1}{25} + C_{10}$$

P6 not used

$$S_{P7} = .025 + C_1$$

$$S_{P8} = .350 + C_4$$

$$S_{P9} = \frac{A_{To}}{200} + C_1$$

$$S_{P10} = .350 + C_4$$

P11 not used

$$S_{P12} = \frac{.500}{.532} S_{TID} S_{(sm)p} S_{(s,r)} M_{\delta} /40 + C_{10}$$

P13 not used

$$S_{P14} = - [M_{\dot{\theta}} + V_A M_{\dot{w}} + S_{rg} S_{(sm)\dot{\theta}} S_{(s,r)} M_{\delta}] \frac{1}{4} + C_4$$

$$S_{P15} = \frac{.500}{.532} S_{TID} S_{(sm)p} S_{(s,r)} Z_{\delta} / V_A + C_1$$

$$S_{P16} = - Z_w 4 + C_4$$

$$S_{P17} = - V_A [M_w + Z_w M_{\dot{w}}] \frac{1}{16} + C_4$$

$$S_{P18} = 1/[1 + SN]5 + C_1$$

$$S_{P19} = \frac{1}{100} [\frac{V_{p(av)}}{V_A} - 1] \frac{2.5}{[1 + SN][PSR]} + C_1$$

$$S_{P20} = .025 (\frac{V_T}{V_A}) + C_1$$

$$S_{P21} = .250 + C_1$$

$$S_{P22} = 1 - (JF) + C_1$$

P 23 and P 24 not used

5. Closed-Loop Tracking System with Controlled-Line Prediction and Tight-Loop Stabilization of the Aircraft.

This tracking system has a prediction computer and radar antenna servo identical with the tracking system of the previous section. However, an integrating rate gyro is used to stabilize the aircraft. The gyro is mounted with its input axis along the pitch axis of the aircraft. The gyro output voltage is

applied to the signal modifier. Any deviations of the aircraft due to rough air or other disturbances are detected by the gyro, and through the action of the signal modifier and elevator servo the elevator is displaced, thus correcting at least in part for the disturbance. The aircraft is maneuvered by applying current to the integrating gyro torque generator. The command signal in this type tracking system comes from the tracking inaccuracy detector, so that as in Eq. E-16

$$\dot{V}_g = S_{g(TL,V)} W_{CL} + S_{g(i,\dot{V})} i_{TID} \qquad \text{E-29}$$

The steady-state angular velocity of the controlled line introduced by a command signal is found from Eq. E-29, by setting $\dot{V}_g = 0$. Then

$$W_{CL} = - \frac{S_{g(i,\dot{V})}}{S_{g(TL,V)}} i_{TID}$$

$$= S_{LCS(i,W)} \, i_{TID} \qquad \text{E-30}$$

Equation E-30 defines the command current — angular velocity sensitivity of the longitudinal control system, $S_{LCS(i,W)}$. Utilizing this sensitivity in Eq. E-29,

$$S_{g(V,CL)} \dot{V}_g = W_{CL} - S_{LCS(i,W)} i_{TID}$$

$$= W_{CL} - S_{TID} S_{LCS(i,W)} [(C)TL] \qquad \text{E-31}$$

Making use of Eq. E-31, the elevator displacement resulting from changes in gyro signal can be written

$$[V_{(sm)} - S_{(sm)\dot{\theta}} \dot{V}_{rg}] S_{(s,r)} =$$

$$S_{g(CL,V)} S_{(sm)p} S_{(s,r)} \left\{ CL - S_{TID} S_{LCS(i,W)} \int [LS + P_R - CL] \, dt \right\} \qquad \text{E-32}$$

The performance of the Closed-Loop Tracking System with Controlled-Line Prediction and Tight-Loop Stabilization of the Aircraft was investigated using Eq. E-32 for the longitudinal stabilization and in addition Eq. E-12D, E-13, E-26, and E-27.

Figure E-6 is a functional diagram of the REAC interconnections for this tracking system. The potentiometer settings, different from those used when obtaining solutions for the Closed-Loop Tracking System with Controlled-Line Prediction, are

$$S_{P12} = - S_{g(CL,V)} S_{(sm)p} S_{(s,r)} M_{\delta} / 40 + C_{10}$$

$$S_{P13} = (2/7) S_{TID} S_{LCS(i,W)} + C_{10}$$

$$S_{P15} = - S_{g(CL,V)} S_{(sm)p} S_{(s,r)} Z_{\delta} / V_A + C_1$$

6. Closed-Loop Tracking System with Tracking Inaccuracy Prediction and and Tight-Loop Stabilization of the Aircraft.

There is considerable advantage in using the command current of the previous section as the pitch rate signal for the prediction computer. Not only are two gyros eliminated but even more important, the prediction computer receives the pitch rate signal in advance, thereby shortening the system solution time. The prediction computer performance equation for this tracking system is obtained simply by substituting Eq. E-30 into Eq. E-25. Then

$$S_{p(W,P)}[1 + SN] [S_{RAS} \dot{V}_{PC}] + [S_{RAS} V_{PC}] =$$

$$S_{p(W,P)} S_{TID} S_{LCS(i,W)} [(C)TL] + S_{p(\alpha,P)} \alpha \qquad \text{E-33}$$

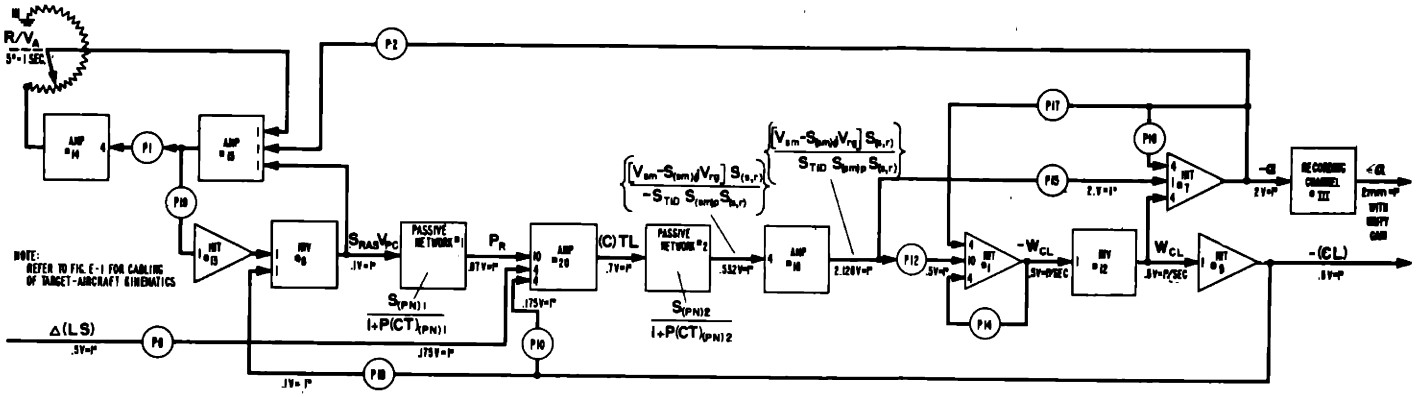

Fig. E–5.–Reac functional diagram for closed-loop tracking system with controlled-line prediction.

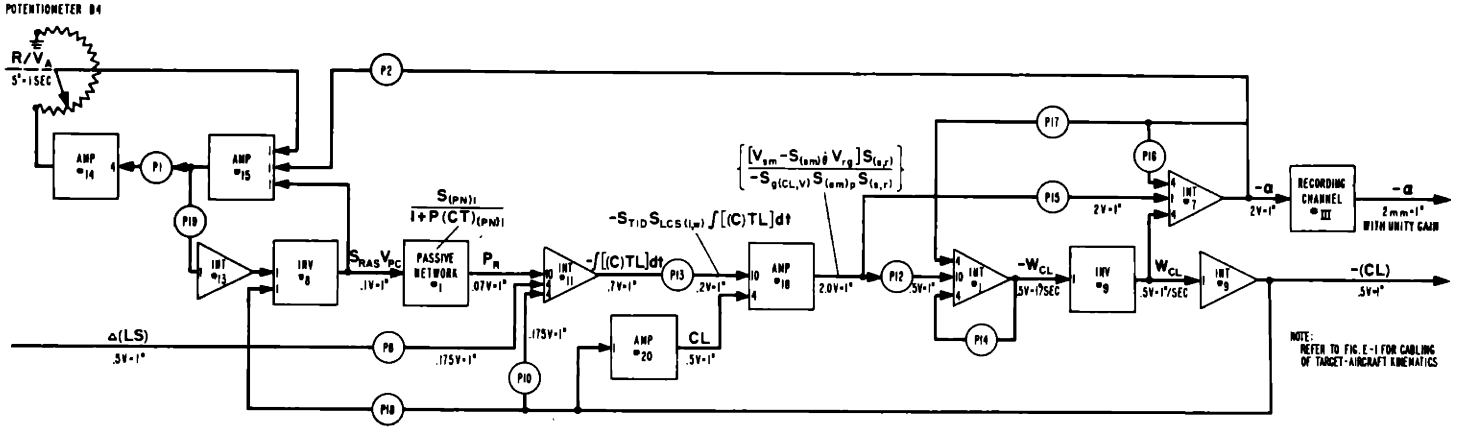

Fig. E–6.–Reac functional diagram for closed-loop tracking system with controlled-line prediction, and tight-loop stabilization of the aircraft.

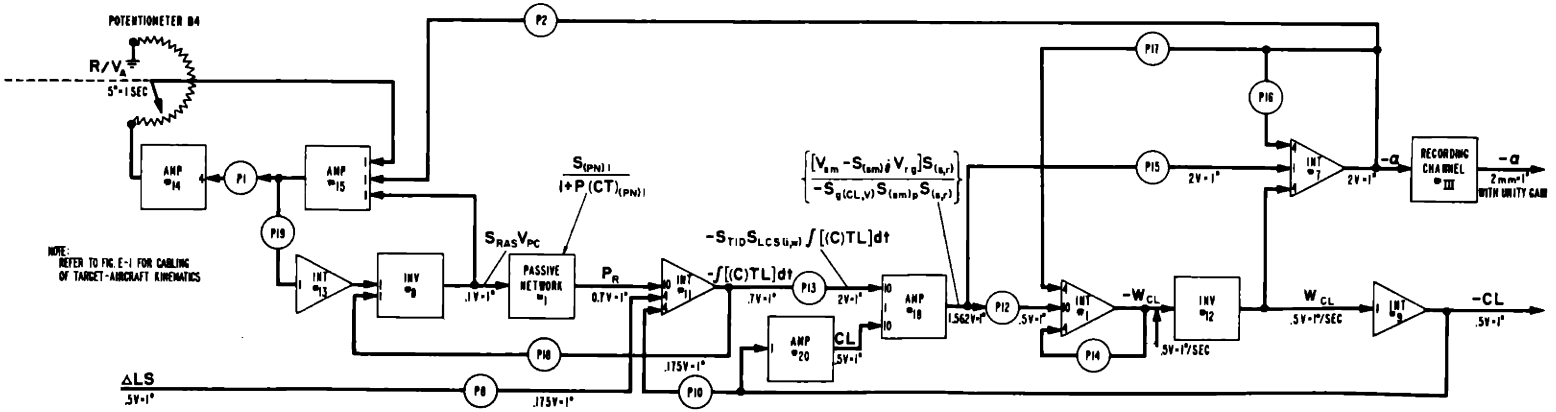

Fig. E–7.–Reac functional diagram for closed-loop tracking system with tracking inaccuracy prediction, and tight-loop stabilization of the aircraft.

Then using the correct value for the prediction sensitivity from Eq. D-55, and integrating

$$[S_{RAS}V_{PC}] = \frac{S_{TID}S_{LCS[i,W]}}{1 + SN}\int [LS + P_R - CL]\,dt$$

$$- \left[\frac{V_{p(av)}}{V_A} - 1\right] \frac{1}{[1 + SN][PSR]} \int \frac{S_{RAS}V_{PC} - S_{p(\alpha,P)}\alpha}{R/V_A}\,dt \qquad E-34$$

Equations E-12D, E-13, E-27, E-32, and E-34 are the basis for the analysis of the Closed-Loop Tracking System with Tracking Inaccuracy Prediction and Tight-Loop Stabilization of the Aircraft.

Figure E-7 is a functional diagram of the REAC cabling for this system. The potentiometer sensitivities, different from the settings for the Closed-Loop Tracking System with Controlled-Line Prediction, are

$$S_{P12} = -S_{g(CL,V)}S_{(sm)p}S_{(s,r)}M_{\delta}/40 + C_{10}$$

$$S_{P13} = (2/7)S_{TID}S_{LCS(i,W)} + C_{10}$$

$$S_{P15} = -S_{g(CL,V)}S_{(sm)p}S_{(s,r)}Z_{\delta}/V_A + C_1$$

$$S_{P18} = (1/7)S_{TID}S_{LCS(i,W)}/[1 + SN] + C_1$$

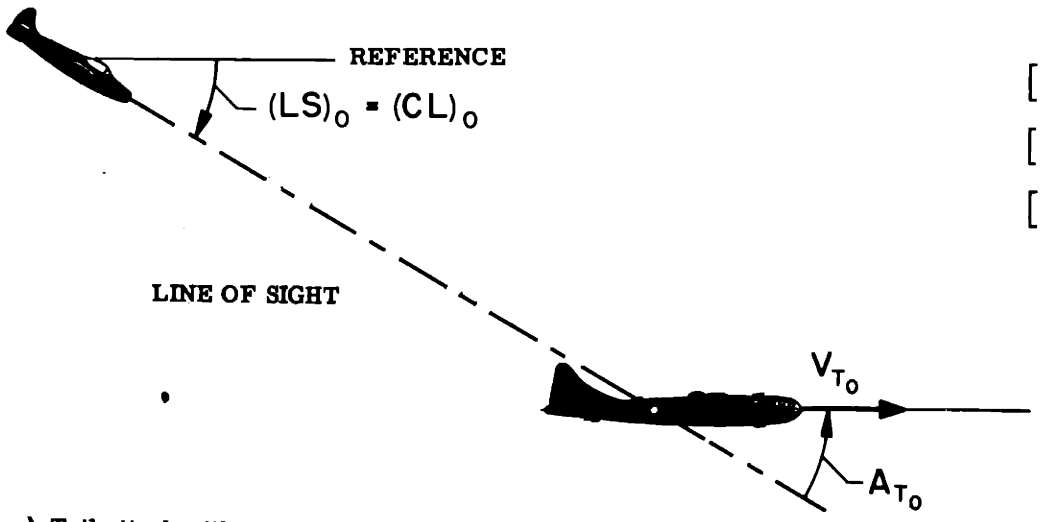

a) Tail attack with $A_{T_0} = 30°$

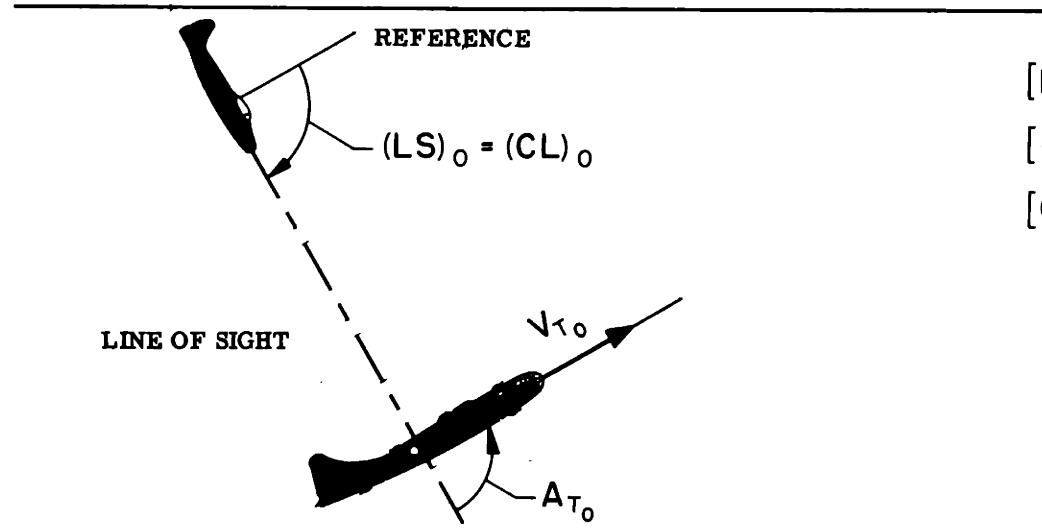

b) Beam attack with $A_{T_0} = 90°$

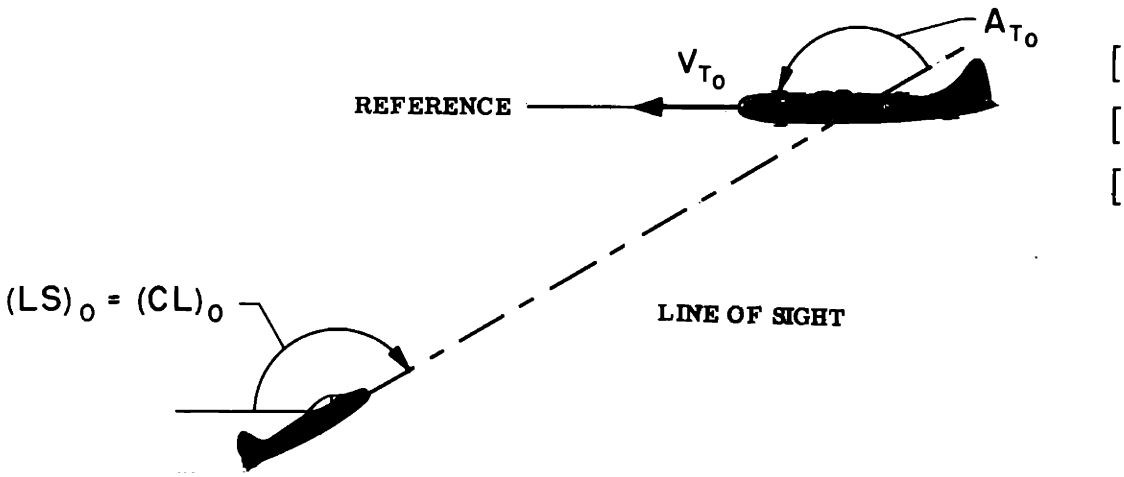

c) Head-on attack with $A_{T_0} = 150°$

Fig. E-8.—Initial headings of the interceptor aircraft and the target.

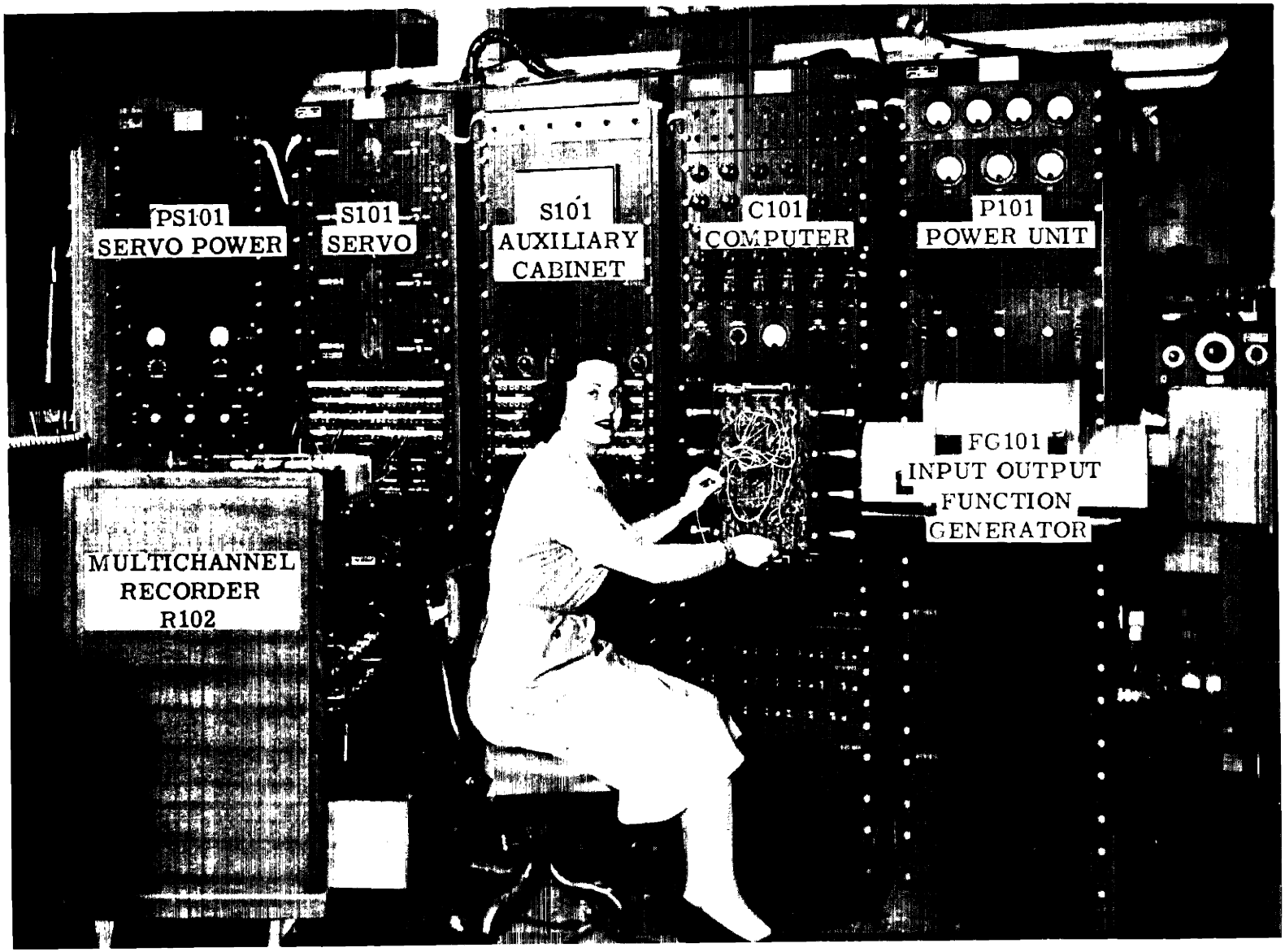

Fig. E–9.–Reac used to determine the controlled-line error.

APPENDIX F

CONCEPTS INVOLVED IN A STATISTICAL ANALYSIS OF INTERFERENCE EFFECTS

This appendix summarizes the concepts used in this thesis when analyzing the effects of gust and radar interference. If other interference effects prove to be important, they can be treated in a similar manner.

As stated in Appendix C, the controlled-line inaccuracy is composed of errors and uncertainties. Static errors can be determined by calibration procedures, and dynamic errors from computer solutions as described in Appendix E. By contrast, the value of the uncertainty at a given instant cannot be predicted beforehand, but must be estimated in terms of its probability of occurrence.

In a discussion of probability[12], it is common to use the root-mean-square value of a quantity, called the standard deviation. The standard deviation of the controlled line, (SD)CL, is related to the controlled line uncertainty, (U)CL, by the expression

$$[(SD)CL] = \sqrt{\frac{1}{n} \sum_{i=1}^{i=n} [(U)CL]_i^2} \qquad F\text{-}1$$

It is assumed in Eq. F-1 that n values of the uncertainty are available and that "i" represents any one value.

The definition for the standard deviation can be applied to the occurrence of any quantity, q, in which case

$[(SD)q]$ = standard deviation of q

$$= \sqrt{\frac{1}{n} \sum_{i=1}^{i=n} [q - q_{(av)}]^2} \qquad \text{F-2}$$

In Eq. F-2, $q_{(av)}$ is the average value of the quantity. For a comprehensive discussion of uncertainties and errors, refer to Chapter 6, "Instrument Engineering," by Draper[20].

For design purposes, it is important to have a method for estimating the standard deviation of the output from a system given the standard deviation of the input. Obviously, a time series must be considered, for when the input quantity deviates even large amounts in a period of time which is short in comparison with the system response, the system output is not affected appreciably. It can be seen that a measure of the time variation of the input quantity is required, as well as the standard deviation. Such a measure is the correlation function, developed by Wiener[19], and is defined

$[(CF)q]$ = the correlation function of the quantity q

$$= \lim_{T \to \infty} \frac{1}{2T} \int_{-T}^{T} q(t)\, q(t + \tau)\, dt \qquad \text{F-3}$$

with t = time and τ = correlation interval.

The process represented by Eq. F-3 is often called "autocorrelation" to differentiate from cross-correlation in which the relation between two different quantities is investigated statistically.

A comparison of Eq. F-2 and F-3 shows that when the average value of q is zero

$$[(CF)q]_{[\tau = 0]} = [(SD)q]^2 \qquad \text{F-4}$$

The correlation function has other useful properties, which are described in a paper by Lee[21]. For example, it can be shown that the correlation function is an even function with respect to the correlation interval, τ; and that the maximum value of the function occurs at zero τ.

The response of a system to a random input can be developed, using correlation functions and the convolution integral. Oftentimes, it is more convenient to carry out the analysis with frequency as the independent variable. Time variables are transformed into the frequency domain by the use of the Fourier integral. The resulting Fourier transform is related to the original quantity in the time domain by the equation

$$[(FT)q] = \int_{-\infty}^{\infty} q e^{-j\omega t}\, dt \qquad \text{F-5}$$

When time is in seconds, the use of Eq. F-5 gives the Fourier transform the dimensions of q/cps. Some engineers prefer to work with radians/second rather than with cycles/second, in which case the integral in Eq. F-5 is multiplied by $1/(2\pi)$. No confusion arises, provided the dimensions are clearly stated.

The Fourier transform of the correlation function is the power spectral density, (PSD), so that

$$[(PSD)q] = \text{power spectral density of } q$$
$$= \int_{-\infty}^{\infty} [(CF)q]\, e^{-j\omega\tau}\, d\tau \qquad \text{F-6}$$

However, since the correlation function is even, Eq. F-6 may be written

$$[(PSD)q] = 2\int_{0}^{\infty} [(CF)q] \cos \omega\tau d\tau \qquad \text{F-7}$$

Given the power spectral density, the correlation function may be found by taking the inverse transform, by which process

$$[(CF)q] = \frac{1}{2\pi}\int_{-\infty}^{\infty} [(PSD)q]\, e^{j\omega\tau}\, d\omega$$

$$= \frac{1}{\pi}\int_{0}^{\infty} [(PSD)q] \cos \omega\tau\, d\omega \qquad \text{F-8}$$

The power spectral density is an even function, thus permitting the simplification shown in Eq. F-8. Equation F-8 can be used to evaluate the correlation function at any time interval, τ. However, when the interval is zero, the correlation function equals the square of the standard deviation, so that from Eq. F-4 and F-8

$$[(SD)q]^2 = \frac{1}{\pi}\int_{0}^{\infty} [PSD)q]\, d\omega \qquad \text{F-9}$$

The standard deviation of the controlled-line displacement is evaluated in Appendix J by the use of Eq. F-9.

When investigating physical systems, the correlation function is frequently in the form

$$[(CF)q] = [(SD)q]^2\, e^{-\frac{\tau}{CT}} \qquad \text{F-10}$$

for $\tau > 0$

in which case, from Eq. F-7, the power spectral density is

$$[(PSD)q] = \frac{2(CT)[(SD)q]^2}{1 + [\omega(CT)]^2} \qquad \text{F-11}$$

There are other occasions when

$$[(CF)q] = [(SD)q]^2 \frac{1}{\sqrt{1 - (DR)^2}}\, e^{-(DR)\omega_n \tau} \cos[\omega_n \sqrt{1 - (DR)^2}\, \tau + \Phi] \qquad \text{F-12}$$

for $\tau > 0$, and where $\Phi = \cos^{-1} \sqrt{1 - (DR)^2}$

Taking the Fourier Integral of Eq. F-12 gives

$$[(PSD)q] = \frac{2\left[\frac{2(DR)}{\omega_n}\right][(SD)q]^2}{1\left[-\left(\frac{\omega}{\omega_n}\right)^2\right]^2 + \left[\frac{2(DR)\omega}{\omega_n}\right]^2} \qquad \text{F-13}$$

The Fourier transform of a system output quantity is more simply related to the Fourier transform of the input than are the two quantities when time is the independent variable. The amplitude of the output quantity, $q_{(out)a}$, equals the product of the amplitude of the input, $q_{(in)a}$, and the amplitude ratio, $(AR)_{S[q_{in},q_{out}]}$. The phase angle of the output quantity, $(PA)_{out}$, equals the sum of the input phase angle, $(PA)_{in}$, and the phase deviation introduced by the system, $(PA)_{S[q_{in},q_{out}]}$. The system amplitude ratio and phase angle are both functions of frequency. It is convenient to define the system sensitivity in such a manner that it equals the amplitude ratio at zero frequency when such a value exists, or

$$S_{s[q_{in},q_{out}]} = (AR)_{s[q_{in}, q_{out}][\omega = 0]} \qquad \text{F-14}$$

For cases where the amplitude ratio is either zero or infinite at zero frequency, the reference sensitivity, $S_{s[q_{in},q_{out}](ref)}$, is used for non-dimensionalizing purposes. The value of the reference sensitivity is selected for maximum ease in carrying out the analysis.

The power spectral density is a real quantity, and hence there is no associated phase angle. Therefore, the relationship between the power spectral density of the system input and the power spectral density of the system output is entirely a function of the system amplitude ratio. It can

be readily shown[13] that

$$[(PSD)q_{out}] = [(PSD)q_{in}]\,(AR)^2_s[q_{in}, q_{out}] \qquad \text{F-15}$$

and, from Eq. F-14, when the value for the amplitude ratio exists at zero frequency,

$$[(PSD)q_{out}]_{[\omega = 0]} = [(PSD)q_{in}]_{[\omega = 0]}\, S^2_s[q_{in}, q_{out}] \qquad \text{F-16}$$

As an example of the use of the correlation function and the power spectral density in determining the standard deviation of a system output quantity, $[(SD)q_{out}]$, let

$$[(CF)q_{in}] = [(SD)q_{in}]^2\, e^{-\frac{\tau}{(CT)_{in}}} \qquad \text{F-17}$$

and

$$(AR)^2_s[q_{in}, q_{out}] = \frac{S^2_s[q_{in}, q_{out}]}{1 + [\omega(CT)_s]^2} \qquad \text{F-18}$$

Then, from Eq. F-11 and F-15,

$$[(PSD)q_{out}] = \left\{\frac{2(CT)_{in}[(SD)q_{in}]^2}{1 + [\omega(CT)_{in}]}\right\} \left\{\frac{S^2_s[q_{in}, q_{out}]}{1 + [\omega(CT)_s]^2}\right\} \qquad \text{F-19}$$

However, the power spectral density for the output quantity is in the same form as Eq. F-13. By equating the coefficients of ω^2 and ω^4 in the denominators of the power spectral density expressions, it is possible to solve for (DR) and ω_n. Then, a combination of Eq. F-13 and F-19 gives

$$[(PSD)q_{out}] = \frac{2[(CT)_{in} + (CT)_s][(SD)q_{out}]^2}{[1 + [\omega(CT)_{in}]^2][1 + [\omega(CT)_s]^2]} \qquad \text{F-20}$$

As a result of Eq. F-20,

$$[(SD)q_{out}] = [(SD)q_{in}]\, S_s[q_{in},q_{out}] \quad \sqrt{\frac{(CT)_{in}}{(CT)_{in} + (CT)_s}} \qquad \text{F-21}$$

Equation F-21 shows the standard deviation of the output quantity equal to the product of the standard deviation of the input and the system sensitivity when the characteristic time of the system, $(CT)_s$, is zero. When the characteristic time has a value other than zero, the standard deviation of the system is reduced. When the input quantity is nearly random with respect to the system response, the input characteristic time is relatively small, and the system standard deviation is considerably reduced.

APPENDIX G

EFFECT OF THE CONTROLLED-LINE INACCURACY ON HIT PROBABILITY

With no uncertainty in the aiming of the controlled line and no dispersion of the projectiles, the probability of a hit would be either zero or 100 percent, depending upon the aiming. However, uncertainty and dispersion are always present; consequently, the distribution of the projectile pattern must be considered. For this purpose, a plane is defined which passes through the center of the vulnerable section of the target and is normal to the impact line (velocity of the projectile when in closest proximity to the target center). As discussed in this thesis, an impact refers to the intersection of a projectile with this plane.

An impact point is the location of an impact on the target plane, and its position is the inaccuracy of the impact, which can be measured in Y_T-Z_T coordinates. Because of the curvature of the trajectory, the target plane is not exactly normal to the controlled line. However, the angular difference between the impact line and the controlled line is small, and consequently Y_T and Z_T can be oriented nearly parallel to the elevation and deflection axes.

The projected area of the vulnerable section of the target is indicated in Fig. G-1. For ease in analysis it is circular, with radius r_T. Actually, its shape may be quite irregular, and may vary with the direction of approach. Also, there may be more than one section of the target that is vulnerable to attack.

Following a gun burst or the launching of several rockets, an impact

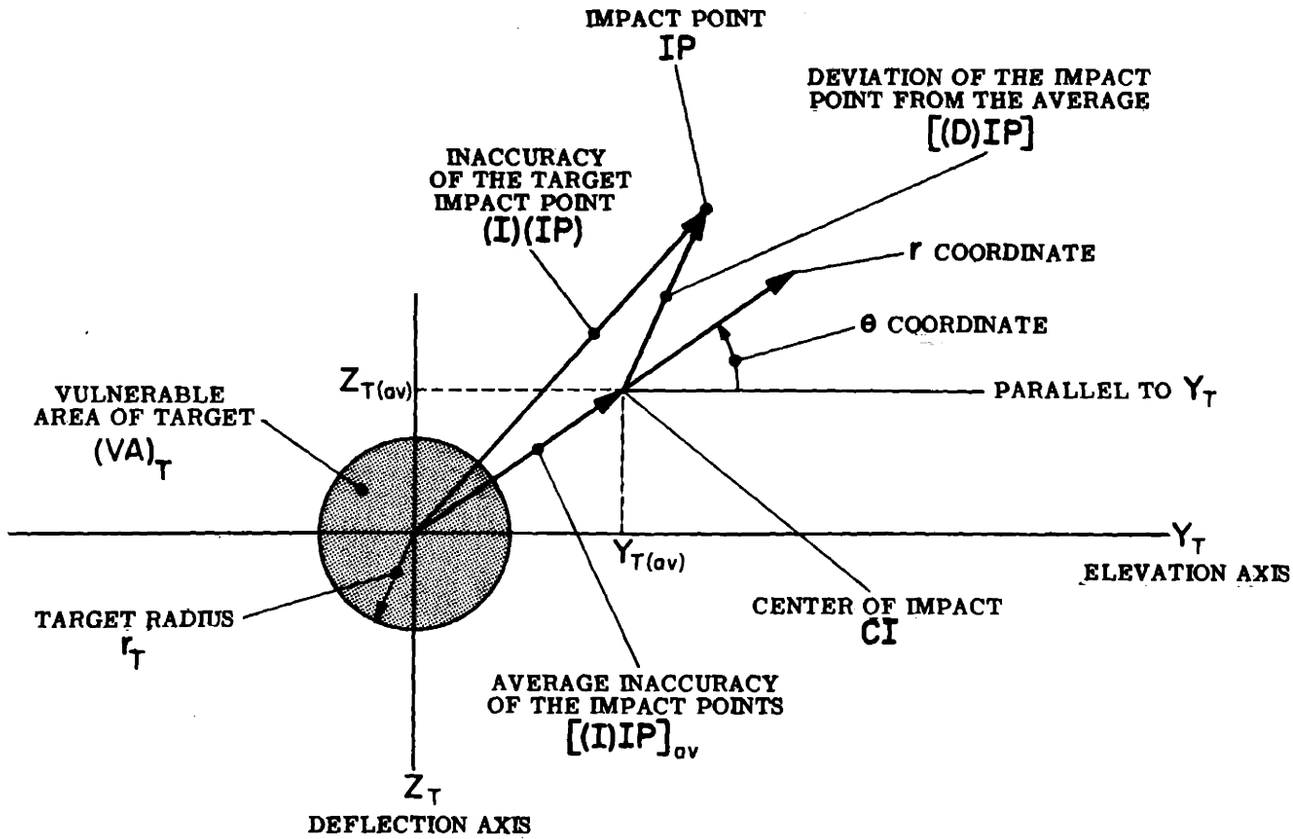

COORDINATES CONTAINED IN A PLANE THROUGH THE CENTER OF GRAVITY OF THE TARGET NORMAL TO THE LINE-OF-FIRE.

$(E)(CI) = \text{ERROR IN CENTER OF IMPACT} = [(I)(IP)]_{av}$

Fig. G-1.–Factors involved in hitting a target.

pattern is found on the target plane. With this impact there is a percentage probability of a hit, $P(VA)_T$, on the target area $[VA]_T$. The hit probability on the infinitesimal section $[dY_T dZ_T]$ equals the product of the hit probability density, $[(PD)(Y_T,Z_T)]$, and the area of the infinitesimal section, or

$$P[dY_T\, dZ_T] = [(PD)(Y_T,Z_T)]\,[dY_T dZ_T] \qquad \text{G-1}$$

The probability of hitting the target then becomes

$$P(VA)_T = \iint_{AT} [(PD)(Y_T,Z_I)]\,[dY_T\, dZ_T] \qquad \text{G-2}$$

In order to evaluate the hit probability, using Eq. G-2, the probability density must be expressed in target coordinates.

The average, or mean, position of the impact points is called the center of impact, with coordinates $Y_{T(av)}$ and $Z_{T(av)}$. It can be seen from Fig. G-1 that the error in the center of impact equals the average inaccuracy of the impact points. The deviation of any one impact from average is shown in Fig. G-1 as (D)(IP), and the standard deviation of the impact points of the complete pattern is (SD)(IP), and can be determined by use of Eq. F-2.

When the impact points have a normal, or Gaussian, distribution, the hit probability density is bell-shaped, with a maximum at the center of impact. Test firings indicate that, for engineering purposes, it is reasonable to assume this type distribution for the impact pattern. With a Gaussian distribution, the probability density expressed in Y_T,Z_T coordinates is

$$[(PD)(Y_T,Z_T)] = \frac{1}{2\pi[(SD)IP]^2}\; e^{-\frac{[Y_T - Y_{T(av)}]^2 + [Z_T - Z_{T(av)}]^2}{2[(SD)IP]^2}} \qquad \text{G-3}$$

or, in polar coordinates, r, θ, with the origin at the center of impact,

$$[(PD)(r,\theta)] = \frac{1}{2\pi[(SD)IP]^2} e^{-\frac{r^2}{2[(SD)IP]^2}} \qquad G\text{-}4$$

It should be noticed that Eq. G-3 and G-4 assume that the dispersion about the elevation axis is the same as the dispersion about the deflection axis.

Finally, expressing Eq. G-2 in polar coordinates, r, , and utilizing the probability density of Eq. G-4, gives

$$P\ (VA)_T = \frac{1}{2\pi[(SD)\ IP]^2} \iint_{AT} e^{-\frac{r^2}{2[(SD)IP]^2}} r dr d\theta \qquad G\text{-}5$$

Even with a circular target area $(VA)_T$, it is difficult to obtain a generalized expression for the hit probability from Eq. G-5.

One special case, which can be readily handled mathematically, arises when the center of impact coincides with the center of the target. Then Eq. G-5 becomes

$$P\ (VA)_T = 1 - e^{-\frac{r_t^2}{2[(SD)IP]^2}} \qquad G\text{-}6$$

From Eq. G-6, when the radius of the target equals the standard deviation, there is a hit probability of .394 or, on a percentage basis, approximately 40 percent of the projectiles can be expected to score a hit. For a 50-percent hit probability, the dispersion must be reduced until the target radius is 1.175 times the standard deviation.

The curves in Fig. G-2, which are derived in a NDRC Memo[31] by Sard from Eq. G-5, give the hit probability for errors in the center of impact

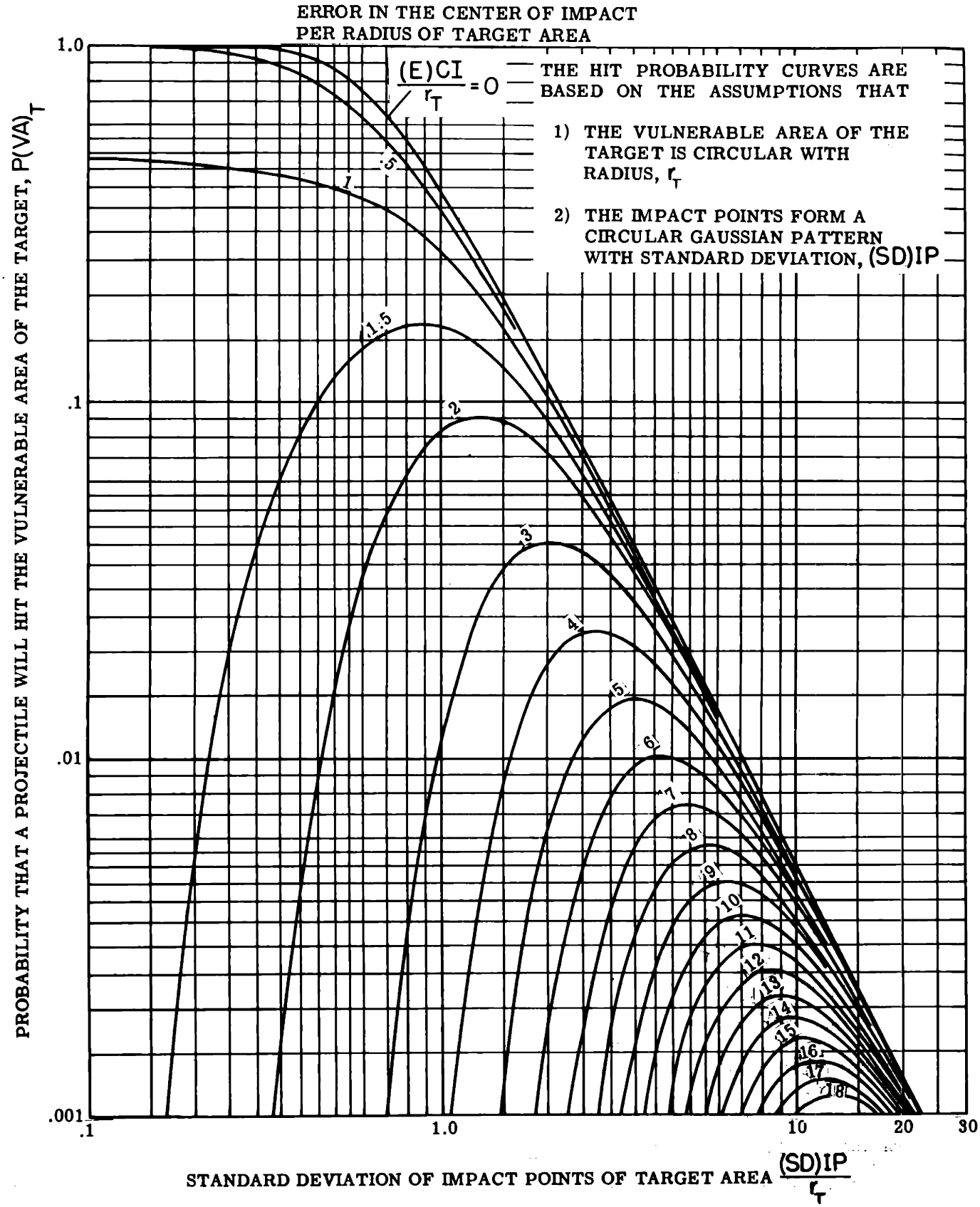

Fig. G-2.—Probability of a hit as a function of dispersion and aiming error.

other than zero. In Fig. G-2, the error and the standard deviation are expressed in ratio form, so that the curves are valid for a circular target of any size.

It can be seen that, for a given error, there is an optimum standard deviation. When the standard deviation is too small, most of the projectiles pass by the target, and when it is too large, the hit density over the target becomes too low.

In this thesis, the error in the center of impact is assumed equal to the controlled-line error. The standard deviation of the impact point is assumed to depend upon the standard deviation of the controlled line and the dispersion of the projectile pattern, with respect to the controlled line in such a manner that

$$[(SD)IP]^2 = [(SD)CL]^2 + [(SD)PP]^2$$

$$= [(SD)CL]^2_{[q_{in} \approx W_G]} + [(SD)CL]^2_{[q_{in} = q_{RI}]} + [(SD)PP]^2 \qquad G\text{-}7$$

APPENDIX H

GUST INTERFERENCE

A B-25J aircraft was assigned to the Instrumentation Laboratory during 1948 and 1949 for the purpose of investigating methods of determining the dynamic performance of aircraft by simple, straight-forward procedures involving as little flight time as possible.

Clementson originally suggested the use of pulse-type control inputs. These inputs, similar to the standard "kick" tests, force the airplane from equilibrium. By measuring the response of the aircraft to pulse disturbances, the longitudinal and lateral characteristics of the airplane can be evaluated. The results of these tests are presented in a thesis by Clementson, a joint thesis by Bain, Michaelis, and Wootton[23], an engineering memorandum[28], and a paper[17] published in the Journal of the Aeronautical Sciences.

Disturbances are applied to an aircraft not only by the control surfaces, but also by roughness in the air. These latter disturbances interfere with the operation of the aircraft, especially when it is being used as a platform for precision fire control.

By the summer of 1949, the B-25 aircraft was well-calibrated and the decision was made to fly the airplane in various types of weather, with the controls fixed. The response of the aircraft in pitch and roll was measured over long intervals of time. The resulting indications were correlated using IBM equipment, as well as with a machine designed especially for the purpose.

The pitch rate correlation function resulting from the atmospheric turbulence, $[(CF)\dot{\theta}_A]$, is presented in Fig. 4-2 of a thesis by Clementson[22]. The power spectral density of the pitch rate, $[(PSD)\dot{\theta}]$, is evaluated from the correlation function according to Eq. F-7, yielding

$$[(PSD)\dot{\theta}_A] = 2\int_0^\infty [(CF)\dot{\theta}_A] \cos \omega\tau d\tau \qquad \text{H-1}$$

The power spectral density, $[(PSD)\dot{\theta}_A]$, equals the product of the power spectral density of the gust disturbances, $[(PSD)W_G]$, and the square of the amplitude ratio, and consequently

$$[(PSD)w_G] = \frac{[(PSD)\dot{\theta}_A]}{(AR)^2_{A(w_G,\dot{\theta})}} \qquad \text{H-2}$$

Values for $[(PSD)\dot{\theta}_A]$ were obtained from Eq. H-1, and the amplitude ratio was computed from Eq. B-17, with

$S_{A(w_G,\theta)(ref)}$ = 2.26 mils per foot/second

$(CT)_{A(w_G,\theta)}$ = .14 second

ω_{n_A} = 2.38 radians per second

DR = .70

These values were computed for the B-25J with its center of gravity at 26% MAC, traveling 175 mph IAS at 8000 ft altitude. The true airspeed was 300 feet per second.

The spectral densities of Eq. H-1 and H-2 and the square of the amplitude ratio are plotted in Fig. 4-3 of Clementson's thesis[22]. However,

the dimensions of the amplitude ratio squared are rad^2/ft^2 not deg^2/ft^2, as indicated. Taking into account this discrepancy, the power spectral density of the air mass velocity, w_G, is replotted in Fig. H-1. A log-log scale is used, and it can be seen that the experimental plots determined by Clementson lie closely along a straight line with a slope of minus two. For this reason, it seems probable that

$$[(CF)w_G] = [(SD)w_G]^2 e^{-\frac{\tau}{(CT)_G}} \quad \text{for} \quad \tau > 0 \qquad \text{H-3}$$

making

$$[(PSD)w_G] = \frac{2(CT)_G[(SD)w_G]^2}{1 + [\omega(CT)_G]^2} \qquad \text{H-4}$$

From Eq. H-4, with $[\omega(CT)_G]^2 >> 1$,

$$[(PSD)w_G] = \left[\frac{2[(SD)w_G]^2}{(CT)_G}\right] \frac{1}{\omega^2} \qquad \text{H-5}$$

A log-log plot of the power spectral density from Eq. H-5 as a function frequency, is a straight line with a slope of minus two. The straight line best averaging the experimental plots has a value of 9.2 ft^2/sec at a frequency of 1 rad/sec, so that

$$\frac{[(SD)w_G]^2}{(CT)_G} = 4.6 \text{ ft}^2/\text{sec}^3$$

Two theoretical curves derived from Eq. H-4 are shown in Fig. H-1. One curve assumes a characteristic time of 3.0 seconds and gust velocity standard deviation of 3.70 ft/sec; the other assumes a characteristic time of 6.0 seconds and gust velocity standard deviation of 5.25 ft/sec. A comparison of the theoretical curves with the experimental data indicates that the gust characteristic time is greater than 3.0 seconds. However, pitch

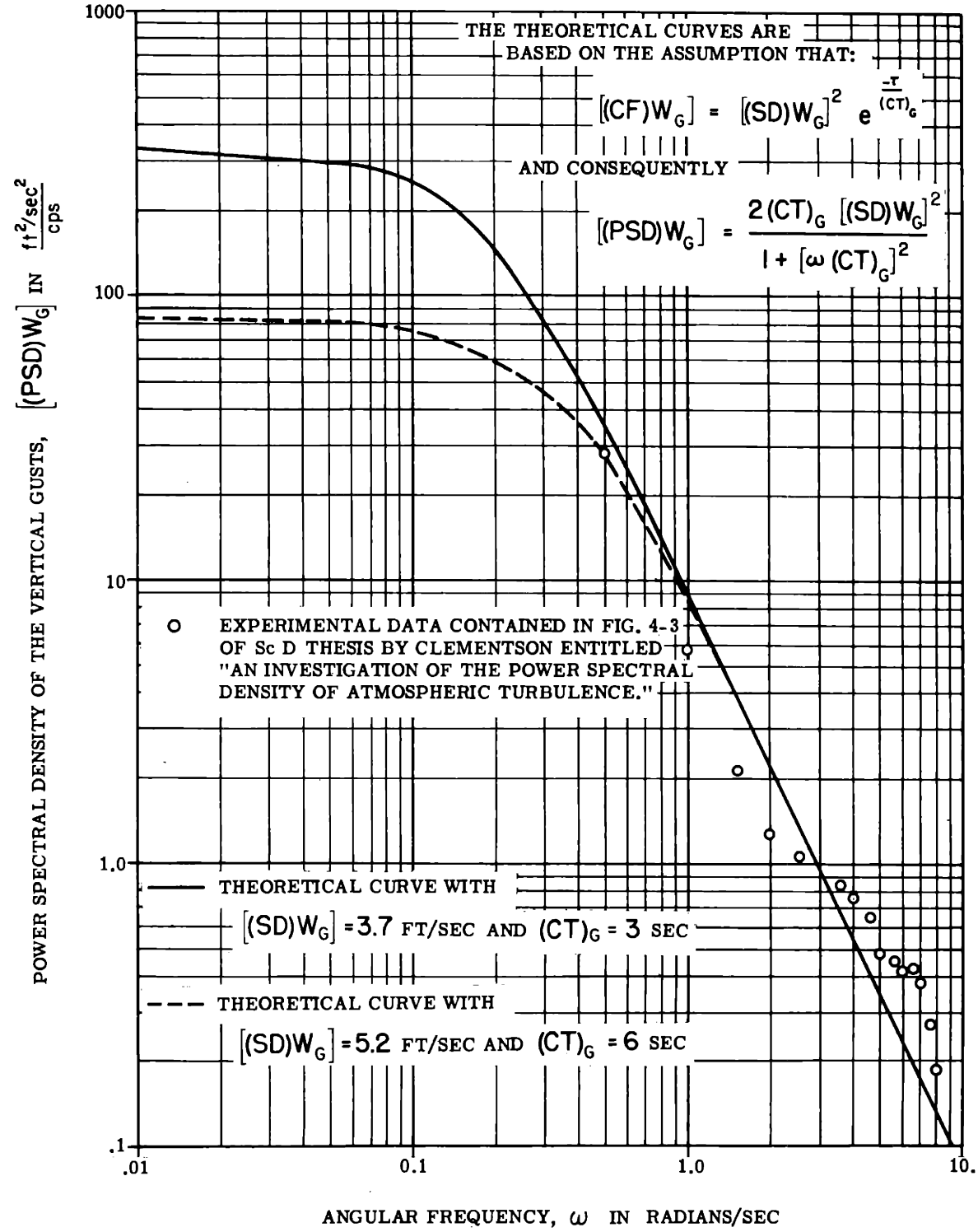

Fig. H-1.—Power spectral density of the vertical velocity of gusts with respect to the earth.

rate data must be obtained at frequencies less than 0.5 rad/sec in order to evaluate the characteristic time more exactly.

In order to check the assumption of Eq. H-3, values of the pitch rate correlation function were obtained on the Rockefeller Differential Analyzer, using Eq. B-17, F-8, H-2, and H-4, with gust characteristic times of 3 and 6 seconds. The results are plotted in Fig. H-2, together with the experimental curve from Fig. 4-2 of Clementson's thesis[22]. The curves are nearly identical for correlation intervals from 0 to 0.7 second. For longer correlation times, the theoretical curves are negative, whereas the experimental curve remains positive. If the amplitude ratio of the airplane is zero at zero frequency, the integral of the pitch rate correlation function must also be zero, and consequently the function must have both positive and negative values. Hence, either the experimental data is inaccurate for times greater than 0.7 second or the assumption of constant forward velocity is not valid because of the time intervals involved.

While the Rockefeller Differential Analyzer was solving for the pitch rate correlation function, it was also obtaining values for the pitch angle correlation function, $[(CF)_{\theta}]$. The expression for $[(CF)_{\theta}]$ differs from $[(CF)_{\dot{\theta}}]$ because the square of the amplitude ratio is in the form

$$(AR)^2_{A(w_G,\theta)} = S^2_{A(w_G,\theta)} \frac{1 + [\omega(CT)_{A(w_G,\theta)}]^2}{[1-(\frac{\omega}{\omega_{n_A}})^2 + [\frac{2(DR)_A}{\omega_{n_A}}\omega]^2} \qquad \text{H-6}$$

Consequently, it has a finite value at zero frequency. Values of $[(CF)_{\theta}]$ with gust characteristic times of 3 and 6 seconds are plotted in Fig. H-3. The curves differ markedly, and indicate that future studies of atmospheric turbulence should be based on pitch angle rather than pitch rate.

A value of 5.25 ft/sec for the standard deviation of the gust velocity is used in the computations of Appendix J. The value is invariant with the forward velo-

THE RATE OF PITCH CORRELATION FUNCTION, $[(CF)\dot{\theta}]$, IS RELATED TO THE POWER SPECTRAL DENSITY OF THE PITCH RATE, $[(PSD)\dot{\theta}]$, BY THE EXPRESSION:

$$[(CF)\dot{\theta}] = \frac{1}{\pi} \int_0^{\infty} [(PSD)\dot{\theta}] \cos \omega \tau \, d\omega$$

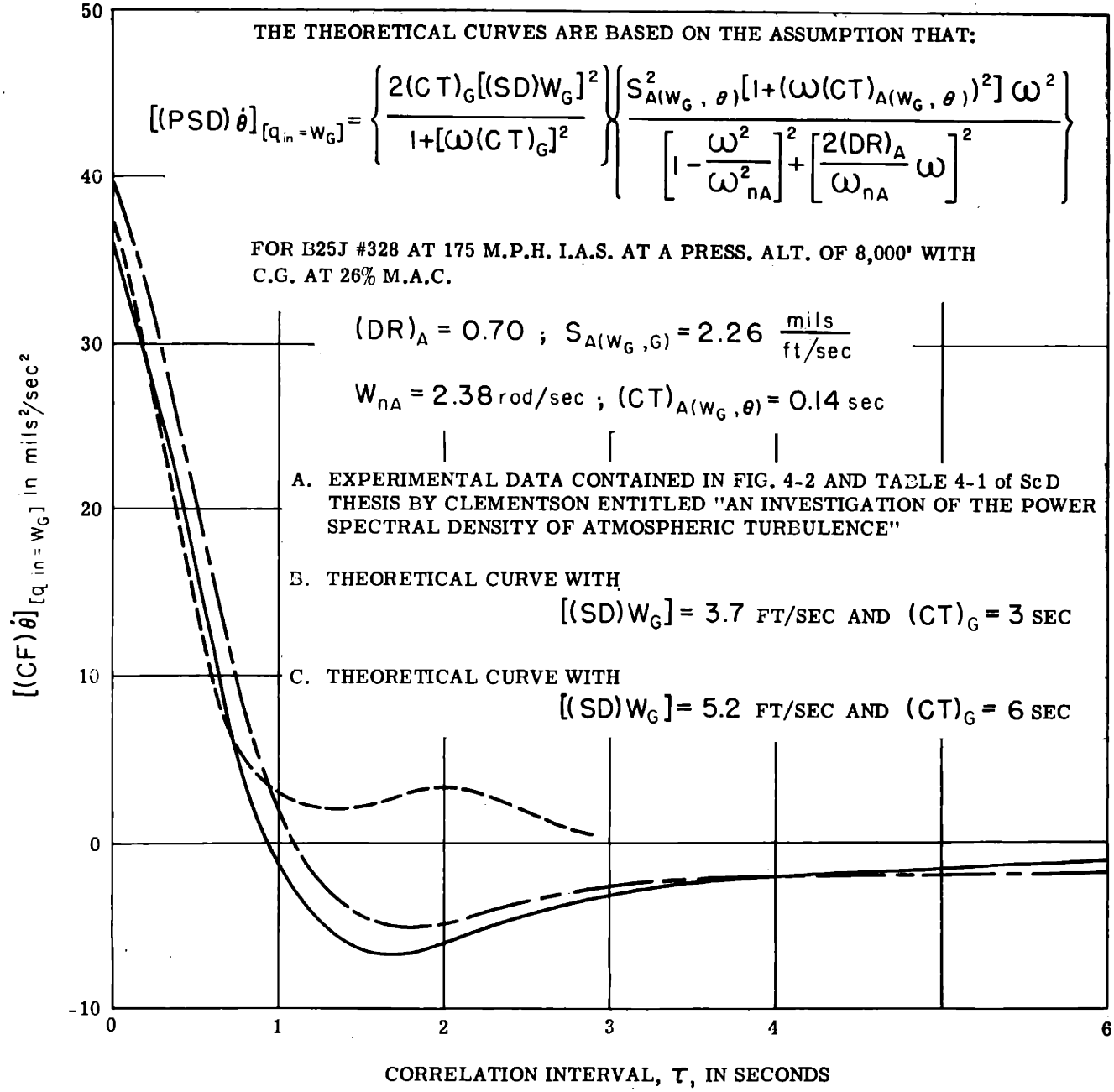

Fig. H-2.–Correlation of the rate of pitch response of a B25J aircraft to vertical gusts.

THE PITCH ANGLE CORRELATION FUNCTION, $[(CF)\theta]$ IS RELATED TO THE POWER SPECTRAL DENSITY OF THE PITCH ANGLE $[(PSD)\theta]$ BY THE EXPRESSION:

$$[(CF)\theta] = \frac{1}{\pi}\int_0^a [(PSD)\theta]\cos\,\omega\,\tau\,d\,\omega$$

THE THEORETICAL CURVES ARE BASED ON THE ASSUMPTION THAT:

$$[(PSD)\theta]_{[q_{in}=\omega_G]} = \left\{\frac{2(CT)_G[(SD)W_G]^2}{1+[\omega\,(CT)_G]^2}\right\}\left\{\frac{S_{A(W_G,G)}\left[1+(\omega\,(CT)_{A(W_G,G)})^2\right]}{\left[1-\frac{\omega^2}{\omega^2_{nA}}\right]^2+\left[\frac{2(DR)_A}{\omega_{nA}}\omega\right]^2}\right\}$$

FOR B-25 J #328 AT 175 MPH I.A.S., AT A PRESSURE ALTITUDE OF 8,000 FT, WITH C. G. AT 26% M.A.C.

$$(DR)_A = 0.70\ ;\ S_{A(W_G,\theta)} = 2.26\ \frac{\text{mils}}{\text{ft/sec}}$$

$$\omega_{nA} = 2.38\ \text{rad/sec}\ ;\ (CT)_{A(W_G,\theta)} = 0.14\ \text{sec}$$

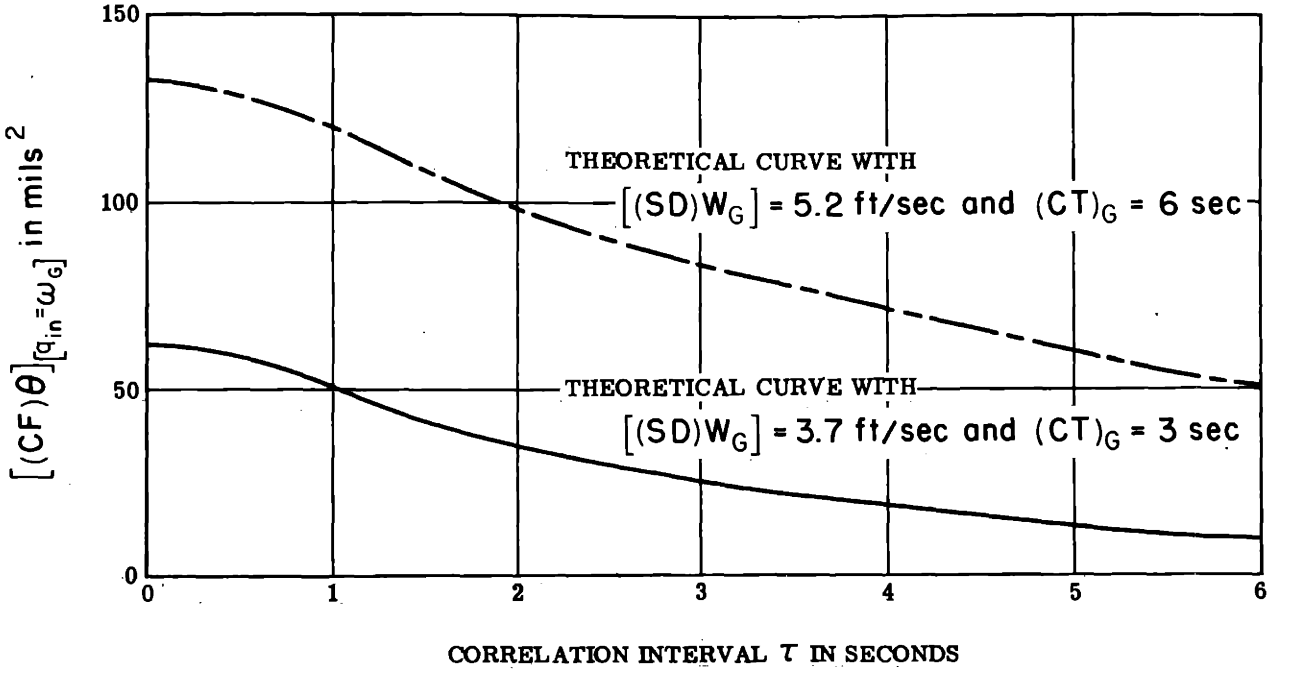

Fig. H-3.—Correlation of pitch angle response of a B25J aircraft to vertical gusts.

city of the aircraft. However, the characteristic time is inversely proportional to the forward speed, and consequently

$$(CT)_{G(V_A = V_{A2})} = (CT)_{G[V_A = V_{A1}]} \left[\frac{V_{A1}}{V_{A2}}\right] \qquad \text{H-7}$$

The B-25J tests were carried out at a true airspeed of 300 ft/sec, whereas the F-94 is assumed to be operating at 737 ft/sec. Consequently, with a gust characteristic time of 6 seconds at 300 ft/ sec,

$$(CT)_{G(V_A = 727)} = 6 \times \frac{300}{727} = 2.5 \text{ seconds}$$

APPENDIX I

RADAR INTERFERENCE

In this appendix, data from different sources is summarized. On the basis of this data, the power spectral density of the radar interference is estimated for both conical scan radar and momupulse radar. All the results are contained in Fig. I-1.

1. Types of Radar Interference.

Radar interference refers to those effects which adversely influence the indication of the radar tracking inaccuracy, and is frequently called radar noise although it is not an acoustical problem. Actually, indications of the radar tracking inaccuracy are uncertain at short range because the target has finite dimensions, giving rise to wander between target reflecting surfaces. At long range, the reflected high frequency signal is of the same order as random voltages generated in the receiver due to thermal agitation in the tubes. At intermediate ranges, conical scan radars introduce inaccuracies caused by changes in the amplitude of the reflected signal from the target. Since these changes occur at frequencies comparable to the scan frequency, it is impossible to detect the desired amplitude modulation due to scanning without introducing an inaccuracy due to target fading. Interference of this type is not found in monopulse radar systems.

To summarize, radar interference is caused by

a. Wander over the target area at short range

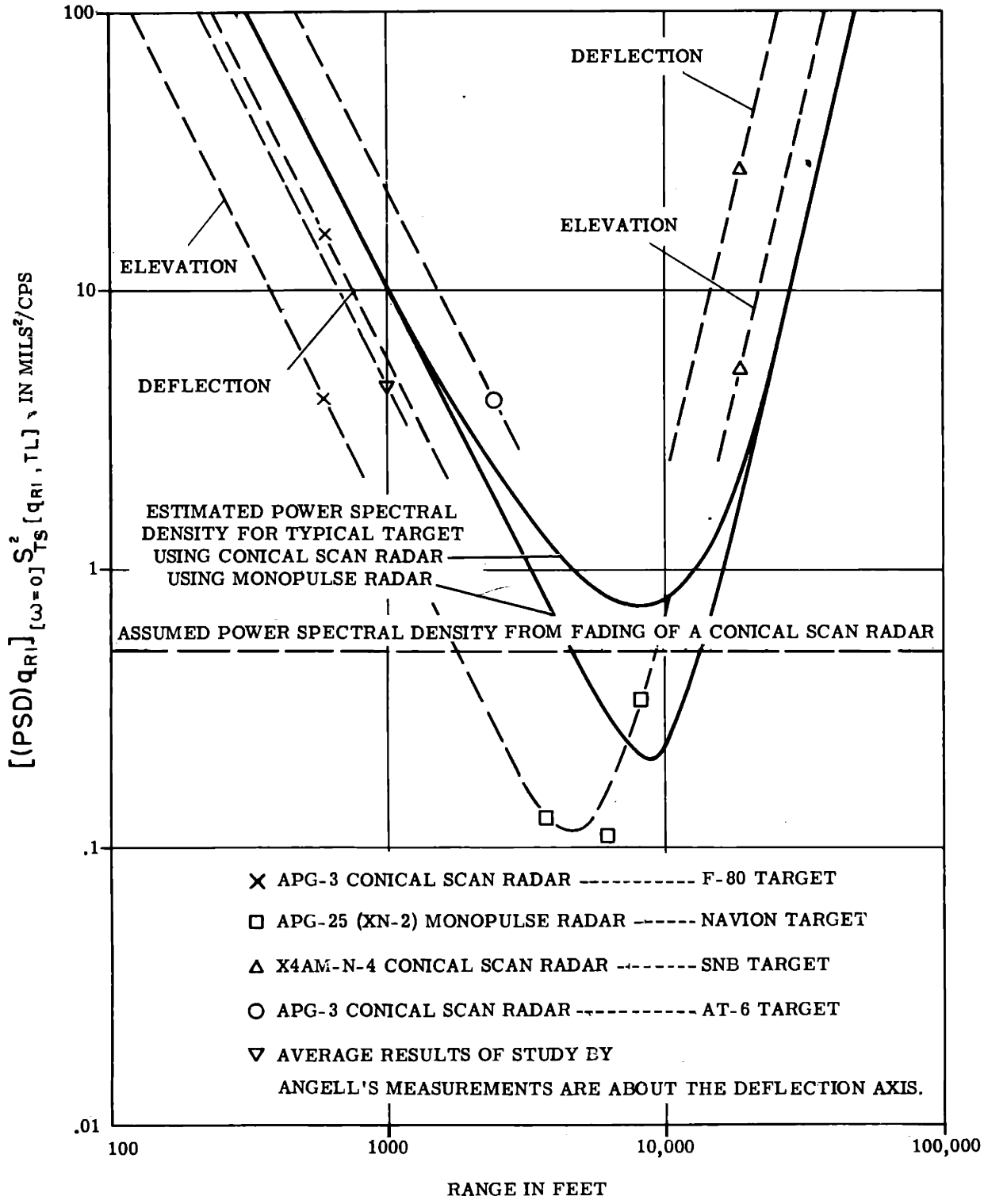

Fig. 1-1.—Power spectral density of radar interference as a function of target range.

b. Amplitude fading when conical scanning at an intermediate range

c. Thermal agitation due to reduction in receiver signal strength at long ranges.

2. Methods for Measuring the Effect of Radar Interference.

Two methods are available for evaluating radar interference. One method involves system tests with a tracking radar of known performance. The other method requires a fundamental study of the interference effects using special test equipment. Results of both methods are presented in this Appendix.

In the first method a radar tracking system is mounted either on a laboratory roof or in an aircraft. Cameras are mounted either on the radar antenna or on a dummy director so that the tracking line inaccuracy can be measured as a function of time. The standard deviation of the tracking line can be readily determined by film measurements and may be of significance in a particular development program. However, for general use, the standard deviation of the tracking line alone is of little value. As shown in Eq. F-21, the standard deviation of the output can be reduced to any desired value by increasing the amount of smoothing in the system. Hence the dynamics of the radar tracking must be considered before the data becomes of general interest.

The quantity of importance to all tracking systems is the power spectral density of the radar interference at zero frequency, $[(PSD)q_{RI}]_{[\omega=0]} S^2_{TS[q_{RI}, TL]}$. The interference quantity, q_{RI}, refers to the effects of wander, fading, and receiver agitation. The radar tracking system sensitivity, $S_{TS[q_{RI}, TL]}$ is used to convert the power spectral density into tracking line mils. The dimensions of the radar interference quantities differ depending upon the effect in question, but the dimensions of $[(PSD)q_{RI}]_{[\omega=0]} S^2_{TS[q_{RI}, TL]}$ are always mils ^{2}/cps, as defined in this appendix.

It can be seen from Eq. F-16 that

$$[(PSD)q_{RI}]_{(\omega=0)} S^2_{TS(q_{RI},TL)} = [(PSD)TL]_{(\omega=0)} \qquad \text{I-1}$$

The power spectral density of the tracking line at zero frequency can be found by the following methods:

a. Autocorrelating the tracking data according to Eq. F-3 and then using Eq. F-7 with $\omega = 0$ to determine the spectral density.

b. Determining the standard deviation of the tracking line from Eq. F-2 and then computing the power spectral density, knowing the characteristics of the radar system.

c. Using a spectrum analyzer to determine the power spectral density directly from the tracking data.

The zero frequency value for the power spectral density is useful, since the over-all performance of tracking systems for interceptor aircraft is not influenced by interference effects occurring at frequencies over 3 cps. In this region, the power spectral density of the radar interference is substantially constant.

3. Radar Interference Data.

It is stated in a report by Meade, Hastings, and Gerwin, entitled "Noise in Tracking Radars,"[25] that the power spectral density resulting from wander is inversely proportional to the square of the range, whereas the receiver agitation causes the spectral density to increase in proportion to BR^4/AP_T. Here, B is the angular beam width, A is the reflecting area of the target, P_T is the transmitting power, and R is the range. The effect of amplitude fading is said to be independent of the range.

a. APG-3 Conical Scan Radar - F-80 Target.

The information presented in Fig. I-1 is derived from Fig. 3 of a General Electric Report by Winn and Schermacher, entitled "Effects of Noise on Automatic Tracking Radar Systems." At 200 yards range, the standard deviation of the tracking line is 2.5 mils in elevation and 5.0 mils in deflection. The servo bandpass is 0.5 cps, and hence the radar characteristic time, $(CT)_R$, equals $1/2\pi$ (0.5), or 0.32 second, on the assumption of first-order radar dynamics. Then, from Eq. F-20 and I-1,

$$[(PSD)TL]_{(\omega=0)} = 2(CT)_R[(SD)TL]^2$$

and making use of Eq. I-1

$$[(PSD)q_{RI}]_{(\omega=0)} S^2_{TS}[q_{RI},TL] = 16 \text{ mils}^2/\text{cps in deflection}$$

$$= 4 \text{ mils}^2/\text{cps in elevation}$$

b. APG Monopulse Radar – Navion Target

A report entitled "Characteristics of Target Generated Noise in Gun Laying Radar," by Burlingame,[26] states that the standard deviation of the radar tracking line of the AP6-25 is 1.58 mils at 1200 yards, 1.46 mils at 2000 yards, and 2.60 mils at 2600 yards. In addition, correlation functions are shown for four runs, in each case to a close approximation of

$$(CF)TL = [(SD)TL]^2 e^{-\frac{\tau}{(CT)_R}} \qquad \tau > 0$$

The radar characteristic time required to best fit the experimental data varied from .022 to .027 second, with an average value of .025 second. Since the standard deviations for these four runs are comparable to the standard deviations already listed, it appears reasonable, from Eq. F-11 and I-1, that

$$[(PSD)q_{RI}]_{(\omega=0)} S^2_{TS}[q_{RI},TL] = .125 \text{ mils}^2/\text{cps at 3600 feet}$$

$$= .107 \text{ mils}^2/\text{cps at 6000 feet}$$

$$= .340 \text{ mils}^2/\text{cps at 7800 feet}$$

c. XAAM-N-4 Conical Scan Radar – SNB Target

The results of run #8 are given on pages C-13 and C-14 of "Ground-to-Air Tracking Tests of XAAM-N-4 Guidance System," by Jacobson[27]. The correlation functions for the elevation and deflection channels at an average range of 18,500 feet are plotted as a function of the correlation time. For both channels,

$$(CF)(TL) = [(SD)TL]^2 \, e^{-\frac{\tau}{(CT)_R}}$$

for correlation times greater than zero and less than 2.0 $(CT)_R$. For the elevation channel, the standard deviation is 2.4 mils, with a characteristic time of .43 second; and for the deflection channel the standard deviation is 3.1 mils, with a characteristic time of 1.40 seconds. Consequently, from Eq F-11 and I-1

$$[(PSD)q_{RI}]_{(\omega = 0)} S^2_{TS}[q_{RI}, TL] = 5.0 \text{ mils}^2/\text{cps in elevation}$$

$$= 27.0 \text{ mils}^2/\text{cps in deflection}$$

d. APG-3 Conical Scan Radar – AT-6 Target

Figure 2-12 of "Theory of Fire-Control System Design,"[29] by Floyd gives the correlation function of the tracking line at an average range of 2500 feet. The standard deviation of the tracking line is 9.2 mils, and the function is nearly exponential with a characteristic time of 0.023 second. Use of Eq. F-11 and I-1 gives

$$[(PSD)q_{RI}]_{(\omega = 0)} S^2_{TS}[q_{RI}, TL] = 4.0 \text{ mils}^2/\text{cps}$$

Recently, the tracking information of Fig. 2-12 was reassessed by the Servomechanisms Laboratory, MIT, using an autocorrelating machine rather than the numerical procedure of Floyd. In this way, more of the data points

were utilized during the 4-second tracking interval. The standard deviation of the tracking line increased to 13 mils, but the characteristic time was reduced to .013 second, so that the power spectral density was only 10 percent larger than the value previously obtained by Floyd.

e. Results of a Study by Angell, using AT-6, AT-11, B-26, and B-29 Targets

James Angell, working under the supervision of Professor Zimmerman in the Research Laboratory for Electronics, MIT, is making fundamental studies of radar wander in conjunction with the Meteor Program sponsored by the Bureau of Ordnance, USN. The receiver signals are multiplied by the range voltage before recording on tape. In this manner, measurements are made in terms of linear displacement at the target. Then, a spectrum analyzer is used to determine the power spectral density of the displacements of the reflecting point. It has been found that the power spectral density at zero frequency has an average value for all targets of 4.5 ft^2/cps at short range. In terms of angular units, this gives a power spectral density of 4.5 $mils^2$/cps at 1000 feet. These results are described in more detail in the Meteor Progress Report for June, 1951[6].

4. Estimated Radar Interference.

The estimated radar interference is shown by the solid curves of Fig. I-1. The upper curve for the conical scan radar assumes the power spectral density due to amplitude fading is 0.5 $mils^2$/cps. The lower curve assumes that, for monopulse radar, the amplitude fading is a negligible effect -- a fact emphasized by data obtained with the APG-25 radar system.

The power spectral density caused by wander is selected equal to 10 ft^2/cps in terms of linear displacement at the target.

The interference internally induced in the receiver is one-third that ob-

tained with the XAAM-N-4. The XAAM-N-4 radar is designed for missile guidance with 50kw peak power. It is felt that higher powered radar systems used in interceptor aircraft will have improved performance.

The estimated radar interference is the sum of the effects of wander, fading, and internal agitation. It should be noted that, for ranges from 1 to 2 - 1/2 miles, monopulse radar shows an improvement over conical scan radar of at least 2 to 1.

APPENDIX J

DETERMINATION OF THE STANDARD DEVIATION OF THE CONTROLLED LINE

There are several possible procedures for determining the standard deviation. Interference effects can be introduced into the REAC in such a way that the controlled-line inaccuracy is determined rather than the controlled-line error, as in Appendix E. However, since the interference is a random process, 25 solutions for a given set of system characteristics are required to evaluate the standard deviation, and hence the hit probability. For this reason, it is advisable to determine the error and the standard deviation separately.

An ideal method that will be available in the near future involves the use of the high-speed electronic simulator developed by Wingate, Green, and Giser[30] in the Instrumentation Laboratory. The tracking system can be represented in analogue form in a manner similar to the procedure used with the REAC. Random voltages can be generated electrically and applied as either gust or radar interference, or both, simultaneously. The electrical indication of the controlled-line displacement can be applied to an R.M.S. voltmeter. When properly calibrated, the voltmeter reading is the desired standard deviation. Since the simulator has a suppressed time scale of approximately 3000 to 1, a good statistical average can be obtained in a short time. At present, generators of random voltage can be obtained commercially, but an R.M.S. voltmeter for use over a reasonable band

of frequencies is difficult to procure.

The standard deviations are computed in this thesis by determining the amplitude ratios of the tracking systems between the input interferences and the controlled-line motion. Then, the power spectral densities can be determined by utilizing the information presented in Appendices H and I. Finally, the power spectral densities are integrated to give the standard deviations.

IBM equipment in the Statistical Center at MIT was used to carry out the computations. The power spectral densities presented in Chapters I, II, IV, and V were evaluated at intervals of 0.1 rad/sec. It is recommended that this procedure be used in the future for check solutions. In addition, it has the advantage of clearly showing the degree of improvement that can be achieved by adding smoothing in various parts of the tracking system.

The equations used in the calculations are summarized in this appendix. Values of the sensitivities and dynamic characteristics are tabulated on the power spectral density curves in each figure.

1. Open-Chain Tracking System with Tracking Line Prediction

The following expressions are derived from Eq. B-8, B-9, E-8, E-11, E-12B, E-14, and H-4.

$(AR)^2_{TS[Closed\ Loop]}$ = the square of the closed-loop amplitude ratio of the tracking system.

$$= \frac{(AR)^2_{TS(ol)}}{1+(AR)^2_{TS(ol)} + 2(AR)_{TS(ol)} \cos(PA)_{(ol)}} \qquad (J-1)$$

$(AR)^2_{TS(ol)}$ = the square of the open-loop amplitude ratio of the tracking system.

$$= \frac{[S_{(sq)(P,V)}\ S_{(sm)P}\ S_{(s,r)}]^2\ S^2_{S(s,\dot{\theta})}\ [1+[\omega(CT)_{A(\delta,\dot{\theta}}]^2]}{\omega^2\left\{[1-(\frac{\omega}{\omega_{nS}})^2]^2 + [\frac{2(DR)_S}{\omega_{nS}}\omega]^2\right\}}$$

$$\times \left\{\frac{[1+S_{p(W,P)}(CT)_R\,\omega^2]^2 + [(SN)S_{p(W,P)}W]^2}{[1+(\omega(CT)_R)^2]\ [1+[(SN)S_{p(W,P)}\ W]^2]}\right\} \qquad J-2$$

$(PA)_{TS(ol)}$ = open-loop phase angle of the tracking system

$$= \tan^{-1}[\omega(CT)_{A(\delta,\dot{\theta})}] + \tan^{-1}\left[\frac{(SN)S_{p(W,P)}W}{1 + S_{p(W,P)}(CT)_R\,\omega}\right]$$

$$-90^\circ - \tan^{-1}\left[\frac{2(DR)_S\left(\frac{\omega}{\omega_{nS}}\right)}{1-\left(\frac{\omega}{\omega_{nS}}\right)^2}\right] - \tan^{-1}[\omega(CT)_R]$$

$$-\tan^{-1}[(SN)S_{p(W,P)}W] \qquad \text{J-3}$$

$(DR)_S$ = system damping ratio

$$= -\frac{M_{\dot{\theta}} + Z_w - u_o M_{\dot{w}} + S_{rg}\,S_{(sm)\dot{\theta}}\,S_{(s,r)}\,M_\delta}{2\,\omega_{nS}} \qquad \text{J-4}$$

ω_{nS} = system undamped natural frequency

$$= \sqrt{Z_w M_{\dot{\theta}} - u_o M_w + Z_w S_{rg} S_{(sm)\dot{\theta}} S_{(s,r)} M_\delta} \qquad \text{J-5}$$

$S_{S(\delta,\dot{\theta})}$ = system elevator displacement–pitch rate sensitivity

$$= \frac{Z_\delta M_w - Z_w M_\delta}{\omega_{nS}^2} \qquad \text{J-6}$$

$$(AR)^2_{TS[LS,CL]} = (AR)^2_{TS[\text{Closed Loop}]}\left\{\frac{1+[(1+SN)S_{p(W,P)}W]^2}{[1+S_{p(W,P)}(CT)_R\,\omega^2]^2+[(SN)S_{p(W,P)}W]^2}\right\} \qquad \text{J-7}$$

$$(AR)^2_{TS[\omega_C,CL]} = \omega^2(AR)^2_{TS[\text{Closed Loop}]}\left[\frac{S_{A(\omega_C,CL)}}{S_{S(\delta,\dot{\theta})}}\right]^2\left\{\frac{1+[\omega(CT)_{A(\omega_C,CL)}]^2}{1+[\omega(CT)_{A(\delta,\dot{\theta})}]^2}\right\}$$

$$\times\left\{\frac{[1+(\omega(CT)_R)^2][1+[(SN)S_{p(W,P)}W]^2]}{[1+S_{p(W,P)}(CT)_R\,\omega^2]^2+[(SN)S_{p(W,P)}W]^2[S_{(sg)(P,V)}\,S_{(sm)P}\,S_{(s,r)}]^2}\right\} \qquad \text{J-8}$$

$$\frac{[(SD)CL]^2_{[q_{in}=q_{RI}]}}{[(PSD)q_{RI}]_{(\omega=0)}\, S^2_{TS[(q_{RI})TL]}} = \frac{1}{\pi}\int_0^{\infty} (AR)^2_{TS[LS,CL]}\, d\omega \qquad \text{J-9}$$

$$[(SD)CL]^2_{[q_{in}=w_G]} = \frac{1}{\pi}\int_0^{\infty} \left[\frac{2(CT)_G\,[(SD)w_G]^2}{1+[\omega(CT)_G]^2}\right](AR)^2_{TS[w_G,CL]}\, d\omega \qquad \text{J-10}$$

2. Open-Chain Tracking System with Tracking Inaccuracy Prediction and Tight-Loop Stabilization of the Radar Antenna.

The following expressions are derived from Eq. B-8, B-9, E-19, E-20, E-21, E-24, and H-4.

$$(AR)^2_{TS[Closed\ Loop]} = \frac{(AR)^2_{TS(ol)}}{1+(AR)^2_{TS(ol)} + 2(AR)_{TS(ol)}\cos(PA)_{(ol)}} \qquad \text{J-11}$$

$$(AR)^2_{TS(ol)} = \frac{[S_{(sg)(P,V)}\, S_{(sm)P}\, S_{(S,r)}]^2}{\omega^2}\left[1+\left(\frac{S_{(sm)i}}{S_{(sm)P}}\right)^2\frac{1}{\omega^2}\right]$$

$$\times \frac{S^2_{S(\delta,\dot{\theta})}\left\{1+[\omega(CT)_{A(\delta,\dot{\theta})}]^2\right\}}{\left\{\left[1-\left(\frac{\omega}{\omega_{nS}}\right)^2\right]^2+\left[\frac{2(DR)_S}{\omega_{nS}}\,\omega\right]^2\right\}}$$

$$\times \left\{\frac{\left\{1-\left[\frac{S_{p(W,P)}}{S_{g(TL,V)}\,S_{R(V,\dot{P})}}+\frac{(SN)\,S_{p(W,P)}}{S_{TID}\,S_{RSS(i,W)}}\right]\omega^2\right\}^2+\left\{\left[\frac{1}{S_{TID}\,S_{RSS(i,W)}}+(SN)S_{p(W,P)}\right]\omega\right\}^2}{\left\{1+[(SN)S_{p(W,P)}W]^2\right\}\left\{\left[1-\frac{\omega^2}{[S_{g(TL,V)}\,S_{R(V,\dot{P})}][S_{TID}\,S_{RSS(i,W)}]}\right]^2+\left[\frac{\omega}{S_{TID}\,S_{RSS(i,W)}}\right]^2\right\}}\right\}$$

J-12

$$(PA)_{(TS)(ol)} = \tan^{-1}[\omega(CT)_{A(\delta,\dot{\theta})}] + \tan^{-1}\left\{\frac{\left[\frac{1}{S_{TID}S_{RSS(i,W)}} + (SN)S_{P(W,P)}\right]\omega}{1-\left[\frac{S_{P(W,P)}}{S_{g(TL,V)}S_{R(V,\dot{P})}} + \frac{(SN)S_{P(W,P)}}{S_{TID}S_{RSS(i,W)}}\right]}\right\}$$

$$-90^\circ - \tan^{-1}\left[\frac{S_{(sm)i}}{S_{(sm)P}}\ \frac{1}{\omega}\right] - \tan^{-1}\left[\frac{2(DR)_S\ \frac{\omega}{\omega_{nS}}}{1-\left(\frac{\omega}{\omega_{nS}}\right)^2}\right]$$

$$-\tan^{-1}\left[(SN)S_{P(W,P)}\omega\right]$$

$$-\tan^{-1}\left\{\frac{\frac{\omega}{[S_{TID}\ S_{RSS(i,W)}]}}{1-\frac{\omega^2}{[S_{g(TL,V)}\ S_{R(V,\dot{P})}][S_{TID}\ S_{RSS(i,W)}]}}\right\} \qquad \text{J-13}$$

$$(AR)^2_{TS(LS,CL)} = (AR)^2_{TS\,[Closed\ Loop]}$$

$$\times\left\{\frac{\left[1-\frac{\omega^2 S_{P(W,P)}}{[S_{g(TL,V)}\ S_{R(V,\dot{P})}]^2}\right]^2 + \left[(1+SN)S_{P(W,P)}W\right]^2}{\left\{1-\left[\frac{S_{P(W,P)}}{S_{g(TL,V)}S_{R(V,\dot{P})}} + \frac{(SN)S_{P(W,P)}}{S_{TID}S_{RSS(i,W)}}\right]\omega^2\right\}^2 + \left\{\left[\frac{1}{S_{TID}S_{RSS(i,W)}} + (SN)S_{P(W,P)}\right]\omega\right\}^2}\right\}$$

J-13A

$$(AR)^2_{TS\,[w_G,CL]} = \omega^2 (AR)_{TS\,[Closed\ Loop]}\left[\frac{S_{A[w_G,CL]}}{S_{S(\delta,\dot{\theta})}}\right]^2\left\{\frac{1+[\omega(CT)_{A[w_G,CL]}]^2}{1+[\omega(CT)_{A(\delta,\dot{\theta})}]^2}\right\}$$

$$\times\left\{\frac{1}{1+\left(\frac{S_{(sm)i}}{S_{(sm)P}W}\right)^2}\right\}\left\{\frac{1+[(SN)S_{P(W,P)}W]^2}{[S_{(sg)(P,V)}S_{(sm)P}S_{(S,T)}]^2}\right\}$$

$$\times\frac{\left[1-\frac{\omega^2}{[S_{g(TL,V)}S_{R(V,\dot{P})}][S_{TID}S_{RSS(i,W)}]}\right]^2 + \left[\frac{\omega}{S_{TID}S_{RSS(i,W)}}\right]^2}{\left\{1-\left[\frac{S_{P(W,P)}}{S_{g(TL,V)}S_{R(V,\dot{P})}} + \frac{(SN)S_{P(W,P)}}{S_{TID}S_{RSS(i,W)}}\right]\omega^2\right\}^2 + \left\{\left[\frac{1}{S_{TID}S_{RSS(i,W)}} + (SN)S_{P(W,P)}\right]\omega\right\}^2}$$

J-14

3. Closed-Loop Tracking System with Controlled-Line Prediction

The following expressions are derived from Eq. B-8, B-9, E-25, E-27, E-28, and H-4.

$(AR)^2_{TS[LS,TL]}$ = the square of the sight-tracking line amplitude ratio of the system

$$= \frac{(AR)^2_{TS(ol)}}{1+(AR)^2_{TS(ol)} + 2(AR)_{TS(ol)} \cos(PA)_{TS(ol)}} \qquad \text{J-15}$$

$$(AR)^2_{TS(ol)} = \frac{[S_{TID}\ S_{(sm)P}\ S_{(s,r)}]^2}{\omega^2} \left\{\frac{[1+[\omega(CT)_{A(\delta,\dot{\theta})}]^2]}{[1+[\omega(CT)_{(sm)}]^2]}\right\}$$

$$\times \left\{\frac{S^2_{S(\delta,\dot{\theta})}}{\left[1-\left(\frac{\omega^2}{\omega^2_{nS}}\right)\right]^2 + \left[\frac{2(DR)_S\,\omega}{\omega_{nS}}\right]^2}\right\}$$

$$\times \left\{\frac{[1-(1+SN)\,S_{p(W,P)}(CT)_R\,\omega^2]^2 + \{[(SN)S_{p(W,P)}+(CT)_R]\omega\}^2}{[1+(1+SN)^2\,S^2_{p(W,P)}\,W^2][1+(\omega(CT)_R)^2]}\right\} \qquad \text{J-16}$$

$$(PA)_{(TS)(ol)} = \tan^{-1}[\omega(CT)_{A(\delta,\dot{\theta})}] + \tan^{-1}\left[\frac{[(SN)S_{p(W,P)}+(CT)_R]\omega}{1-(1+SN)S_{p(W,P)}(CT)_R\,\omega^2}\right]$$

$$-90^\circ - \tan^{-1}[\omega(CT)_{(sm)}]$$

$$-\tan^{-1}\left[\frac{2(DR)_S\left(\frac{\omega}{\omega_{nS}}\right)}{1-\frac{\omega^2}{\omega^2_{nS}}}\right] - \tan^{-1}[1+SN]\,S_{p(W,P)}\,W$$

$$-\tan^{-1}[\omega(CT)_R] \qquad \text{J-17}$$

$$(AR)^2_{(TS)(LS,CL)} = \frac{[1+(1+SN)^2 S^2_{p(W,P)} W^2][1+(\omega(CT)_R)^2](AR)^2_{(TS)(LS,TL)}}{\{1-(1+SN)S_{p(W,P)}(CT)_R\,\omega^2\}^2 + \{[(SN)S_{p(W,P)}+(CT)_R]\omega\}^2} \qquad \text{J-18}$$

$$(AR)^2_{(TS)[w_G,CL]} = \frac{\omega^2 (AR)^2_{(TS)[LS,CL]}}{[S_{TID}\, S_{(sm)P}\, S_{(s,r)}]^2} \left[\frac{S_{A[w_G,CL]}}{S_{A(\delta,\dot{\theta})}}\right]^2 \times \left[\frac{1+[\omega(CT)_{A[w_G,\theta]}]^2}{1+[\omega(CT)_{A(\delta,\dot{\theta})}]^2}\right] \left[1+[\omega(CT)_{(sm)}]^2\right] \qquad \text{J-19}$$

4. Closed-Loop Tracking System with Tracking Inaccuracy Prediction and Tight-Loop Stabilization of the Aircraft

The following expressions are dervied from Eq. B-8, B-9, E-27, E-32, E-33, and H-4.

$$(AR)^2_{TID}(AR)^2_{LCS(i,W)} = \frac{[S_{TID}\, S_{LCS(i,W)}]^2 (AR)^2_{LCS(ol)}}{\omega^2 [1+(AR)^2_{LCS(ol)} + 2(AR)_{LCS(ol)} \cos(PA)_{LCS(ol)}]} \qquad \text{J-20}$$

$$(PA)_{LCS(i,W)} = (PA)_{LCS(ol)} - 90^\circ - \tan^{-1}\left[\frac{(AR)_{LCS(ol)} \sin(PA)_{LCS(ol)}}{1+(AR)_{LCS(ol)} \cos(PA)_{LCS(ol)}}\right] \qquad \text{J-21}$$

$$(AR)^2_{LCS(ol)} = \frac{[S_{q(CL,V)}\, S_{(sm)P}\, S_{(s,r)}]^2 [1+(\omega(CT)_{A(\delta,\dot{\theta})})^2]}{\omega^2\left\{\left[1-\frac{\omega^2}{\omega^2_{nS}}\right]^2 + \left[\frac{2(DR)_S}{\omega_{nS}}\omega\right]^2\right\}} \qquad \text{J-22}$$

$$(PA)_{LCS(ol)} = \tan^{-1}[\omega(CT)_{A(\delta,\dot{\theta})}] - 90^\circ - \tan^{-1}\left\{\frac{2(DR)_S\left(\frac{\omega}{\omega_{nS}}\right)}{1-\frac{\omega^2}{\omega^2_{nS}}}\right\} \qquad \text{J-23}$$

$$(AR)^2_{[TID,PC,RAS]} = \frac{[S_{TID}\, S_{LCS(i,W)}]^2 [S_{P(W,P)}]^2}{[1+(1+SN)^2 S^2_{P(W,P)} W^2][1+(\omega(CT)_R)^2]} \qquad \text{J-24}$$

$$(PA)_{[TID,PC,RAS]} = -\tan^{-1}\left[(1+SN)\,S_{p(W,P)}W\right]-\tan^{-1}\left[\omega(CT)_R\right] \qquad \text{J-25}$$

$$(AR)^2_{TS[LS,CL]} = \frac{(AR)^2_{TID}\,(AR)^2_{LCS(i,W)}}{\left\{\left[1+(AR)_{TID}(AR)_{LCS(i,W)}\cos(PA)_{LCS(i,W)}-(AR)_{[TID,PC,RAS]}\cos(PA)_{[TID,PC,RAS]}\right]^2 + \left[(AR)_{TID}(AR)_{LCS(i,W)}\sin(PA)_{LCS(i,W)}-(AR)_{[TID,PC,RAS]}\sin(PA)_{[TID,PC,RAS]}\right]^2\right\}} \qquad \text{J-26}$$

$$(AR)^2_{TS[W_G,CL]} = \left[\frac{\omega^2}{S_{TID}\,S_{LCS(i,W)}}\right]^2 \frac{(AR)^2_{TS(LS,CL)}}{\left[S_{g(CL,V)}\,S_{(sm)P}\,S_{(s,r)}\right]^2} \times\left\{\frac{S_{A(W_G,CL)}}{S_{S(\delta,\dot{\theta})}}\right\}^2\left\{\frac{1+\left[\omega(CT)_{A(W_G,\theta)}\right]^2}{1+\left[\omega(CT)_{A(\delta,\dot{\theta})}\right]^2}\right\} \times\left\{1+(AR)^2_{[TID,PC,RAS]}-2(AR)_{[TID,PC,RAS]}\cos(PA)_{[TID,PC,RAS]}\right\} \qquad \text{J-27}$$

APPENDIX K

1. Weymouth, R. and Benjes, A. C., Jr., "Design Consideration for All-Weather Fighter Fire Control System"; Engineering Memo No. 6445-T-24, MIT, Sept., 1949 (Confidential).
2. Eckhardt, H. D., "Theoretical Lateral Frequency Response of Douglas A-26 Airplane to (a) A Sinusoidally Varying Rudder Angle with Fixed Ailerons and (b) A sinusoidally Varying Aileron Angle with Fixed Rudder"; Instrumentation Laboratory, MIT, Engineering Memorandum No. 6445-E-7, Sept., 1947.
3. Van Meter, J. T., "The Effect of Various Flight Configurations on the Longitudinal Performance of an Airplane"; Instrumentation Laboratory, MIT, Report No. 6445-T-15.
4. Design Study Report, "Automatic Gun Laying Turret -- Tail Aero X5A Using AN/APG-25 Radar," Vol. I and II; General Electric Company.
5. Project Meteor Quarterly Report; MIT, Dec., 1950 (Secret).
6. Project Meteor Quarterly Report; MIT, June, 1951 (Secret).
7. Geometric Problems Associated with Fire Control Systems of the Disturbed-Sight Type; Theory and Correction of the Cross-Roll Error; Interrelationships of Smoothing and Solution Time; Comparison of Naval AA Fire Control Systems"; Instrumentation Laboratory, MIT, Nav/ord Report 3-47, Pt. II, Vol. III, April, 1949 (Confidential).
8. "Maintenance Instructions of Simulator Model II"; Direction of Chief of Bureau of Aeronautics, August, 1949 (Confidential)
9. Seamans, R. C., Jr., Wilkins, F. P., and Brainerd, H. B., "Application of Minneapolis Honeywell Type C-1a Servo Pilot Components to Automatic Tracking Systems"; Instrumentation Laboratory, MIT, Tracking Control Progress Report No. 6445-P-3, June, 1946 (Confidential).
10. Seamans, R. C., Jr., Muzzey, C. L., and Whitaker, H., "Determination of the Performance Operators of Army Attack Bomber A-26C No. 898";

Instrumentation Laboratory, MIT, Tracking Control Progress Report No. 6445-P-4, Sept., 1947 (Confidential).

11. Seamans, R. C., Jr., and Whitaker, H. P., "Dynamic Performance of Aircraft Tracking Systems"; Instrumentation Laboratory, MIT, Tracking Control Progress Report No. 6445-P-5, Sept., 1948 (Confidential).

12. Brainerd, H. B., "Summary of Concepts Associated with the Normal Probability Law"; Instrumentation Laboratory, MIT, Jan., 1949 (Confidential).

13. Loh, Yuan-Chin, "Design of Linear Systems for Minimum Mean Integral Square Error"; Aeronautical Engineering Department, MIT, 1949.

14. "Detailed Theory and Computations for the A-1 Sight for the Control of Gunfire from Fixed Guns, Rocketfire, and Bombing from Aircraft"; Vol. II, Instrumentation Laboratory, MIT, Dec., 1945 (Restricted).

15. Rea, J. B., "Automatic Tracking Control of Aircraft"; Report No. 6445-T-8, Instrumentation Laboratory, MIT, 1947 (Confidential).

16. Durand, W. F., Editor in Chief, "Aerodynamic Theory," Vol. V, Division Nav/ord.

17. Seamans, R. C., Jr., Blasingame, B. P., and Clementson, G. C., "The Pulse Method for the Determination of Aircraft Dynamic Performance"; Journal of the Institute of Aeronautical Sciences, Vol. 17, No. 1, Jan., 1950.

18. Kidder, R. C., "Dynamic Longitudinal Stability Flight Test of an F-80 Airplane by the Forced Oscillation and Step Function Methods Including Measured Horizontal Tail Loads"; Report TB495-F-11, Cornell Aero Laboratory, Feb., 1950.

19. Wiener, N., "The Extrapolation, Interpolation, and Smoothing of Stationary Time Series"; John Wiley & Sons, New York, 1949.

20. Draper, C. S., "Instrument Engineering"; Instrumentation Laboratory, MIT, Sept., 1950.

21. Lee, Y. W., "Communication Applications of Correlation Analysis"; Symposium on Applications of Autocorrelation Analysis to Physical Problems, Research Laboratory of Electronics, MIT, June, 1949.

22. Clementson, G. C., "An Investigation of the Power Spectral Density of Atmosphere Turbulence"; Report No. 6445-T-31, Instrumentation Laboratory, MIT, May, 1950.

23. Bain, J. B., Michaelis, F. H., and Wootton, J. C., "Investigation of Aircraft Lateral Motion Performance Function of Pulse Technique"; Report No. 6445-T-23, Instrumentation Laboratory, May, 1949.

24. "Recommendations for the Design of Automatic Interceptor Control Systems"; Engineering Memorandum No. 6445-E-35, Instrumentation Laboratory, MIT, Dec., 1949 (Confidential).

25. Meade, J. E., Hastings, A. E., and Gerwin, H. L., "Noise in Tracking Radars"; Report NRL 3759, Naval Research Laboratory, Washington, D. C., Nov., 1950 (Confidential).

26. Burlingame, "Characteristics of Target Generated Noise in Gun Laying Radar, AN/APG-25(XN-2)"; Engineering Report No. R49A0329, Dec., 1949 (Confidential).

27. Jacobson, S., "Ground-to-Air Tracking Tests of XAAM-N-4 Guidance System"; Engineering Report No. 3796, Glenn L. Martin, June, 1950 (Confidential).

28. "Dynamic Response of a B-25J Airplane to Pulse Shape Elevation Disturbances"; MIT, July, 1949 (Confidential).

29. Floyd, G. F., Jr., "Design of Fire-Control Systems"; Servomechanisms Laboratory, MIT, June, 1950 (Confidential).

30. "Demonstration of Automatic Interceptor Control Systems"; Fig. V-34 through V-41; Instrumentation Laboratory, MIT, Feb., 1950 (Confidential).

31. Sard, A., "The Combination of a Random and a Systematic Error"; Columbia University, AMP Memo 104.4M, Sept., 1945 (Restricted).

32. Clementson, G. C., "Investigation of the Response of an Aircraft to a Finite Pulse Input"; Report No. 6445-T-18, Instrumentation Laboratory, MIT, Sept., 1948.

33. Greene, F. H., Jr., "Results of Experimental Flight Test Program on A-1 Gun-Bomb-Rocket Sight Installed in XP-38R No. 236"; Instrumentation Laboratory, MIT, Report No. 6445-E-21, March, 1949 (Confidential).

APPENDIX L

GLOSSARY OF SYMBOLS USED IN CHAPTERS I THROUGH V

A_T - Target angle.

$(VA)_T$ - Vulnerable area of the target.

CL - Controlled line is used for boresighting purposes and is fixed to the interceptor aircraft. For the purposes of this thesis the controlled line is parallel to the longitudinal axis of the aircraft, X_A.

(C)TL - Tracking line correction measured from the tracking line to the line of sight.

(C)V - Correction voltage.

$(CT)_{sm}$ - Characteristic time of the signal modifier.

$(CT)_R$ - Radar characteristic time.

δ - Elevator displacement.

(E)CI - Error in the center of impact.

(I)TL - Tracking line inaccuracy measured from line of sight to the tracking line.

LS - Line of sight drawn from the interceptor aircraft to the vulnerable area of the target.

$P(VA)_T$ - Probability of a projectile hitting the vulnerable area of the target.

P_R - Radar prediction angle measured from the radar tracking line to the controlled line.

$\dot{P}_R$ - Radar prediction angle rate.

PSR - Prediction sensitivity ratio.

R - Range measured from the interceptor aircraft to the target.

r_T - Radius of the vulnerable area of the target assumed circular.

$(SD)IP$ - Standard deviation of the impact point.

$S_{g(CL,V)}$ - Controlled-line displacement input — voltage output sensitivity of the integrating rate gyro.

$S_{g(TL,V)}$ - Tracking-line displacement input — voltage output sensitivity of the integrating gyro unit.

$S_{LCS(i,W)}$ - Current input angular velocity output sensitivity of the longitudinal control system.

SN - Stability number of the prediction computer.

$S_{p(W,P)}$ - Angular velocity input-prediction angle output sensitivity of the prediction computer.

S_{RAS} - Sensitivity of the radar antenna servo.

$S_{(sg)(P,V)}$ - Prediction angle-voltage output sensitivity of the radar antenna signal generator.

$S_{(sg)(V,P)}$ - Reciprocal of $S_{(sg)(P,V)}$.

$S_{(sm)i}$ - Integrating sensitivity of the signal modifier.

$S_{(sm)p}$ - Proportional sensitivity of the signal modifier.

$S_{(sm)\dot{\theta}}$ - Pitch rate sensitivity of the signal modifier.

$S_{(s,r)}$ - Sensitivity of the elevator servo and rigging. This sensitivity includes the effect of elevator hinge moments.

$S_{(rg)}$ - Sensitivity of the rate gyro.

$S_{RSS(i,W)}$ - Current input-angular velocity output sensitivity of the radar stabilization system analyzed in Chapter II.

$S_{R(V,\dot{P})}$ - Voltage input-prediction rate output sensitivity of the antenna servo drive.

S_{TID} - Sensitivity of the tracking inaccuracy detector.

TL - Tracking line.

$(TL)_R$ - Radar tracking line, a line fixed to the radar antenna, which is along the line of sight when the output from the tracking inaccuracy detector is zero. In this thesis the subscript is omitted.

V_A - Velocity of the interceptor aircraft with respect to air-mass coordinates.

$V_{p(av)}$ - Average velocity of the projectile with respect to air-mass coordinates.

V_{PC} - Voltage output from the prediction computer.

$\dot{V}_{PC}$ - Voltage rate output from the prediction computer.

V_T - Target velocity.

W_{CL} - Angular velocity of the controlled line.

W_{TL} - Angular velocity of the tracking line.

APPENDIX M

BIOGRAPHICAL SKETCH

Robert Channing Seamans, Jr. was born in Salem, Massachusetts on October 30, 1918. He graduated from the Tower School in Salem in 1931, and from the Lenox School for Boys in 1936. He entered Harvard College the same year, where he concentrated on Engineering Sciences. He graduated from Harvard with the degree of Bachelor of Science in 1939, as of the class of 1940.

After taking a preparatory course for Medical School, he returned to engineering and enrolled at Massachusetts Institute of Technology, in September, 1940. There he received the degree of Master of Science in Aeronautical Engineering in February, 1942.

He was an instructor in the Aeronautical Engineering Department of MIT for four years, commencing September, 1941; an assistant professor for an additional three years, commencing in September, 1945; and has been an associate professor from June 1949 to the present.

In 1946 he received a leave of absence in order to direct the Tracking Control Project, which was carried out by the Instrumentation Laboratory, MIT, under the auspices of the Division of Industrial Corporation.

He worked at the Consolidated Engineering Corporation in Pasadena, California from June until September, 1942, and has been a Technical Consultant for the Office of Air Research, Air Materiel Command, USAF. He is a member of the Subcommittee on Stability and Control of the NACA.

He is co-author of two papers that have been published in the "Journal of the Aeronautical Sciences". One of the papers, in which he co-authored with Dr. B. G. Bromberg and Mr. L. E. Payne, is entitled "Application of the Performance Operator to Aircraft Automatic Control" (Vol. 15, No. 9, Sept. 1948); the other, in which he co-authored with Major B. P. Blasingame, USAF, and Major G. C. Clementson, USAF, is entitled "The Pulse Method for the Determination of Aircraft Dynamic Performance"(Vol. 17, No. 1, January 1950).